PB34-192178

REPORT NO.
UCB/EERC-83/22
OCTOBER 1983

EARTHQUAKE ENGINEERING RESEARCH CENTER

HYBRID MODELLING OF SOIL-STRUCTURE INTERACTION IN LAYERED MEDIA

by

TSAIR-JYH TZONG
JOSEPH PENZIEN

Report to the National Science Foundation

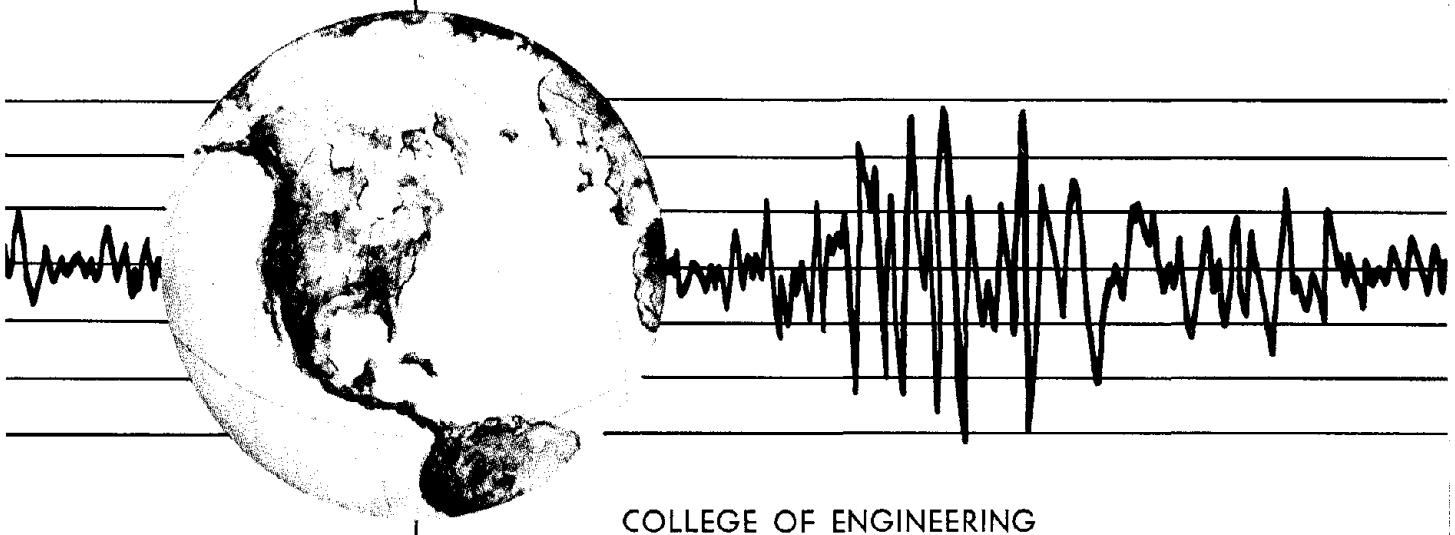

COLLEGE OF ENGINEERING

UNIVERSITY OF CALIFORNIA · Berkeley, California

For sale by the National Technical Information Service, U.S. Department of Commerce, Springfield, Virginia 22161.

See back of report for up to date listing of EERC reports.

DISCLAIMER

Any opinions, findings, and conclusions or recommendations expressed in this publication are those of the authors and do not necessarily reflect the views of the National Science Foundation or the Earthquake Engineering Research Center, University of California, Berkeley

50272-101

REPORT DOCUMENTATION PAGE	1. REPORT NO. NSF/CEE - 83035	2.	3. Recipient's Accession No. PB84 192178
4. Title and Subtitle: Hybrid Modelling of Soil-Structure Interaction in Layered Media			5. Report Date: October 1983 6.
7. Author(s): Tsair-Jyh Tzong and Joseph Penzien			8. Performing Organization Rept. No. UCB/EERC - 83/22
9. Performing Organization Name and Address: Earthquake Engineering Research Center, University of California, 1301 South 46th Street, Richmond, CA 94804			10. Project/Task/Work Unit No. 11. Contract(C) or Grant(G) No. (C) (G) CEE81-05790
12. Sponsoring Organization Name and Address: National Science Foundation, 1800 "G" Street, NW, Washington, DC 20550			13. Type of Report & Period Covered 14.

15. Supplementary Notes

16. Abstract (Limit: 200 words)

The hybrid modelling approach, which effectively solves soil-structure interaction problems, is extended for use in layered soil media. This approach partitions the entire structure-soil system into a near field which consists of the structure and a portion of its surrounding soil, modelled by the finite element method, and a far field which is responsible for energy travelling away from the near field represented by an impedance model. Two analytical methods, appropriate to different layered soil systems, are employed to simulate the semi-infinite far-field region. The system identification method, which determines the approximate far-field impedance functions along the interface between the near and far fields, is applied to the single-layer halfspace in which a rigorous representation of the far-field is difficult to obtain by direct solution. A boundary solution method is developed to calculate the exact far-field impedance matrix for cases involving layers of soil having a rigid lower boundary. By this method, the theoretical solution of the far field is combined with the near-field finite elements through the variational principle.

17. Document Analysis a. Descriptors

b. Identifiers/Open-Ended Terms

c. COSATI Field/Group

18. Availability Statement: Release Unlimited	19. Security Class (This Report)	21. No. of Pages: 154
	20. Security Class (This Page)	22. Price

(See ANSI-Z39.18) See Instructions on Reverse

OPTIONAL FORM 272 (4-77)
(Formerly NTIS-35)
Department of Commerce

HYBRID MODELLING OF SOIL-STRUCTURE INTERACTION IN LAYERED MEDIA

by

Tsair-jyh Tzong
and
Joseph Penzien

A Report to the
National Science Foundation

Report No. UCB/EERC-83/22
Earthquake Engineering Research Center
University of California
Berkeley, California

October 1983

ABSTRACT

The hybrid modelling approach, which effectively solves the soil-structure interaction problems, is extended herein for use in layered soil media. This approach partitions the entire structure-soil system into a near field and a far field with a smooth interface. The near field which consists of the structure and a portion of its surrounding soil is modelled by the finite element method. The far field which is responsible for energy travelling away from the near field is represented by an impedance model. Two analytical methods, appropriate to different layered soil systems, are employed to simulate the semi-infinite far-field region. The system identification method, which determines the approximate far-field impedance functions along the interface between the near and far fields, is applied to the single-layer halfspace in which a rigorous representation of the far-field is difficult to obtain by direct solution. A boundary solution method is developed to calculate the exact far-field impedance matrix for cases involving layers of soil having a rigid lower boundary. By this method, the theoretical solution of the far field is combined with the near-field finite elements through the variational principle.

Since the theoretical solution of rigid plates vibrating on the layered halfspace is required in the system identification procedure, the dynamic behavior of the infinite rigid strip on a single-layer halfspace is determined.

The modified Gauss-Newton method, which considers the second derivatives of the proposed error function, is applied to systematically identify the far-field impedance functions for the plane-strain case in the single-layer halfspace. Numerical results obtained using the identified impedance functions indicate that these functions are efficient and effective in solving the soil-structure interaction problem involving a single-layer halfspace.

The principle of the virtual work employed in the far field and the variational principle employed in the near field constitute the boundary solution method. By evaluating the dynamic behavior of the infinite rigid strip and the circular disk on the layers of soil with a rigid lower boundary, the far-field impedance matrix generated by the boundary solution method

successfully shows its ability to account for energy travelling away from the structure, waves reflecting and refracting from the layer interfaces, and waves reflecting from the rigid lower boundary.

The effectiveness and efficiency of the hybrid modelling for soil-structure interaction analysis in layered media are demonstrated by simulating the far field using the system identification method and the boundary solution method for different aforementioned soil conditions.

ACKNOWLEDGEMENTS

The authors wish to thank Professor J. Lysmer and Professor B. Bolt for their valuable suggestions and for reviewing the manuscript. This report also constitutes Tsair-jyh Tzong's doctoral dissertation submitted to the University of California at Berkeley.

Financial support, provided by the National Science Foundation under Grant No. CEE81-05790, is greatly appreciated. Computer facilities were provided by the University of California at Berkeley and the Lawrence Berkeley Laboratory.

TABLE OF CONTENTS

I. INTRODUCTION

In recent years, the analysis of soil-structure interaction and its effects on the earthquake response of structures becomes significant because of the high safety and reliability requirements for massive structures such as nuclear power plants, offshore gravity towers, and dams. Numerous investigations have been reported on this subject, however, many difficulties still remain in obtaining the true response of these structures. These difficulties are caused primarily by the semi-infinite nature of the soil medium and the embedment of the structures. The nonhomogeneity and strain dependency of the soil and the uncertainties associated with seismic input excitations further complicate the analysis. Since a rigorous mathematical representation of the real structure and its surrounding soil is extremely difficult to define using the present state of the art, several modelling methods are provided herein to approximate real conditions. The analysis methods can be categorized into the substructure method and the direct method.

In the usual substructure method of analysis the soil is idealized as a homogeneous or horizontally layered halfspace and the structure is simplified using a stick model connected to a rigid foundation with simple geometry such as a rigid circular disk [1,2,3,4,5] or an infinite rigid strip [6,7,8,9]. The interaction problem is then reduced to the evaluation of the frequency dependent impedance functions of the rigid foundation which when combined with the structure allow the response to be evaluated through the frequency domain. This simple method is economical and it realistically considers the radiation of energy away from the foundation and into the halfspace. However, it is restricted to structures which satisfy the rigid plate foundation conditions mentioned above and to soil conditions which can be approximated by an elastic or viscoelastic halfspace.

The direct method of analysis models the structure and a large portion of surrounding soil as a single system using finite elements. This method can easily accommodate the embedment of a structure and nonlinear soil properties; however, radiation damping is usually not properly

represented even though viscous dashpots are sometimes placed on the boundaries [10] to allow outward wave transmission to simulate true radiation damping. In addition to the problem associated with wave transmission across the boundaries, waves are artificially reflected from the finite element interfaces due to the the nonuniformity of the displacement fields assumed in the finite elements [11]. These reflections further distort the solution.

A hybrid model has been used in the substructure method in an attempt to include the advantages and avoid the disadvantages of the above two methods. In this method, finite elements are used in the near field to model the structure and a portion of its surrounding soil so that structural embedment and the nonhomogeneity and strain dependency of soil can be treated. Since the soil region in the near field is limited in size, the number of degrees of freedom and the influence of artificial wave reflections can be greatly reduced. To treat radiation damping, the far field, which shares a common interface with the near field, is represented by an impedance matrix of a size corresponding to the number of degrees of freedom at the interface. This impedance matrix, which accounts for the radiation of energy, can be determined using the system identification method [12,13] or the infinite element method [14]. The soil-structure interaction problem is then solved efficiently and economically by the substructure method of analysis in the frequency domain.

In the previous hybrid modelling studies, the soil medium was restricted to a homogeneous, isotropic and elastic halfspace. Engineers are however often interested in the dynamic behavior of structures built on a layered soil deposit. It is therefore the purpose of this research to generalize the hybrid model to accommodate layered soil media. A far-field impedance matrix, which accounts for both radiation and viscous damping, is determined by two methods suitable to different soil deposits. The continuous far-field impedance functions along a common interface between the near and far fields are determined by the method of system identification for a single-layer halfspace which has wide application in modelling site conditions. A boundary solution technique is used to solve the soil-structure interaction problem for systems having a rigid lower boundary under the soil layers. Although, Waas [15] and

Kausel [16] solved the similar problem, i.e. layered soils terminated by a rigid boundary, their formulation leads to a quadratic complex-valued eigenvalue problem which requires much computational effort. The current method avoids this shortcoming and is more flexible to be used.

To calculate far-field impedance functions, the dynamic behavior of an infinite rigid strip on the single-layer halfspace is determined in Chapter II. Results for different material properties of the layer and the halfspace are shown and compared with some existing data. The calculated strip response is then employed in Chapter III where the continuous far-field impedance functions are determined iteratively by the system identification method. Two dimensional inplane problems which can simulate the dynamic behavior of long tunnels, dams and other massive long structures are considered. In Chapter IV, the boundary solution method, which combines the continuous solution of the far field with a finite element formulation of the near field using the variational principle and the principle of virtual work, is used to treat an extreme case, i.e. the case of layers of soil underlain by rigid rock. In this special case, it is not practical to generate boundary impedances by the system identification method. Numerical results are presented and a comparison is made between the characteristics of the boundary solution method and the semi-analytic method introduced by Waas and Kausel. Conclusions and suggestions for future research are presented in Chapter V.

II. VIBRATION OF AN INFINITE RIGID STRIP ON LAYERED MEDIA

A. General

The dynamic behavior of simple geometries, e.g. an infinitely long rigid strip as used in two dimensional problems and a rigid circular disk as used in three dimensional problems, plays an important role in soil-structure interaction analysis. Many investigations have been conducted on this subject during the past decade, which basically involves two methods. One method introduces the relaxed boundary assumption, i.e. it ignores the shearing stresses under the plate for the vertical and rocking motions and the normal stress for the translational motion; thus, the calculation of the plate response becomes a mixed boundary value problem represented by dual integral equations which can be reduced to a single Fredholm integral equation. The response of the plate is then obtained by numerically solving the Fredholm integral equation. Employing this method, Karasudhi et al. [7], Luco and Westmann [8] solved the problem of the rigid strip vibrating on the homogeneous halfspace and Robertson [5] and Luco [2] solved the same problem for the circular disk. Luco [3,4] also extended this method for the case of layered halfspace. The other method allows a distribution of stresses under the plate expressed in terms of unknown constants. The response of a surface foundation, either rigid or flexible, can thus be obtained by the principle of virtual work with known or assumed displacement shape functions of the foundation. Oien [9] obtained the response of the rigid strip on the halfspace by assuming the stress as the combination of a series of Tchebychev polynominals. With the assumption of constant stress distribution between nodal points on the surface under the strip, Dasgutpa [17] calculated frequency dependent stiffness matrices for the corresponding surface degrees of freedom. By employing a similar constant stress assumption and discretization of the foundation, Wong and Luco [18] solved the vibration problem involving a rigid surface footing with arbitrary geometry on the homogeneous halfspace. Bycroft [1] found the vertical response of the circular disk on the halfspace by adopting the static stress distribution under the plate and the Hankel transform. However, due to the complexity for the

Hankel transform for three dimensional axisymmetric problems, the response of the circular disk with a more complicated stress condition than the static stress distribution is difficult to obtain.

Two dimensional problems may be solved by the Fast Fourier Transform method and its inversion. Gazetas and Roësset [6] used this method to calculate the dynamic behavior of the rigid strip on a horizontally layered halfspace. It can be shown however that Simpson rule or Gaussian quadrature is a much more efficient and more accurate method for solving these problems. For the case of a rigid boundary under soil layers, Waas [15] and Kausel [16] introduced a vertical semi-analytic transmitting boundary. The advantage of the transmitting boundary is that one can easily treat embedded structures. This method is however computationally expensive due to the complex-valued quadratic eigenvalue solution required.

In the following sections, the finite element discretization is employed to calculate the response of surface foundations. With the aid of the principle of virtual work and the linear stress assumption between nodes under the foundation, it is shown that solutions of the rigid strip and other plane-strain flexible surface footings on a viscoelastic layered soil system can be obtained accurately.

B. Basic Equations

1. Equations of Motion

For the two dimensional inplane wave propagation problems, motion in the normal y-direction is taken to be invariant; thus, the energy will be restricted to radiate or reflect in the $x-z$ plane.

In Fig. 2.1, a system of n-1 horizontal layers of soil resting on a halfspace is considered. These soil layers are assumed to be homogeneous, isotropic and elastic or viscoelastic, and are welded to each other at the interfaces. Within each layer or halfspace, the equations of motions, written in terms of displacement u and w, are

$$(\lambda+G)\frac{\partial \Delta}{\partial x} + G\nabla^2 u = \rho \ddot{u}$$

$$(\lambda+G)\frac{\partial \Delta}{\partial z} + G\nabla^2 w = \rho \ddot{w} \tag{2.1}$$

giving the corresponding stress components

$$\sigma_{xx} = \lambda\Delta+2G\frac{\partial u}{\partial x}$$

$$\sigma_{zz} = \lambda\Delta+2G\frac{\partial w}{\partial z} \tag{2.2}$$

$$\tau_{xz} = G\left(\frac{\partial u}{\partial z}+\frac{\partial w}{\partial x}\right)$$

where λ and G are the Lame's constants, $\Delta=\frac{\partial u}{\partial x}+\frac{\partial w}{\partial z}$ is the change of volume per unit volume, ∇ is the gradient operator, and ρ is the mass density.

In order to avoid the complex nature of the displacement equations of motion, the above equations are transformed into a simpler set of equations by introducing the dilatational and shear wave potentials ϕ and ψ which satisfy

$$u=\frac{\partial \phi}{\partial x}-\frac{\partial \psi}{\partial z}$$

$$w=\frac{\partial \phi}{\partial z}+\frac{\partial \psi}{\partial x} \tag{2.3}$$

Substituting Eqs. 2.3 into Eqs. 2.1 with appropriate manipulations, two uncoupled equations are obtained, namely

$$\nabla^2\phi = \frac{\ddot{\phi}}{C_p^2}$$

$$\nabla^2\psi = \frac{\ddot{\psi}}{C_s^2} \tag{2.4}$$

in which $C_p=\sqrt{(\lambda+2G)/\rho}$ and $C_s=\sqrt{G/\rho}$ are the dilatational and shear wave velocities, respectively.

The general solution of the above equations for a steady state harmonic motion with an excitation frequency ω can be expressed as

$$\phi = (Ae^{-\upsilon z}+Be^{\upsilon z})\ e^{i(\omega t-kx)}$$

$$\psi = (Ce^{-\upsilon' z}+De^{\upsilon' z})\ e^{i(\omega t-kx)} \tag{2.5}$$

where k is the horizontal wave number, $\upsilon=\sqrt{k^2-k_\alpha^2}$, $\upsilon'=\sqrt{k^2-k_\beta^2}$, $k_\alpha=\omega/C_p$ and $k_\beta=\omega/C_s$; A, B, C and D are constants which are determined by the loading or source condition.

Substituting Eqs. 2.5 into Eqs. 2.3 and 2.2, the displacements and stresses can be written in matrix form as

$$\begin{Bmatrix} u \\ w \\ \tau_{xz} \\ \sigma_{zz} \end{Bmatrix} = \begin{bmatrix} -ik & -ik & \upsilon' & -\upsilon' \\ -\upsilon & \upsilon & -ik & -ik \\ i2kG\upsilon & -i2kG\upsilon & -G(2k^2-k_\beta^2) & -G(2k^2-k_\beta^2) \\ G(2k^2-k_\beta^2) & G(2k^2-k_\beta^2) & i2kG\upsilon' & -i2kG\upsilon' \end{bmatrix} \mathbf{e} \begin{Bmatrix} A \\ B \\ C \\ D \end{Bmatrix} e^{i(\omega t-kx)} \tag{2.6}$$

or

$$\mathbf{Y} = \mathbf{E}\,\mathbf{e}\,\mathbf{A}\ e^{i(\omega t-kx)} \tag{2.6a}$$

in which $\mathbf{Y}=< u,\ w,\ \tau_{xz},\ \sigma_{zz} >^T$ is the displacement-stress vector, and $\mathbf{e}$ is the diagonal matrix $diag(\ e^{-\upsilon z},\ e^{\upsilon z},\ e^{-\upsilon' z},\ e^{\upsilon' z}\ )$.

2. Transfer Matrix

The compatibility and equilibrium conditions at the horizontal interfaces between different layers must be satisfied in order to obtain the displacements and stresses in all soil layers. Thomson [19] and Haskell [20] introduced an efficient transfer matrix for this purpose which not only assures compatibility and equilibrium at each interface but also indicates the relationship between the displacement-stress vectors of different layers.

In Fig. 2.1, the transfer matrix between the (j-1)th and jth interfaces can be obtained from the material properties of the jth layer. The term $e^{i(\omega t-kx)}$ is a common factor to all layers and can be ignored for simplicity. By shifting the origin of the z axis to the (j-1)th horizontal interface, the displacement-stress vectors at the (j-1)th and jth interfaces are, respectively,

$$\mathbf{Y}_{j-1} = \mathbf{E}_j \, \mathbf{e}_j(0) \, \mathbf{A}_j$$

$$\mathbf{Y}_j = \mathbf{E}_j \, \mathbf{e}_j(h_j) \, \mathbf{A}_j$$

where $\mathbf{e}_j(0)$ is an identity matrix, h_j is the thickness of the jth layer, and the subscript "j" indicates the material properties of the jth layer are adopted.

Vector $\mathbf{Y}_{j-1}$ can be expressed in terms of vector $\mathbf{Y}_j$ as

$$\mathbf{Y}_{j-1} = \mathbf{E}_j \, \mathbf{e}_j(-h_j) \, \mathbf{E}_j^{-1} \, \mathbf{Y}_j \tag{2.7}$$

or

$$\mathbf{Y}_{j-1} = \mathbf{a}_j \, \mathbf{Y}_j \tag{2.7a}$$

where $\mathbf{e}_j(-h_j)=\mathbf{e}_j^{-1}(h_j)$, since $\mathbf{e}_j$ is a diagonal matrix, and $\mathbf{a}_j=\mathbf{E}_j \, \mathbf{e}_j(-h_j) \, \mathbf{E}_j^{-1}$.

Ignoring the subscript "j" for simplicity, the transfer matrix **a** can be written explicitly as

$$\mathbf{a} = \begin{bmatrix} \frac{2k^2}{k_\beta^2}(CH-CH')+CH' & \frac{ik}{k_\beta^2}(2\upsilon' SH'-(2k^2-k_\beta^2)\frac{SH}{\upsilon}) \\ \frac{ik}{k_\beta^2}(-2\upsilon SH+(2k^2-k_\beta^2)\frac{SH'}{\upsilon'}) & CH-\frac{2k^2}{k_\beta^2}(CH-CH') \\ \frac{G}{k_\beta^2}(-4k^2\upsilon SH+(2k^2-k_\beta^2)^2\frac{SH'}{\upsilon'}) & \frac{2ikG}{k_\beta^2}(2k^2-k_\beta^2)(CH-CH') \\ \frac{2ikG}{k_\beta^2}(2k^2-k_\beta^2)(CH-CH') & \frac{G}{k_\beta^2}((2k^2-k_\beta^2)\frac{SH}{\upsilon}-4k^2\upsilon' SH') \end{bmatrix}$$

$$\begin{bmatrix} \frac{1}{Gk_\beta^2}(-k^2\frac{SH}{\upsilon}+\upsilon' SH') & \frac{ik}{Gk_\beta^2}(CH-CH') \\ \frac{ik}{Gk_\beta^2}(CH-CH') & \frac{1}{Gk_\beta^2}(\upsilon SH-k^2\frac{SH'}{\upsilon'}) \\ CH'+\frac{2k^2}{k_\beta^2}(CH-CH') & \frac{ik}{k_\beta^2}(-2\upsilon SH+(2k^2-k_\beta^2)\frac{SH'}{\upsilon'}) \\ \frac{ik}{k_\beta^2}(2\upsilon' SH'-2k\frac{SH}{\upsilon}) & CH-\frac{2k^2}{k_\beta^2}(CH-CH') \end{bmatrix} \tag{2.8}$$

in which SH=sinhυh, SH'=sinh$\upsilon' h$, CH=coshυh, and CH'=cosh$\upsilon' h$.

With the aid of the transfer matrix, the displacement-stress vector at any depth may be expressed in terms of the displacement-stress vector at another depth. For example, the relationship between the (j-1)th and (n-1)th interfaces is

$$\mathbf{Y}_{j-1} = \mathbf{a}_j \, \mathbf{a}_{j+1} \, \cdots \, \mathbf{a}_{n-1} \, \mathbf{Y}_{n-1} \tag{2.9}$$

In addition, it is observed that the elements in the transfer matrix **a** are either even or odd functions of the wave number k. Matrix **a** then has the form

$$\mathbf{a} = \begin{bmatrix} e & o & e & o \\ o & e & o & e \\ e & o & e & o \\ o & e & o & e \end{bmatrix} \tag{2.10}$$

where an "e" indicates an even function and an "o" indicates an odd function. The product of any two matrices of this form is also a matrix of the same form. This characteristic will be

employed later to simplify the computation of the plate response.

C. Displacement and Stress Relationship at Surface

The soil profile usually consists of multiple horizontal layers of soil underlain by rock with the lower soil layers being stiffer than the upper layers. If the thickness of any particular soil layer is large compared with the structural dimension, it is practical to assume this particular soil layer as a halfspace. If the rock underlying all soil layers is much stiffer than the soil, the rock can be assumed to be completely rigid.

1. Halfspace

If the nth layer in Fig. 2.1 is a halfspace, waves which penetrate through the (n-1)th interface will never return. In other words, energy will radiate continuously along the (n-1)th interface. Recognizing this radiation condition, those terms corresponding to $e^{\nu z}$ and $e^{\nu' z}$ in Eq. 2.5 can be omitted. Therefore, the dilatational and shear wave potentials become

$$\phi = Ae^{-\nu z} e^{i(\omega t - kx)}$$

$$\psi = Ce^{-\nu' z} e^{i(\omega t - kx)}$$

Shifting the origin of the z axis to the (n-1)th interface, the dispacement-stress vector at that location has the form

$$\begin{Bmatrix} u \\ w \\ \tau_{xz} \\ \sigma_{zz} \end{Bmatrix}_{n-1} = \begin{bmatrix} -ik & \upsilon' \\ -\upsilon & -ik \\ i2kG\upsilon & -G(2k^2-k_\beta^2) \\ G(2k^2-k_\beta^2) & i2kG\upsilon' \end{bmatrix}_n \begin{Bmatrix} A \\ C \end{Bmatrix}_n \tag{2.11}$$

or

$$\mathbf{Y}_{n-1} = \mathbf{g}_n \, \mathbf{A}_n' \tag{2.11a}$$

By employing Eq. 2.9, the displacement-stress vector at the top surface can be written as

$$\mathbf{Y}_0 = \mathbf{a}_1 \, \mathbf{a}_2 \, \cdots \, \mathbf{a}_{n-1} \, \mathbf{g}_n \, \mathbf{A}_n' \tag{2.12}$$

or

$$\begin{Bmatrix} \mathbf{u} \\ \mathbf{s} \end{Bmatrix}_0 = \begin{bmatrix} \mathbf{R}_1 \\ \mathbf{R}_2 \end{bmatrix} \mathbf{A}_n' \tag{2.12a}$$

where $\mathbf{R}_1$ and $\mathbf{R}_2$ are 2×2 matrices, $\mathbf{u}=<u, \; w>^T$, and $\mathbf{s}=<\tau_{xz}, \; \sigma_{zz}>^T$.

If the top surface is horizontal and only surface tractions are applied, the displacements and stresses at surface may be related through the Fourier transform and its inversion. In Eq. 2.12a, the surface tractions at location x for a specific horizontal wave number k are

$$\mathbf{s}_0 = \mathbf{R}_2 \, \mathbf{A}_n' \, e^{-ikx} \tag{2.13}$$

Moving factor e^{-ikx} to the left side of the above equation and integrating it along the entire x axis, the Fourier transform of the surface tractions can be obtained as

$$\begin{Bmatrix} \tau_{xz}^*(k) \\ \sigma_{zz}^*(k) \end{Bmatrix}_0 = \mathbf{s}_0^*(k) = \int_{-\infty}^{\infty} \mathbf{s}_0(x) \; e^{ikx} \, dx = \mathbf{R}_2 \, \mathbf{A}_n' \tag{2.14}$$

with its inverse transform being

$$\begin{Bmatrix} \tau_{xz}(x) \\ \sigma_{zz}(x) \end{Bmatrix}_0 = \mathbf{s}_0(x) = \frac{1}{2\pi} \int_{-\infty}^{\infty} \mathbf{s}_0^*(k) \; e^{-ikx} \, dk \tag{2.15}$$

Similarly, the Fourier transform pairs for displacements are

$$\begin{Bmatrix} u^*(k) \\ w^*(k) \end{Bmatrix}_0 = \mathbf{u}_0^*(k) = \int_{-\infty}^{\infty} \mathbf{u}_0(x)\ e^{ikx}\,dx = \mathbf{R}_1\ \mathbf{A}_n' \tag{2.16}$$

and

$$\begin{Bmatrix} u(x) \\ w(x) \end{Bmatrix}_0 = \mathbf{u}_0(x) = \frac{1}{2\pi}\int_{-\infty}^{\infty} \mathbf{u}_0^*(k)\ e^{-ikx}\,dk \tag{2.17}$$

To calculate the response of the surface foundation, it is important to know the displacements in terms of the surface tractions. Substituting Eqs. 2.14 and 2.16 into Eq. 2.17 and eliminating vector $\mathbf{A}_n'$ gives

$$\begin{aligned} \mathbf{u}_0(x) &= \frac{1}{2\pi}\int_{-\infty}^{\infty} \mathbf{R}_1\ \mathbf{R}_2^{-1} \int_{-\infty}^{\infty} \mathbf{s}_0(\xi)\ e^{-ik\xi}\,d\xi\ e^{ikx}\,dx \\ &= \frac{1}{2\pi}\int_{-\infty}^{\infty} \mathbf{R}' \int_{-\infty}^{\infty} \mathbf{s}_0(\xi)\ e^{-ik\xi}\,d\xi\ e^{ikx}\,dx \end{aligned} \tag{2.18}$$

Therefore, if the stress distribution along the horizontal surface is known, the displacements at any point on the surface can be found from the above equations.

The physical meaning of the Fourier transform in this problem is the response corresponding to a specific wave number k in the system resulting from the general sources or loadings. The corresponding analogy of the inverse transform is that the waves generated by such sources or loadings will propagate in all directions.

In addition, comparing Eqs. 2.14, 2.16 with Eq. 2.12a, the displacements and stresses in Eq. 2.12a may be thought of directly as their corresponding Fourier transforms.

2. Rigid Rock

If the bottom material is rigid, waves will be restricted to propagate between the top surface and the rigid lower boundary. Energy generated by any source will not dissipate unless there is energy dissipation in the soil materials. Assuming no slippage occurs during wave propagation, the displacements at the rigid boundary are zero. Using Eq. 2.9, displacements and stresses at the top surface can be written as

$$\begin{Bmatrix} u \\ w \\ \tau_{xz} \\ \sigma_{zz} \end{Bmatrix}_0 = \mathbf{a}_1\ \mathbf{a}_2\ \cdots\ \mathbf{a}_{n-1} \begin{Bmatrix} 0 \\ 0 \\ \tau_{xz} \\ \sigma_{zz} \end{Bmatrix}_n \tag{2.19}$$

or

$$\begin{Bmatrix} \mathbf{u} \\ \mathbf{s} \end{Bmatrix}_0 = \begin{bmatrix} \mathbf{T}_1 \\ \mathbf{T}_2 \end{bmatrix} \mathbf{s}_n \tag{2.19a}$$

where $\mathbf{T}_1$ and $\mathbf{T}_2$ are 2×2 matrices.

Comparing the above equation with Eq. 2.12a, the stresses at the rigid rock interface may be taken as unknown coefficients. A similar derivation, as in the case of the halfspace, may be obtained by replacing the matrix $\mathbf{R}_i$ by matrix $\mathbf{T}_i$. Therefore, displacements at the top surface become

$$\mathbf{u}_0(x) = \frac{1}{2\pi} \int_{-\infty}^{\infty} \mathbf{T}_1\ \mathbf{T}_2^{-1} \int_{-\infty}^{\infty} \mathbf{s}_0(\xi)\ e^{-ik\xi}\, d\xi\ e^{ikx}\, dx$$

$$= \frac{1}{2\pi} \int_{-\infty}^{\infty} \mathbf{T}' \int_{-\infty}^{\infty} \mathbf{s}_0(\xi)\ e^{-ik\xi}\, d\xi\ e^{ikx}\, dx \tag{2.20}$$

D. Linear Stress Model

In the mixed boundary value problem, stress and displacement conditions are specified separately over different portions of the boundary, e.g. stresses at the free boundaries and displacements under rigid plates. There is no direct method to solve this kind of problem. Although, Karasudhi et al. [7] and Luco [2,3,4,8] solved the response of rigid plate by the Fredholm integral equations, the shortcoming is that they had to simplify the system with relaxed boundary conditions. In addition, the Fredholm integral equation cannot be used to solve the same problem for a flexible surface foundation.

In the two dimensional problems, a model established from the proposed stress distribution with unknown coefficients under the surface foundation gives a satisfactory and efficient solution. There are many possible stress models, either continuous or discrete. The selection of a suitable model depends significantly on the foundation type, e.g., flexible or rigid. For wider application and easier understanding, the finite element model for the foundation is selected. In Fig. 2.2, the massless plate is partitioned into several intervals with uniform spacing b. The stress components at the surface of the upper soil stratum are assumed to be linearly distributed within each interval as expressed by

$$\tau_{xz} = \left(\sum_{j=-n+1}^{n-1} h_j(x)\, q_j + h_{-n}\, q_{-n} + h_n\, q_n \right) e^{i\omega t}$$

$$\sigma_{zz} = \left(\sum_{j=-n+1}^{n-1} h_j(x)\, p_j + h_{-n}\, p_{-n} + h_n\, p_n \right) e^{i\omega t} \qquad (2.21)$$

where q_j and p_j, which depend on the motion of the foundation, are the nodal values of shearing stress and normal stress at node j, respectively; n and $-n$ are two edge nodes having zero stress on one side, and

$$h_j(x) = \begin{cases} 1+\dfrac{(x-jb)}{b} & \text{if } (j-1)\,b<x<jb, \quad -n+1\leqslant j\leqslant n \\ 1-\dfrac{(x+jb)}{b} & \text{if } jb<x<(j+1)\,b, \quad -n\leqslant j\leqslant n-1 \\ 0 & \text{otherwise} \end{cases} \tag{2.22}$$

Since the motion is analyzed in the frequency domain, the common harmonic factor $e^{i\omega t}$ will be ignored for simplicity. In addition, only stress τ_{xz} will be considered in the following derivations.

Substituting Eqs. 2.21 and 2.22 into Eq. 2.14, the Fourier transform of the jth component of τ_{xz} is

$$\tau_{xz_j}{}^*(k) = \left(\int_{(j-1)\,b}^{jb} (1+\frac{x-jb}{b})\, e^{ikx}\, dx + \int_{jb}^{(j+1)\,b} (1-\frac{x+jb}{b})\, e^{ikx}\, dx\right)\, q_j$$

$$= \frac{4}{bk^2}\sin^2\frac{kb}{2}\, e^{ijkb}\, q_j \tag{2.23}$$

and the Fourier transforms corresponding to edge nodes n and -n are, respectively,

$$\tau_{xz_n}{}^*(k) = \int_{(n-1)\,b}^{nb} (1+\frac{x-nb}{b})\; e^{ikx}\, dx\; q_n = (\frac{1}{ik}+\frac{1-e^{-ikb}}{bk^2})\, e^{inkb}\; q_n \tag{2.24}$$

and

$$\tau_{xz_{-n}}{}^*(k) = \int_{-nb}^{-(n-1)\,b} (1-\frac{x+nb}{b})\; e^{ikx}\, dx\; q_{-n} = (\frac{-1}{ik}+\frac{1-e^{-ikb}}{bk^2})\; e^{-inkb}\; q_{-n} \tag{2.25}$$

Combining the contributions of all nodes to the Fourier transform of shearing stress results in

$$\tau_{xz}^{*}(k) = \frac{4}{bk^2}\sin^2\frac{kb}{2}\{e^{-i(n-1)kb}, \cdots, e^{-ikb}, 1, e^{ikb}, \cdots, e^{i(n-1)kb}\}\begin{Bmatrix} q_{-n+1} \\ \cdot \\ \cdot \\ q_{-1} \\ q_0 \\ q_1 \\ \cdot \\ \cdot \\ q_{n-1} \end{Bmatrix}$$

$$+ \left(-\frac{1}{ik}+\frac{1-e^{-ikb}}{bk^2}\right) e^{-inkb}\, q_{-n} + \left(\frac{1}{ik}+\frac{1-e^{-ikb}}{bk^2}\right) e^{inkb}\, q_n \tag{2.26}$$

To calculate the response of the surface foundation, it is advantageous to simplify the above equation by considering separately the symmetric and antisymmetric foundation motions. If the stress under the foundation is symmetric with respect to its central axis, i.e., $q_{-j}=q_j$, Eq. 2.26 becomes

$$\tau_{xz}^{*}(k) = \frac{8}{bk^2}\sin^2\frac{kb}{2}\{\frac{1}{2}, \cos kb, \cdots, \cos(n-1)kb,\}\begin{Bmatrix} q_0 \\ q_1 \\ \cdot \\ \cdot \\ q_{n-1} \end{Bmatrix}$$

$$+ \left(\frac{2}{k}\sin nkb+\frac{2}{bk^2}(\cos nkb-\cos(n-1)kb)\right) q_n$$

$$= \mathbf{d}_1^T \mathbf{q}_1 \tag{2.27}$$

If the stress is antisymmetric during the motion, i.e. $q_j=-q_{-j}$ and $q_0=0$, Eq. 2.26 becomes

$$\tau_{xz}^{*}(k) = \frac{8}{bk^2}\sin^2\frac{kb}{2}\{i\sin kb,\ i\sin 2kb,\ \cdots,\ i\sin(n-1)kb\}\begin{Bmatrix} q_1 \\ q_2 \\ . \\ . \\ q_{n-1} \end{Bmatrix}$$

$$+ \left(\frac{2\cos nkb}{ik} + \frac{2}{bk^2}(i\sin nkb - i\sin(n-1)kb)\right) q_n$$

$$= \mathbf{d}_2^T \mathbf{q}_2 \tag{2.28}$$

It can be shown that both terms corresponding to q_n in Eqs. 2.27 and 2.28 are equal to zero when k approaches zero. For different motions of the surface foundation, the shearing and normal stresses are different. When symmetric loading is applied to the foundation, the normal stress is symmetric; whereas, the shearing stress is antisymmetric. The stress vector may be written as

$$\begin{Bmatrix} \tau_{xz}^{*}(k) \\ \sigma_{zz}^{*}(k) \end{Bmatrix} = \begin{bmatrix} \mathbf{d}_2^T & 0^T \\ 0^T & \mathbf{d}_1^T \end{bmatrix} \begin{Bmatrix} \mathbf{q}_2 \\ \mathbf{p}_1 \end{Bmatrix} \tag{2.29}$$

or

$$\mathbf{s}^{*} = \mathbf{G}_s\ \mathbf{r}_s \tag{2.29a}$$

If the foundation is subjected to antisymmetric motion, the shearing stress is symmetric but the normal stress is antisymmetric; thus,

$$\begin{Bmatrix} \tau_{xz}^{*}(k) \\ \sigma_{zz}^{*}(k) \end{Bmatrix} = \begin{bmatrix} \mathbf{d}_1^T & 0^T \\ 0^T & \mathbf{d}_2^T \end{bmatrix} \begin{Bmatrix} \mathbf{q}_1 \\ \mathbf{p}_2 \end{Bmatrix} \tag{2.30}$$

or

$$\mathbf{s}^{*} = \mathbf{G}_a\ \mathbf{r}_a \tag{2.30a}$$

in which $\mathbf{p}_1$ and $\mathbf{p}_2$ are vectors of the nodal values of normal stress having a number of terms

similar to $\mathbf{q}_1$ and $\mathbf{q}_2$, respectively. The term 0 designates a zero vector.

E. Compliance and Impedance of the Rigid Strip

For the steady state harmonic motion, it is appropriate to use the principle of virtual work to obtain the compliance or impedance matrix of the system. The expression of the virtual work is

$$\delta W = \int_{-a}^{a} \delta \mathbf{t}^T(x)\ \mathbf{u}(x)\ dx \tag{2.31}$$

where $\delta \mathbf{t}$ is a 2-component vector of admissible virtual forces under the foundation, $\mathbf{t} \equiv \mathbf{s}$, $\mathbf{u}$ is the corresponding 2-component real displacement vector, and a is the half width of the foundation.

Substituting Eqs. 2.29a or 2.30a into Eq. 2.18 or Eq. 2.20 gives

$$\left\{ \begin{matrix} u(x) \\ w(x) \end{matrix} \right\}_0 = \frac{1}{2\pi} \int_{-\infty}^{\infty} \mathbf{Q}\ \mathbf{G}_j\ \mathbf{r}_j\ e^{-ikx}\, dx \tag{2.32}$$

where $\mathbf{Q} = \mathbf{R}'$ for the case of bottom boundary as a halfspace, or $\mathbf{Q} = \mathbf{T}'$ for the case of rigid bottom boundary; $j=s$ for symmetric loading, or $j=a$ if the foundation is in antisymmetric motion.

Substitution of Eq. 2.32 into Eq. 2.31 gives

$$\delta W = \frac{1}{2\pi} \int_{-\infty}^{\infty} \int_{-a}^{a} \delta \mathbf{t}^T(x)\ e^{-ikx}\, dx\ \mathbf{Q}\ \mathbf{G}_j\ \mathbf{r}_j\ dk \tag{2.33}$$

It is obvious that the integration of the virtual forces along x in the above equation is the complex conjugate of the Fourier transform of itself. With the aid of the discretization of the foundation, Eq. 2.33 becomes

$$\delta W = \delta \mathbf{r}_j^T \left(\frac{1}{2\pi} \int_{-\infty}^{\infty} \overline{\mathbf{G}}_j^T\ \mathbf{Q}\ \mathbf{G}_j\ dk \right) \mathbf{r}_j \tag{2.34}$$

or

$$\delta W = \delta \mathbf{r}_j^T \mathbf{F}_j \mathbf{r}_j \tag{2.34a}$$

in which $\bar{\mathbf{G}}_j$ is the complex conjugate of matrix $\mathbf{G}_j$, and $\mathbf{F}_j$ is the compliance matrix of nodal degrees of freedom under the foundation.

It is difficult to recognize the symmetry of matrix $\mathbf{F}_j$ from Eq. 2.34. However, if the symmetry can be demonstrated in the integrand, then there is no doubt that $\mathbf{F}_j$ is symmetric. In Fig. 2.3 two nodes I and J of the surface foundation are considered. The submatrix which represents the displacements at node I due to unit forces applied at node J for a specific wave number k is

$$\mathbf{f}_{IJ} = (\bar{\mathbf{G}}_j^T \mathbf{Q} \mathbf{G}_j)_{IJ}$$

, or more explicitly, for the case of symmetric loading applied to the foundation,

$$(\mathbf{f}_{IJ})_s = (\frac{8}{bk^2}\sin^2\frac{kb}{2})^2 \begin{bmatrix} -i\sin Ikb & 0 \\ 0 & \cos Ikb \end{bmatrix} \begin{bmatrix} Q_{11} & Q_{12} \\ Q_{21} & Q_{22} \end{bmatrix} \begin{bmatrix} i\sin Jkb & 0 \\ 0 & \cos Jkb \end{bmatrix}$$

$$= (\frac{8}{bk^2}\sin^2\frac{kb}{2})^2 \begin{bmatrix} Q_{11}\sin Ikb\sin Jkb & -iQ_{12}\sin Ikb\cos Jkb \\ iQ_{21}\cos Ikb\sin Jkb & Q_{22}\cos Ikb\cos Jkb \end{bmatrix} \tag{2.35}$$

where Q_{lm} are functions of k only and characterize the material properties and the layering condition of the system; and $Q_{21}=-Q_{12}$.

Interchanging I and J in above equation results in

$$(\mathbf{f}_{JI})_s = (\frac{8}{bk^2}\sin^2\frac{kb}{2})^2 \begin{bmatrix} Q_{11}\sin Jkb\,\sin Ikb & -iQ_{12}\sin Jkb\cos Ikb \\ iQ_{21}\cos Jkb\sin Ikb & Q_{22}\cos Jkb\cos Ikb \end{bmatrix} \tag{2.36}$$

Comparing Eq. 2.35 with Eq. 2.36, it is obvious that $(\mathbf{f}_{IJ})_s=(\mathbf{f}_{JI})_s^T$. A similar proof can be shown, if node I or J is at the foundation edge or if antisymmetric loading is applied. Therefore, the compliance matrix of those surface nodal degrees of freedom is symmetric. In addition, it has been shown in Eq. 2.10 that the elements of matrix **a** are always even or odd

functions of k. A similar condition can be found in Q_{lm}, giving

$$\mathbf{Q} = \begin{bmatrix} e & o \\ o & e \end{bmatrix}$$

Thus elements of matrix **f** are even functions of the wave number. Equation 2.34 may be simplified further as

$$\delta W = \delta \mathbf{r}_j^T \left(\frac{1}{\pi} \int_0^{\infty} \bar{\mathbf{G}}_j^T \mathbf{Q}\, \mathbf{G}_j \, dk \right) \mathbf{r}_j \tag{2.37}$$

In order to find the response of the surface foundation, it is required to know its displacement shape functions at the surface. For a flexible foundation, it is possible to approximate displacements by another finite element model. However, the focus in this chapter is on the response of the rigid strip so that its behavior can be described by rigid body motion. There are three degrees of freedom, i.e., vertical, translational and rotational displacements at the center of the plate. Under vertical loading, the displacement vector $\mathbf{u}(x)$ at the surface is

$$\begin{Bmatrix} u(x) \\ w(x) \end{Bmatrix} = \begin{Bmatrix} 0 \\ 1 \end{Bmatrix} \Delta_V \tag{2.38}$$

; for translational and rocking motions, the displacement vector becomes

$$\begin{Bmatrix} u(x) \\ w(x) \end{Bmatrix} = \begin{bmatrix} 1 & 0 \\ 0 & x \end{bmatrix} \begin{Bmatrix} \Delta_H \\ \Delta_M \end{Bmatrix} \tag{2.39}$$

where Δ_V, Δ_H and Δ_M are the vertical, translational and rotational displacements of the rigid strip; and $|x| \leqslant a$.

Substituting the above two displacement shape functions into Eq. 2.31, virtual work can be expressed in the form of

$$\delta W = \delta \mathbf{r}_s^T \left\{0,\ 0,\ \cdots,\ 0,\ b,\ 2b,\ \cdots,\ 2b,\ b\right\}^T \Delta_V$$

$$= \delta \mathbf{r}_s\ \mathbf{B}_V\ \Delta_V \tag{2.40}$$

for vertical motion or in the form of

$$\delta W = \delta \mathbf{r}_a^T \begin{bmatrix} b & 2b & \cdots & 2b & b & 0 & 0 & \cdots & 0 & 0 \\ 0 & 0 & \cdots & 0 & 0 & 2b^2 & 4b^2 & \cdots & 2(n-1)\,b^2 & (n-\frac{1}{3})\,b^2 \end{bmatrix}^T \begin{Bmatrix} \Delta_H \\ \Delta_M \end{Bmatrix}$$

$$= \delta \mathbf{r}_a^T\ \mathbf{B}_C \begin{Bmatrix} \Delta_H \\ \Delta_M \end{Bmatrix} \tag{2.41}$$

for translational and rocking motions.

Since $\delta \mathbf{r}_s$ is arbitrary, Eqs. 2.34a and 2.40 lead to

$$\mathbf{F}_s\ \mathbf{r}_s = \mathbf{B}_V\ \Delta_V \tag{2.42}$$

or

$$\mathbf{U}_V = \mathbf{B}_V\ \Delta_V \tag{2.42a}$$

where $\mathbf{U}_V$ represents the displacements of the discrete nodes at the top surface for vertical motion of the plate.

By employing the reciprocal theorem, the applied vertical loading at the center of the plate can be expressed in terms of the nodal forces $\mathbf{r}_s$ as given by

$$V = \mathbf{B}_V^T\ \mathbf{r}_s$$

The relationship between vertical loading and vertical displacement of the rigid strip is

$$V = \mathbf{B}_V^T\ \mathbf{F}_s^{-1}\ \mathbf{B}_V\ \Delta_V = K_{VV}\ \Delta_V \tag{2.43}$$

in which K_{VV} is the vertical impedance of the rigid strip with its corresponding compliance

being $C_{VV}=1/K_{VV}$. Similarly in translational and rocking motions, the horizontal force H and rocking moment M of the plate are related to Δ_H and Δ_M through

$$\begin{Bmatrix} H \\ M \end{Bmatrix} = \mathbf{B}_C^T \, \mathbf{F}_a^{-1} \, \mathbf{B}_C \begin{Bmatrix} \Delta_H \\ \Delta_M \end{Bmatrix} = \begin{bmatrix} K_{HH} & K_{HM} \\ K_{MH} & K_{MM} \end{bmatrix} \begin{Bmatrix} \Delta_H \\ \Delta_M \end{Bmatrix} \tag{2.44}$$

where K_{HH} and K_{MM} are the principal impedances of the translational and rocking motions, respectively; and $K_{HM}=K_{MH}$ is the coupling impedance between the two motions. The compliances of the two motions are given by the inversion of the corresponding impedance matrix.

F. Numerical Computation

1. Truncation Error

Owing to the limitation of computer accuracy, numerical error may be significant if the soil is horizontally layered. This problem occurs when the real part of νh in Eq. 2.7 is larger than the real part of $\nu' h$ by a certain amount in a specific layer with thickness h. After various subtractions are carried out, the number of significant digits in the result may be reduced to zero. This problem has been discussed in several references [21,22,23]. To demonstrate the significance of this problem explicitly, one soil layer with thickness h over the halfspace is considered. Referring to Eq. 2.12, the displacements and stresses at the top surface can be written in terms of the unknown constants $\bar{\mathbf{A}}$ as given by

$$\begin{Bmatrix} \mathbf{u} \\ \mathbf{s} \end{Bmatrix} = \mathbf{a} \, \bar{\mathbf{g}} \, \bar{\mathbf{A}} = \begin{bmatrix} \mathbf{R}_1 \\ \mathbf{R}_2 \end{bmatrix} \bar{\mathbf{A}} \tag{2.45}$$

where $\mathbf{a} = \mathbf{E}\,\mathbf{e}\,\mathbf{E}^{-1}$ and $\mathbf{e} = diag(\, e^{\nu h},\ e^{-\nu h},\ e^{\nu' h},\ e^{-\nu' h}\,)$.

For the extreme case, i.e., the quantity of $e^{\nu h}$ is much larger than the other exponential terms, matrix $\mathbf{e}$ may be expressed numerically as

$$\mathbf{e}' = diag(\, e^{\nu h},\ 0,\ 0,\ 0)$$

Thus, Eq. 2.45 becomes

$$\begin{Bmatrix} \mathbf{u} \\ \mathbf{s} \end{Bmatrix} = \mathbf{E}\,\mathbf{e}'\,\mathbf{E}^{-1}\,\bar{\mathbf{g}}\,\bar{\mathbf{A}} = \mathbf{a}'\,\bar{\mathbf{g}}\,\bar{\mathbf{A}} = \begin{bmatrix} \mathbf{R}_1' \\ \mathbf{R}_2' \end{bmatrix} \bar{\mathbf{A}}$$

In order to obtain displacements $\mathbf{u}$ in terms of stresses $\mathbf{s}$, the inversion of matrix $\mathbf{R}_2'$ is necessary. However, $\mathbf{a}'$ is a rank one matrix, i.e., all 2×2 submatrices are singular; therefore, the inversion of $\mathbf{R}_2'$ is trivial. Since the elements in the matrix $\mathbf{R}_2'$ have a common factor $e^{\nu h}$, the determinant of $\mathbf{R}_2'$ equals to zero multiplied by the factor $e^{2\nu h}$. Because of the truncation in actual calculations, the determinant never vanishes in above situation. Once $e^{\nu h}$ becomes much larger than other exponential terms, the truncation error multiplied by $e^{2\nu h}$ will dominate; thus, distorting the true determinant of $\mathbf{R}_2'$. In this case, accurate integration of Eq. 2.35 is not possible.

Dunkin [21] developed a good numerical scheme to solve this difficulty. In his derivation, terms having the factor $e^{(\nu+\nu')h}$ were recognized as more important in the calculation of the determinant of $\mathbf{R}_2'$. Other terms having $e^{2\nu h}$, $e^{2\nu' h}$, $e^{(\nu-\nu')h}$ etc. as factors are considered to be zero or negligible. However, Dunkin did not realize the importance of $e^{-\nu' h}$ when the quantity $e^{\nu' h}$ is relatively small. More correctly, the determinant of $\mathbf{R}_2$ should include both $e^{(\nu+\nu')h}$ and $e^{(\nu-\nu')h}$ terms. In the following, a simpler and more complete procedure than Dunkin's method is developed.

Considering a multi-layered system on the halfspace, the displacements and stresses at the top surface may be expressed as

$$\begin{Bmatrix} \mathbf{u} \\ \mathbf{s} \end{Bmatrix}_0 = \mathbf{a}_1\,\mathbf{a}_2\,\cdots\,\mathbf{a}_{j-1}\,(\mathbf{b}_j'+\mathbf{b}_j'')\,\mathbf{a}_{j+1}\,\cdots\,\mathbf{a}_{n-1}\,\mathbf{g}_n\,\mathbf{A}_n$$

$$= \left(\begin{bmatrix} \mathbf{R}_1^{(1)} \\ \mathbf{R}_2^{(1)} \end{bmatrix} + \begin{bmatrix} \mathbf{R}_1^{(2)} \\ \mathbf{R}_2^{(2)} \end{bmatrix} \right) \mathbf{A}_n \qquad (2.46)$$

where $\mathbf{b}_j'=\mathbf{E}_j\,\mathbf{e}_j'\,\mathbf{E}_j^{-1}$, $\mathbf{b}_j''=\mathbf{E}_j\,\mathbf{e}_j''\,\mathbf{E}_j^{-1}$ in which $\mathbf{e}_j''=diag(\,0,\,0,\,e^{\nu_j' h_j},\,e^{-\nu_j' h_j}\,)$, and $\mathbf{R}_i^{(1)}$ and $\mathbf{R}_i^{(2)}$

are products of $\mathbf{b}_j'$, $\mathbf{b}_j''$ and other transfer matrices, respectively. Since $\mathbf{b}_j'$ is a rank one matrix, the most important contribution to the $det(\mathbf{R}_2^{(1)}+\mathbf{R}_2^{(2)})$ comes from the interproduct of columns with each other. If $\mathbf{b}_j''$ is also rank one, $det(\mathbf{R}_2)$ can be written as

$$\begin{aligned}\det(\mathbf{R}_2) &= det(\mathbf{R}_2^{(1)}+\mathbf{R}_2^{(2)}) \\ &= \det\left(\begin{bmatrix} r_{31}^{(1)} & r_{32}^{(1)} \\ r_{41}^{(1)} & r_{42}^{(1)} \end{bmatrix} + \begin{bmatrix} r_{31}^{(2)} & r_{32}^{(2)} \\ r_{41}^{(2)} & r_{42}^{(2)} \end{bmatrix} \right) \\ &= (r_{31}^{(1)} r_{42}^{(2)} - r_{41}^{(1)} r_{32}^{(2)}) + (r_{31}^{(2)} r_{42}^{(1)} - r_{41}^{(2)} r_{32}^{(1)})\end{aligned} \tag{2.47}$$

If $\mathbf{b}_j''$ is of higher rank,

$$det(\mathbf{R}_2) = (r_{31}^{(1)} r_{42}^{(2)} - r_{41}^{(1)} r_{32}^{(2)}) + (r_{31}^{(2)} r_{42}^{(1)} - r_{41}^{(2)} r_{32}^{(1)}) + (r_{31}^{(2)} r_{42}^{(2)} - r_{41}^{(2)} r_{32}^{(2)}) \tag{2.48}$$

In Eq. 2.47, all terms have the common factor $e^{(\nu_j+\nu'_j)h_j}$. The factors in Eq. 2.48 are not explicit; however, terms having factors of $e^{(\nu_j+\nu'_j)h_j}$, $e^{(\nu_j-\nu'_j)h_j}$, and unity which comes from $e^{(\nu'_j-\nu'_j)h_j}=1$ are all included in the determinant. Therefore, the truncation error due to the large numerical value of $e^{\nu_j h_j}$ is avoided and the accuracy of solution is retained.

If more than one layer of soil have the truncational problem, the solution procedure can be extended simply by separating each corresponding troubled transfer matrix into the sum of two matrices. For example, if two layers j and j+1 are involved, displacement-stress vector becomes

$$\begin{aligned}\begin{Bmatrix} \mathbf{u} \\ \mathbf{s} \end{Bmatrix}_0 &= \mathbf{a}_1 \cdots \mathbf{a}_{j-1} (\mathbf{b}_j'+\mathbf{b}_j'') (\mathbf{b}_{j+1}'+\mathbf{b}_{j+1}'') \mathbf{a}_{j+2} \cdots \mathbf{a}_{n-1} \mathbf{g}_n \mathbf{A}_n \\ &= \mathbf{a}_1 \cdots \mathbf{a}_{j-1} (\mathbf{b}_j'\mathbf{b}_{j+1}'+\mathbf{b}_j'\mathbf{b}_{j+1}''+\mathbf{b}_j''\mathbf{b}_{j+1}'+\mathbf{b}_j''\mathbf{b}_{j+1}'') \mathbf{a}_{j+2} \cdots \mathbf{a}_{n-1} \mathbf{g}_n \mathbf{A}_n\end{aligned} \tag{2.49}$$

or

$$\begin{Bmatrix} \mathbf{u} \\ \mathbf{s} \end{Bmatrix}_0 = \left(\begin{bmatrix} \mathbf{R}_1^{(1)} \\ \mathbf{R}_2^{(1)} \end{bmatrix} + \begin{bmatrix} \mathbf{R}_1^{(2)} \\ \mathbf{R}_2^{(2)} \end{bmatrix} + \begin{bmatrix} \mathbf{R}_1^{(3)} \\ \mathbf{R}_2^{(3)} \end{bmatrix} + \begin{bmatrix} \mathbf{R}_1^{(4)} \\ \mathbf{R}_2^{(4)} \end{bmatrix} \right) \mathbf{A}_n = \begin{bmatrix} \mathbf{R}_1 \\ \mathbf{R}_2 \end{bmatrix} \mathbf{A}_n$$

The reason for choosing the jth and (j+1)th layers is for convenience. Seclection of any two or more layers will not affect the solution procedure. If all $\mathbf{b}_i'$ and $\mathbf{b}_i''$ are rank one, the determinant of $\mathbf{R}_2$ may be obtained by an equation similar to Eq. 2.47, i.e. by the sum of the interproduct of columns of two different $\mathbf{R}_2^{(m)}$. The contributions to the determinant then only include terms with the factor $e^{(v_j+v_j')h_j+(v_{j+1}+v_{j+1}')h_{j+1}}$. If $\mathbf{b}_i''$ is not rank one, an equation similar to Eq. 2.48 should be adopted to include other important terms. However, the determinant calculations in Eqs. 2.47 and 2.48 are not explicit when the number of layers having numerical problems are more than one. In Fig. 2.4, a table is presented giving the contribution of each multiplication. Each entry in the table is the multiplication of the first column elements of the corresponding matrix in the first column of the table and the second column elements of the corresponding matrix in the first row of the table. The determinant of $\mathbf{R}_2$ is then the sum of those nonzero entries. Figure 2.4 shows that if all $\mathbf{R}_2^{(m)}$ are rank one, only the inverse diagonal entries, i.e. the asterisk positions, exist. However, if the importance of $e^{-v_j h_j}$ and/or $e^{-v_{j+1}h_{j+1}}$ cannot be ignored, all inverse lower triangular entries, i.e. asterisk and cross positions, should be included when obtaining the determinant of $\mathbf{R}_2$. The contributions from other entries are zero. The derivation of the results in Fig. 2.4 can be obtained by considering the characteristics of the rank one matrix, which is not shown here.

The truncational problem also occurs in the calculation of $\mathbf{R}_1\mathbf{R}_2^{-1}$ of Eq. 2.18. In this case, a procedure similar to finding the determinant of $\mathbf{R}_2$ may be applied. However, the interproducts of columns between different matrices as in Eqs. 2.47 and 2.48 should be replaced by the corresponding matrix multiplications. If only one soil layer has the truncational problem, it can be shown that

$$\mathbf{R}_1\,\mathbf{R}_2^{-1} = (\,\mathbf{R}_1^{(1)} + \mathbf{R}_1^{(2)})\,\frac{(\,adj(\mathbf{R}_2^{(1)}) + adj(\mathbf{R}_2^{(2)}))}{\det(\mathbf{R}_2)}$$

$$= \left(\begin{bmatrix} r_{11}^{(1)} & r_{12}^{(1)} \\ r_{41}^{(1)} & r_{22}^{(1)} \end{bmatrix} + \begin{bmatrix} r_{11}^{(2)} & r_{12}^{(2)} \\ r_{21}^{(2)} & r_{22}^{(2)} \end{bmatrix} \right) \left(\begin{bmatrix} \bar{r}_{31}^{(1)} & \bar{r}_{32}^{(1)} \\ \bar{r}_{41}^{(1)} & \bar{r}_{42}^{(1)} \end{bmatrix} + \begin{bmatrix} \bar{r}_{31}^{(2)} & \bar{r}_{32}^{(2)} \\ \bar{r}_{41}^{(2)} & \bar{r}_{42}^{(2)} \end{bmatrix} \right) \tag{2.50}$$

$$= \begin{bmatrix} t_1^* & t_2^* \\ t_3^* & t_4^* \end{bmatrix}$$

where $adj(\mathbf{R}_2^{(i)})$ is the adjoint matrix of $\mathbf{R}_2^{(i)}$; and

$$t_1^* = (r_{11}^{(1)}\bar{r}_{31}^{(2)} + r_{12}^{(1)}\bar{r}_{41}^{(2)}) + (r_{11}^{(2)}\bar{r}_{31}^{(1)} + r_{12}^{(2)}\bar{r}_{41}^{(1)})$$

if $\mathbf{b}_j^*$ is rank one; or

$$t_1^* = (r_{11}^{(1)}\bar{r}_{31}^{(2)} + r_{12}^{(1)}\bar{r}_{41}^{(2)}) + (r_{11}^{(2)}\bar{r}_{31}^{(1)} + r_{12}^{(2)}\bar{r}_{41}^{(1)}) + (r_{11}^{(2)}\bar{r}_{31}^{(2)} + r_{12}^{(2)}\bar{r}_{41}^{(2)})$$

if $\mathbf{b}_j^*$ is not of rank one. Similar calculations can be carried out for other t_i^*.

For two or more troubled layers, a similar table as Fig. 2.4 used for the calculation of t_i^* is shown in Fig. 2.5, in which $\overline{\mathbf{R}}_2^{(i)}$ represents $adj(\mathbf{R}_2^{(i)})/det(\mathbf{R}_2)$. The entries in the table become the product of one row in $\mathbf{R}_1^{(i)}$ by one column in $\overline{\mathbf{R}}_2^{(i)}$. The required row and column in this calculation depend on the calculated t_i^*, and the relations in Fig. 2.4, i.e. asterisk, cross and zero, remains in Fig. 2.5. If more layers possess the truncational problem, Figs. 2.4 and 2.5 can be expanded simply by mounting other $\mathbf{R}_l^{(i)}$ matrices in the first row and first column respectively, and those entries in the inverse upper triangular part are always equal to zero.

In addition, if m layers have trouble with the term e^{vh}, the number of matrices in the first row or column of Figs. 2.4 and 2.5 is 2^m. A similar procedure may be applied to a layered system with rigid lower boundary by changing $\mathbf{g}_n\mathbf{A}_n$ to $\mathbf{U}_n$ in Eq. 2.46.

2. Numerical Integration

Direct numerical evaluation of the integrals in Eq. 2.38 is impossible due to the singularities existing on the axis of wave number k, when materials of the layered system are elastic. These singularities come from the zero determinant of matrix $\mathbf{R}_2$ in Eq. 2.18 or matrix $\mathbf{T}_2$ in

Eq. 2.20. Ewing et al. [24] avoided these singularities by transforming the integration to the complex plane and evaluating it by contour integration. If the elastic halfspace is chosen for the lower boundary, the integral of Eq. 2.18 can be separated into several poles and two branch cut integrations as shown in Fig. 2.6. The poles which correspond to singularities represent the Rayleigh surface waves. The surface waves are generated from multiple reflections of waves between the horizontal interfaces. The branch cuts, which end respectively at the dilatational wave number k_{α_n} and shear wave number k_{β_n} of the halfspace, represent the wave refractions or energy transmission into the halfspace. For the case of rigid lower boundary, there is no energy radiation. The integral in Eq. 2.20 can be transformed into an infinite series of Rayleigh modes, i.e. an infinite number of poles.

Owing to the complexity of evaluating the integration in the complex plane caused by zero damping, viscoelastic behavior of the soil is introduced, which also has the additional benefit of giving more realistic solutions. The equations governing harmonic motions of viscoelastic material are identical to those of elastic media, except that the elastic constants λ and G are replaced by their complex moduli λ^* and G^*. The complex moduli depend on the viscoelastic model assumed for the material. For a Voigt solid

$$\lambda^*(\omega) = \lambda\ (1+i\omega\frac{\lambda'}{\lambda})$$

$$G^*(\omega) = G\ (1+i\omega\frac{G'}{G}) \tag{2.51}$$

where ω is the excitation frequency, λ' and G' are constants of viscosity.

If $\eta=\lambda'/\lambda=G'/G$ is introduced [25], the number of viscous constants is reduced to one. It implies that the viscoelastic behavior is the same in both dilatational and shear deformations. Equation 2.51 may now be written as

$$\lambda^* = \lambda\ (1+i\eta\omega)$$

$$G^* = G\ (1+i\eta\omega)$$

For a Voigt solid, the energy loss per cycle of harmonic vibration is proportional to the excitation frequency. However, over a considerable range of frequencies, several materials including rocks and soils exhibit energy loss substantially independent of the frequency of vibration [8]. Such materials may be idealized as a constant hysteretic solid which differ from Voigt model in the value assigned to η. In the voigt model, η is considered to be constant and energy loss is proportional to ω. For a hysteretic solid, η is replaced by $2\xi/\omega$, where ξ is a constant, and the energy loss is then independent of ω. Therefore, for a constant hysteretic soild

$$\lambda^* = \lambda\ (1+i2\xi)$$

$$G^* = G\ (1+i2\xi)$$

For the purpose of practical use, the following numerical results are calculated for a constant hysteretic model.

After damping is introduced into the soil property, the poles and branch cuts in Fig. 2.7 will deviate from the real axis and move into the lower half plane. The extent of deviation depends on the percentage of critical damping in materials. In this case, there is no singularity on the real k axis so that direct integration is possible. Although the convergent rate of direct integration may not be as fast as the complex domain integration, the existence of the factor $1/k^4$ in the integrand of Eq. 2.35 greatly improves the convergence. The upper limit of integration is truncated to as low as 50.0 in the following numerical results.

When the upper limit of integration is finite, Gaussian quadrature is very efficient in evaluating the integral. The integrand function is approximated by a polynomial in Gaussian quadrature. If the integration domain is big and the integrand is complicated, it is difficult to obtain a good evaluation by the lower quadrature integration through the whole domain. It is

also inappropriate to use many quadrature points, i.e. a very high order polynomial. In addition, the integrand in Eq. 2.37, which depends on the condition of the soil profile, involves some transcendental functions such as sinh, cosh, sin and cos. However, this difficulty can be treated by partitioning the whole integration domain into smaller subdomains, and adopting an appropraite order of quadrature integration in each subdomain. The selection of subdomain depends on the integrand value of that region. There are some inherent domain separators, i.e. $k_{\alpha_j}=\omega/C_{p_j}$ and $k_{\beta_j}=\omega/C_{s_j}$ of the jth soil stratum. If the soil is elastic, choosing k_{α_j} as a domain separator, the values of $v=\sqrt{k^2-k_{\alpha_j}^2}$ will convert from real to complex numbers when k moves form the right side of k_{α_j} to the left side on the k axis. A similar relation can be found between v' and k_{β_j}. Although the soil is assumed viscoelastic, similar phase conversion will affect the accuracy of integration, if k_{α_j} or k_{β_j} is included within a subdomain carelessly. However, the influence of k_{α_j} and k_{β_j} may be negligible if a large critical damping ratio, e.g., 0.10, is introduced into the materials. Also, subdomains around k_{α_j} and k_{β_j} are usually more important to the integration than those subdomains with higher k values. Therefore, larger subdomains are chosen for large values of k and finer subdomains should be adopted close to k_{α_j} and k_{β_j}.

Another factor influencing the solution is the number of finite elements under the plate. It is reasonable to use a coarse approximation for the lower frequencies and more elements for the higher frequencies.

Damping in material, thickness of soil layer, and stiffness ratio between layers are three possible factors which will affect the required number of subdomains along the k axis and the number of elements under the plate. In the following, numerical solutions are obatined for the case of only one soil layer over the halfspace or rigid rock. These solutions provide good guidance for the determination of solutions for multi-layered systems. Tables 2.1 and 2.2 show the required subdomain and element numbers for the single-layer system with different material dampings and with different stiffness ratios. The results for cases indicated in Tables

2.1 and 2.2 converge up to five significant digits. In Table 2.1, the subdomain numbers are satisfactory for wave number k from 0.0 to 10.0. Eight equal subdomains are exploited for large k values, i.e. from 10.0 to 50.0. The first columns in Tables 2.1 and 2.2 show the numbers necessary for the nondimensional frequency, $a_0=\omega a/C_{s_1}$, equal to 0.01, in which a is the half width of the plate and C_{s_1} is the shear wave velocity of soil layer. The second columns show the required numbers for a_0 equal to 3.0. For medium frequencies, both subdomain and element numbers are adjusted between the two values given in the first and second columns. In addition, 10-point Gaussian integration is employed in each subdomain. Upon numerical calculation, the influence of layer thickness on the numbers of subdomains and elements is of minor importance.

Although it may be more appropriate to evaluate the integrals involved in the solution for the case of rigid lower boundary by the residue theorem, direct integration will be used subsequently for all solutions.

3. Numerical Results

By employing the above procedure, the response of an infinite rigid strip on a single-layer system is evaluated for discrete nondimensional frequencies a_0 from 0.0 to 3.0. In these studies, the influence of certain parameters, namely, damping in the soil, stiffness ratio for soil layer and halfspace, and the ratio of layer depth to plate width, on the plate response are investigated. A Poisson ratio of 1/3, which is a fairly representive value for soils, is used in all solutions. A relaxed boundary condition, which includes only the normal stress under the plate for the vertical and rocking motion cases and only the shearing stress for the translational motion, is used so as to compare the results with the results of exact solutions.

Although similar solutions for the single-layer system has been calculated [6], they are not used herein for comparision, because the solution calculated by the Fast Fourier Transform method is not as accurate as the solution calculated by the principle of virtual work, especially when evaluating the peak values.

In Fig. 2.8, the solution of a viscoelastic homogeneous halfspace is shown and is compared with the elastic solution modified by the correspondence principle [26] to account for internal damping. The agreement between them is very good for the vertical, translational and coupling compliances over the whole frequency range considered. Although slightly bigger differences are observed for the rocking motion, possibly due to the approximate nature of the correspondence principle, the agreement is still satisfactory. It is therefore verified that the linear stress model with finite element discretization under the plate provides an accurate and efficient method to evaluate the response of the surface foundation.

The solutions for different stiffness ratios between layer and halfspace are shown in Figs. 2.9 and 2.10. The ratios chosen are $C_{s_2}^2/C_{s_1}^2$= 1.0, 3.0, 10.0 and ∞, in which 1.0 represents a system which is totally homogeneous and ∞ represents a single layer system with a rigid lower boudary. The real part of the translational compliance exhibits several peaks in the nondimensional frequency range from 0.0 to 3.0. Considering only the case of rigid boundary, the first peak corresponds to a frequency very close to $a_0=0.1\pi$ which is the first natural frequency of the soil layer excited by the vertical propagating shear waves, as predicted by the one-dimensional amplification theory, $a_0=\pi a/2H$, where H is the depth of the layer. The second peak which is at $a_0=0.2\pi$ is due to the first natural frequency of the stratum excited by the vertical dilatational waves, $a_0=\pi a C_{p_1}/2HC_{s_1}$. The third peak and those following correspond to the second, third, etc., natural frequencies due to the vertical shear wave excitation. The value of the third peak is less than that of the fourth, possibly due to the interference of the dominant dilatational waves on the shear waves. Thus, only the dominant dilatational waves affect the translational response with the influence from other dilatational waves being minor. The shear wave effect is not shown explicitly in the vertical compliance; therefore, dilatational waves govern the vertical motion of the plate. There is only one peak shown in the rocking response, which is at a frequency close to the first natural frequency of the stratum due to the vertical dilatational waves, since rocking is influenced primarily by the dilatational waves and only secondarily by the shear waves. The behavior of the coupling compliance is interesting, in the

sense that the first peak corresponds to the dominant vertical dilatational waves and the second corresponds to the third natural frequency for the vertical shear waves. When the stiffness ratio decreases, the compliance peak becomes wider and lower; thus, approaching the homogeneous halfspace solution. This observation is attributed in part to the phemomenon of energy being transmitted into the lower halfspace.

The compliance solutions corresponding to different ratios of layer depth to plate width, H/a, are shown in Figs. 2.11 and 2.12. Although the peaks corresponding to different H/a ratios shift with respect to the nondimensional frequency a_0, they shift very little with respect to the actual frequency ω. When the depth ratio increases, it is apparent that the peak values decrease, with the plate response becoming closer to the homogeneous halfspace solution. It is also shown that the rocking compliance corresponding to H/a=5.0 and the compliance for the halfspace are almost identical over a large range of nondimensional frequencies.

For different damping ratios, ξ =2%, 5% and 10%, the solutions are shown in Figs. 2.13 and 2.14. The real parts of the compliances decrease and their peaks become flatter when the damping increases. However, the imaginary parts of the compliances, which represent the energy dissipataion during plate motion, increase with damping in the lower frequency range and decrease in the higher frequency range. The behavior is possibly due to the larger proportion of energy dissipated by material damping in the lower frequency range but by radiation damping in the higher frequency range.

The solution for the relaxed boundary condition case can be obtained by removing the coupling submatrices of the nodal degrees of freedom between the normal and shearing stresses from the compliance matrix $\mathbf{F}$ of Eq. 2.34a. The comparison between solutions with complete restricted and relaxed boundaries are shown in Figs. 2.15, 2.16, 2.17 and 2.18 for different depth ratios, stiffness ratios and critical damping ratios. The response is completely matched for the translational motion and has only minor differences for the vertical motion. The discrepencies in the rocking compliances are greater; but, they are still acceptable. The differences between the solutions for two different boundary conditions, i.e. halfspace or rigid

boundary under the layers of soil, are minor with respect to depth, stiffness, and damping ratio.

Solutions of systems with more than one soil layer can be obtained by the same procedure. Certainly, the nature of the plate compliances becomes more complicated.

Solutions presented in this section will be employed later to find the corresponding far-field impedance functions through the method of system identification.

III. SYSTEM IDENTIFICATION METHOD

A layer of soil with medium depth over the homogeneous viscoelastic halfspace is considered in the present study. The purpose is to supplement previous works which modelled the soil as a homogeneous halfspace. The hybrid formulation is applied here for the analysis of plane-strain problems, e.g., long gravity dams or tunnels where it is reasonable to assume two dimensional behavior, with the far-field impedance matrix being determined by the method of system identification. Although most of the concepts used are similar to those presented before [12,13], they are briefly repeated here for the sake of completeness.

A. Hybrid Modelling Approach

1. Hybrid Model

The hybrid model is obtained by partitioning the total soil-structure system into two substructures, namely the near field and the far field. The near field consists of the structure concerned and a portion of the foundation soil within the smooth interface shown in Fig. 3.1. The far field consists of the remaining soil region outside this interface. In the previous investigations [12,13] the interfaces were chosen to be hemispherical for three-dimensional problems and semi-cylindrical for plane-strain problems in the case of a homogeneous elastic halfspace. Although, one soil layer of medium depth over the halfspace is of interest in this investigation, the interface remains to be a semi-cylinder as shown in Fig. 3.1c. However, it is not permitted to intersect the horizontal boundary between the soil layer and the halfspace. Selecting the interface in this manner keeps a homogeneous boundary; thus, reducing the complexity of the proposed impedance model.

Both the structure and the soil in the near field may be modelled in discrete form using the finite element method, thus taking advantage of its ability to accommodate irregular geometries such as those encountered with embedded foundations. Nonhomogeneous and

nonlinear soil properties in the immediate vicinity of the foundation can also be modelled by assigning appropriate properties to the affected finite elements.

In the present investigation, the far field is one soil layer over a halfspace with a semi-cylindrical cavity in the top layer, sharing a common interface with the near field. It takes into account not only the loss of energy due to the waves travelling away from the foundation but also the energy reflecting back into the near field from the horizontal boundary between the layer and the halfspace. To represent this behavior accurately, the development of a far-field impedance matrix which corresponds to the degrees of freedom at the common interface is necessary. Since a rigorous solution to layered soil problems with a semi-cylindrical pit appears mathematically intractable at present, the far field is modelled in this investigation by continuous impedance functions distributed over the interface. The far field impedance matrix may then be obtained by the principle of virtual work. This matrix, when combined with the near-field equations of motion, effectively and efficiently simulates the total soil-structure system.

2. Equation of Motion

The equation of motion for the isolated near field subjected to ground excitation along the interface can be written as

$$\mathbf{M}\ddot{\mathbf{u}} + \mathbf{C}\dot{\mathbf{u}} + \mathbf{K}\mathbf{u} = \mathbf{p}(t) + \mathbf{f}(t) \tag{3.1}$$

in which $\mathbf{u}(t)$ is the vector of nodal point displacements in the near field (including interface nodes) relative to the motion of the boundary, and $\dot{\mathbf{u}}$ and $\ddot{\mathbf{u}}$ are the corresponding velocity and acceleration vectors. $\mathbf{M}$ and $\mathbf{K}$ are the near-field mass and stiffness matrices, respectively. Viscous damping matrix $\mathbf{C}$ accounts for energy dissipation in the near field due to material damping. Vector $\mathbf{p}(t)$ contains the components of effective inertia loading on the system due to earthquake ground motion, and vector $\mathbf{f}(t)$ contains the far-field interaction forces corresponding to the interface degrees of freedom.

For steady state response, Eq. 3.1 can be transformed into the frequency domain, giving

$$(-\omega^2\mathbf{M} + i\omega\mathbf{C} + \mathbf{K})\ \mathbf{U}(\omega) = \mathbf{P}(\omega) + \mathbf{F}(\omega) \tag{3.2}$$

or

$$\mathbf{S}(\omega)\ \mathbf{U}(\omega) = \mathbf{P}(\omega) + \mathbf{F}(\omega) \tag{3.2a}$$

where $\mathbf{S}(\omega)=-\omega^2\mathbf{M}+i\omega\mathbf{C}+\mathbf{K}$ is the frequency dependent impedance matrix which characterizes the mass, damping and stiffness properties of the near field. $\mathbf{U}(\omega)$, $\mathbf{P}(\omega)$ and $\mathbf{F}(\omega)$ are the Fourier transforms of the displacement, loading and interaction force vectors, respectively, and ω is the excitation frequency.

The vector $\mathbf{U}$ of nodal point displacements can be partitioned into two parts: $\mathbf{U}_b$ corresponding to the nodal displacements at the boundary common to the near and far fields, and $\mathbf{U}_n$ corresponding to the remaining nodal displacements of the near field. Thus, Eq. 3.2a can then be written in the partitioned form

$$\begin{bmatrix} \mathbf{S}_{nn} & \mathbf{S}_{nb} \\ \mathbf{S}_{nb}^T & \mathbf{S}_{bb} \end{bmatrix} \begin{Bmatrix} \mathbf{U}_n \\ \mathbf{U}_b \end{Bmatrix} = \begin{Bmatrix} \mathbf{P}_n \\ \mathbf{P}_b \end{Bmatrix} + \begin{Bmatrix} 0 \\ \mathbf{F}_b \end{Bmatrix} \tag{3.3}$$

Because there is no interaction force in the interior of the near field, only vector $\mathbf{F}_b$ corresponding to the interface degrees of freedom exists in the vector $\mathbf{F}(\omega)$.

For the isolated far field, the interface dynamic force-deflection relationship is

$$\mathbf{S}_f(\omega)\ \mathbf{U}_f(\omega) = \mathbf{F}_f(\omega) \tag{3.4}$$

where $\mathbf{S}_f(\omega)$ is the far-field impedance matrix which has to be determined by a separate analysis. In rigorous form, it is a full matrix of which the elements characterize the mass, both radiation and viscous damping, stiffness properties, and layering condition of the far field. It is complex valued and frequency dependent.

The equations of motion for the far field are incorporated into the frequency domain near-field equations by employing the conditions of compatibility and equilibrium at the interface, i.e.,

$$\mathbf{U}_f = \mathbf{U}_b$$

$$\mathbf{F}_f + \mathbf{F}_b = 0 \tag{3.5}$$

Substitution of Eqs. 3.4 and 3.5 into Eq. 3.3 leads to the following equations of motion for the hybrid model of the entire soil-structure system.

$$\begin{bmatrix} \mathbf{S}_{nn} & \mathbf{S}_{nb} \\ \mathbf{S}_{nb}^T & \mathbf{S}_{bb}+\mathbf{S}_f \end{bmatrix} \begin{Bmatrix} \mathbf{U}_n \\ \mathbf{U}_b \end{Bmatrix} = \begin{Bmatrix} \mathbf{P}_n \\ \mathbf{P}_b \end{Bmatrix} \tag{3.6}$$

or

$$\hat{\mathbf{S}}(\omega)\ \mathbf{U}(\omega) = \mathbf{P}(\omega) \tag{3.6a}$$

where $\hat{\mathbf{S}}(\omega)$ is the impedance matrix of the total hybrid system including both the near and far fields.

3. Dynamic Response

For a prescribed earthquake input motion, the Fourier amplitude, $\mathbf{P}(\omega)$, of the resulting load vector, $\mathbf{p}(t)$, can be obtained from

$$\mathbf{P}(\omega) = \int_0^{T_d} \mathbf{p}(t)\ e^{-i\omega t}\, dt \tag{3.7}$$

where T_d is the time duration of excitation. The time histories of response of the system can then be obtained by the inverse Fourier transformation of the complex frequency response, i.e., solution $\mathbf{U}(\omega)$ of Eq. 3.6, into the time domain using

$$\mathbf{u}(t) = \frac{1}{2\pi} \int_{-\infty}^{\infty} \mathbf{U}(\omega)\ e^{i\omega t}\, d\omega \tag{3.8}$$

The transform pairs of Eqs. 3.7 and 3.8 can be evaluated efficiently and economically by using the Fast Fourier Transform (FFT) techniques.

The definition of a realistic input motion to the soil-structure systems is still a debatable issue. The seismic energy arriving at a particular site depends upon so many factors, such as fault rupture mechanism, travel path of the seismic waves, and local soil conditions, that a complete characterization of the earthquake ground motion unique to a particular site seems impossible and impractical. Therefore, it is reasonable and prudent to specify a site-dependent response spectrum from which time histories of motion can be generated to be used as input to the soil-structure system.

B. Far-Field Impedance Functions

1. Mathematical Model

The main purpose of the hybrid modelling approach is to find an accurate representation of both the radiation and viscous damping in the far-field soil region and the energy reflection from the horizontally layered boundary. The development of the far-field impedance matrix, $\mathbf{S}_f(\omega)$, requires the solution of sets of partial differential equations with prescribed boundary conditions at the interface common to both the near and far fields and at the horizontal boundary between the layer and halfspace. Since such analytical solution is difficult to obtain, a semi-analytical approach is adopted. A dynamic equivalent Winkler's assumption which was used successfully to simulate the far field in the case of elastic halfspace will be extended for the single-layer system of this study. In this assumption the far field soil region is represented by different continuous impedance functions in principal directions. This is equivalent to decomposing the far-field soil region into infinite infinitesimally thin soil elements in the radial direction which have only principal directional impedances to account for both stiffness and damping. Also, these elements act independently of each other. Although, the material may not be uniform within each infinitesimally thin soil element due to the soil layer, the proposed

far-field impedance function may be chosen as a smoothly varying function along the semi-cylindrical interface. The success of the dynamic equivalent Winkler's assumption is assured by placing the interface at a reasonable distance from the structure since the influence of foundation irregularities on stresses and displacements along the semi-cylindrical boundary diminishes with distance from the foundation.

In general, the far-field impedances can be expressed in terms of a Fourier series involving the angle ϕ. Since for horizontally layered halfspaces the far field possesses material and geometric symmetry about the vertical axis, the impedance functions must be symmetric in ϕ; thus giving

$$S_R(R,H,\phi,C_{s_1},C_{s_2},\xi_1,\xi_2,b_0) = \sum_0^\infty S_{R_n}(R,H,C_{s_1},C_{s_2},\xi_1,\xi_2,b_0)\cos n\phi$$

$$S_\phi(R,H,\phi,C_{s_1},C_{s_2},\xi_1,\xi_2,b_0) = \sum_0^\infty S_{\phi_n}(R,H,C_{s_1},C_{s_2},\xi_1,\xi_2,b_0)\cos n\phi \tag{3.9}$$

in which S_R and S_ϕ are the complex valued far-field impedances per unit area in the radial and tangential directions to the semi-cylindrical interface as shown in Fig. 3.2. Coefficients S_{R_n} and S_{ϕ_n} characterize all properties of soil layer and halfspace, which are functions of the interface radius R, the layer depth H, the shear velocities C_{s_1} and C_{s_2} and damping ratios ξ_1 and ξ_2 corresponding to soil layer and halfspace, respectively, and also the non-dimensional frequency parameter b_0 defined by $b_0=\omega R/C_{s_1}$ where ω is the excitation frequency, $C_{s_i}=\sqrt{G_i/\rho_i}$, G_i and ρ_i are the shear modulus and mass density of the corresponding material.

The number of terms required in Eqs. 3.9 to properly represent the far field depends upon the complexity of the soil condition. A constant distributed impedance function along the interface was appropriate for the elastic halfspace. However, a more sophisticated impedance function is required to represent the far field of the single-layer system. For the sake of minimizing the number of unknown coefficients to be determined, Eqs. 3.9 are limited to the first two terms, i.e., the constant and the first trigonometric terms, in this investigation; thus,

giving

$$S_R(H/R,\phi,C_{s_2}/C_{s_1},\xi_1,\xi_2,b_0) = S_{R_0}+S_{R_1}\cos\phi = (\eta_{R_0}+i\zeta_{R_0}) + (\eta_{R_1}+i\zeta_{R_1})\cos\phi$$

$$S_\phi(H/R,\phi,C_{s_2}/C_{s_1},\xi_1,\xi_2,b_0) = S_{\phi_0}+S_{\phi_1}\cos\phi = (\eta_{\phi_0}+i\zeta_{\phi_0}) + (\eta_{\phi_1}+i\zeta_{\phi_1})\cos\phi \qquad (3.10)$$

where the η's and ζ's are the real and imaginary parts, respectively, of the coefficients of the unknown far-field impedance functions.

These continuous far-field impedance functions can be discretized at the boundary nodes to obtain the far-field impedance matrix. This can be achieved by using the principle of virtual work expressed as

$$\delta W = \int \delta \mathbf{u}^T \mathbf{p}\, ds \qquad (3.11)$$

where $\delta\mathbf{u}$ is the 2-component vector of kinematically admissible virtual displacements on the interface, and $\mathbf{p}$ is the corresponding 2-component vector of real interface forces in equilibrium, and s is the distance along the interface.

According to the assumed model of the far field, the interface forces and displacements are related by

$$\begin{Bmatrix} p_r \\ p_\phi \end{Bmatrix} = \begin{bmatrix} S_R & 0 \\ 0 & S_\phi \end{bmatrix} \begin{Bmatrix} u_r \\ u_\phi \end{Bmatrix} \qquad (3.12)$$

where S_R and S_ϕ are the continuous far-field impedance functions defined in Eqs. 3.10.

For consistency, the far-field displacements expressed in cylindrical coordinates will be transformed into Cartesian coordinates, as used for the near-field finite element model, by the relation

$$\begin{Bmatrix} u_r \\ u_\phi \end{Bmatrix} = \begin{bmatrix} \sin\phi & \cos\phi \\ \cos\phi & -\sin\phi \end{bmatrix} \begin{Bmatrix} u_x \\ u_z \end{Bmatrix} \qquad (3.13)$$

Substituting Eqs. 3.12 and 3.13 into Eq. 3.11 gives

$$\delta W = \int \delta < u_x \; u_z >^T \begin{bmatrix} S_R \sin^2\phi + S_\phi \cos^2\phi & (S_R - S_\phi)\sin\phi\cos\phi \\ (S_R - S_\phi)\sin\phi\cos\phi & S_R \cos^2\phi + S_\phi \sin^2\phi \end{bmatrix} \begin{Bmatrix} u_x \\ u_z \end{Bmatrix} r \; d\phi \tag{3.14}$$

The displacements on the interface may now be expressed in terms of the same interpolation functions as used for the near-field finite element discretization to ensure compatibility of displacements along the interface. Thus, for element "p" on the interface

$$\begin{Bmatrix} u_x \\ u_z \end{Bmatrix} = \begin{bmatrix} \mathbf{N} & \\ & \mathbf{N} \end{bmatrix} \begin{Bmatrix} \mathbf{u}_x \\ \mathbf{u}_z \end{Bmatrix}_p \tag{3.15}$$

where $\mathbf{u}_x$ and $\mathbf{u}_z$ are the nodal point displacement vectors at the interface, and $\mathbf{N}$ are the finite element interpolation functions.

The contribution of element "p" to the total virtual work can then be obtained by substituting Eq. 3.15 into 3.14 , giving

$$\delta W^p = \delta < \mathbf{u}_x^T \, \mathbf{u}_z^T >_p \; \mathbf{S}_f^p \begin{Bmatrix} \mathbf{u}_x \\ \mathbf{u}_z \end{Bmatrix}_p \tag{3.16}$$

in which,

$$\mathbf{S}_f^p = \int_p \begin{bmatrix} (S_R \cos^2\phi + S_\phi \sin^2\phi)\mathbf{N}^T\mathbf{N} & (S_R - S_\phi)\sin\phi\cos\phi\,\mathbf{N}^T\mathbf{N} \\ (S_R - S_\phi)\sin\phi\cos\phi\,\mathbf{N}^T\mathbf{N} & (S_R \sin^2\phi + S_\phi \cos^2\phi)\mathbf{N}^T\mathbf{N} \end{bmatrix} r \; d\phi \tag{3.16a}$$

$\mathbf{S}_f^p$ is the 6×6, consistent far-field impedance matrix in Cartesian coordinates for element "p" on the interface. Because of the complexity of the terms in Eq. 3.16a, six and seven Gaussian quadrature points along an element interface are needed for the constant and trigonometric terms in Eqs. 3.10 ,respectively, to avoid incomplete integration.

The far-field impedance matrix for the entire interface may be obtained by standard finite element assembly procedure [27], and then used in the hybrid system as indicated by Eq. 3.6 to solve the soil-structure interaction problem.

2. Parameter Identification

The unknown far-field impedance functions S_R and S_ϕ are determined by the method of system identification. System identification is an iterative process in which the unknown parameters of the postulated model are determined by systematically adjusting them so that the resulting model provides a best fit to the actual observed behavior of the system. In the present investigation, which is concerned with two dimensional problems, the "observed behavior" is taken as the theoretical solutions for the dynamic response of an infinitely long, rigid, massless strip footing on the viscoelastic layered halfspace in the vertical and coupled translation-rocking modes of vibration. These solutions have been obtained in Chapter II by a proposed stress model under the plate, as defined by

$$\begin{Bmatrix} \Delta_V \\ \Delta_H \\ \Delta_M \end{Bmatrix} = \begin{bmatrix} C_{VV} & & \\ & C_{HH} & C_{HM} \\ & C_{MH} & C_{MM} \end{bmatrix} \begin{Bmatrix} V \\ H \\ M \end{Bmatrix} \tag{3.17}$$

In this equation, the coupling compliance C_{HM} equals C_{MH} owing to the reciprocal condition. The corresponding hybrid model of the rigid strip, with the near field modelled by finite elements and far field by impedance functions, must reproduce these known solutions within some prescribed tolerance level.

For a prescribed value of the excitation frequency and for the assumed values of far-field impedance functions, the equation of motion for the hybrid system, Eq. 3.6, can be solved to yield the complex displacement amplitudes (compliances) of the rigid massless strip footing. These compliances depend on the assumed far-field impedances and will, in general, be in error with the known compliances. To systematically minimize these errors using the methods of system identification, an error function containing the sum of squared errors of all the strip compliances considered is formed giving,

$$J(\beta,\omega) = \sum_{i=1}^{NC} \left| U_i(\beta,\omega) - C_i \right|^2$$

$$= \sum_{i=1}^{NC} \left\{ [Re(U_i) - Re(C_i)]^2 + [Im(U_i) - Im(C_i)]^2 \right\} \tag{3.18}$$

in which, $\boldsymbol{\beta}$ is an n-dimensional vector containing all of the far-field impedance coefficients (in the present case $\boldsymbol{\beta}$ has 8 parameters, η_{R_i}, ζ_{R_i}, etc., given by Eqs. 3.10), $U_i = U_i(\boldsymbol{\beta},\omega)$ are the strip compliances from the hybrid model, $C_i = C_i(\omega)$ are the known strip compliances, ω is the excitation frequency, and NC is the total number of strip compliances considered in the solution.

The error function $J(\boldsymbol{\beta},\omega)$, which can be visualized as a surface in an n-dimensional space corresponding to the n parameters in the far-field impedance vector $\boldsymbol{\beta}$, is minimized for discrete values of ω to give the corresponding $\boldsymbol{\beta}$ over the desired range of frequencies. Methods of system identification are used to systematically adjust the originally assumed values of the far-field impedance coefficients. There are several iterative methods [28] which can be used for this purpose. To speed the rate of convergence, the modified Gauss-Newton method [29] which makes use of the information on second derivatives is selected for the present study. The procedure of this method is to expand the error function $J(\boldsymbol{\beta},\omega)$ into a Tayler's series, neglecting the terms of order higher than two, and then equating the gradient to zero which leads to the equation

$$\mathbf{g}(\boldsymbol{\beta}_{i-1},\omega) + \mathbf{h}(\boldsymbol{\beta}_{i-1},\omega)\ (\boldsymbol{\beta}_i - \boldsymbol{\beta}_{i-1}) = 0 \tag{3.19}$$

where $\boldsymbol{\beta}_{i-1}$ and $\boldsymbol{\beta}_i$ are the parameter vectors at iterative steps $i-1$ and i, respectively,

$$\mathbf{g}^T(\boldsymbol{\beta},\omega) = \left\{ \frac{\partial J}{\partial \beta_1}, \frac{\partial J}{\partial \beta_2}, \cdots, \frac{\partial J}{\partial \beta_n} \right\} \tag{3.19a}$$

is the gradient vector, and

$$\mathbf{h}(\boldsymbol{\beta},\omega) = \begin{bmatrix} \dfrac{\partial^2 J}{\partial \beta_1^{\,2}} & \cdots & \dfrac{\partial^2 J}{\partial \beta_1 \partial \beta_n} \\ \vdots & \ddots & \vdots \\ \dfrac{\partial^2 J}{\partial \beta_n \partial \beta_1} & \cdots & \dfrac{\partial^2 J}{\partial \beta_n^{\,2}} \end{bmatrix} \tag{3.19b}$$

is the n×n Hessian matrix.

If the Hessian matrix is invertible, $\boldsymbol{\beta}_i$ can be expressed as

$$\boldsymbol{\beta}_i = \boldsymbol{\beta}_{i-1} - \lambda\ \mathbf{h}^{-1}(\boldsymbol{\beta}_{i-1},\omega)\ \mathbf{g}(\boldsymbol{\beta}_{i-1},\omega) \tag{3.20}$$

or

$$\boldsymbol{\beta}_i = \boldsymbol{\beta}_{i-1} - \lambda\ \mathbf{d}_{i-1} \tag{3.20a}$$

where $\mathbf{d}_{i-1} = \mathbf{h}^{-1}(\boldsymbol{\beta}_{i-1},\omega)\ \mathbf{g}(\boldsymbol{\beta}_{i-1},\omega)$ is the search direction vector as defined by the modified Gauss-Newton method, and scalar λ is a positive parameter selected to ensure a decrease in error within each iteration cycle.

The components of gradient vector in Eq. 3.19a are obtained by taking the partial derivatives of the error function at $\boldsymbol{\beta}_{i-1}$, i.e.,

$$\frac{\partial J}{\partial \beta_j} = 2 \sum_{i=1}^{NC} \left\{ [Re(U_i) - Re(C_i)] \frac{\partial Re(U_i)}{\partial \beta_j} + [Im(U_i) - Im(C_i)] \frac{\partial Im(U_i)}{\partial \beta_j} \right\} \tag{3.21}$$

Similarly, the coefficients of the Hessian matrix are

$$\frac{\partial^2 J}{\partial \beta_j \partial \beta_k} = 2 \sum_{i=1}^{NC} \left\{ \frac{\partial Re(U_i)}{\partial \beta_j} \frac{\partial Re(U_i)}{\partial \beta_k} + [Re(U_i) - Re(C_i)] \frac{\partial^2 Re(U_i)}{\partial \beta_j \partial \beta_k} \right.$$

$$\left. + \frac{\partial Im(U_i)}{\partial \beta_j} \frac{\partial Im(U_i)}{\partial \beta_k} + [Im(U_i) - Im(C_i)] \frac{\partial^2 Im(U_i)}{\partial \beta_j \partial \beta_k} \right\} \tag{3.22}$$

Since the effort required to calculate the second derivatives in Eq. 3.22 is prohibitive, the coefficients in the Hessian matrix are approximated by

$$\frac{\partial^2 J}{\partial \beta_j \partial \beta_k} = 2 \sum_{i=1}^{NC} \left[\frac{\partial Re(U_i)}{\partial \beta_j} \frac{\partial Re(U_i)}{\partial \beta_k} + \frac{\partial Im(U_i)}{\partial \beta_j} \frac{\partial Im(U_i)}{\partial \beta_k} \right] \tag{3.23}$$

A justification for neglecting the two higher order terms in Eq. 3.22 is that near the minimum these terms are small compared with the first order terms. The approximation given by Eq.

3.23 makes the Hessian matrix positive semi-definite, a property that the original matrix based on Eq. 3.22 does not possess. To ensure that the inverse of the Hessian matrix in Eq. 3.20, does exist, it is necessary only to add a small positive constant to the diagonal elements. The added term can be considered as an approximation to the higher order terms ignored in Eq. 3.23, and it improves the search direction. In addition, since the response quantity $U_i(\boldsymbol{\beta},\omega)$ is not an explicit function of $\boldsymbol{\beta}$, but is obtained through a numerical process involving the solution of Eq. 3.6, the partial derivatives $\partial U_i/\partial\beta_j$ in Eqs. 3.21 and 3.23 are replaced by finite differences $\Delta U_i/\Delta\beta_j$.

The error function $J(\boldsymbol{\beta},\omega)$ defines an n-dimensional surface which in two dimensions is easy to visualize as shown in Fig. 3.3. The modified Gauss-Newton method is an iterative process in which the error is minimized by obtaining successively better estimates of the far-field impedance vector $\boldsymbol{\beta}$ until a point $\boldsymbol{\beta}^*$ is located where the slope of the error surface approaches zero. The slope of the error profile at a point $\boldsymbol{\beta}_i$ along the search direction $\mathbf{d}_{i-1}$ is obtained by differentiating the error function with respect to the step size λ, giving

$$\alpha_{i-1}(\boldsymbol{\beta}_i) = -\mathbf{g}^T(\boldsymbol{\beta}_i,\omega)\ \mathbf{d}_{i-1} \tag{3.24}$$

At any step $i-1$, a typical iteration cycle proceeds a follows -- The far-field impedance matrices corresponding to the parameter vector $\boldsymbol{\beta}_{i-1}$ are formed as explained earlier and then they are combined with the near-field finite element equations to give the equations of motion, Eq. 3.6, for the hybrid model. These equations are solved to obtain the response U_i of the rigid strip and the error is evaluated according to Eq. 3.18. The slope of the error surface, $\alpha_{i-1}(\boldsymbol{\beta}_{i-1})$ is obtained by substituting $\boldsymbol{\beta}_{i-1}$ for $\boldsymbol{\beta}_i$ in Eq. 3.24 which is then compared against a specified tolerance on slope taken sufficiently close to zero. If the slope is less than the specified tolerance, the error surface is considered flat and the error J is assumed to be minimized. The parameter vector $\boldsymbol{\beta}_{i-1}$ in that case is the desired far-field impedance vector $\boldsymbol{\beta}^*$. If the slope is greater than the specified tolerance, a line search along the direction $\mathbf{d}_{i-1}$ is made as shown in Fig. 3.3. According to Eq. 3.20 each value of the step size parameter λ defines a different point

β_i along this direction. Within a line search, the step size λ is systematically adjusted so that a point β_i is obtained where the slope of the error profile is sufficiently small and the error is minimized in that direction. The parameter vector β_i so obtained is then used as the next point in the iteration process.

To start the iterative process one must have an initial estimate β_0 of the far-field impedance function. The success of the method depends upon the accuracy of this estimate. If the starting vector β_0 is far from the true minimum, either the convergence may be very slow or the solution never converges. It is possible that, even the iterative process converges to a minimum, the error at that point is still large. This implies one of two possibilities -- either it is a local minimum, or it is a global minimum but the model chosen for the far-field impedance is not adequate. In the first eventuality, one may start from a different set of starting values β_0 until the true minimum is achieved. In the second case, one may try including additional terms in the Fourier expansion of Eqs. 3.9. If that does not work either, then it implies that the chosen model is not realistic. If, however, at the minimum the error approaches zero, it signifies that the chosen mathematical model for the far-field impedances is adequate and that the iterative process has converged to the true minimum.

C. Numerical Computation

1. Finite Element Model and Soil Condition

A quadratic planar 9-node element [30] is employed to discretize the near field. The accuracy and stability of this element has been attributed to the addition of the ninth node to the center of the more conventional 8-node element. The ninth node increases the flexibility of the 8-node element under geometric distortion, which is especially valuable to the wave propagation problems. A typical finite element mesh selected for system identification procedure is shown in Fig. 3.4. The dimension of each element varys smoothly to diminish most artificial reflection of energy due to the nonuniformity of the assumed displacement field within the

finite elements. The element size chosen is not bigger than 1/4 of the shortest shear wave length considered to ensure the error due to the finite element approximation being negligible. This selection is based on the study of one-dimensional wave propagation problem; however, very good results have been shown for multi-dimensional problems [12,13] by satisfying this requirement. Since the entire system employed to generate the far-field impedance functions is a simple rigid strip on the layered halfspace, its dynamic behavior can be decomposed into a symmetrical and an antisymmetrical motions. Therefore, only half of the system with some appropriate boundary conditions imposed on the central axis is required.

A single-layer halfspace is considered in the present study. The radius of the common boundary between the near and far fields, R, has been assigned to 3/4 of the depth of the top layer, H. The Poisson's ratios chosen for top layer and halfspace are $\nu_1 = \nu_2 = 1/3$ which fairly represent the typical value of soils. To account for the hysteretic behavior of the soil, a small damping ratio, 2%, is assigned to both the layer and halfspace. The impedance function will be evaluated with respect to different stiffness ratios between the layer and the halfspace. This ratio is defined as $C_{s_2}^2 / C_{s_1}^2$, where C_{s_1} and C_{s_2} are the shear wave velocities of the layer and the halfspace, respectively.

The computational detail about the condensation of the near-field impedance matrix, S, and the assembly of the near-field and far-field impedance matrices through their interface degrees of freedom to calculate the plate response is almost identical to the previous report [13]. It is therefore not repeated here.

2. Numerical Results

Since there are 8 unknown parameters, $\boldsymbol{\beta}^T = <\eta_{R_0}, \zeta_{R_0}, \eta_{\phi_0}, \zeta_{\phi_0}, \eta_{R_1}, \zeta_{R_1}, \eta_{\phi_1}, \zeta_{\phi_1}>$, in the far-field impedance functions, the number of components of plate response required for system identification procedure should be more than the undetermined parameters. Two sets of plate response for $R/a = 3.75$ and 2.8125 are selected, which are obtained through the numerical procedure in Chapter II by changing the half width of the rigid strip "a" with respect

to a fixed depth of layer H. Therefore, the selected interface radius R and the determined impedance functions are constant for different R/a ratios. Those identified impedance parameters have been plotted in a nondimensional form in Figs. 3.5 to 3.8 as a function of the nondimensional frequency $b_0 = \omega R / C_{s_1}$. For any particular frequency, those distributed far-field impedance functions are directly proportional to the shear modulus, G_1, of the top layer, and are inversely proportional to the interface radius R. Therefore, with specified stiffness, depth ratios between soil layer and halfspace and with associated damping and Poisson ratios of the materials, the identified impedance functions for any size of the far field with any shear modulus and mass density can be obtained from these nondimensional curves.

In Figs. 3.5 to 3.8, three sets of impedance parameters corresponding to stiffness ratios of $C_{s_2}^2 / C_{s_1}^2 = 1.0$, 3.0 and 10.0 are shown. Because there is only one constant term assumed in Eqs. 3.9 for the homogeneous halfspace, $C_{s_2}^2 / C_{s_1}^2 = 1.0$, the corresponding data are only shown in the first two figures. In addition,the original impedance data of $C_{s_2}^2 / C_{s_1}^2 = 1.0$ were calculated upon elastic property, the correspondence principle is then applied to consider the material damping, 2%, in the soil medium. Although, some figures show a similar behavior as in the plate response, i.e., the fluctuation in solution for larger stiffness ratio is higher, there is no obvious relationship between impedance parameter and the propagation of waves. It is due to the approximate nature of the impedance functions and the numerical iterative searching procedure.

To show how the impedance function varies along the cylindrical interface, four locations corresponding to $\phi = 0^o$, 30^o, 60^o and 90^o are chosen. Equations 3.10 are applied to calculate the impedance functions at each location. The impedance functions corresponding to $C_{s_2}^2 / C_{s_1}^2 = 3.0$ and 10.0 are shown in Figs. 3.9 and 3.10, respectively. The impedance values at $\phi = 0^o$, 30^o, 60^o and 90^o are quite different in the whole frequency range considered. The peaks of $\phi = 0^o$ are usually the deeps of $\phi = 90^o$. It is possibly due to the fact that at $\phi = 0^o$ the reflecting waves which influence this location are dominately generated by those waves emitting from its own direction. However, the wave propagating in all ϕ directions will reflect to the

free surface, ϕ=90°, and then affect the corresponding impedance values. Therefore, the impedance function corresponding to ϕ=0° can be considered as the result of the direct reflection of waves from the horizontal soil boundary. Impedance functions at ϕ=30°, 60° and 90° are more or less influenced by the waves emitting from other directions and the waves having multiple reflections.

There are some nodal points in Figs. 3.9 and 3.10, in which the impedance function at each location passes. It can be considered at those specific frequencies the corresponding impedance function may be represented by a constant term in Eqs. 3.10. However, those nodal points are primarily due to numerical calculation. No relationship could be found between the nodal points and the soil condition.

The identified far-field impedance functions corresponding to $C_{s_2}^2/C_{s_1}^2=3.0$ are exploited to calculate the plate response which is then compared with analytic solution in Figs. 3.11 and 3.12. Very good agreement between two solutions has been shown for R/a of 2.8125 and 3.75 in the whole frequency range considered. Although, there are some peaks corresponding to the natural frequencies of the layered system in the plate response, the error between the two solutions never exceed 5%. Because the calculation is based on the physical frequency ω, the range of nondimensional frequency a_0 transformed from ω for different R/a is not constant. To investigate the range of applicability of the proposed far-field impedance function, the compliances of rigid strip for R/a ratios of 2.25 and 4.5 are shown in Figs. 3.13 and 3.14. Although, a somewhat larger error of 15% is observed in the rocking compliance, good agreement between the calculated and analytic solutions still remains. In addition, the two R/a ratios used represent a reasonable range of the interface distance of the near field. For R/a ratio greater than 4.5, the economy and efficiency of the hybrid modelling diminish because the required near-field finite element system becomes too large. For R/a less than 2.25, the nonuniformity of stress and displacement fields due to irregularity of foundation or local nonlinearity of soil property may affect the accuracy of the solution.

The identified impedance functions of $C_{s_2}^2/C_{s_1}^2=10.0$ are also applied for R/a ratios of 2.25, 2.8125, 3.75 and 4.5. Fairly accurate solutions have been shown in Figs. 3.15, 3.16 and 3.18 by the proposed impedance model for the cases of 2.8125, 3.75 and 4.5. The error observed in the result of R/a=2.25, Fig. 3.17, is somewhat larger especially in the high frequencies. However, it is still within reasonable range.

There is a tendency that the error corresponding to the larger stiffness ratio is bigger. The reason is that the identified far-field impedance functions are numerically governed by those strip compliances with higher fluctuation in the system identification procedure. The errors in other compliances are then mitigated. It is therefore concluded that the assumed continuous impedance functions gradually lose its effectiveness to simulate the real soil-structure interaction behavior when the stiffness ratio between layer and halfspace is getting large. It is possible to include more trigonometric terms in Eqs. 3.10 to modify current assumption; however, the computational efforts required by the procedure of system identification increase significantly. When the halfspace is much stiffer than the above soil layers, those soil layers can be assumed being underlain by a rigid boundary since only negligible amount of energy is radiated into the very stiff halfspace. Upon this assumption, there is alternative way in which an analytic solution is exploited to find an exact far-field impedance matrix, which will be introduced in the next chapter.

IV. BOUNDARY SOLUTION METHOD

A. General

If the stiffness of underlying rock is very large compared with the stiffness of the upper soil layers, one can assume the rock as a rigid base for the soil. Wave propagation in the layered system is now different from the case of layered soil over a flexible halfspace, since there is no energy transfer into the rigid rock. All energy in the soil will reflect and propagate between the rigid base and the free surface resulting in an infinite number of surface wave modes. If the soil is purely elastic, for a specified excitation frequency there are a finite number of real Rayleigh and Love surface modes and an infinite number of damped Rayleigh and Love surface modes. These real modes, which do not dissipate energy, radiate energy in the form of wave propagation; however, the damped modes dissipate and radiate energy in their travelling path.

There are some disadvantages in using the system identification method to find far-field impedances for layered soil underlain by rigid rock. The most significant disadvantage results from the highly oscillatory behavior of plate response with respect to the frequency when the soil layers are elastic or have low damping. The system identification method minimizes an error function between true response and calculated response through a set of far-field impedance parameters. If the proposed far-field model is not able to represent the true boundary impedances, the minimum error may be unacceptably large. Because of the above mentioned oscillatory behavior of the plate response, the number of Fourier expansion terms needed in Eq. 3.9 for the proposed far-field impedances may be so large that the computational effort is unacceptable; thus, making the system identification approach impractical. Also when rigid base rock is present, the uncoupled far-field impedances along a semi-cylindrical or a hemispherical boundary around the structure cannot adequately represent the wave reflections at the rigid boundary. Because of these problems, a boundary solution procedure is used, which combines finite element modelling of the near field with a true continuum model of the

far field.

B. Boundary Solution Method

The boundary solution procedure simulates a field where the standard finite element approximation is not feasible or inefficient by a set of trial functions having parameters for unknown displacements or stresses. These functions which are independent of each other satisfy the governing equations in their homogeneous forms. The parameters are determined by approximately satisfying the boundary conditions of the field. Certainly the choice of trial functions is more difficult than the finite element shape functions. However, in the following discussion analytic solution, which satisfies both equations of motion and some boundary conditions, is determined to substitute for those trial functions.

The boundary solution method is to minimize the discrepancy between an analytic solution of the far field and a finite element approximation of the near field at their interface through the variational principle and the principle of virtual work. It is equivalent to finding a hyperelement for the far-field region by employing appropriate functions as the element shape functions. These functions are chosen so that the governing equations of the far field are automatically satisfied. In Fig. 4.1, the near field which includes the structure is discretized by finite elements and the far field, which has a semi-infinite domain, is represented by the degrees of freedom at the interface. The selection of the interface is not arbitrary but depends on the analytic solution of the far field.

The displacements and stresses at any point on the interface may be expressed by a series of uncoupled modes of the analytic solution as

$$\mathbf{u}(s) = \mathbf{N}(s)\ \mathbf{c}$$

$$\mathbf{t}(s) = \mathbf{G}(s)\ \mathbf{c} \tag{4.1}$$

where $\mathbf{N}(s)$ and $\mathbf{G}(s)$ are the matrices of modal displacement and stress vectors respectively, $\mathbf{c}$ is the vector of corresponding modal participation factors, and s is the distance of the common

boundary between near and far fields. Also, $\mathbf{G}(s)$ is the differential of $\mathbf{N}(s)$ multiplied by the elastic constants.

The finite element approximate displacements on the interface can be written as

$$\bar{\mathbf{u}}(s) = \bar{\mathbf{N}}(s)\ \mathbf{U}_b \tag{4.2}$$

in which $\bar{\mathbf{N}}(s)$ is the finite element shape functions exploited in the near field and at the interface, and $\mathbf{U}_b$ is the nodal displacement vector containing the interface degrees of freedom.

Considering the far field independently and prescribing the interface displacements in terms of the finite element approximate displacements, i.e., $\mathbf{u}=\bar{\mathbf{u}}$, the principle of virtual work gives

$$\int_{s_u} \delta\mathbf{t}^T(\mathbf{u} - \bar{\mathbf{u}})\ ds = 0 \tag{4.3}$$

where $\delta\mathbf{t}$ is the variation of forces along the interface.

In above equation, the error or residual due to the discrepancy of displacements between the near and far fields is then forced to zero in an average sense. Substitution of Eqs. 4.1 and 4.2 into Eq. 4.3 gives

$$\delta\mathbf{c}^T \left(\int_{s_u} \mathbf{G}^T\mathbf{N}\ ds\ \mathbf{c} - \int_{s_u} \mathbf{G}^T\bar{\mathbf{N}}\ ds\ \mathbf{U}_b\right) = 0 \tag{4.4}$$

Ignoring the arbitrary quantity $\delta\mathbf{c}$ above, modal participation factors can be expressed as

$$\mathbf{c} = \left(\int_{s_u} \mathbf{G}^T\mathbf{N}\ ds\ \right)^{-1} \left(\int_{s_u} \mathbf{G}^T\bar{\mathbf{N}}\ ds\ \right) \mathbf{U}_b \tag{4.5}$$

or

$$\mathbf{c} = \mathbf{K}_c^{-1}\mathbf{K}_{cb}\mathbf{U}_b \tag{4.5a}$$

in which $\mathbf{K}_c = \int_{s_u} \mathbf{G}^T\mathbf{N}\ ds$ and $\mathbf{K}_{cb} = \int_{s_u} \mathbf{G}^T\bar{\mathbf{N}}\ ds$.

Since the interface is the only nontrivial displacement boundary of the far field, boundary integration is thus limited along the interface.

Now considering only the near field and prescribing the interface as a force boundary, i.e. taking the interface forces as the sum of uncoupled modal forces of the far field, the variational expression of the equations of motion and the force boundary conditions is then given by

$$\int_V \delta\bar{\mathbf{u}}^T (div\boldsymbol{\sigma} - \rho\ddot{\bar{\mathbf{u}}})\ dV - \int_{s_t} \delta\bar{\mathbf{u}}^T (\bar{\mathbf{t}} - \mathbf{t})\ ds = 0$$

where $\boldsymbol{\sigma}$ is the symmetric stress tensor, $\delta\bar{\mathbf{u}}$ are the displacement variations of the near field, and $\bar{\mathbf{t}}$ are the real forces applied in the near field and on the interface.

Integrating the above equation by parts and analyzing the motion in the frequency domain leads to

$$\int_s \delta\bar{\mathbf{u}}^T \boldsymbol{\sigma}\cdot\bar{\mathbf{n}} ds - \int_V tr(\delta\nabla\bar{\mathbf{u}}^T\boldsymbol{\sigma})\ dV + \int_V \delta\bar{\mathbf{u}}^T \omega^2\rho\bar{\mathbf{u}}\ dV - \int_{s_t} \delta\bar{\mathbf{u}}^T (\bar{\mathbf{t}} - \mathbf{t})\ ds = 0 \tag{4.6}$$

in which $\bar{\mathbf{n}}$ is the unit normal vector of the near-field boundary, tr is the trace of the multiplication of two matrices, ω is the excitation frequency, and $s=s_t+s_u$. Since, $\boldsymbol{\sigma}\cdot\bar{\mathbf{n}}=\bar{\mathbf{t}}$, $\delta\bar{\mathbf{u}}=0$ on s_u and $tr(\delta\nabla\bar{\mathbf{u}}^T\boldsymbol{\sigma})=tr(\delta\boldsymbol{\epsilon}\boldsymbol{\sigma})$, where $\boldsymbol{\epsilon}$ is the symmetric strain tensor, Eq. 4.6 can be written as

$$-\int_V tr(\delta\boldsymbol{\epsilon}\ \boldsymbol{\sigma})\ dV + \omega^2\int_V \delta\bar{\mathbf{u}}^T\rho\bar{\mathbf{u}}\ dV + \int_{s_t} \delta\bar{\mathbf{u}}^T\mathbf{t}\ ds = 0 \tag{4.7}$$

Substituting Eq. 4.1 and the finite element approximation of the near field into Eq. 4.7, the equation of motion due to harmonic loadings becomes

$$-\delta\mathbf{U}^T(\int_V \mathbf{B}^T\mathbf{D}\,\mathbf{B}\ dV - \omega^2\int_V \rho\bar{\mathbf{N}}^T\bar{\mathbf{N}}\ dV)\mathbf{U} + \delta\mathbf{U}_b^T\int_{s_t} \bar{\mathbf{N}}^T\mathbf{G}\ ds\ \mathbf{c} = -\delta\mathbf{U}^T\mathbf{P} \tag{4.8}$$

in which $\mathbf{B}$ is the differential of $\bar{\mathbf{N}}$, $\mathbf{D}$ is the 6×6 constitutive matrix, $\mathbf{U}$ is the displacement vector including the degrees of freedom of both the near field and the interface, and $\mathbf{P}$ contains boundary forces other than the interactive forces at the interface. In addition, the boundary s_t

in the above equation is identical to the boundary s_u in Eq. 4.5.

Substituting Eq. 4.5 into Eq. 4.8 and expressing $\mathbf{K}=\int_V \mathbf{B}^T\mathbf{D}\mathbf{B}dV$, $\mathbf{M}=\int_V \rho\bar{\mathbf{N}}^T\bar{\mathbf{N}}dV$ and $\mathbf{S}=\mathbf{K}-\omega^2\mathbf{M}$, one obtains

$$\mathbf{S}\,\mathbf{U} - (\mathbf{K}_{cb}^T\mathbf{K}_c^{-1}\mathbf{K}_{cb})\,\mathbf{U}_b = \mathbf{P} \tag{4.9}$$

or

$$\begin{bmatrix}\mathbf{S}_{nn} & \mathbf{S}_{nb}\\ \mathbf{S}_{nb}^T & \mathbf{S}_{bb}+\mathbf{S}_f\end{bmatrix}\begin{Bmatrix}\mathbf{U}_n\\ \mathbf{U}_b\end{Bmatrix} = \begin{Bmatrix}\mathbf{P}_n\\ \mathbf{P}_b\end{Bmatrix} \tag{4.9a}$$

where subscripts "n" and "b" represent degrees of freedom of the near field and the interface, respectively; $\mathbf{S}_f=-\mathbf{K}_{cb}^T\mathbf{K}_c^{-1}\mathbf{K}_{cb}$ is the far-field impedance matrix corresponding to the nodal displacements at the interface, $\mathbf{P}_n$ and $\mathbf{P}_b$ represent the earthquake input or other loadings applied to the hybrid system. $\mathbf{S}_f$ is a full symmetric matrix provided $\mathbf{K}_c$ is symmetric.

Considering two different modes i and j with respect to a specified frequency ω, the corresponding modal displacements and stresses are $\mathbf{u}_i$, $\mathbf{u}_j$, $\mathbf{t}_i$ and $\mathbf{t}_j$, and the equations of motion for each mode are

$$div\boldsymbol{\sigma}_k + \omega^2\rho\mathbf{u}_k = 0 \qquad\qquad k=i \text{ or } j$$

Multipling the equations of motion of mode j by the displacements of mode i and integrating throughout the far field leads to

$$\int_V \mathbf{u}_i^T(div\boldsymbol{\sigma}_j + \omega^2\rho\mathbf{u}_j)\,dV = 0$$

Integrating by parts gives

$$\int_s \mathbf{u}_i^T\boldsymbol{\sigma}_j\cdot\bar{\mathbf{n}}\,ds - \int_V tr(\nabla\mathbf{u}_i^T\boldsymbol{\sigma}_j)\,dV + \omega^2\int_V \rho\mathbf{u}_i^T\mathbf{u}_j\,dV = 0 \tag{4.10}$$

or

$$\int_s \mathbf{u}_i^T \mathbf{t}_j \, ds - \int_V tr(\boldsymbol{\epsilon}_i \boldsymbol{\sigma}_j) \, dV + \omega^2 \int_V \rho \mathbf{u}_i^T \mathbf{u}_j \, dV = 0 \tag{4.10a}$$

Similarly, by considering the equations of motion of mode i and the displacements of mode j gives

$$\int_s \mathbf{u}_j^T \mathbf{t}_i \, ds - \int_V tr(\boldsymbol{\epsilon}_j \boldsymbol{\sigma}_i) \, dV + \omega^2 \int_V \rho \mathbf{u}_j^T \mathbf{u}_i \, dV = 0 \tag{4.11}$$

Since $tr(\boldsymbol{\epsilon}_i \boldsymbol{\sigma}_j) = tr(\boldsymbol{\epsilon}_j \boldsymbol{\sigma}_i)$, subtracting Eq. 4.10a from Eq. 4.11 gives

$$\int_s \mathbf{u}_i^T \mathbf{t}_j \, ds = \int_s \mathbf{u}_j^T \mathbf{t}_i \, ds \tag{4.12}$$

In Eq. 4.12, s includes both the force boundary s_t and the displacement boundary s_u. However, the entire force boundary of the far field except the interface is free from stress, therefore, only the interface is then involved in the energy integration. In addition,

$$\mathbf{u}_i = \mathbf{n}_i \, c_i$$

$$\mathbf{u}_j = \mathbf{n}_j \, c_j$$

$$\mathbf{t}_i = \mathbf{g}_i \, c_i$$

$$\mathbf{t}_j = \mathbf{g}_j \, c_j$$

; thus, Eq. 4.12 can be further modified to give

$$c_i \int_s \mathbf{n}_i^T \mathbf{g}_j \, ds \, c_j = c_j \int_s \mathbf{n}_j^T \mathbf{g}_i \, ds \, c_i \tag{4.13}$$

or

$$c_i (\mathbf{K}_c)_{ji} c_j = c_j (\mathbf{K}_c)_{ij} c_i \tag{4.13a}$$

Matrix $\mathbf{K}_c$ is then a symmetric matrix.

In the above derivation, it is implicit that no matter how complicated the continuous far field is, the boundary solution method can simplify the problem tremendously if the analytic solution of the far field is available.

C. One Dimensional Wave Propagation

The one dimensional problem can be visualized as uniform plane waves propagating in a multi-dimensional homogeneous space. A simple example is adopted to verify the boundary solution method. In Fig. 4.2a, a periodic loading is applied at one end of a homogeneous bar with the other end extending to infinity. This problem can be solved by the following equation,

$$E\frac{\partial^2 u}{\partial x^2} = \rho\frac{\partial^2 u}{\partial t^2}$$

To satisfy the radiation condition, the displacement is chosen as

$$u(x,t) = Ae^{i\omega(t-\frac{x}{C})} = u(x)\,e^{i\omega t}$$

and the stress is

$$\sigma(x,t) = -E\frac{i\omega}{C}u(x)\,e^{i\omega t}$$

where A is an unknown constant; $C=\sqrt{E/\rho}$ is the longitudinal wave velocity of the bar, E is Young's modulus and ρ is the mass density.

There are two ways to calculate the far-field impedances. Since the wave front is uniform and the cross section of the bar is homogeneous, the impedance may be obtained by simply dividing the stress by the displacement. Therefore,

$$S_f = -\frac{\sigma(x)}{u(x)} = E\frac{i\omega}{C} = i\rho\omega C \tag{4.14}$$

A minus sign in the above equation indicates the opposite directions of the displacement and the stress at the far-field end.

Another method just follows the derivation of the boundary solution procedure. In Fig. 4.2b, the bar is modelled by a few one dimensional finite elements in the near field and the far field is represented by a dashpot attached at the interface point. Referring to Eqs. 4.1 and 4.2 and ignoring $e^{i\omega t}$ for simplicity, the modal and finite element shape functions are, respectively,

$$N(x) = e^{\frac{-i\omega x}{C}}$$

$$M(x) = -E\frac{i\omega}{C}e^{-\frac{i\omega x}{C}}$$

and

$$\bar{N}(x) = 1$$

since there is only one mode corresponding to plane waves.

Substituting the above equations into Eqs. 4.5 and 4.9a, it is seen that.

$$K_c = M(x)N(x)|_{x=x_0} = -E\frac{i\omega}{C}e^{-\frac{i2\omega x_0}{C}}$$

$$K_{cb} = M(x)\bar{N}(x)|_{x=x_0} = -E\frac{i\omega}{C}e^{-\frac{i\omega x_0}{C}} \tag{4.15}$$

$$S_f = -\frac{K_{cb}^2}{K_c} = E\frac{i\omega}{C} = i\rho\omega C$$

The impedance coefficient S_f is exactly the same as in Eq. 4.14; thus, the feasibility of the boundary solution method is verified.

D. Two Dimensional Wave Propagation

The major part of the derivation for the two dimensional inplane wave propagation problems has been shown in Chapter II. Due to the difficulty in handling the radiation of energy into the halfspace, the boundary solution method is restricted to the problems of layered soil

underlain by rigid rock, in which the analytic solution of the far field can be discretized by uncoupled modes. With a lower rigid boundary as shown in Fig. 4.3, only Rayleigh surface waves exist in the inplane motion of the system.

The displacements and stresses at the top surface can be expressed in terms of the stresses at the lower rigid boundary as

$$\begin{Bmatrix} u \\ w \\ \tau_{xz} \\ \sigma_{zz} \end{Bmatrix}_0 = \mathbf{a}_1\ \mathbf{a}_2\ \cdots\ \mathbf{a}_{n-1} \begin{Bmatrix} 0 \\ 0 \\ \tau_{xz} \\ \sigma_{zz} \end{Bmatrix}_n = \begin{bmatrix} t_{13} & t_{14} \\ t_{23} & t_{24} \\ t_{33} & t_{34} \\ t_{43} & t_{44} \end{bmatrix} \begin{Bmatrix} \tau_{xz} \\ \sigma_{zz} \end{Bmatrix}_n \tag{4.16}$$

or

$$\begin{Bmatrix} \mathbf{u} \\ \mathbf{s} \end{Bmatrix}_0 = \begin{bmatrix} \mathbf{T}_1 \\ \mathbf{T}_2 \end{bmatrix} \mathbf{s}_n \tag{4.16a}$$

To calculate the Rayleigh surface modes, the boundary condition of the free surface, $\mathbf{s}_0=0$, is used. For nontrivial $\mathbf{s}_n$, the determinant of $\mathbf{T}_2$ must vanish. This introduces the characteristic function of the Rayleigh surface waves. Within the Rayleigh function, besides the boundary conditions of the free top surface and rigid bottom rock, the assumption of homogeneous and infinite horizontal soil layers is also implied. Consequently, the interface which separates the near and far fields is chosen to be vertical throughout all the layers as shown in Fig. 4.3. Boundary stresses at the vertical interface are different from the stresses employed in the calculation of the transfer matrix, which are σ_{xx} in the x-direction and τ_{xz} in the z-direction. By employing Eqs. 2.2 and 2.7 , σ_{xx} and τ_{xz} in the jth layer at depth z can be written in terms of the unknown constants $\mathbf{A}_j$ as

$$\begin{Bmatrix} \sigma_{xx}(z) \\ \tau_{xz}(z) \end{Bmatrix} = \begin{bmatrix} -G(2\upsilon^2+k_\beta^2) & -G(2\upsilon^2+k_\beta^2) & -i2kG\upsilon' & i2kG\upsilon' \\ i2kG\upsilon & -i2kG\upsilon & -G(2k^2-k_\beta^2) & -G(2k^2-k_\beta^2) \end{bmatrix}_j \mathbf{e}_j'\,\mathbf{A}_j \tag{4.17}$$

in which $\mathbf{e}_j'=diag(\ e^{\upsilon_j(d_j-z)},\ e^{-\upsilon_j(d_j-z)},\ e^{\upsilon_j'(d_j-z)},\ e^{-\upsilon_j'(d_j-z)})$.

Substituting Eq. 2.6 into Eq. 4.17, the displacements and stresses at the vertical interface at any depth may be expressed in terms of the displacements and stresses at the successive lower horizontal interface as

$$\begin{Bmatrix} u(z) \\ w(z) \\ \sigma_{xx}(z) \\ \tau_{xz}(z) \end{Bmatrix} = \begin{bmatrix} -ik & -ik & \nu' & -\nu' \\ -\nu & \nu & -ik & -ik \\ -G(2\nu^2+k_\beta^2) & -G(2\nu^2+k_\beta^2) & -i2kG\nu' & i2kG\nu' \\ i2kG\nu & -i2kG\nu & -G(2k^2-k_\beta^2) & -G(2k^2-k_\beta^2) \end{bmatrix} \mathbf{e}_j' \, \mathbf{E}_j^{-1} \begin{Bmatrix} u \\ w \\ \tau_{xz} \\ \sigma_{zz} \end{Bmatrix}_j$$

$$= \mathbf{f}_j(z) \; \mathbf{Y}_j$$

in which

$$\mathbf{f} = \begin{bmatrix} \frac{2k^2}{k_\beta^2}(CH-CH')+CH' & \frac{ik}{k_\beta^2}(-(2k^2-k_\beta^2)\frac{SH}{\nu}+2\nu' SH') \\ \frac{ik}{k_\beta^2}(-2\nu SH+(2k^2-k_\beta^2)\frac{SH'}{\nu'}) & CH-\frac{2k^2}{k_\beta^2}(CH-CH') \\ \frac{i2kG}{k_\beta^2}(-(2\nu^2+k_\beta^2)CH+(2k^2-k_\beta^2)CH') & \frac{G}{k_\beta^2}(-(2\nu^2+k_\beta^2)(2k^2-k_\beta^2)\frac{SH}{\nu}+4k^2\nu' SH') \\ \frac{G}{k_\beta^2}(-4k^2\nu SH+(2k^2-k_\beta^2)^2\frac{SH'}{\nu'}) & \frac{i2kG}{k_\beta^2}(2k^2-k_\beta^2)(CH-CH') \end{bmatrix}$$

$$\begin{bmatrix} \frac{1}{Gk_\beta^2}(-k^2\frac{SH}{\nu}+\nu' SH') & \frac{ik}{Gk_\beta^2}(CH-CH') \\ \frac{ik}{Gk_\beta^2}(CH-CH') & \frac{1}{Gk_\beta^2}(\nu SH-k^2\frac{SH'}{\nu'}) \\ \frac{ik}{k_\beta^2}((2\nu^2+k_\beta^2)\frac{SH}{\nu}-2\nu' SH') & \frac{(2\nu^2+k_\beta^2)}{k_\beta^2}CH-\frac{2k^2}{k_\beta^2}CH' \\ \frac{2k^2}{k_\beta^2}(CH-CH')+CH' & \frac{ik}{k_\beta^2}(-2\nu SH+(2k^2-k_\beta^2)\frac{SH'}{\nu'}) \end{bmatrix}$$

; while SH_j, SH_j', CH_j and CH_j' are different from the definitions indicated in Eq. 2.8, they are

$$SH_j = \sinh\nu_j(d_j-z) \qquad SH_j' = \sinh\nu_j'(d_j-z)$$

$$CH_j = \cosh\nu_j(d_j-z) \qquad CH_j' = \cosh\nu_j'(d_j-z)$$

Due to the discontinuities at the horizontal interfaces and the undetermined number of layers, an explicit form of the modal displacement-stress vector is difficult to obtain. With the aid of the transfer matrix between the layer interfaces, the displacements and stresses at the vertical interface can be written in terms of the stresses on the rock surface as

$$\begin{Bmatrix} u(z) \\ w(z) \\ \sigma_{xx}(z) \\ \tau_{xz}(z) \end{Bmatrix} = \mathbf{f}_j(z)\ \mathbf{a}_{j+1}\ \cdots\ \mathbf{a}_{n-1} \begin{Bmatrix} 0 \\ 0 \\ \tau_{xz} \\ \sigma_{zz} \end{Bmatrix}_n \tag{4.18}$$

In order to express displacements and stresses as the sum of uncoupled modes, the modal participation factor needs to be chosen. Since the top surface is free from stress, Eq. 4.16 gives

$$\begin{Bmatrix} 0 \\ 0 \end{Bmatrix} = \begin{bmatrix} t_{33}(k_i) & t_{34}(k_i) \\ t_{43}(k_i) & t_{44}(k_i) \end{bmatrix} \begin{Bmatrix} \tau_{xz}{}^i \\ \sigma_{zz}{}^i \end{Bmatrix}_n$$

for the ith Rayleigh mode with wave number k_i.

Either $\tau_{xz}{}^i$ or $\sigma_{zz}{}^i$ can be taken as the unknown factor of mode i. Therefore, if $\alpha_i = \tau_{xz}{}^i$ is chosen,

$$\begin{Bmatrix} \tau_{xz}{}^i \\ \sigma_{zz}{}^i \end{Bmatrix}_n = \begin{Bmatrix} 1 \\ \xi_i \end{Bmatrix} \alpha_i \tag{4.19}$$

where $\xi_i = -\dfrac{t_{33}(k_i)}{t_{34}(k_i)} = -\dfrac{t_{43}(k_i)}{t_{44}(k_i)}$.

Substituting Eq. 4.19 into Eq. 4.18, the ith modal displacements and stresses at the vertical interface at depth z are

$$\begin{Bmatrix} u^i(z) \\ w^i(z) \\ \sigma_{xx}{}^i(z) \\ \tau_{xz}{}^i(z) \end{Bmatrix} = \mathbf{f}_j^i(z)\ \mathbf{a}_{j+1}^i\ \cdots\ \mathbf{a}_{n-1}^i \begin{Bmatrix} 0 \\ 0 \\ 1 \\ \xi_i \end{Bmatrix} \alpha_i \tag{4.20}$$

These modal displacements and stresses will be adopted in Eqs. 4.5 and 4.9a to calculate the far-field impedance matrix for the two dimensional inplane motion. If the soil profile at the right side of the near field is different from the left side, two independent far-field impedance matrices for either side have to be evaluated, because Rayleigh surface waves which propagate in the right region are not the same as in the left region.

E. Axisymmetrical Three Dimensional Wave Propagation

1. General Equations

In the cylindrical coordinate system, the displacements u, v and w in the radial, vertical and circumferential directions, respectively, can be written as

$$\begin{Bmatrix} u \\ v \\ w \end{Bmatrix} = \begin{Bmatrix} \sum_{n=0}^{\infty} (\bar{u}_s^n \cos n\theta + \bar{u}_a^n \sin n\theta) \\ \sum_{n=0}^{\infty} (\bar{w}_s^n \cos n\theta + \bar{w}_a^n \sin n\theta) \\ \sum_{n=0}^{\infty} (-\bar{v}_s^n \sin n\theta + \bar{v}_a^n \cos n\theta) \end{Bmatrix} \tag{4.21}$$

or

$$\begin{Bmatrix} u \\ v \\ w \end{Bmatrix} = \begin{Bmatrix} \sum_n \bar{u}^n \begin{Bmatrix} \cos n\theta \\ \sin n\theta \end{Bmatrix} \\ \sum_n \bar{w}^n \begin{Bmatrix} \cos n\theta \\ \sin n\theta \end{Bmatrix} \\ \sum_n \bar{v}^n \begin{Bmatrix} -\sin n\theta \\ \cos n\theta \end{Bmatrix} \end{Bmatrix} \tag{4.21a}$$

which contain symmetric and antisymmetric components about θ=0 axis. These generalized displacements $\bar{u}$, $\bar{v}$ and $\bar{w}$ are functions of r and z only and do not depend on θ. The purpose of using a minus sign in the sine term for the circumferential displacement is to obtain the same stiffness for both the symmetric and antisymmetric components.

The strain-displacement relations expressed in the cylindrical coordinates are

$$\begin{Bmatrix} \epsilon_{rr} \\ \epsilon_{\theta\theta} \\ \epsilon_{zz} \\ \gamma_{rz} \\ \gamma_{r\theta} \\ \gamma_{\theta z} \end{Bmatrix} = \begin{Bmatrix} \dfrac{\partial u}{\partial r} \\ \dfrac{u}{r}+\dfrac{1}{r}\dfrac{\partial v}{\partial \theta} \\ \dfrac{\partial w}{\partial z} \\ \dfrac{\partial u}{\partial z}+\dfrac{\partial w}{\partial r} \\ \dfrac{1}{r}\dfrac{\partial u}{\partial \theta}+\dfrac{\partial v}{\partial r}-\dfrac{v}{r} \\ \dfrac{1}{r}\dfrac{\partial w}{\partial \theta}+\dfrac{\partial v}{\partial z} \end{Bmatrix} = \begin{Bmatrix} \sum_n \overline{\epsilon_{rr}}^n \begin{cases} \cos n\theta \\ \sin n\theta \end{cases} \\ \sum_n \overline{\epsilon_{\theta\theta}}^n \begin{cases} \cos n\theta \\ \sin n\theta \end{cases} \\ \sum_n \overline{\epsilon_{zz}}^n \begin{cases} \cos n\theta \\ \sin n\theta \end{cases} \\ \sum_n \overline{\gamma_{rz}}^n \begin{cases} \cos n\theta \\ \sin n\theta \end{cases} \\ \sum_n \overline{\gamma_{r\theta}}^n \begin{cases} -\sin n\theta \\ \cos n\theta \end{cases} \\ \sum_n \overline{\gamma_{\theta z}}^n \begin{cases} -\sin n\theta \\ \cos n\theta \end{cases} \end{Bmatrix} \tag{4.22}$$

in which

$$\begin{Bmatrix} \overline{\epsilon_{rr}} \\ \overline{\epsilon_{\theta\theta}} \\ \overline{\epsilon_{zz}} \\ \overline{\gamma_{rz}} \\ \overline{\gamma_{r\theta}} \\ \overline{\gamma_{\theta z}} \end{Bmatrix} = \begin{bmatrix} \dfrac{\partial}{\partial r} & & \\ \dfrac{1}{r} & & -\dfrac{n}{r} \\ & \dfrac{\partial}{\partial z} & \\ \dfrac{\partial}{\partial z} & \dfrac{\partial}{\partial r} & \\ \dfrac{n}{r} & & \left(\dfrac{\partial}{\partial r}-\dfrac{1}{r}\right) \\ & \dfrac{n}{r} & \dfrac{\partial}{\partial z} \end{bmatrix} \begin{Bmatrix} \bar{u} \\ \bar{w} \\ \bar{v} \end{Bmatrix}$$

The symmetric and antisymmetric components of the stresses may also be written as

$$\begin{Bmatrix} \sigma_{rr} \\ \sigma_{\theta\theta} \\ \sigma_{zz} \\ \tau_{rz} \\ \tau_{r\theta} \\ \tau_{\theta z} \end{Bmatrix} = \mathbf{D} \begin{Bmatrix} \epsilon_{rr} \\ \epsilon_{\theta\theta} \\ \epsilon_{zz} \\ \gamma_{rz} \\ \gamma_{r\theta} \\ \gamma_{\theta z} \end{Bmatrix} = \begin{Bmatrix} \sum_n \overline{\sigma_{rr}}^n \begin{cases} \cos n\theta \\ \sin n\theta \end{cases} \\ \sum_n \overline{\sigma_{\theta\theta}}^n \begin{cases} \cos n\theta \\ \sin n\theta \end{cases} \\ \sum_n \overline{\sigma_{zz}}^n \begin{cases} \cos n\theta \\ \sin n\theta \end{cases} \\ \sum_n \overline{\tau_{rz}}^n \begin{cases} \cos n\theta \\ \sin n\theta \end{cases} \\ \sum_n \overline{\tau_{r\theta}}^n \begin{cases} -\sin n\theta \\ \cos n\theta \end{cases} \\ \sum_n \overline{\tau_{\theta z}}^n \begin{cases} -\sin n\theta \\ \cos n\theta \end{cases} \end{Bmatrix} \tag{4.23}$$

where **D** is the 6×6 constitutive matrix of the isotropic and elastic or viscoelastic materials.

The general equations of wave propagation expressed in the cylindrical coordinates are

$$\begin{aligned} \rho \ddot{u} &= (\lambda+2G)\frac{\partial \Delta}{\partial r} - \frac{2G}{r}\frac{\partial \omega_r}{\partial \theta} + 2G\frac{\partial \omega_\theta}{\partial z} \\ \rho \ddot{w} &= (\lambda+2G)\frac{\partial \Delta}{\partial z} - \frac{2G}{r}\frac{\partial (r\omega_\theta)}{\partial r} + \frac{2G}{r}\frac{\partial \omega_r}{\partial \theta} \\ \rho \ddot{v} &= (\lambda+2G)\frac{1}{r}\frac{\partial \Delta}{\partial \theta} - 2G\frac{\partial \omega_r}{\partial z} + 2G\frac{\partial \omega_z}{\partial r} \end{aligned} \tag{4.24}$$

where, λ and G are real or complex Lame's constants depending on the material, $\Delta = \frac{1}{r}\frac{\partial (ru)}{\partial r} + \frac{1}{r}\frac{\partial v}{\partial \theta} + \frac{\partial w}{\partial z}$ is the dilatation, and

$$2\omega_r = \frac{1}{r}\frac{\partial w}{\partial \theta} - \frac{\partial v}{\partial z}$$

$$2\omega_z = \frac{1}{r}\left(\frac{\partial (rv)}{\partial r} - \frac{\partial u}{\partial \theta}\right)$$

$$2\omega_\theta = \frac{\partial u}{\partial z} - \frac{\partial w}{\partial r}$$

are the rotations in r, z and θ directions respectively, and ρ is the mass density.

Sezawa [31] solved Eqs. 4.24 for a homogeneous halfspace by employing the Fourier expansions of the displacements, i.e., Eq. 4.21, as

$$u = \sum_n (A^n k H_n' e^{-\nu z} + B^n \frac{n}{r} H_n e^{-\nu' z} - C^n \nu' H_n' e^{-\nu' z}) \begin{Bmatrix} \cos n\theta \\ \sin n\theta \end{Bmatrix} e^{i\omega t}$$

$$w = \sum_n (-A^n k \nu H_n e^{-\nu z} + C^n k^2 H_n e^{-\nu' z}) \begin{Bmatrix} \cos n\theta \\ \sin n\theta \end{Bmatrix} e^{i\omega t} \tag{4.25}$$

$$v = \sum_n (A^n \frac{n}{r} k H_n e^{-\nu z} + B^n H_n' e^{-\nu' z} - C^n \nu' \frac{n}{r} H_n e^{-\nu' z}) \begin{Bmatrix} -\sin n\theta \\ \cos n\theta \end{Bmatrix} e^{i\omega t}$$

where k is the horizontal wave number, $H_n' = \dfrac{dH_n(kr)}{dr}$, ν and ν' are the same as in Eq. 2.5, A^n, B^n and C^n are constants. Also, $H_n = H_n^{(2)}(kr)$ is the second kind of Hankel's function of order n. H_n and the exponential terms represent waves that propagate away from the source in the r and z directions, respectively.

To write Eq. 4.25 in matrix form, the nth Fourier components of the displacements are

$$\begin{Bmatrix} \bar{u} \\ \bar{w} \\ \bar{v} \end{Bmatrix}^n = \begin{bmatrix} kH_n' & \frac{n}{r}H_n & -\nu' H_n' \\ -k\nu H_n & & k^2 H_n \\ \frac{n}{r}kH_n & H_n' & -\nu' \frac{n}{r} H_n \end{bmatrix} \begin{bmatrix} e^{-\nu z} & & \\ & e^{-\nu' z} & \\ & & e^{-\nu' z} \end{bmatrix} \begin{Bmatrix} A \\ B \\ C \end{Bmatrix}^n \tag{4.26}$$

Owing to the existence of the soil layers, not only the outgoing waves but also the incoming waves in the z direction must be included. Also, the following derivations are applicable to all components of the Fourier expansion, the superscripts "n" and "$\bar{\ }$" will no longer be held for simplicity. Eq. 4.26 is then expanded as

$$\begin{Bmatrix} u \\ w \\ v \end{Bmatrix} = \begin{bmatrix} kH_n' & \frac{n}{r}H_n & -\nu' H_n' \\ -k\nu H_n & & k^2 H_n \\ \frac{n}{r}kH_n & H_n' & -\nu' \frac{n}{r} H_n \end{bmatrix} \begin{bmatrix} e^{-\nu z} & & \\ & e^{-\nu' z} & \\ & & e^{-\nu' z} \end{bmatrix} \begin{Bmatrix} A_1 \\ B_1 \\ C_1 \end{Bmatrix}$$

$$+\begin{bmatrix} kH_n' & \frac{n}{r}H_n & v'H_n' \\ kvH_n & & k^2H_n \\ \frac{n}{r}kH_n & H_n' & v'\frac{n}{r}H_n \end{bmatrix}\begin{bmatrix} e^{vz} & & \\ & e^{v'z} & \\ & & e^{v'z} \end{bmatrix}\begin{Bmatrix} A_2 \\ B_2 \\ C_2 \end{Bmatrix} \tag{4.27}$$

or

$$\begin{Bmatrix} u \\ w \\ v \end{Bmatrix} = \begin{bmatrix} H_n' & & \frac{n}{r}H_n \\ & kH_n & \\ \frac{n}{r}H_n & & H_n' \end{bmatrix}\begin{bmatrix} k & k & & & -v' & v' \\ -v & v & & & k & k \\ & & 1 & 1 & & \end{bmatrix}\mathbf{e}\,\mathbf{A} \tag{4.27a}$$

where $\mathbf{e} = diag(\, e^{-vz},\ e^{vz},\ e^{-v'z},\ e^{v'z},\ e^{-v'z},\ e^{v'z})$ and $\mathbf{A} = (A_1, A_2, B_1, B_2, C_1, C_2)^T$.

2. Transfer Matrix

To set up the transfer matrix between layers, the continuity of displacements and stresses at the layer interface must be satisfied. In cylindrical coordinates the contacted stresses τ_{rz}, σ_{zz} and $\tau_{\theta z}$ may be obtained by Eqs. 4.23 and 4.27. After some adjustments, the displacements and stresses can be written together as

$$\begin{Bmatrix} u \\ w \\ \tau_{rz} \\ \sigma_{zz} \\ v \\ \tau_{\theta z} \end{Bmatrix} = \begin{bmatrix} H_n' & & & & \frac{n}{r}H_n & \\ & kH_n & & & & \\ & & H_n' & & & \frac{n}{r}H_n \\ & & & kH_n & & \\ \frac{n}{r}H_n & & & & H_n' & \\ & & \frac{n}{r}H_n & & & H_n' \end{bmatrix}$$

$$\begin{bmatrix} k & k & -v' & v' & & \\ -v & v & k & k & & \\ -2kGv & 2kGv & G(2k^2-k_\beta^2) & G(2k^2-k_\beta^2) & & \\ G(2k^2-k_\beta^2) & G(2k^2-k_\beta^2) & -2kGv' & 2kGv' & & \\ & & & & 1 & 1 \\ & & & & -Gv' & Gv' \end{bmatrix} \mathbf{e}\,\mathbf{A}' \tag{4.28}$$

or

$$\mathbf{Y} = \mathbf{H}(r) \begin{bmatrix} \mathbf{E}' & \\ & \mathbf{E}'' \end{bmatrix} \mathbf{e}(z)\ \mathbf{A}' = \mathbf{H}(r)\ \mathbf{E}\ \mathbf{e}(z)\ \mathbf{A}' \tag{4.28a}$$

where $\mathbf{A}' = (A_1, A_2, C_1, C_2, B_1, B_2)^T$.

The purpose of rearranging the displacements and stresses in this order is to decouple the characteristic equations of Rayleigh and Love waves.

Shifting the origin of the z axis to the jth horizontal interface, the displacement-stress vector at the jth and (j+1)th interfaces can be obtained by employing the material properties of the jth layer,

$$\mathbf{Y}_j = \mathbf{H}\,\mathbf{E}_j\,\mathbf{A}_j'$$

$$\mathbf{Y}_{j+1} = \mathbf{H}\,\mathbf{E}_j\,\mathbf{e}_j(h_j)\,\mathbf{A}_j' \tag{4.29}$$

The displacements and stresses at the jth interface are then written in terms of the displacements and stresses at the (j+1)th interface as

$$\mathbf{Y}_j = \mathbf{H}\,\mathbf{E}_j\,\mathbf{e}_j^{-1}(h_j)\,\mathbf{E}_j^{-1}\,\mathbf{H}^{-1}\,\mathbf{Y}_{j+1} \tag{4.30}$$

Since $h_j = d_{j+1} - d_j$ is the thickness of the jth layer and $\mathbf{e}$ is a diagonal matrix, the above equation becomes

$$\mathbf{Y}_j = \mathbf{H}\,\mathbf{E}_j\,\mathbf{e}_j(-h_j)\,\mathbf{E}_j^{-1}\,\mathbf{H}^{-1}\,\mathbf{Y}_{j+1} \tag{4.31}$$

or

$$\mathbf{Y}_j = \mathbf{H}\,\mathbf{a}_j\,\mathbf{H}^{-1}\,\mathbf{Y}_{j+1} \tag{4.31a}$$

where

$$\mathbf{a}_j = \mathbf{E}_j\,\mathbf{e}_j(-h_j)\,\mathbf{E}_j^{-1} = \begin{bmatrix} \mathbf{a}_j' & \\ & \mathbf{a}_j'' \end{bmatrix} \tag{4.32}$$

in which

$$\mathbf{a}' = \begin{vmatrix} \frac{2k^2}{k_\beta^2}(CH-CH')+CH' & \frac{k^2}{k_\beta^2}((2k^2-k_\beta^2)\frac{SH}{\upsilon}-2\upsilon' SH') \\ \frac{k}{k_\beta^2}(-2\upsilon SH+(2k^2-k_\beta^2)\frac{SH'}{\upsilon'}) & CH-\frac{2k^2}{k_\beta^2}(CH-CH') \\ G(-\frac{4k^2}{k_\beta^2}\upsilon SH+\frac{(2k^2-k_\beta^2)^2}{k_\beta^2}\frac{SH'}{\upsilon'}) & -\frac{2kG}{k_\beta^2}(2k^2-k_\beta^2)(CH-CH') \\ \frac{2kG}{k_\beta^2}(2k^2-k_\beta^2)(CH-CH') & G(\frac{(2k^2-k_\beta^2)^2}{k_\beta^2}\frac{SH}{\upsilon}-\frac{4k^2}{k_\beta^2}\upsilon' SH') \end{vmatrix}$$

$$\begin{vmatrix} \frac{1}{Gk_\beta^2}(\upsilon' SH'-k^2\frac{SH}{\upsilon}) & -\frac{k}{Gk_\beta^2}(CH-CH') \\ \frac{k}{Gk_\beta^2}(CH-CH') & \frac{1}{Gk_\beta^2}(\upsilon SH-k^2\frac{SH'}{\upsilon'}) \\ \frac{2k^2}{k_\beta^2}(CH-CH')+CH' & \frac{k}{k_\beta^2}(2\upsilon SH-(2k^2-k_\beta^2)\frac{SH'}{\upsilon'}) \\ -\frac{k}{k_\beta^2}((2k^2-k_\beta^2)\frac{SH}{\upsilon}-2\upsilon' SH') & CH-\frac{2k^2}{k_\beta^2}(CH-CH') \end{vmatrix}$$

and

$$\mathbf{a}'' = \begin{bmatrix} CH' & -\frac{SH'}{G\upsilon'} \\ -G\upsilon' SH' & CH' \end{bmatrix}$$

, $\mathbf{a}_j$ is the transfer matrix of the jth layer, and

$$CH = \cosh\upsilon h\,, \qquad CH' = \cosh\upsilon' h$$

$$SH = \sinh\upsilon h\,, \qquad SH' = \sinh\upsilon' h$$

The displacement-stress vector at the top surface can thus be expressed in terms of the displacement-stress vector at the bottom rigid boundary as

$$\mathbf{Y}_0 = \mathbf{H}\,\mathbf{a}_1\,\mathbf{a}_2\,\cdots\,\mathbf{a}_{n-1}\,\mathbf{H}^{-1}\,\mathbf{Y}_n = \mathbf{H}\,\mathbf{T}\,\mathbf{H}^{-1}\,\mathbf{Y}_n \tag{4.33}$$

or

$$\begin{Bmatrix} u \\ w \\ \tau_{rz} \\ \sigma_{zz} \\ v \\ \tau_{\theta z} \end{Bmatrix}_0 = \mathbf{H} \begin{bmatrix} t_{11} & t_{12} & t_{13} & t_{14} & & \\ t_{21} & t_{22} & t_{23} & t_{24} & & \\ t_{31} & t_{32} & t_{33} & t_{34} & & \\ t_{41} & t_{42} & t_{43} & t_{44} & & \\ & & & & t_{55} & t_{56} \\ & & & & t_{65} & t_{66} \end{bmatrix} \mathbf{H}^{-1} \begin{Bmatrix} u \\ w \\ \tau_{rz} \\ \sigma_{zz} \\ v \\ \tau_{\theta z} \end{Bmatrix}_n \tag{4.33a}$$

If there is no slippage at the surface of the rigid rock, the stresses at the top surface are

$$\begin{Bmatrix} \tau_{rz} \\ \sigma_{zz} \\ \tau_{\theta z} \end{Bmatrix}_0 = \mathbf{H}' \begin{bmatrix} t_{33} & t_{34} & \\ t_{43} & t_{44} & \\ & & t_{66} \end{bmatrix} \mathbf{H}'^{-1} \begin{Bmatrix} \tau_{rz} \\ \sigma_{zz} \\ \tau_{\theta z} \end{Bmatrix}_n = \mathbf{H}'\,\mathbf{T}'\,\mathbf{H}'^{-1} \begin{Bmatrix} \tau_{rz} \\ \sigma_{zz} \\ \tau_{\theta z} \end{Bmatrix}_n \tag{4.34}$$

where

$$\mathbf{H}' = \begin{bmatrix} H_n' & & \frac{n}{r}H_n \\ & kH_n & \\ \frac{n}{r}H_n & & H_n' \end{bmatrix}$$

If the top surface is free from stress, the nontrivial stresses at the rigid boundary is guaranteed by equating the determinant of $\mathbf{H}'\,\mathbf{T}'\,\mathbf{H}'^{-1}$ to zero. Since the determinant must vanish for arbitrary r, the possible solutions are restricted to k=0 or to the case where the determinant of $\mathbf{T}'$ equals to zero. However, k=0 representing standing waves occurs only when the excitation frequency is equal to one of the natural frequencies of the layered system and when the soil is purely elastic. It is also a trivial solution. Therefore, the characteristic values of k come from

$$t_{33}\ t_{44} - t_{34}\ t_{43} = 0 \tag{4.35}$$

and

$$t_{66} = 0 \tag{4.36}$$

The solutions of Eq. 4.35 represent the wave numbers of the circular Rayleigh waves with respect to a specific frequency ω. Similarly, Eq. 4.36 generates the wave numbers of the circular Love waves. Although, the derivation of Rayleigh functions is slightly different between the two and three dimensional problems, i.e., $i=\sqrt{-1}$ exists in the transfer matrix of the two dimensional case, the final characteristic equations are the same. Therefore, the wave numbers of Rayleigh surface modes are identical in both cases.

3. Modal Stresses and Displacements

The derivation of the transfer matrix simply depends upon the boundary conditions of the top free surface and the bottom rigid rock; therefore, in order to use boundary solution method, the interface between the near and far fields is again chosen vertically throughout all the layers as shown in Fig. 4.3.

The boundary stresses at the vertical interface in the cylindrical coordinates are σ_{rr}, τ_{rz} and $\tau_{r\theta}$. Using Eqs. 4.22, 4.23 and 4.27, the nth Fourier components of the boundary stresses are obtained as

$$\begin{Bmatrix} \sigma_{rr} \\ \tau_{rz} \\ \tau_{r\theta} \end{Bmatrix} = \left(\begin{bmatrix} & kH_n \\ H_n' & \frac{n}{r}H_n \end{bmatrix} \begin{bmatrix} -2kGv & 2kGv & G(2k^2-k_\beta^2) & G(2k^2-k_\beta^2) & \\ -G(2v^2+k_\beta^2) & -G(2v^2+k_\beta^2) & 2kGv' & -2kGv' & \\ & & & & -Gv' \quad Gv' \end{bmatrix} \right.$$

$$+\begin{bmatrix} (-\frac{H_n'}{r}+\frac{n^2}{r^2}H_n) & (\frac{n}{r}H_n'-\frac{n}{r^2}H_n) \\ (\frac{n}{r}H_n'-\frac{n}{r^2}H_n) & (-\frac{H_n'}{r}+(\frac{n^2}{r^2}-\frac{k^2}{2})H_n) \end{bmatrix} \begin{bmatrix} 2kG & 2kG & -2Gv' & 2Gv' \\ & & 2G & 2G \end{bmatrix} \mathbf{e}\,\mathbf{A}' \quad (4.37)$$

or

$$\bar{\mathbf{s}} = (\mathbf{H}_1\,\mathbf{F}_1 + \mathbf{H}_2\,\mathbf{F}_2)\,\mathbf{e}\,\mathbf{A}' \quad (4.37a)$$

Eliminating the common factor $\mathbf{A}'$ in Eqs. 4.29 and 4.37, σ_{rr}, τ_{rz} and $\tau_{r\theta}$ can also be written in terms of the displacement-stress vector at the rigid rock. Therefore, the boundary stresses in the jth layer at depth z become

$$\bar{\mathbf{s}}_j(z) = (\mathbf{H}_1\,\mathbf{F}_1 + \mathbf{H}_2\,\mathbf{F}_2)_j\,\mathbf{e}_j(d_j-z)\,\mathbf{E}_j^{-1}\,\mathbf{a}_{j+1}\,\cdots\,\mathbf{a}_{n-1}\,\mathbf{H}^{-1}\,\mathbf{Y}_n \quad (4.38)$$

where $\mathbf{e}(d-z) = diag(\,e^{v(d-z)},\ e^{-v(d-z)},\ e^{v'(d-z)},\ e^{-v'(d-z)},\ e^{v'(d-z)},\ e^{-v'(d-z)})$.

To write the above equation explicitly, $\mathbf{F}_i$, $\mathbf{e}$ and $\mathbf{E}^{-1}$ are multiplied together as

$$\mathbf{F}_1\,\mathbf{e}\,\mathbf{E}^{-1} = \begin{bmatrix} \frac{G}{k_\beta^2}(-4k^2vSH+(2k^2-k_\beta^2)^2\frac{SH'}{v'}) & -\frac{2kG}{k_\beta^2}(2k^2-k_\beta^2)(CH-CH') \\ \frac{2kG}{k_\beta^2}(-(2v^2+k_\beta^2)CH+(2k^2-k_\beta^2)CH') & \frac{G}{k_\beta^2}(-(2k^2-k_\beta^2)(2v^2+k_\beta^2)\frac{SH}{v}+4k^2v'SH') \end{bmatrix}$$

$$\begin{bmatrix} \frac{2k^2}{k_\beta^2}(CH-CH')+CH' & \frac{k}{k_\beta^2}(2vSH-(2k^2-k_\beta^2)\frac{SH'}{v'}) & \\ \frac{k}{k_\beta^2}((2v^2+k_\beta^2)\frac{SH}{v}-2v'SH') & \frac{1}{k_\beta^2}((2v^2+k_\beta^2)CH-2k^2CH') & \\ & & -Gv'SH' \quad CH' \end{bmatrix}$$

and

$$\mathbf{E}_2\ \mathbf{e}\ \mathbf{E}^{-1} = \begin{bmatrix} 2G\left(\frac{2k^2}{k_\beta^2}(CH-CH')+CH'\right) & \frac{2kG}{k_\beta^2}\left((2k^2-k_\beta^2)\frac{SH}{\upsilon}-2\upsilon' SH'\right) \\ \frac{2}{k_\beta^2}(\upsilon' SH'-k^2\frac{SH}{\upsilon}) & -\frac{2k}{k_\beta^2}(CH-CH') \\ & 2GCH' \end{bmatrix}$$

$$\begin{bmatrix} & \\ & \\ -2\frac{SH'}{\upsilon'} & \end{bmatrix}$$

where SH, SH', CH and CH' are functions of z as in Eq. 4.18.

Due to the discontinuity between different layers, the modal shape functions of displacements and stresses cannot be shown explicitly. However, the transfer matrix, Eq. 4.32, corresponding to each layer plays an important role in the calculation of the displacements and stresses at any point on the vertical interface.

It is necessary to choose modal participation factors of the Rayleigh and Love modes before determining the corresponding displacement and stress functions. The characteristic equations corresponding to the Rayleigh and Love waves have been shown in Eqs. 4.35 and 4.36, respectively. Owing to the decoupling of the Rayleigh and Love waves, the boundary displacements and stresses corresponding to different kinds of surface modes can be evaluated individually.

If the ith mode of the Rayleigh wave number is substituted into Eq. 4.34, one obtains

$$\begin{bmatrix} t_{33}(k_i) & t_{34}(k_i) & \\ t_{43}(k_i) & t_{44}(k_i) & \\ & & t_{66}(k_i) \end{bmatrix} \mathbf{H}'^{-1} \begin{Bmatrix} \tau_{rz} \\ \sigma_{zz} \\ \tau_{\theta z} \end{Bmatrix}_n = \begin{Bmatrix} 0 \\ 0 \\ 0 \end{Bmatrix} \tag{4.39}$$

The numerical values of the stresses at rigid rock are not required; therefore, they may be combined with $\mathbf{H}'^{-1}$ to give

$$\begin{bmatrix} t_{33}(k_i) & t_{34}(k_i) & \\ t_{43}(k_i) & t_{44}(k_i) & \\ & & t_{66}(k_i) \end{bmatrix} \begin{Bmatrix} \alpha_i \\ \beta_i \\ \eta_i \end{Bmatrix} = \begin{Bmatrix} 0 \\ 0 \\ 0 \end{Bmatrix}$$

Since $t_{66}(k_i) \neq 0$ and $t_{33}(k_i)\ t_{44}(k_i) - t_{34}(k_i)\ t_{43}(k_i) = 0$ with respect to the Rayleigh wave number k_i, the above equation can be simplified to

$$\begin{bmatrix} t_{33}(k_i) & t_{34}(k_i) & \\ t_{43}(k_i) & t_{44}(k_i) & \\ & & t_{66}(k_i) \end{bmatrix} \begin{Bmatrix} 1 \\ \xi_i \\ 0 \end{Bmatrix} \alpha_i = \begin{Bmatrix} 0 \\ 0 \\ 0 \end{Bmatrix} \tag{4.40}$$

in which $\xi_i = -\dfrac{t_{33}(k_i)}{t_{34}(k_i)} = -\dfrac{t_{43}(k_i)}{t_{44}(k_i)}$, and α_i is the unknown modal participation factor of the ith Rayleigh mode. Similarly, if k_j is the wave number of the jth Love mode, Eq. 4.39 becomes

$$\begin{bmatrix} t_{33}(k_j) & t_{34}(k_j) & \\ t_{43}(k_j) & t_{44}(k_j) & \\ & & t_{66}(k_j) \end{bmatrix} \begin{Bmatrix} 0 \\ 0 \\ 1 \end{Bmatrix} \gamma_j = \begin{Bmatrix} 0 \\ 0 \\ 0 \end{Bmatrix} \tag{4.41}$$

, since $t_{33}(k_j)\ t_{44}(k_j) - t_{34}(k_j)\ t_{43}(k_j) \neq 0$. γ_j is the unknown modal participation factor of the jth Love mode. When choosing α_i and γ_j as the modal participation factors of the Rayleigh and Love modes, respectively, the corresponding displacements and stresses can be determined by Eqs. 4.33 and 4.38 after substituting for $\mathbf{H}^{-1}\ \mathbf{Y}_n$ using $(0, 0, 1, \xi_i, 0, 0)^T$ for the Rayleigh modes and $(0, 0, 0, 0, 0, 1)^T$ for the Love modes. Since the calculation of the Rayleigh and Love waves can be separated, it is not necessary to evaluate the whole 6×6 transfer matrix for each wave mode. The calculation of the modal displacements and stresses of the Rayleigh waves requires only the $\mathbf{E}'$ of Eq. 4.28a and $\mathbf{a}'$ of Eq. 4.31a. Similarly, only $\mathbf{E}''$ and $\mathbf{a}''$ are required for the calculation of the Love waves.

The final modal displacements and stresses of the nth Fourier components at depth z on the vertical interface can be written as

$$\begin{Bmatrix} u \\ w \\ \sigma_{rr} \\ \tau_{rz} \\ v \\ \tau_{r\theta} \end{Bmatrix} = \begin{bmatrix} H_n' & & kH_n & \\ & kH_n & & \\ 2G(-\frac{H_n'}{r}+\frac{n^2}{r^2}H_n) & & & kH_n \\ & & H_n' & \\ \frac{n}{r}H_n & & & \\ 2G(\frac{n}{r}H_n'-\frac{n}{r^2}H_n) & & & \end{bmatrix} \begin{Bmatrix} r_1 \\ r_2 \\ r_3 \\ r_4 \end{Bmatrix} \tag{4.42}$$

for the Rayleigh waves and as

$$\begin{Bmatrix} u \\ w \\ \sigma_{rr} \\ \tau_{rz} \\ v \\ \tau_{r\theta} \end{Bmatrix} = \begin{bmatrix} \frac{n}{r}H_n & \\ 2G(\frac{n}{r}H_n'-\frac{n}{r}H_n) & \\ & \frac{n}{r}H_n \\ H_n' & \\ 2G(-\frac{H_n'}{r}+(\frac{n^2}{r^2}-\frac{k^2}{2})H_n) & \end{bmatrix} \begin{Bmatrix} l_1 \\ l_2 \end{Bmatrix} \tag{4.43}$$

for the Love waves. r_i and l_j are functions of the specific Rayleigh and Love wave numbers, respectively, and depth z. They are calculated by employing the previous equations such as Eqs. 4.31, 4.38, 4.40 and 4.41. In addition, r_j and l_j are independent of the order of the Fourier component. The computational effort is thus greatly reduced if a large number of the Fourier components are required to simulate the general motion of the near-field. Using Eqs. 4.42 and 4.43, the boundary displacement and stress formulations for the axisymmetrical three dimensional problems are found. These equations are used in the boundary solution method to generate the far-field impedance matrix as required for a soil-structure interaction analysis.

In the axisymmetrical three dimensional problems, there are some interesting observations to be noted. If an axisymmetrical structure is in simple torsional motion, all displacements and stresses in Eq. 4.43, except v and $\tau_{r\theta}$, are zero. The corresponding far-field impedance matrix can be obtained completely by employing Eq. 4.43 with n=0, which means

that only the Love waves will radiate energy into the far field. If the same structure is subjected to symmetrical vertical loading, only the Rayleigh waves will carry energy away from the near field. On the contrary, the far-field impedance matrix can be obtained by choosing n=0 in Eq. 4.42; however, Eq. 4.43 is no longer adopted to ensure that v and $\tau_{r\theta}$ are zero. If more Fourier components are needed to simulate the structural dynamic behavior, n is greater than zero. In this case, both the Rayleigh and Love waves are responsible for transmitting energy through the interface between the near and far fields.

The numerical computation of the far-field impedance matrix can be reduced using the characteristics of matrix $\mathbf{K}_c$. In matrix $\mathbf{K}_c$, the elements corresponding to two different Love modes always vanish. Thus, if only Love waves are present, $\mathbf{K}_c$ becomes a diagonal matrix. To prove this advantage, two different Love modes i and j are considered. Substitution of the corresponding displacement and stress functions into Eq. 4.5 leads to

$$(\mathbf{K}_c)_{ij} = \int_s (\sigma_{rr_i}\, u_j + \tau_{r\theta_i}\, v_j)\; ds = \int_s (\sigma_{rr_j}\, u_i + \tau_{r\theta_j}\, v_i)\; ds = (\mathbf{K}_c)_{ji}$$

in which $ds = r_0 d\theta\, dz$ for the axisymmetrical problems, r_0 is a constant, and the integrations with respect to θ and z are independent.

Employing Eq. 4.43, the above equation becomes

$$\alpha\pi \int_z [2G(\frac{n}{r_0}H_n' - \frac{n}{r_0^2}H_n)_i 1_{1_i} (\frac{n}{r_0}H_n)_j 1_{1_j} + 2G(-\frac{H_n'}{r_0} + (\frac{n^2}{r_0^2} - \frac{k_i^2}{2})H_n)_i 1_{1_i} (H_n')_j 1_{1_j}]\; dz$$

$$= \alpha\pi \int_z [2G(\frac{n}{r_0}H_n' - \frac{n}{r_0^2}H_n)_j 1_{1_j} (\frac{n}{r_0}H_n)_i 1_{1_i} + 2G(-\frac{H_n'}{r_0} + (\frac{n^2}{r_0^2} - \frac{k_j^2}{2})H_n)_j 1_{1_j} (H_n')_i 1_{1_i}]\, dz$$

or

$$W_{ij} \int_z 1_{1_i} 1_{1_j} dz = W_{ji} \int_z 1_{1_i} 1_{1_j} dz$$

where $W_{ij} = 2G\alpha\pi[(\frac{n}{r_0}H_n' - \frac{n}{r_0^2}H_n)_i (\frac{n}{r_0}H_n)_j + (-\frac{H_n'}{r_0} + (\frac{n^2}{r_0^2} - \frac{k_i^2}{2})H_n)_i (H_n')_j]$, α =1 or 2

depending on the Fourier component number n, and H_n' and H_n are functions of k and r_0 only.

Since W_{ij} is not necessarily equal to W_{ji}, the only way to satisfy the above equation is to require that $\int_z l_{1_i} l_{1_j} dz=0$. In this case, $(\mathbf{K}_c)_{ij}$ and $(\mathbf{K}_c)_{ji}$ will vanish. A similar condition can be found in two dimensional antiplane motions. However, this numerical evaluation advantage does not exist if the off-diagonal entries are related to the Rayleigh waves.

F. Numerical Results

1. Wave Number, Numerical Integration and Near-Field Model

Because the lower boundary is taken to be rigid, the response of undamped structures tends toward infinity at resonance when the soil is elastic. It is therefore practical to include some internal damping in the soil system to reduce the peak values of response so that more realistic behavior of the soil can be obtained. Results shown later are calculated using the constant hysteretic model, i.e. Eq. 2.33.

It is necessary to determine the wave numbers of the Rayleigh and Love modes before evaluating the boundary integration of Eq. 4.5. The characteristic equations of Rayleigh and Love waves have been shown in Eqs. 4.35 and 4.36, respectively. They are complex-valued transcendental functions. In general, the roots of these nonlinear equations cannot be evaluated straightforward. They usually must be found by a numerical searching procedure with good initial approximations. The nature of complex value of these functions further complicates the calculation. These difficulties can however be overcome by employing Muller's method [32], which can find any prescribed number of roots, real or complex, of arbitrary functions efficiently. Muller's method, which is an extension of the secant method, approximates a root using a parabola which goes through three existing points. If the roots are real, this situation may be pictured graphically as in Fig. 4.4. The process is then repeated using three out of four known points as basic approximations. Muller's method is iterative, converges almost

quadratically in the vicinity of the root, and does not require the evaluation of the derivative of the function. To avoid the repeated detection of the same root during iteration, all known roots should be factored out of the function. Another advantage of the Muller's method is that only a rough initial approximation of the root is needed.

Since the Rayleigh and Love equations are even functions of wave number k, if k_m is one root of either one of them, $-k_m$ should be another root. In addition, in the development of the far-field impedance matrix, only those modes which decay or transmit energy in the positive x or r-direction are included. Therefore,if $k=\alpha+i\beta$ is a modal wave number, only modes with negative β values need be involved. If $\beta=0$, which occurs in the elastic case, only modes with positive wave number are chosen in the calculation. Although the number of surface modes in the system of soil layers over rigid boundary is infinite, it is not necessary to include all of them in the calculation. Since surface waves dissipate energy in the path of propagation, the required number of surface modes can be determined by considering their individual contributions to the dissipation of energy from the near field.

Gaussian quadrature is always a good selection for finite domain integration. The evaluation of the boundary integral can be achieved by using Gauss-Legendre integration along each element boundary at the interface. Since transcendental functions are involved, the required number of quadrature points needs to be determined numerically.

The quadratic 9-node element is again selected for the near field because of its accuracy and stability in wave propagation problems. Although, the dimension chosen for the 9-node element must be no greater than 1/4 of the shortest shear wave length for which accuracy of representation is required, its selection here is based on the study of one dimenaional waves propagating through a semi-infinite rod. For the two dimensional inplane and three dimensional axisymmetric problems. the corresponding element size will be investigated subsequently.

2. Two Dimensional Problems

The vibration of an infinite rigid strip over a single-layer system is considered to investigate the accuracy and efficiency of the boundary solution method. In Fig. 4.5, three different meshes with 3, 4 and 6 elements at the vertical interface are used and 6 quadrature points are applied along each element. The nondimensional frequency, $a_0=\omega a/C_s$, is used in the calculation over the range 0.0 to π, where a is the halfwidth of the plate and C_s is the shear wave velocity of the top layer. Therefore, the element dimensions of the 3 meshes shown corresponding to $a_0=\pi$ are 1/3, 1/4 and 1/6 of its shear wave length, respectively.

The calculated plate compliances are shown in Figs. 4.6 to 4.8 and are compared with the solutions evaluated by Waas' semi-analytic transmitting boundary in [33]. Good agreement is observed between them. The very small differences shown may come from the different finite element discretizations used in the near field by the two methods. Results using different finite element meshes, i.e. 3, 4 and 6 elements at interface, are also compared. The maximium error observed between the coarse mesh, 1/3, and the fine mesh, 1/6, is in the rocking response, which is less than 4%. In other responses the difference is lower than 1%. The bigger error in the rocking response is possibly due to the fact that the stress variation under the rigid plate in rocking motion cannot be sufficiently approximated using only a few, less than 3, elements. It is therefore concluded that 1/3 of the shortest shear wave length considered can be used as the element dimension with the errors of solution being limited to 4%.

Although 1/3 of the wave length as the element dimension is satisfactory, 1/4 is used conservatively to investigate other important factors such as required quadrature points along each element boundary at the interface and the necessary number of surface modes in the far field.

In Fig. 4.9, results based on 3, 4 and 6 quadrature points along each element at the interface are calculated. Since the differences between them are difficult to resolve from the figures, only one set of data is plotted. Therefore, if the element dimension is satisfied by the wave length requirement, integration by 3 quadrature points along each element boundary can bring

very satisfactory result.

The number of modes required is another important factor, which dominates the computational effort needed to generate the far-field impedance matrix. In the two dimensional inplane motion, there is a common factor e^{-ikx} in both the displacement and stress functions. If $k=\alpha-i\beta$ is chosen, e^{-ikx} becomes $e^{-\beta x}\ e^{-i\alpha x}$, where $e^{-i\alpha x}$ represents the wave propagating with horizontal wave length $2\pi/\alpha$ and $e^{-\beta x}$ is a decay factor which represents the attenuation of the wave amplitude. If the factor $e^{-\beta x_0}$ of a specific surface mode at distance x_0 is very small, it may be considered that this mode has already dissipated most of its energy before reaching the boundary common to the near and far fields so that it can be ignored in the calculation. To investigate the necessary number of wave modes, the interface is located at a nondimensional distance $x_0/a=1.50$ from the central axis. Results including surface modes with the largest β limited to 5.0, 8.0 and 10.0 are calculated. The differences between them are less than 0.5%. The corresponding numbers of Rayleigh modes used in the above analysis are listed in Table 4.1 for $a_0=0.05\pi$ and $a_0=\pi$, respectively. The numbers of modes for medium frequencies are adjusted between values corresponding to the above two frequencies. In Table 4.1, it is shown that the solution can be obtained accurately using only a few modes. The freedom of choosing the number of modes shows the flexibility of the boundary solution method. Further reduction of modes is possible; however, the computational cost paid for the far-field impedance calculations is already minor compared to the cost paid for the near-field finite element calculation in the soil-structure interaction analysis.

The solution calculated by the boundary solution method is also compared with the solution of the proposed stress model under the plate in Chapter II. A very good agreement between them is observed in Fig. 4.10. Again, the biggest error is in the rocking response for the case of coarse finite element discretization in the near field. However, this error is within 8%.

3. Axisymmetrical Three Dimensional Problems

The modal displacement and stress functions of Eqs. 4.42 and 4.43 are employed in the boundary solution method to evaluate the behavior of a simple circular disk resting on a single-layer system. Since there is no available analytic solution, the impedance instead of the compliance of the circular disk calculated by Kausel's semi-analytic transmitting boundary [33] is used for comparison.

Similar investigations to those previously described for the two dimensional problems, which consider element dimension, quadrature points and number of modes, are pursued for nondimensional frequencies $a_0=\omega a/C_s$ in the range 0.0 to 2.0π, in which a is the radius of the circular disk. The elements chosen have dimensions of 1/2, 1/3 and 1/4 of the shear wave length for $a_0=2.0\pi$ as shown in Fig. 4.11. In Figs. 4.12 to 4.15, results of different finite element meshes are shown and compared with the solution calculated by Kausel's semi-analytic method. The agreement is very good for nondimensional frequencies as high as $a_0=1.5\pi$. For higher frequencies, the solutions based on an element size of 1/2 of the shear wave length for $a_0=2.0\pi$ become worse, which means that the corresponding finite element mesh in the near field is unable to transmit waves with frequencies higher than $a_0=1.5\pi$. However, the solutions using element sizes of 1/3 and 1/4 of the shear wave length for $a_0=2.0\pi$ are quite satisfactory. There is a peak shift which occurs in the high frequency range between solutions by the boundary solution method and the semi-analytic method. This discrepancy may come from the different finite element discretizations at the interface, where it is approximated by two-node linear elements in the semi-analytic method and by the more efficient quadratic elements in the boundary solution method. In addition, the peak shift is more significant in the torsional and translational motions than in the vertical and rocking motions. This is because the behavior of the first two motions is governed by the shear waves, while the latter two are governed by the longer dilatational waves.

Solutions using 3, 4 and 6 quadrature points along an element boundary at the interface have been calculated. The differences between them are not obvious in Figs. 4.16 and 4.17. A

similar conclusion, as in the two dimensional problems, is reached. If the element dimension is less than 1/3 of the shear wave length of the highest frequency considered, 3-points integration along an element boundary can produce very good results.

Table 4.2 shows the numbers of the Rayleigh and Love waves employed for a_0=0.1π and a_0=2.0π corresponding to the largest β= 5.0, 8.0 and 10.0, respectively, where r_0/a=1.333 is chosen. The differences between the results using different β values are also negligible, i.e. less than 0.5%. Therefore, only a few Rayleigh and Love modes are required in the far field to give a very accurate solution. The numbers of surface modes for medium frequencies are between the two numbers corresponding to a_0=0.1π and 2.0π respectively.

Moreover, because the 9-node ring elements are used to approximate the near field in the axisymmetrical problems, the agreement between the solutions using different finite element meshs in the case of a circular disk is not as good as that described previously for the two dimensional rigid strip, where 9-node planar elements were employed.

4. Comparison with Semi-Analytic Method

There are some advantages in using the boundary solution method over the semi-analytic transmitting boundaries introduced by Waas and Kausel.

(1) No eigenvalue solution is required in using the boundary solution method; only the modal wave numbers need to be determined by the Muller's method.

(2) The computational effort required is less. In the boundary solution method, the major operations necessary are tm^2n to generate $\mathbf{K}_c$ and $\mathbf{K}_{cb}$, $m^3/6$ for LU decomposition of $\mathbf{K}_c$, m^2n for $\mathbf{K}_c^{-1}\,\mathbf{K}_{cb}$, and mn^2 to generate $\mathbf{S}_f$; in which t depends on the operations required to calculate the transfer matrices of Eqs. 4.20 and 4.31, m is the number of modes employed, and n is the degrees of freedom on the interface. Also, m is usually small comparing with n.

The total operations required for the semi-analytic method are pn^2 for the solution of the eigenvalue problem and for some intermediate manipulations and qn^3 to generate

the impedance matrix, where q is greater than 1, p is usually a large number which depends dominantly on the iterations required to solve the quadratic complex-valued eigenvalue problems. It is therefore concluded that the computer cost to generate the far-field impedance marix increases quadratically by the boundary solution method and cubically by the semi-analytic method as n increases.

(3) It is not necessary to recalculate the modal wave numbers in the boundary solution method if a different finite element mesh is used in the near field. However, all calculations must be repeated when using the semi-analytic method.

(4) Any kind of element may be applied in the near field without increasing the computational effort in the boundary solution method. However, the use of sophisticated elements along the interface, e.g. quadratic element, will signifcantly increase the cost of computation in the semi-analytic method. This increase is mainly due to the required solution of the eigenvalue problems.

(5) In the boundary solution method, the selection of the number of surface modes is flexible. In the semi-analytic method, all eigenvectors are required to ensure the inversion of the matrix of eigenvectors.

5. Remarks

If the soil is elastic and if the excitation frequency is over the first natural frequency of the system, there is a finite number of real modes, i.e. their wave numbers are real. After introducing damping in the system, these real modes switch to damped modes but with relatively small imaginary parts, β. It is important to include all these modes in the calculation of the far-field impedance matrix, because most energy is carried away from the near field by them.

The truncation error mentioned in Chapter II exists in the calculation of the Rayleigh wave numbers. The same procedure described in that chapter must be applied in finding the Rayleigh wave numbers. However, the truncational problem never occurs in the calculations of

Love wave numbers [21] and the far-field impedance matrix.

V. CONCLUSIONS AND RECOMMENDATIONS

Based on the numerical results presented herein, several conclusions can be drawn:

1. The far-field impedances as generated by the system identification method for the case of a single-layer halfspace and by the boundary solution method for the case of multiple layers having a rigid lower boundary can be used effectively and efficiently in the hybrid modelling of soil-structure interaction.
2. The continuous impedance functions for the single-layer halfspace should be applied within the range $2.25 < R/a < 4.5$.
3. The formulation of the boundary solution method is independent of the near field. Therefore, the dynamic behavior of an arbitrary semi-buried structure can be analyzed and the interface between the near and far fields can be placed as close as possible to the structure.
4. The dimension of 9-node element for wave propagation problems must be no greater than 1/3 of the shortest shear wave length considered.
5. In the boundary solution method, a few modes of surface waves and the 3-point Gaussian quadrature along a finite element boundary suffice to obtain the correct far-field impedance matrix.
6. To calculate the far-field impedance matrix for the case of layers of soil on rigid rock, it is more advantageous to use the boundary solution method than the semi-analytic method introduced by Waas [15] and Kausel [16].

Both methods presented herein for finding far-field impedances as used in the hybrid model can be extended to accommodate more sophisticated problems. The following studies are recommended:

1. The continuous far-field impedance functions distributed along a semi-spherical boundary for three dimensional problems involving a single-layer halfspace can be obtained by the system identification method by involving an additional impedance component on the interface in the circumferential direction.

2. There is a disadvantage in the boundary solution method for deep soil deposits due to the large number of finite elements needed in the near field. However, a hyperelement approach, as described in Refs. 33 and 34, may be substituted for the lower region of the near field to greatly reduce the degrees of freedom. The boundary solution technique or Ritz vectors [35] may be used in defining the hyperelement.

3. The boundary solution method can be extended to solve the general three dimensional soil-structure interaction problem, in which a small cylinder discretized by the solid finite elements is chosen to model the near field. The displacements and stresses in the far field can be approximated by adopting a finite number of Fourier components [36]. The generalized far-field impedance matrix corresponding to the degrees of freedom on the cylindrical surface can then be obtained.

4. If only surface waves propagating in the system of soil layers with a rigid lower boundary are considered as the earthquake excitation to the structures, a formulation which is similar to the boundary solution method can be derived to find the consistent earthquake input to the near field. In this formulation, both the incoming and outgoing wave effects must be included in the displacements and stresses of the far field.

REFERENCES

1. Bycroft, G. N., "Forced Vibrations of a Rigid Circular Plate on a Semi-Infinite Elastic Space or on an Elastic Stratum," *Philosophical Transactions, Royal Society of London*, 327-368, 1956.

2. Luco, J. E. and Westmann, R. A., "Dynamic Response of Circular Footings," *Journal of the Engineering Mechanics Division*, ASCE, Vol. 97, No. EM5, 1381-1395, 1971.

3. Luco, J. E., "Impedance Functions for a Rigid Foundation on a Layered Medium," *Nuclear Engineering* and *Design*, Vol. 31, 204-217, 1974.

4. Luco, J. E., "Vibrations of a Rigid Disc on a Layered Viscoelastic Medium," *Nuclear Engineering* and *Design*, Vol. 36, No. 3, 325-340, 1976.

5. Robertson, I. A., "Forced Vertical Vibration of a Rigid Circular Disc on a Semi-Infinite Elastic Solid," *Proceedings, Cambridge Philosophical Society*, 62, 547-553, 1966.

6. Gazetas, G. C. and Roësset, J. M., "Forced Vibrations of Strip Footings on Layered Soils," *Methods of Structural Analysis*, ASCE, Vol. 1, 115-131, 1976.

7. Karasudhi, P., Keer, L. M. and Lee, S. L., "Vibratory Motion of a Body on an Elastic Half Plane," *Journal of Applied Mechanics*, ASME, Vol. 35, No. E4, 697-705, 1968.

8. Luco, J. E., and Westmann, R. A., "Dynamic Response of a Rigid Footing Bonded To an Elastic Halfspace," *Journal of Applied Mechanics*, ASME, Vol. 39, No. E2, 527-534, 1972.

9. Oien, M. A., "Steady State Motion of a Rigid Strip Bonded to an Elastic Halfspace," *Journal of Applied Mechanics*, ASME, Vol. 8, No. E2, 328-334, June 1971.

10. Lysmer, J. and Kuhlemeyer, R. L., "Finite Dynamic Model for Infinite Media," *Journal of the Engineering Mechanics Division*, ASCE, Vol. 95, No. EM4, 859-877, 1969.

11. Day, S. M., "Finite Element Analysis of Seismic Scattering Problems," *Ph.D. Thesis*, University of California, San Diego, 1977.

12. Gupta, S., Lin, T. W., Penzien, J., and Yeh, C. S., "Hybrid Modelling of Soil-Structure Interaction," *Report No. UCB/EERC*–80/09, University of California, Berkeley, 1980.

13. Tzong, T. J., Gupta, S. and Penzien, J., "Two Dimensional Hybrid Modelling of Soil-Structure Interaction," *Report No. UCB/EERC*–81/11, University of California, Berkeley, 1981.

14. Medina, F., "Modelling of Soil-Structure Interaction by Finite and Infinite Elements," *Report No. UCB/EERC*–80/43, University of California, Berkeley, 1980.

15. Waas, G., "Linear Two-Dimensional Analysis of Soil Dynamic Problems in Semi-Infinite Layered Media," *Ph.D. Thesis*, University of California, Berkeley, 1972.

16. Kausel, E., "Forced Vibrations of Circular Footings on Layered Media," *MIT Research Report R*74–11, Massachusetts Institute of Technology, 1974.

17. Dasgupta, G. and Chopra, A. K., "Dynamic Stiffness Matrices for Homogeneous Viscoelastic Halfplanes," *Report No. UCB/EERC*–77/26, University of California, Berkeley, 1977.

18. Wong, H. L. and Luco, J. E., "Dynamic Response of Rigid Foundations of Arbitrary Shape," *Earthquake Engineering* and *Structural Dynamics*, Vol. 4, 579-587, 1976.

19. Thomson, W. T., "Transmission of Elastic Waves through a Stratified Solid Medium," *Journal of Applied Physics*, 21, 89-93, 1950.

20. Haskell, N. A., "The Dispersion of Surface Waves on Multilayered Media," *Bulletin of the Seismological Society of America*, 43, 17-34, 1953.

21. Dunkin, J. W., "Computation of Modal Solutions in Layered, Elastic Media at High Frequencies," *Bulletin of the Seismological Society of America*, 55, 335-358, 1965.

22. Knopoff, L., "A Matrix Method for Elastic Wave Problems," *Bulletin of the Seismological Society of America*, 54, 431-438, 1964.

23. Thrower, E. N., "The Computation of the Dispersion of Elastic Waves in Layered Media," *Journal of Sound Vibration*, 2, 210-226, 1965.

24. Ewing, M., Jardetzky, W. and Press, F., *Elastic Waves in Layered Media*, McGraw-Hill, 1957.

25. Kolsky, H., *Stress Waves in Solids*, Dover, 1963.

26. Liang, V. C., "Dynamic Response of Structures in Layered Soils," *MIT Research Report R*74–10, Massachusetts Institute of Technology, 1974.

27. Zienkiewicz, O. C., *The Finite Element Method*, 3rd edition, McGraw-Hill, 1977.

28. Bekey, G. A., "System Identification - An Introduction and a Survey," *Simulation*, Vol. 5, No. 4, 151-166, 1970.

29. Matzen, V. C., and McNiven, H. D., "Investigation of the Inelastic Characteristics of a Single Story Steel Structure Using System Identification and Shaking Table Experiments," *Report No. UCB/EERC*–76/20, University of California, Berkeley, 1976.

30. Hollings, J. P., and Wilson, E. L., "3-9 Node Isoparametric Planar or Axisymmetric Finite Element," *Report No. UCB/SESM* 78–3, University of California, Berkeley, 1977.

31. Sezawa, K. "Further Studies on Rayleigh Waves Having Some Azimuthal Distribution," *Bulletin of Earthquake Research Institute, Tokyo*, Vol. 6,1-18, 1929.

32. Conte, S. D. and de Boor, C., *Elementary Numerical Analysis*, 2nd edition, McGraw-Hill, 1972.

33. Tassoulas, J. L., "Elements for the Numerical Analysis of Wave Motion in Layered Media," *MIT Reserach Report R*81–2, Massachusetts Institute of Technology, 1981.

34. Kausel, E. and Roësset, J. M., "Semianalytic Hyperelement for Layered Strata," *Journal of the Engineering Mechanics Division*, ASCE, Vol. 103, No. EM4, 569-588, 1977.

35. Wilson, E. L., Yuan, M. W. and Dickens, J. M., "Dynamic Analysis by Direct Superposition of Ritz Vectors," *Earthquake Engineering* and *Structural Dynamics*, Vol. 10, 813-823, 1982.

36. Bayo, E. and Wilson, E. L., "Numerical Techniques for the Evaluation of Soil-Structure Interaction Effects in the Time Domain," *Reprot No. UCB/EERC*–83/04, University of California, Berkeley, 1983.

$C_{s_2}^2/C_{s_1}^2$	$\xi = 0.02$		$\xi = 0.05$	
	$a_0 = 0.01$	$a_0 = 3.0$	$a_0 = 0.01$	$a_0 = 3.0$
3.0	36	28	26	20
10.0	30	24	22	18
∞	--	--	18	14

TABLE 2.1 NUMBER OF SUBDOMAINS FOR INTEGRATION

$C_{s_2}^2/C_{s_1}^2$	$\xi = 0.02$		$\xi = 0.05$	
	$a_0 = 0.01$	$a_0 = 3.0$	$a_0 = 0.01$	$a_0 = 3.0$
3.0	26	44	26	44
10.0	34	52	32	50
∞	--	--	36	54

TABLE 2.2 NUMBER OF DISCRETE ELEMENTS UNDER RIGID STRIP

β	$a_0 = 0.05\pi$	$a_0 = \pi$
5.0	7	7
8.0	11	11
10.0	12	13
∞	∞	∞

TABLE 4.1 NUMBERS OF RAYLEIGH MODES FOR DIFFERENT IMAGINARY PARTS OF WAVE NUMBER (ξ=0.05, H/a =2.0, ν=0.30)

β	$a_0 = 0.01\pi$		$a_0 = 2\pi$	
	RAYLEIGH	LOVE	RAYLEIGH	LOVE
5.0	7	3	9	5
8.0	11	5	13	6
10.0	13	6	15	8
∞	∞	∞	∞	∞

TABLE 4.2 NUMBERS OF RAYLEIGH AND LOVE MODES FOR DIFFERENT IMAGINARY PARTS OF WAVE NUMBER (ξ=0.05, H/a = 2.0, ν=1/3)

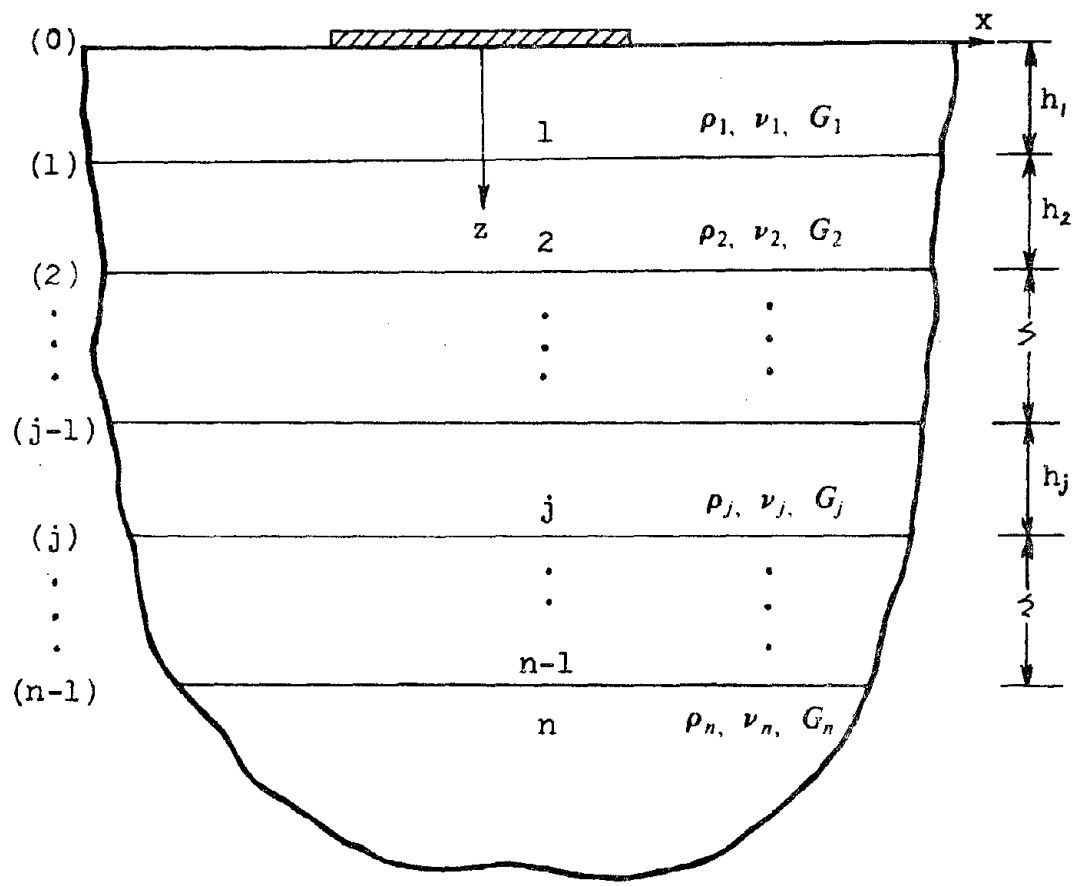

FIG. 2.1 SURFACE FOOTING ON LAYERED SOIL SYSTEM

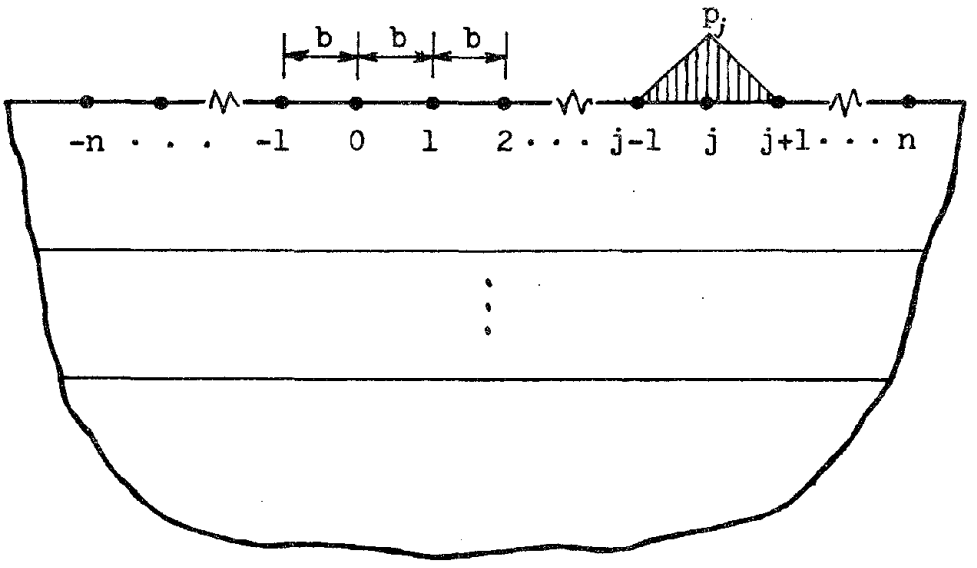

FIG. 2.2 DISCRETIZATION OF SURFACE FOUNDATION

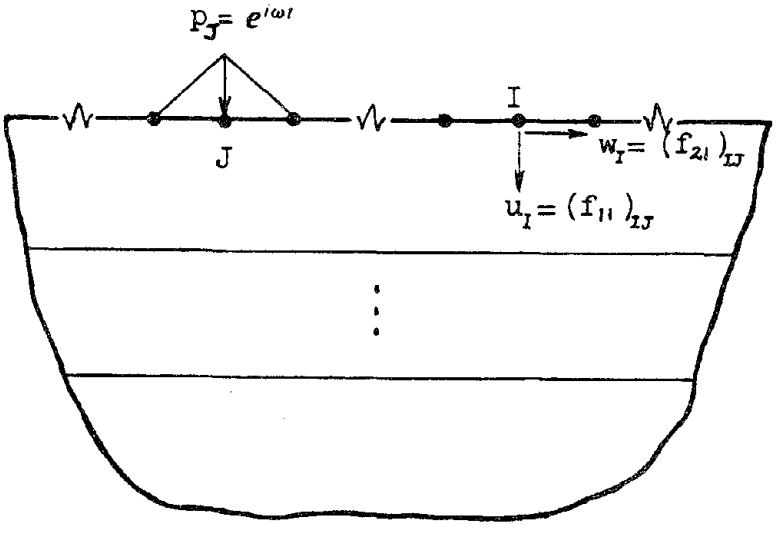

FIG. 2.3 DYNAMIC LOAD-DISPLACEMENT RELATIONSHIP BETWEEN TWO NODES

--	$\mathbf{R}_2^{(1)}$	$\mathbf{R}_2^{(2)}$	$\mathbf{R}_2^{(3)}$	$\mathbf{R}_2^{(4)}$
$\mathbf{R}_2^{(1)}$	0	0	0	*
$\mathbf{R}_2^{(2)}$	0	0	*	×
$\mathbf{R}_2^{(3)}$	0	*	×	×
$\mathbf{R}_2^{(4)}$	*	×	×	×

FIG. 2.4 CALCULATION OF DETERMINANT OF $\mathbf{R}_2$

--	$\overline{\mathbf{R}}_2^{(1)}$	$\overline{\mathbf{R}}_2^{(2)}$	$\overline{\mathbf{R}}_2^{(3)}$	$\overline{\mathbf{R}}_2^{(4)}$
$\mathbf{R}_1^{(1)}$	0	0	0	*
$\mathbf{R}_1^{(2)}$	0	0	*	×
$\mathbf{R}_1^{(3)}$	0	*	×	×
$\mathbf{R}_1^{(4)}$	*	×	×	×

FIG. 2.5 CALCULATION OF $\mathbf{R}_1\,\mathbf{R}_2^{-1}$

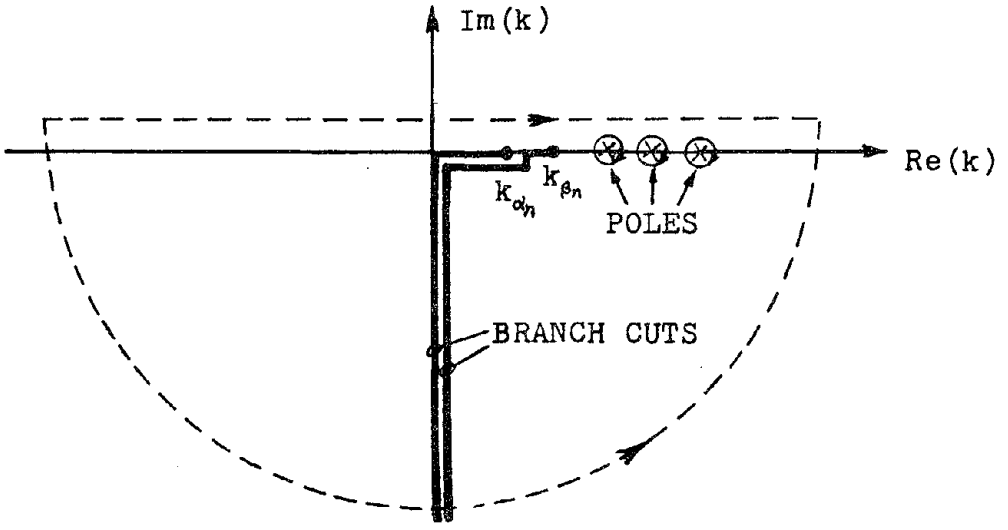

FIG. 2.6 CONTOUR INTEGRATION ON THE COMPLEX PLANE

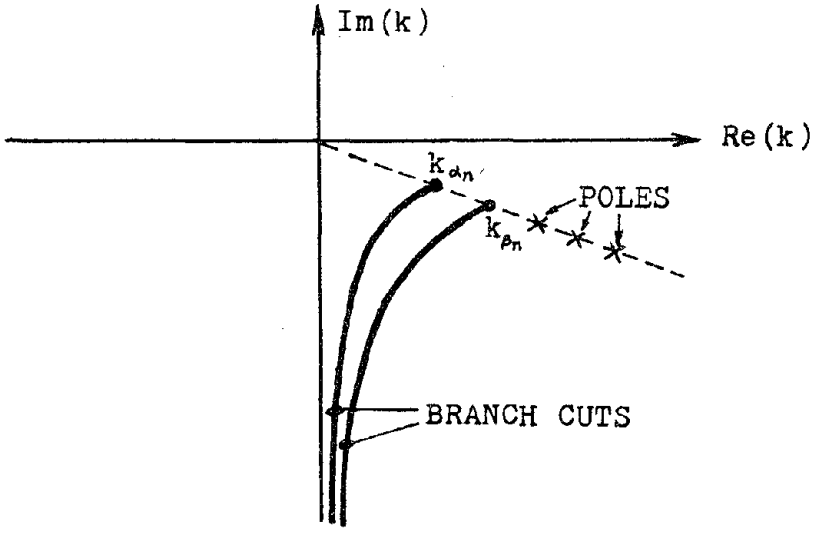

FIG. 2.7 BRANCH POINTS AND POLES MOVING FROM REAL AXIS

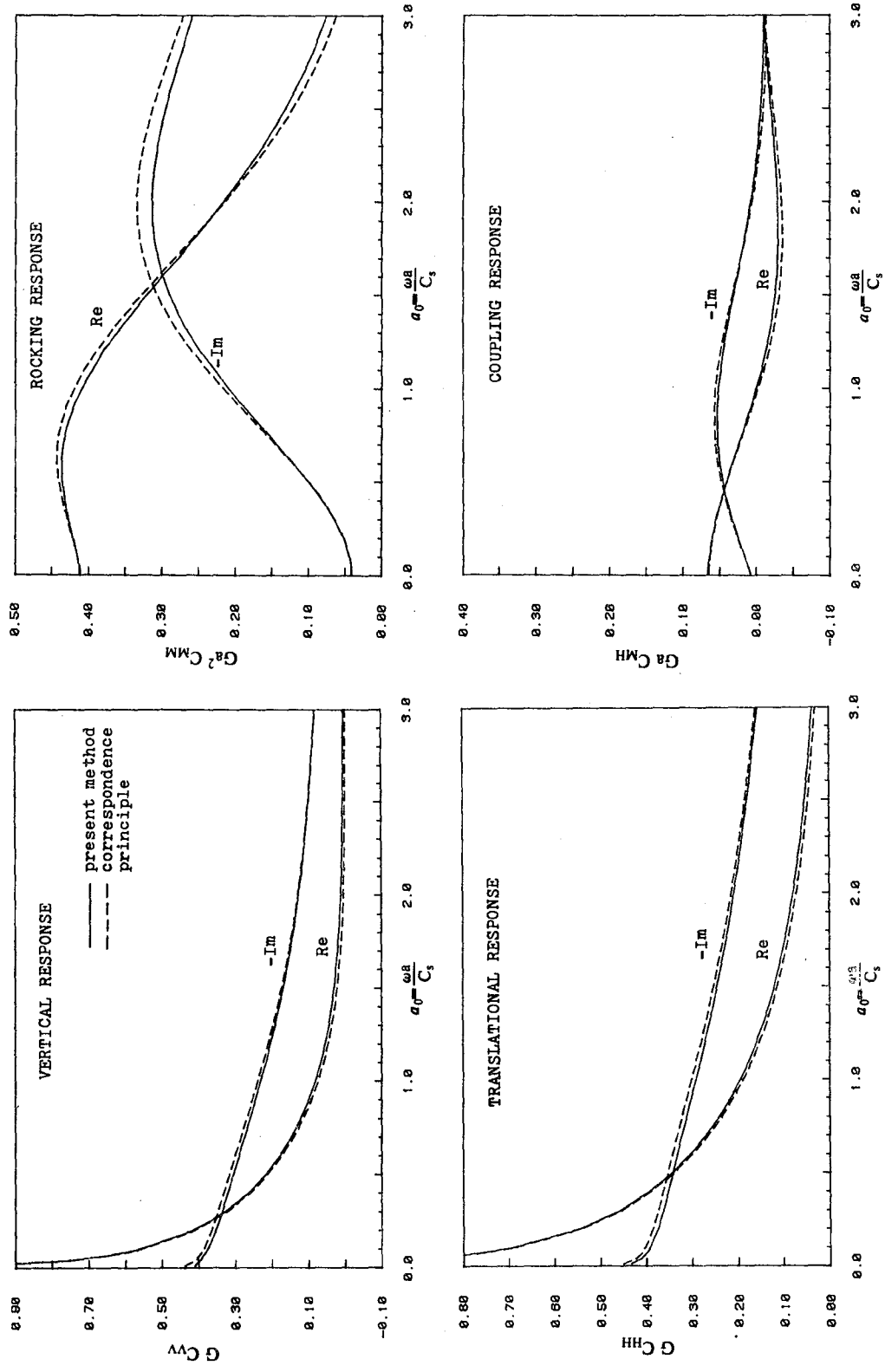

FIG. 2.8 COMPARISON OF STRIP COMPLIANCES USING CORRESPONDENCE PRINCIPLE ($\xi = 0.05, \nu = 1/3$)

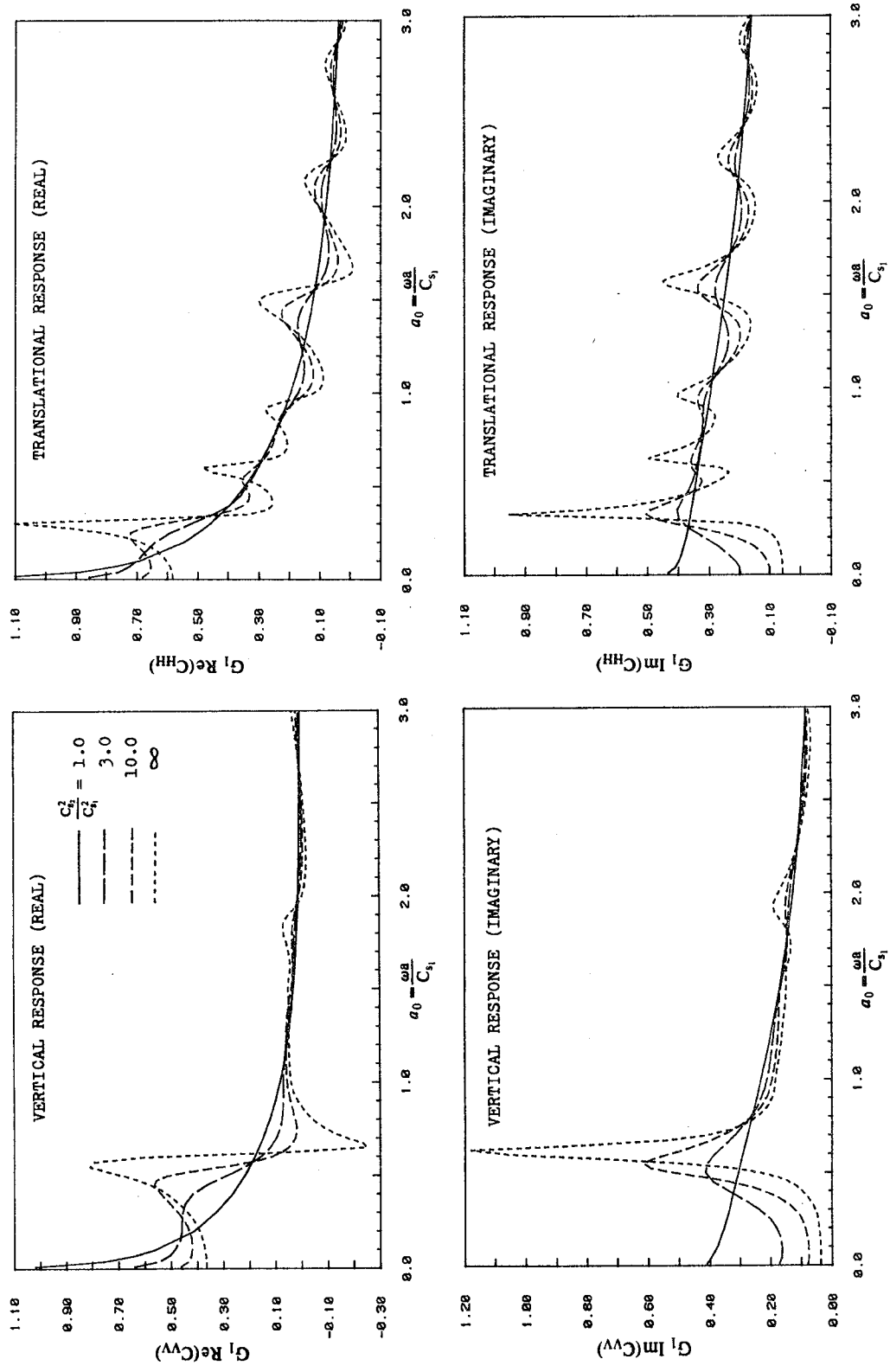

FIG. 2.9 COMPARISON OF STRIP COMPLIANCES FOR DIFFERENT $C_{s_2}^2/C_{s_1}^2$ RATIOS ($\xi_1 = \xi_2 = 0.05$, $\nu_1 = \nu_2 = 1/3$, H/a = 5.0)

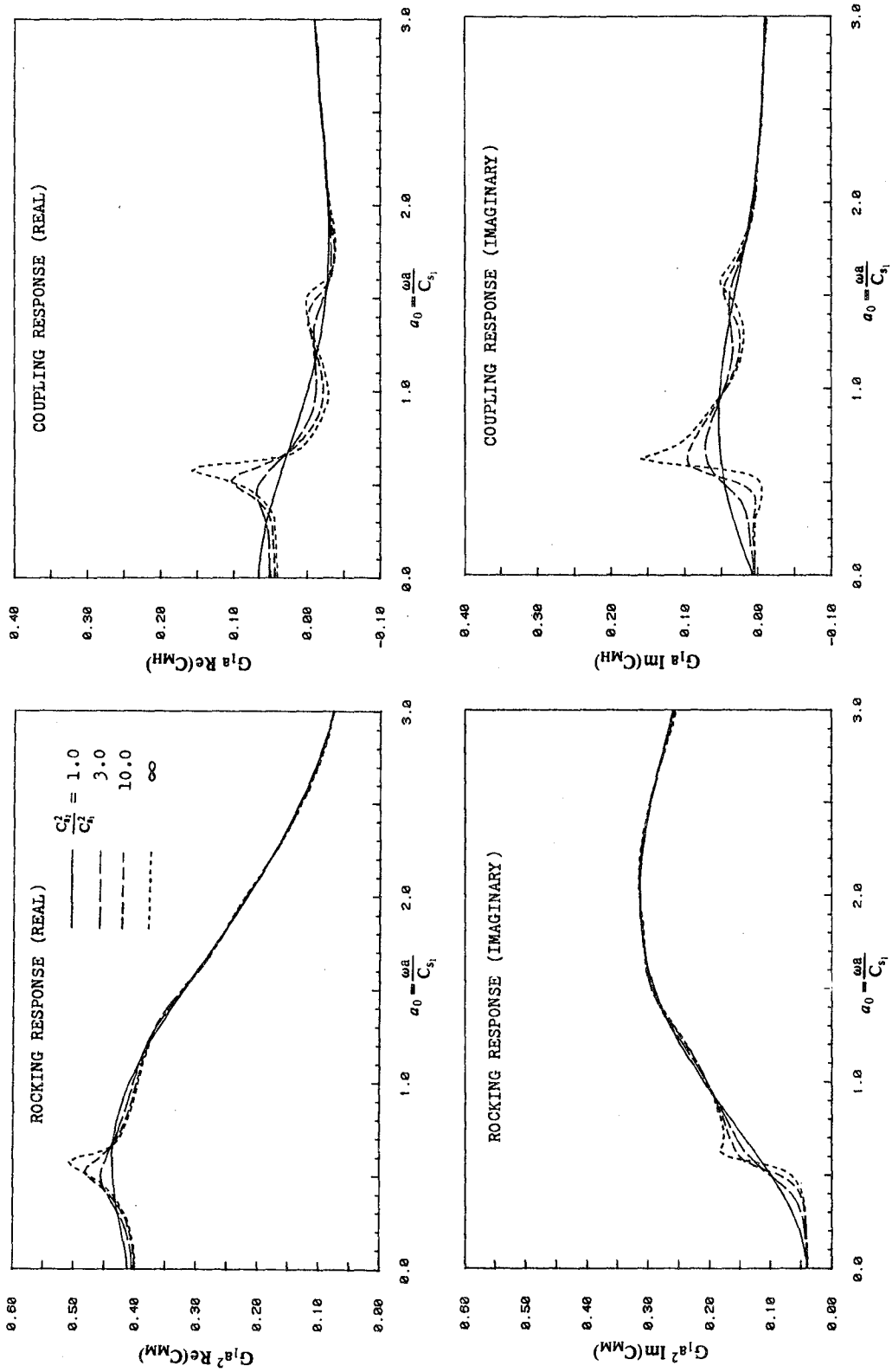

FIG. 2.10 COMPARISON OF STRIP COMPLIANCES FOR DIFFERENT $C_{s_2}^2/C_{s_1}^2$ RATIOS ($\xi_1 = \xi_2 = 0.05$, $\nu_1 = \nu_2 = 1/3$, $H/a = 5.0$)

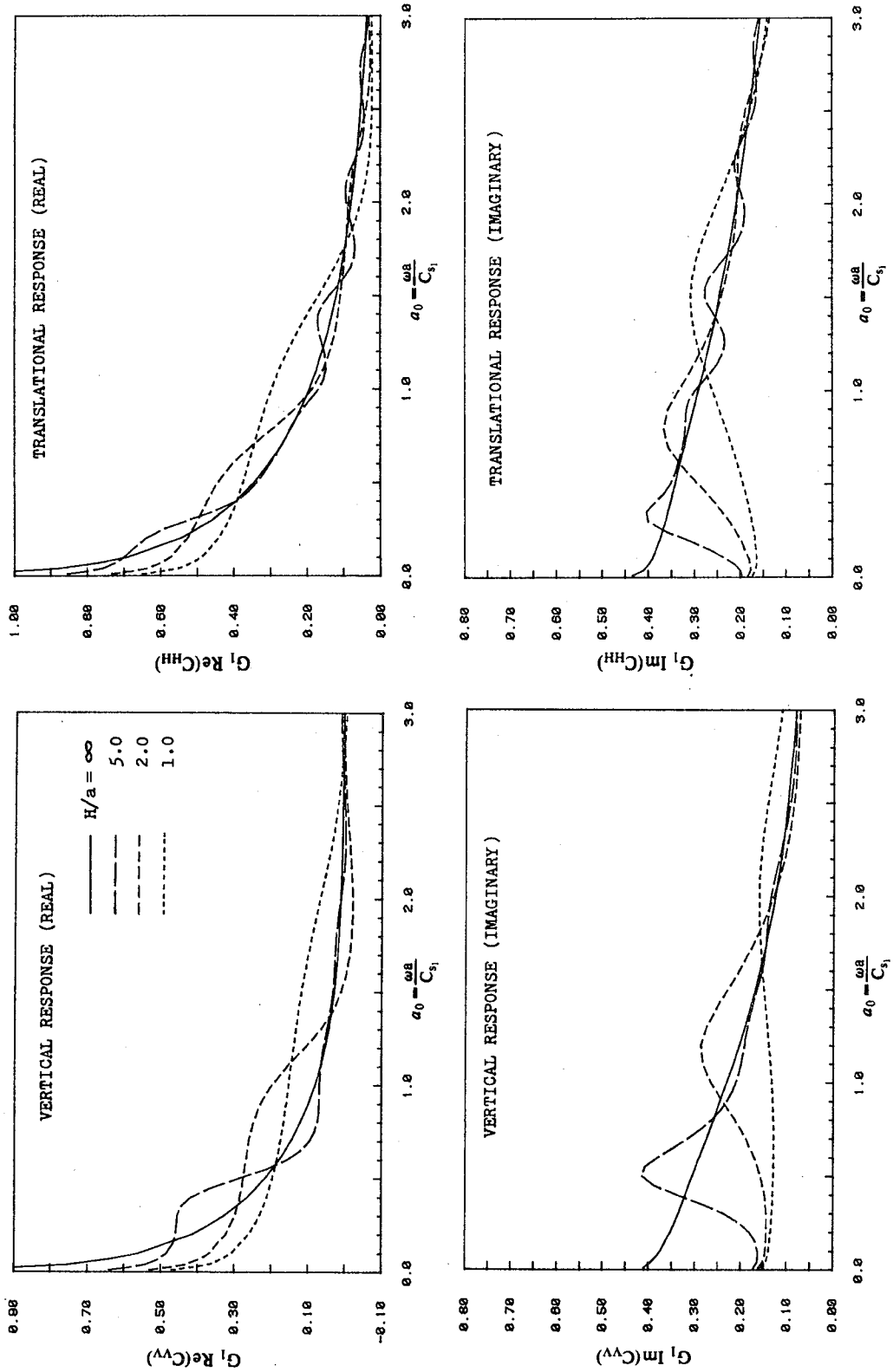

FIG. 2.11 COMPARISON OF STRIP COMPLIANCES FOR DIFFERENT DEPTH RATIOS ($\xi_1 = \xi_2 = 0.05$, $\nu_1 = \nu_2 = 1/3$, $C_{s_2}^2/C_{s_1}^2 = 3.0$)

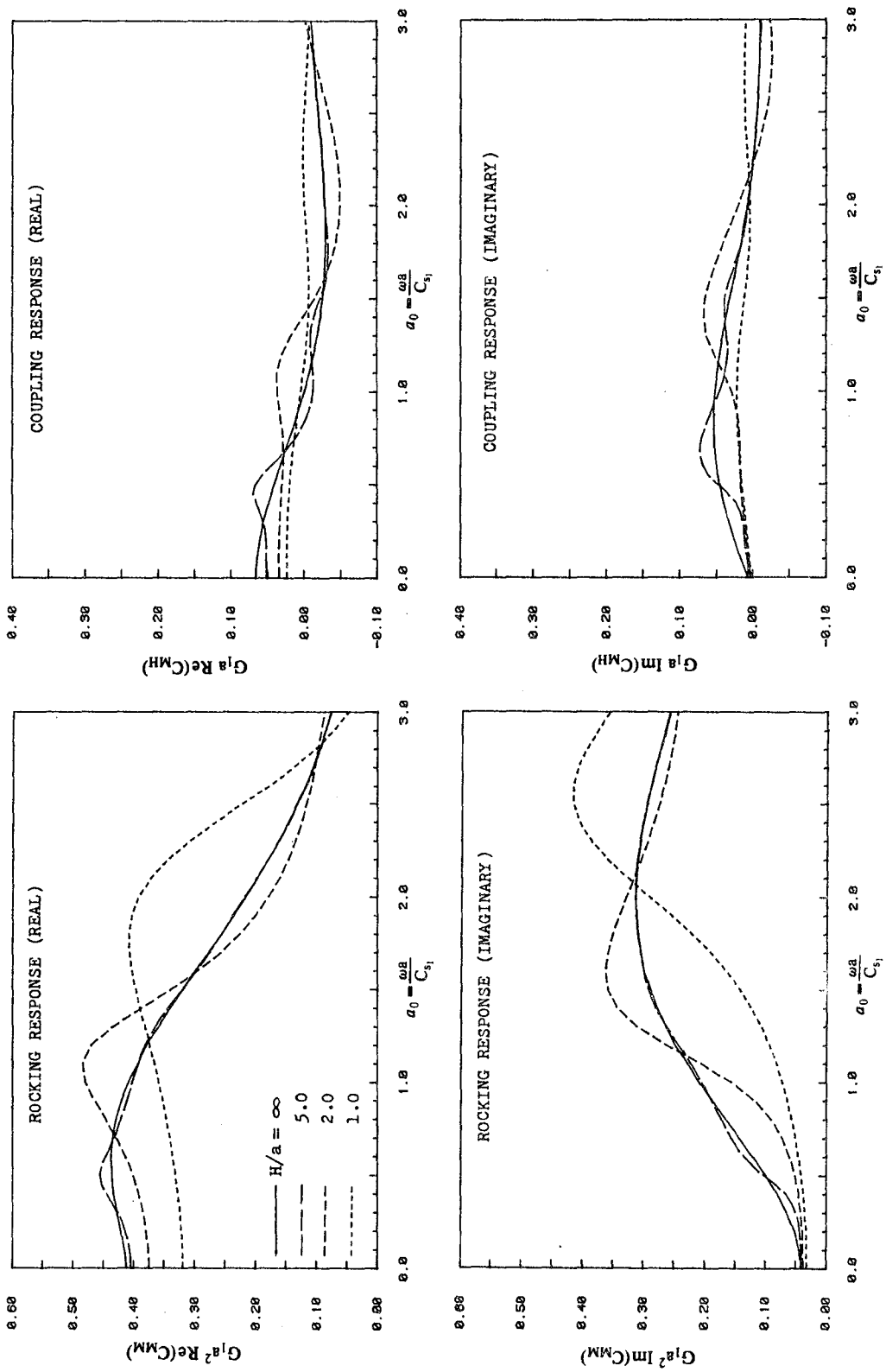

FIG. 2.12 COMPARISON OF STRIP COMPLIANCES FOR DIFFERENT DEPTH RATIOS ($\xi_1 = \xi_2 = 0.05$, $\nu_1 = \nu_2 = 1/3$, $C_{s_2}^2/C_{s_1}^2 = 3.0$)

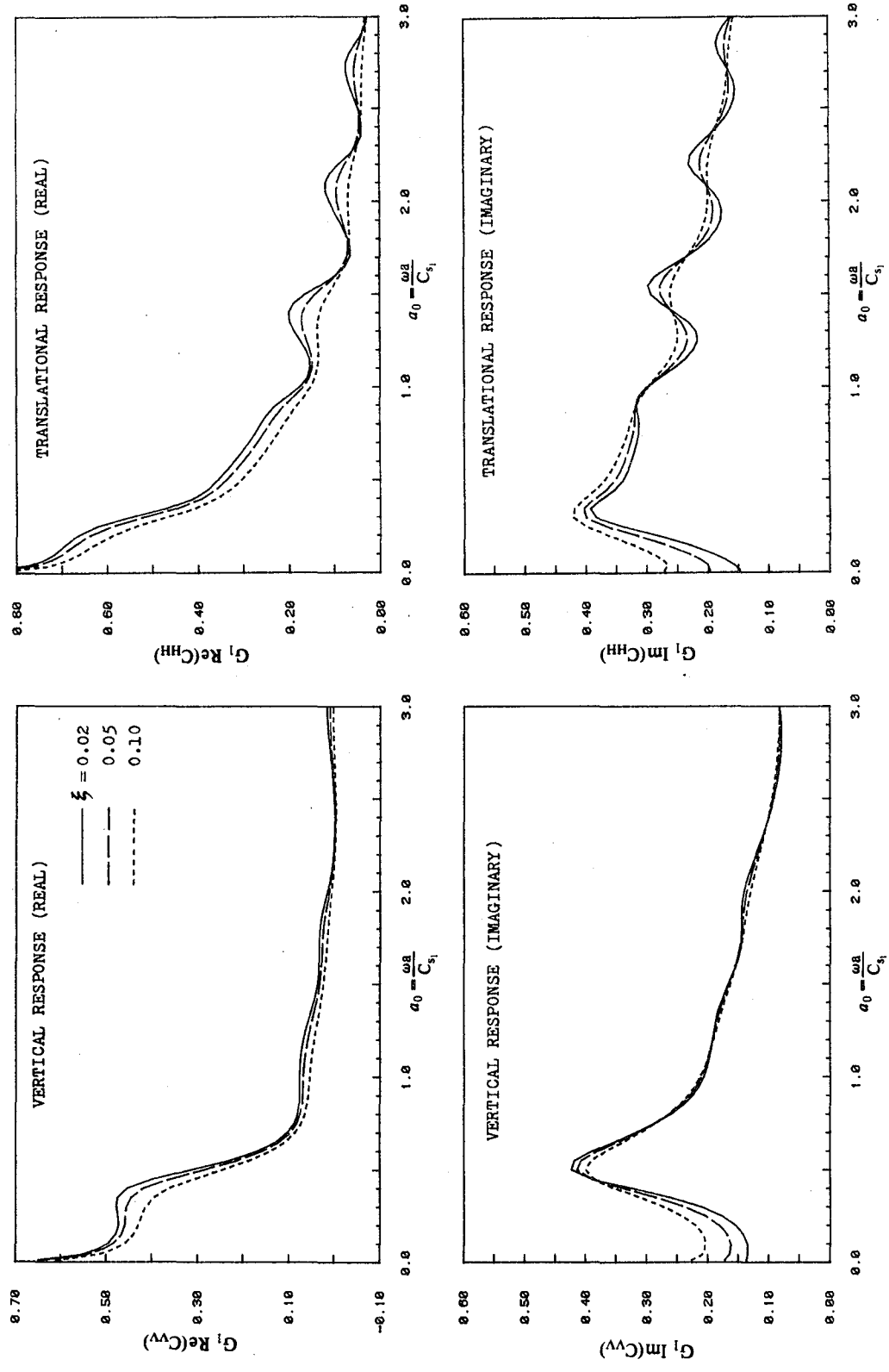

FIG. 2.13 COMPARISON OF STRIP COMPLIANCES FOR DIFFERENT DAMPING RATIOS ($\nu_1 = \nu_2 = 1/3$, H/a = 5.0, $C_{s_2}^2/C_{s_1}^2 = 3.0$)

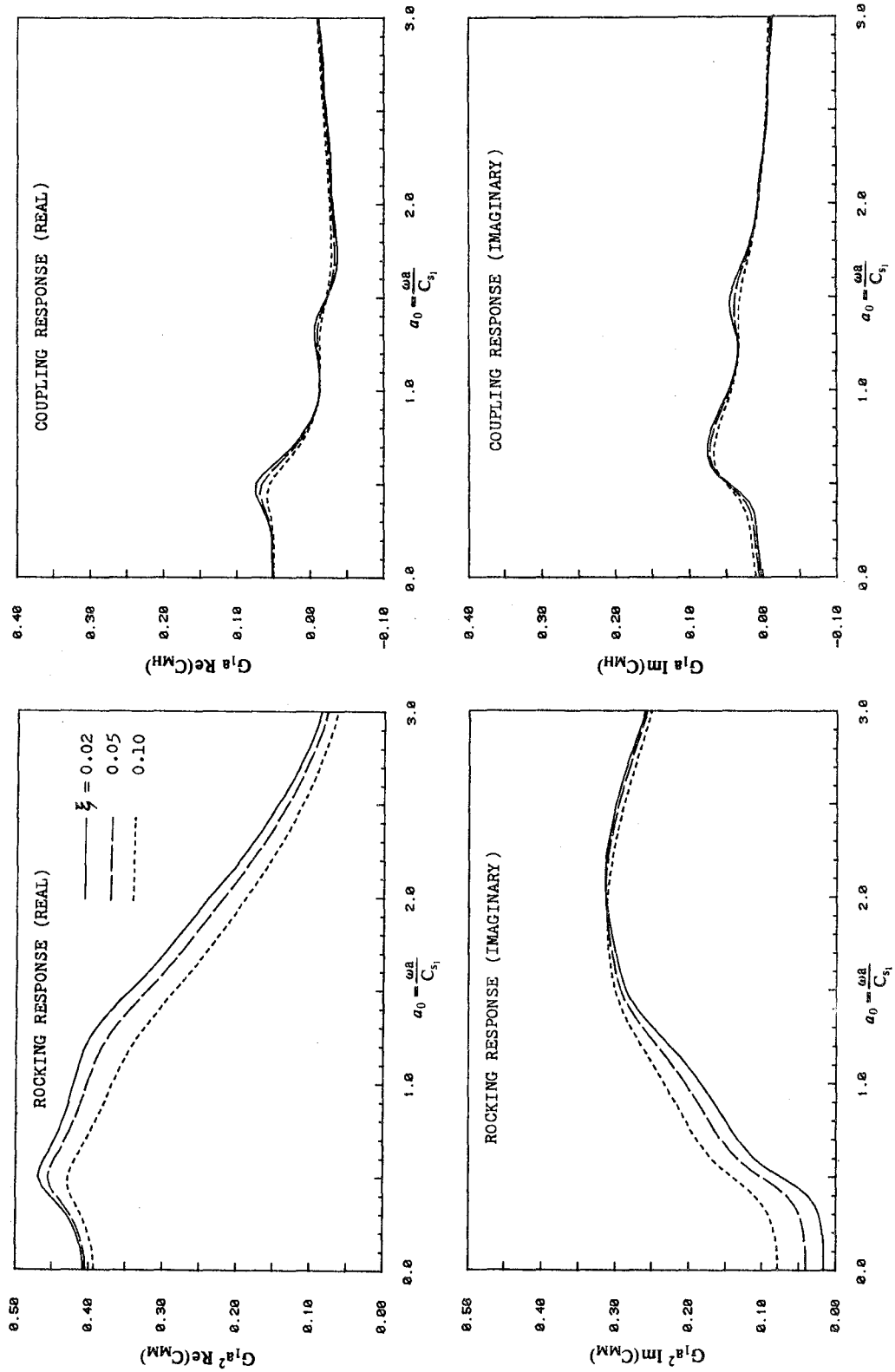

FIG. 2.14 COMPARISON OF STRIP COMPLIANCES FOR DIFFERENT DAMPING RATIOS ($\nu_1 = \nu_2 = 1/3$, H/a = 5.0, $C_{s_2}^2/C_{s_1}^2 = 3.0$)

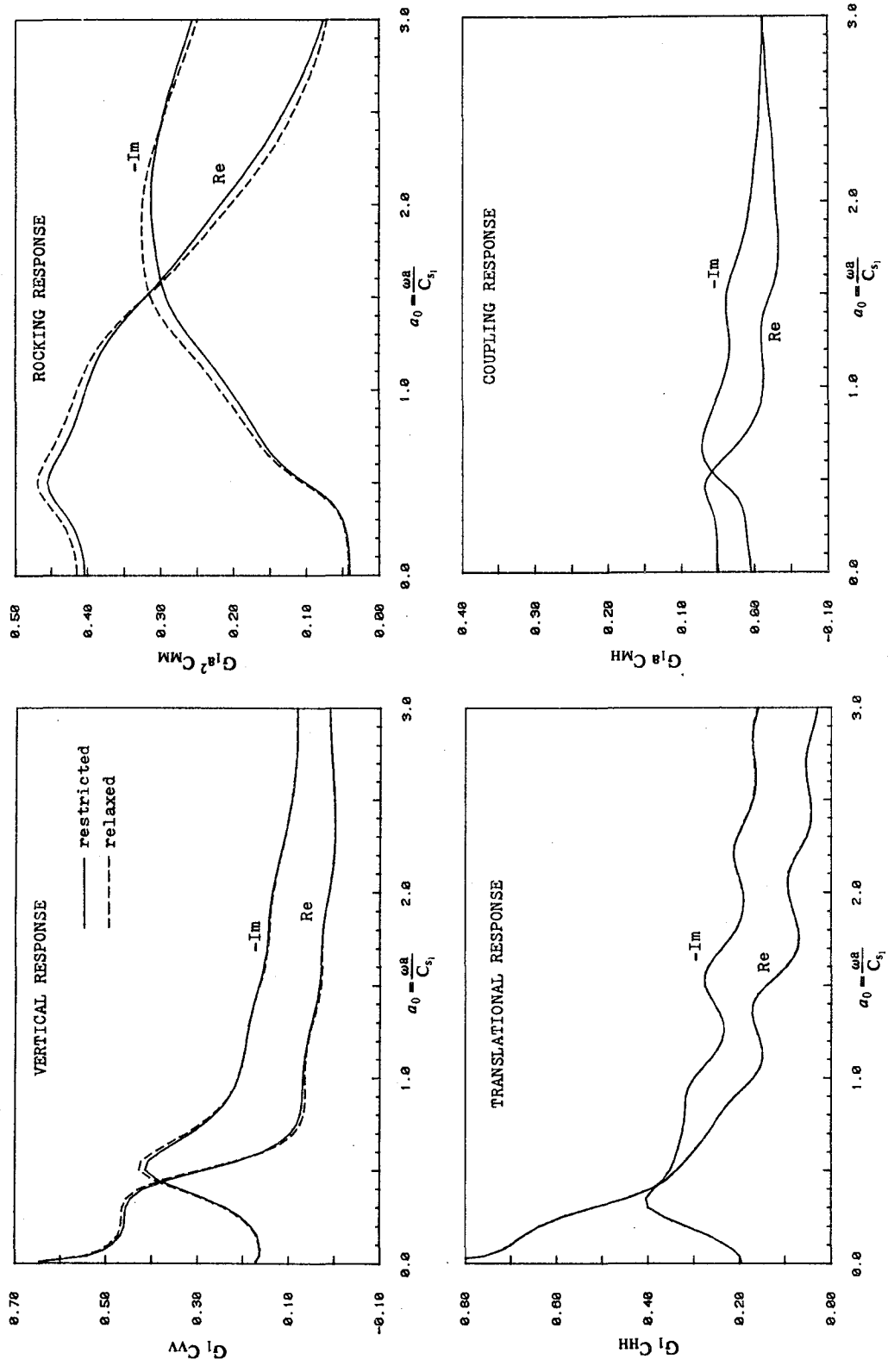

FIG. 2.15 COMPARISON OF STRIP COMPLIANCES FOR RESTRICTED AND RELAXED BOUNDARIES ($\xi_1 = \xi_2 = 0.05$, $\nu_1 = \nu_2 = 1/3$, H/a = 5.0, $C_{s_2}^2/C_{s_1}^2 = 3.0$)

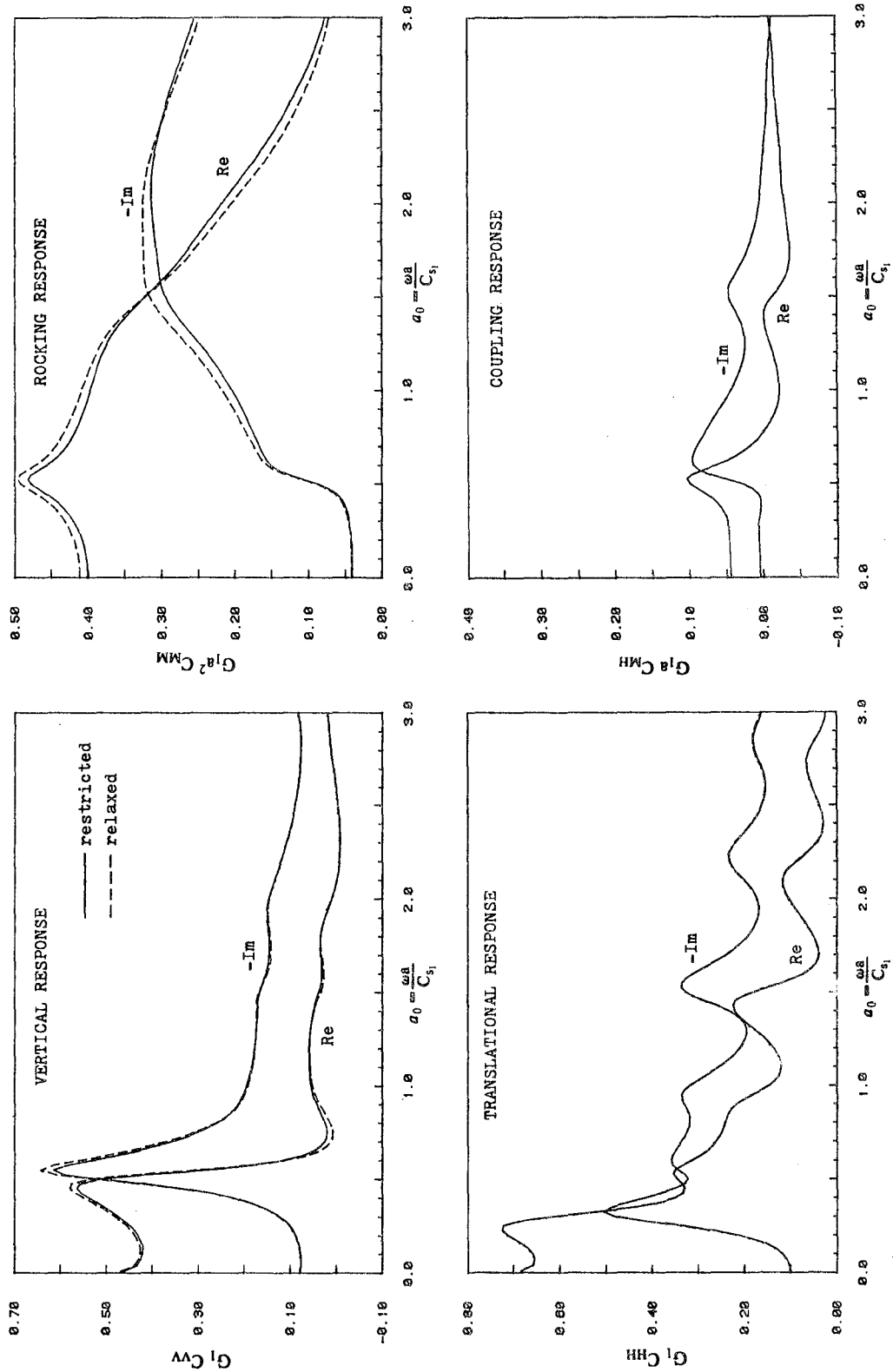

FIG. 2.16 COMPARISON OF STRIP COMPLIANCES FOR RESTRICTED AND RELAXED BOUNDARIES ($\xi_1 = \xi_2 = 0.05$, $\nu_1 = \nu_2 = 1/3$, $H/a = 5.0$, $C_{s_2}^2/C_{s_1}^2 = 10.0$)

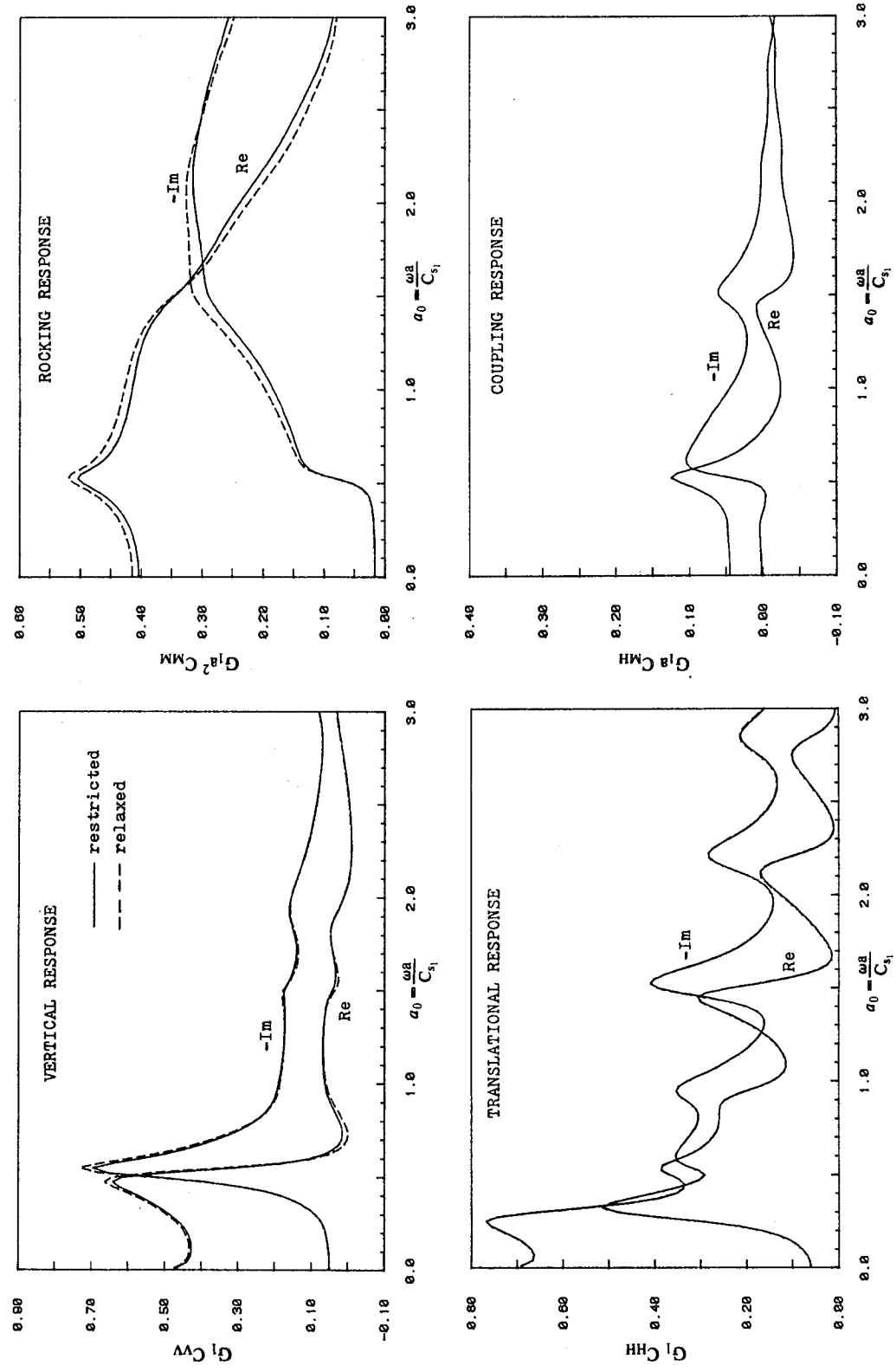

FIG. 2.17 COMPARISON OF STRIP COMPLIANCES FOR RESTRICTED AND RELAXED BOUNDARIES ($\xi_1 = \xi_2 = 0.02$, $\nu_1 = \nu_2 = 1/3$, H/a = 5.0, $C_{s_2}^2/C_{s_1}^2 = 10.0$)

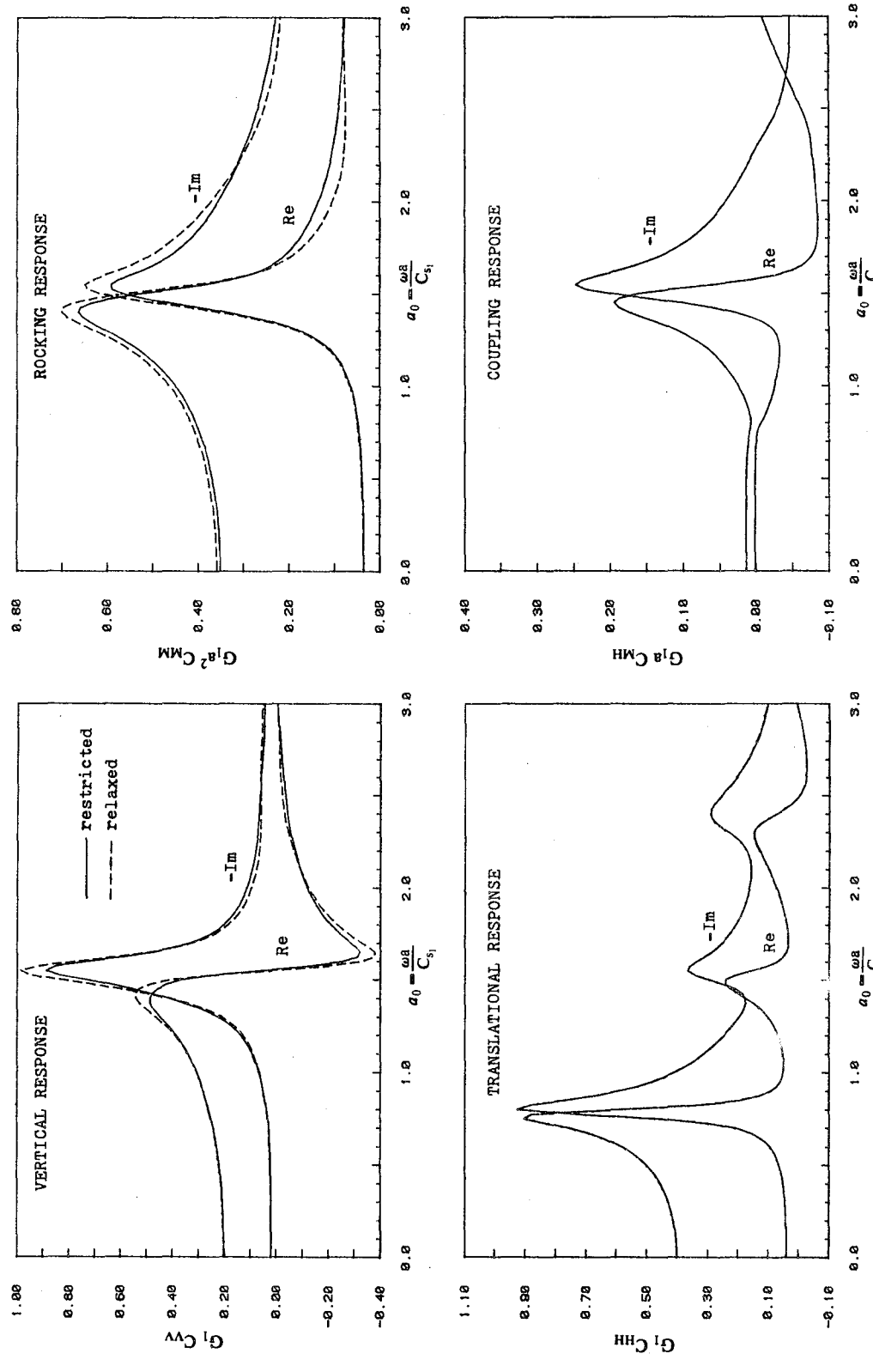

FIG. 2.18 COMPARISON OF STRIP COMPLIANCES FOR RESTRICTED AND RELAXED BOUNDARIES ($\xi = 0.05$, $\nu = 1/3$, $H/a = 2.0$, $C_{s_2}^2/C_{s_1}^2 = \infty$)

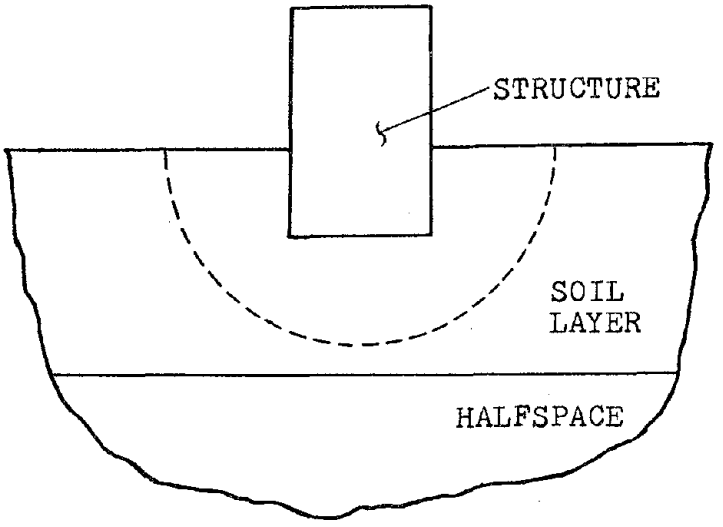

(a) STRUCTURE IN LAYERED HALFSPACE

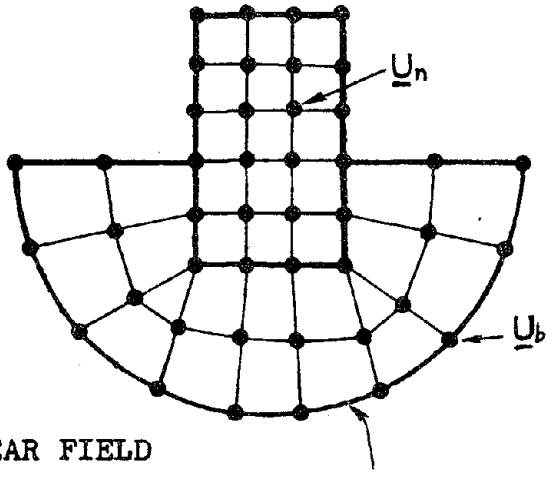

(b) NEAR FIELD

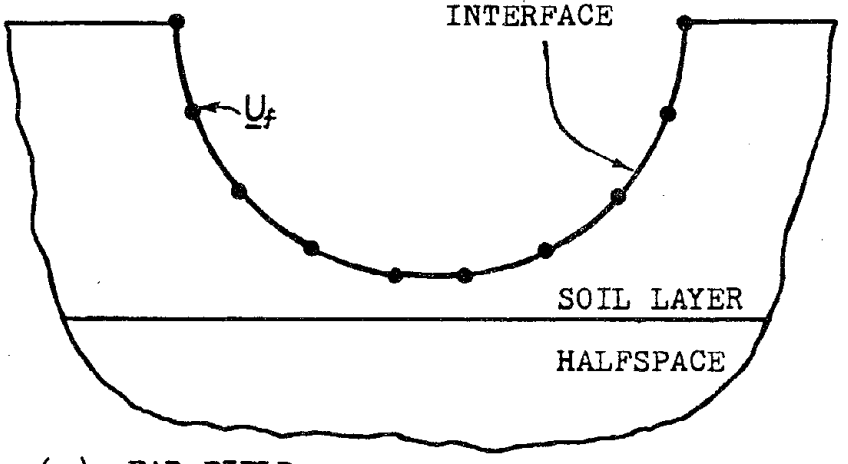

(c) FAR FIELD

FIG. 3.1 HYBRID MODELLING OF SOIL-STRUCTURE INTERACTION IN LAYERED HALFSPACE

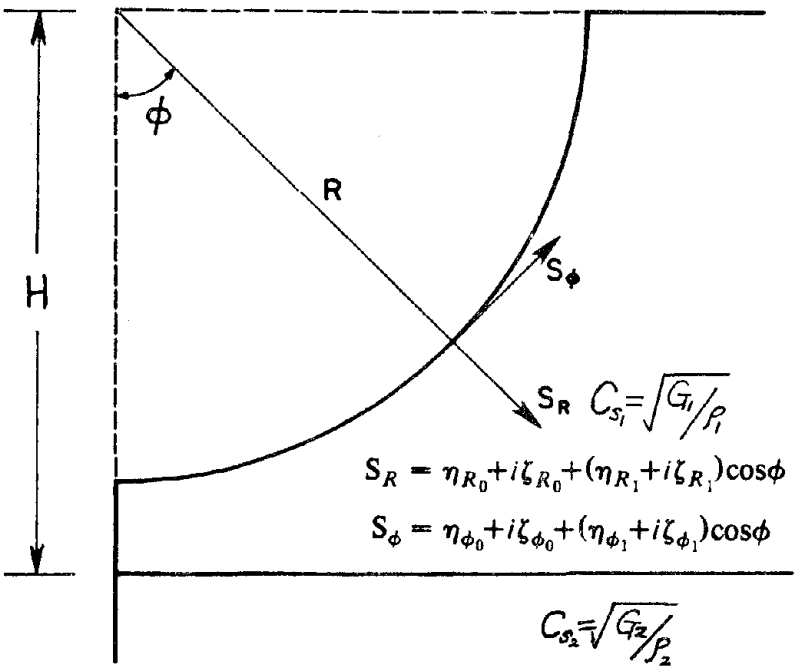

(a) CONTINUOUS FAR-FIELD IMPEDANCES

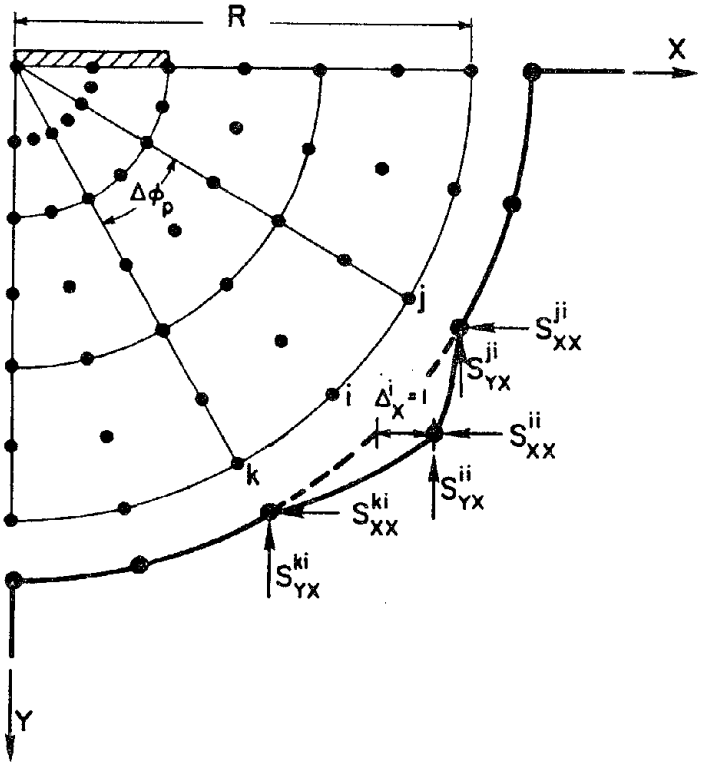

(b) FINITE-ELEMENT CONSISTENT IMPEDANCES

FIG. 3.2 FAR-FIELD MODELLING BY IMPEDANCE FUNCTIONS

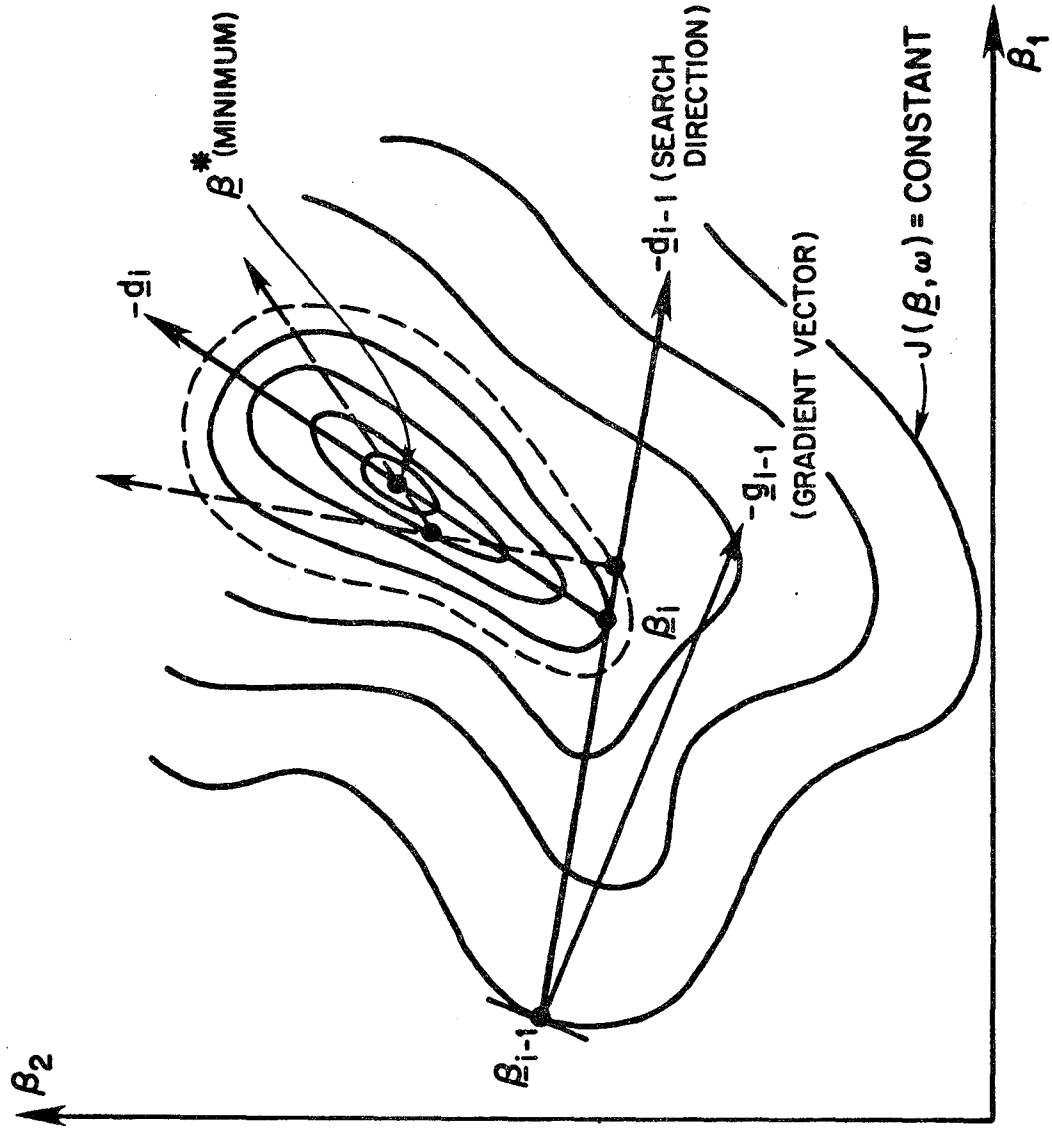

FIG. 3.3 ERROR SURFACE FOR TWO PARAMETERS

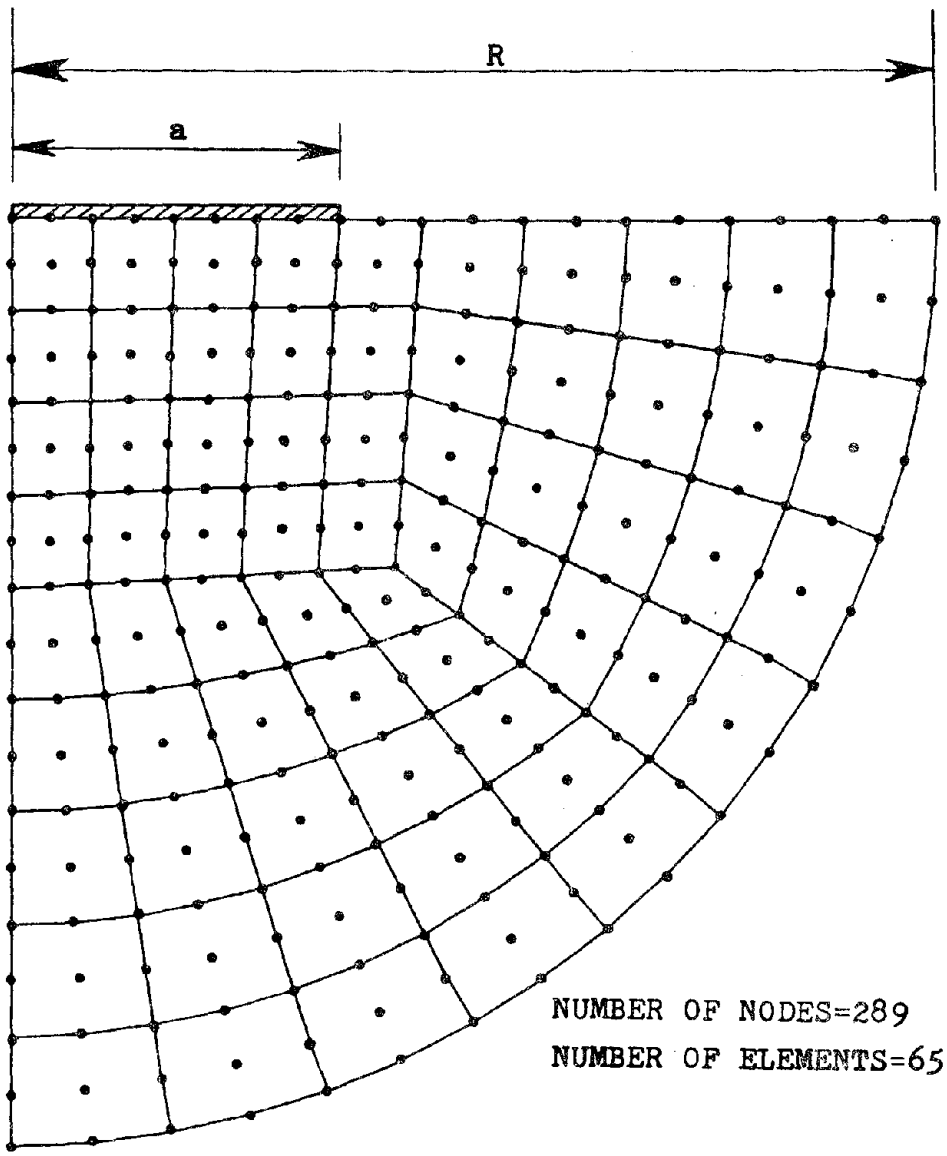

FIG. 3.4 NEAR-FIELD FINITE ELEMENT MESH FOR GENERATING FAR-FIELD IMPEDANCE FUNCTIONS

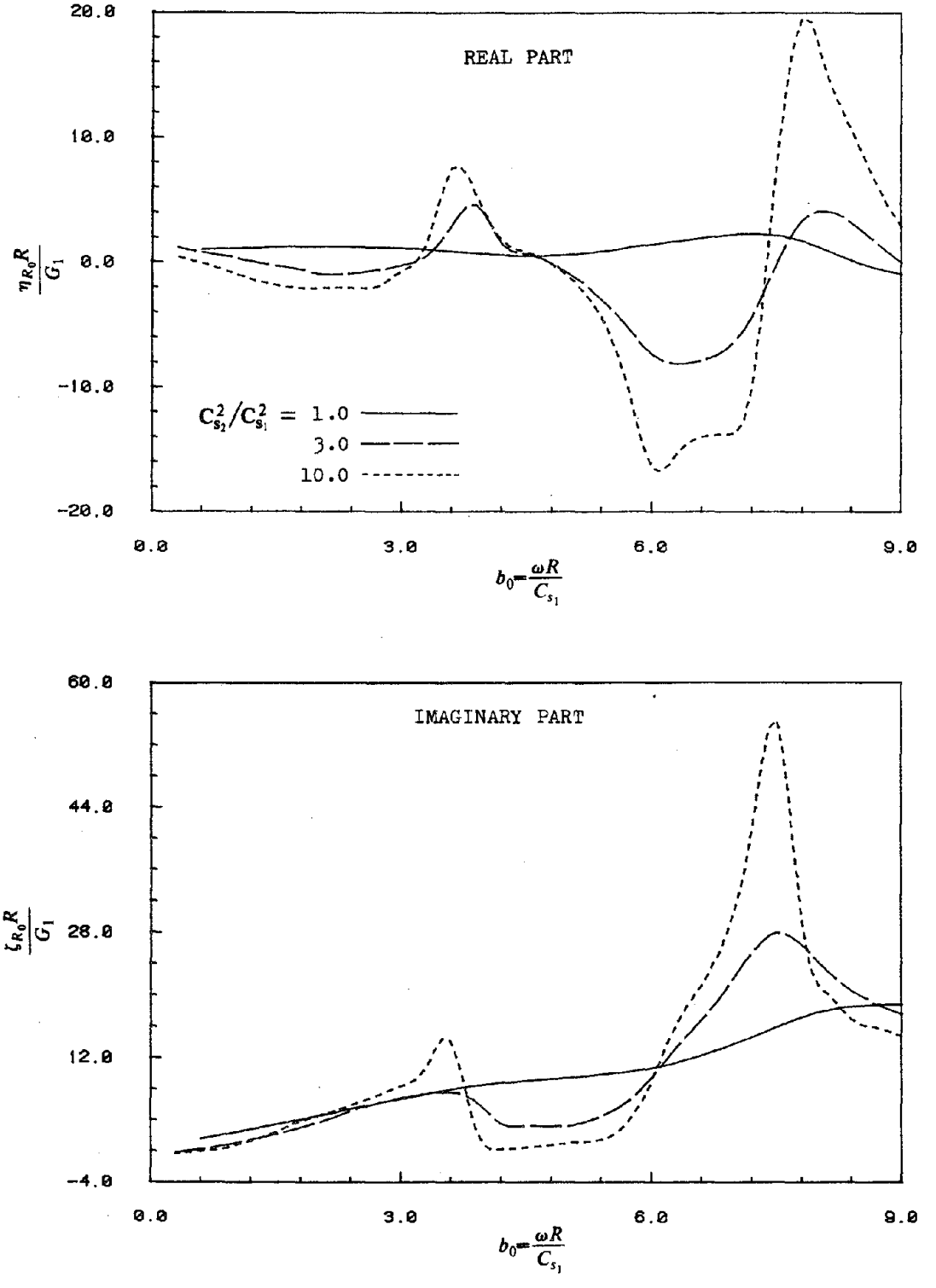

FIG. 3.5 FAR-FIELD IMPEDANCE FUNCTIONS - CONSTANT TERM OF RADIAL COMPONENT ($\nu_1=\nu_2=1/3$, $\xi_1=\xi_2=0.02$, H/R =4/3)

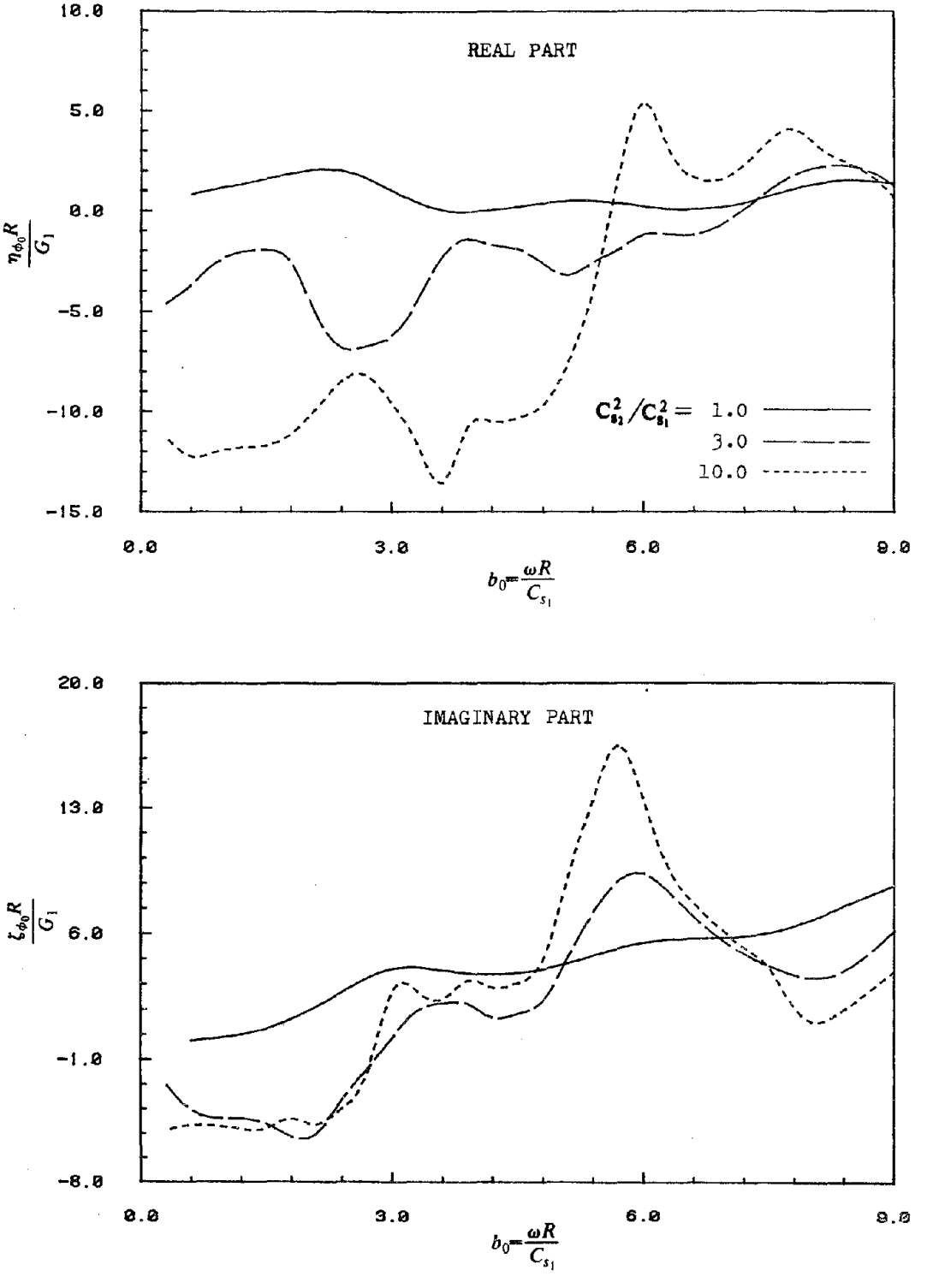

FIG. 3.6 FAR-FIELD IMPEDANCE FUNCTIONS - CONSTANT TERM OF TANGENTIAL COMPONENT ($\nu_1 = \nu_2 = 1/3$, $\xi_1 = \xi_2 = 0.02$, H/R $= 4/3$)

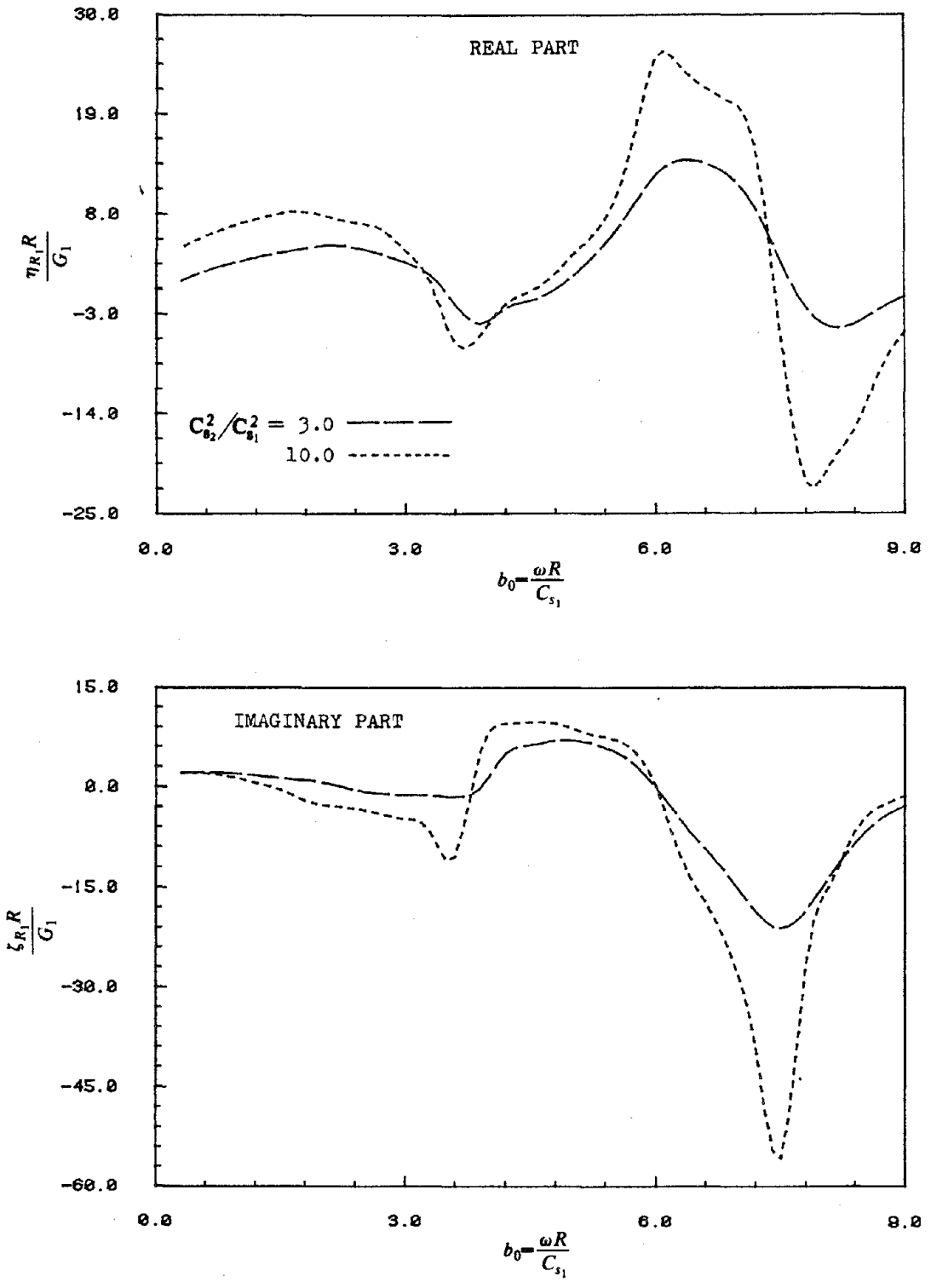

FIG. 3.7 FAR-FIELD IMPEDANCE FUNCTIONS - TRIGONOMETRIC TERM OF RADIAL COMPONENT ($\nu_1 = \nu_2 = 1/3$, $\xi_1 = \xi_2 = 0.02$, H/R = 4/3)

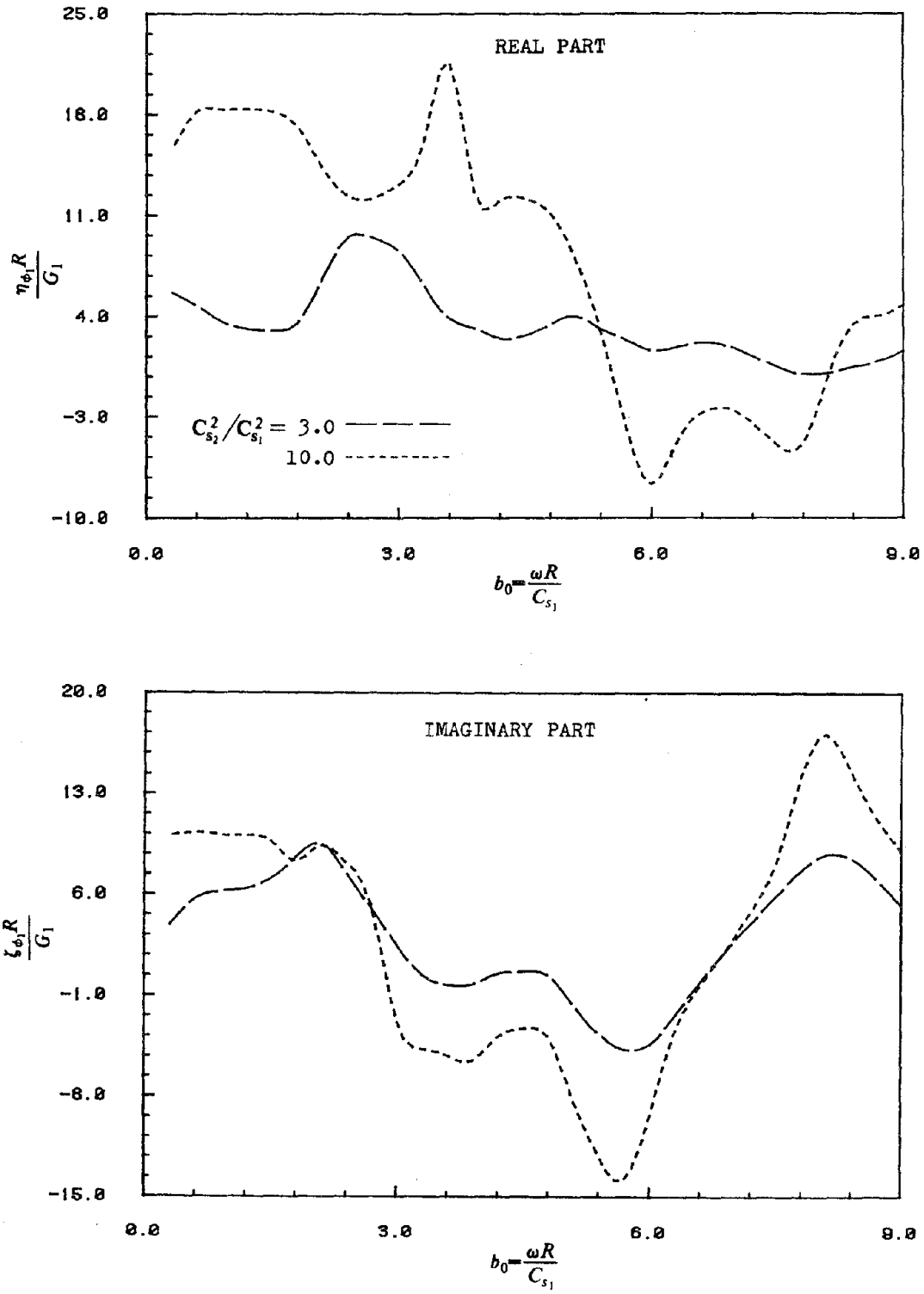

FIG. 3.8 FAR-FIELD IMPEDANCE FUNCTIONS - TRIGONOMETRIC TERM OF TANGENTIAL COMPONENT ($\nu_1 = \nu_2 = 1/3$, $\xi_1 = \xi_2 = 0.02$, H/R $= 4/3$)

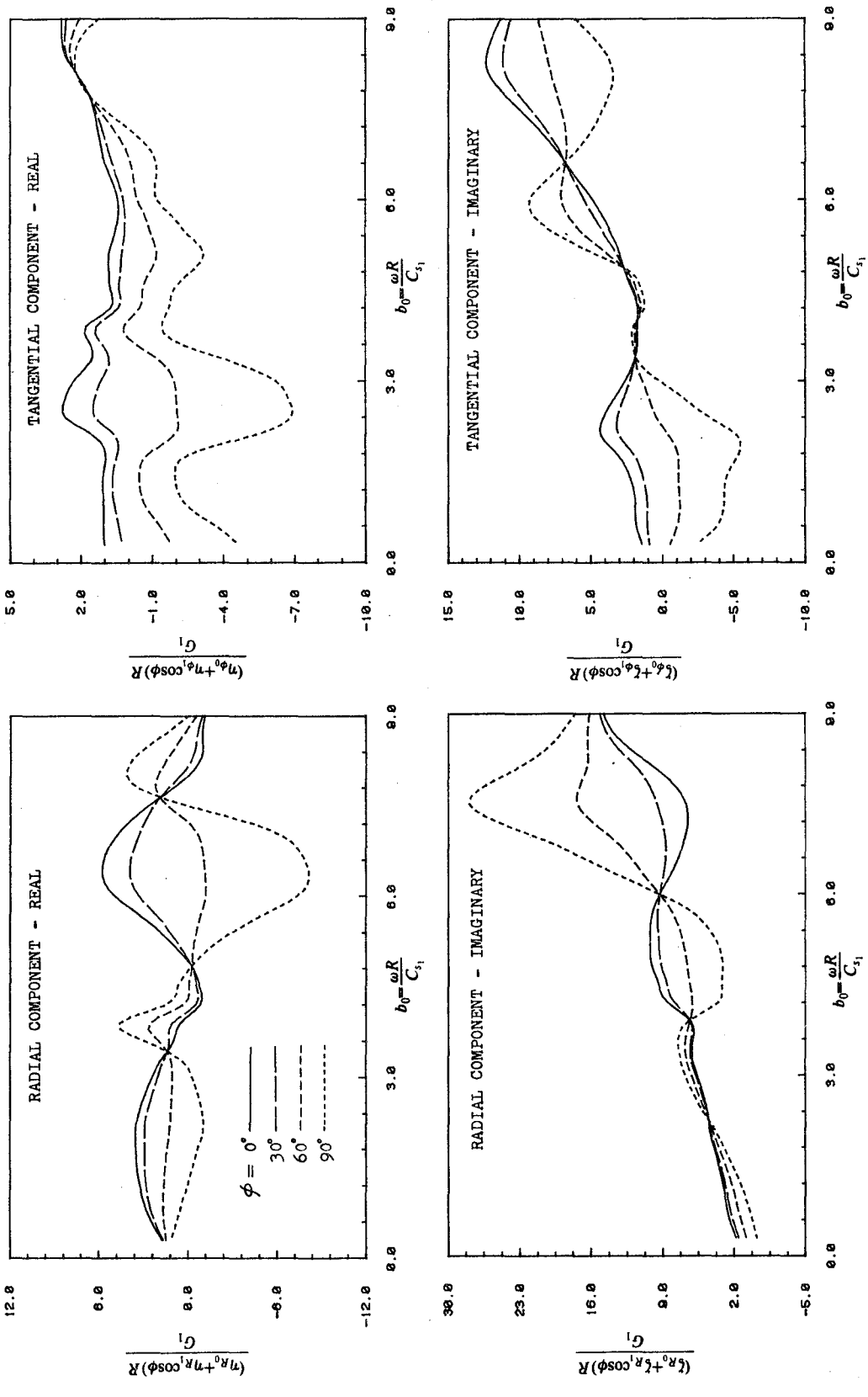

FIG. 3.9 FAR-FIELD IMPEDANCE FUNCTIONS AT DIFFERENT LOCATIONS
($C_{s_2}^2/C_{s_1}^2 = 3.0$, $\nu_1 = \nu_2 = 1/3$, $\xi_1 = \xi_2 = 0.02$, H/R = 4/3)

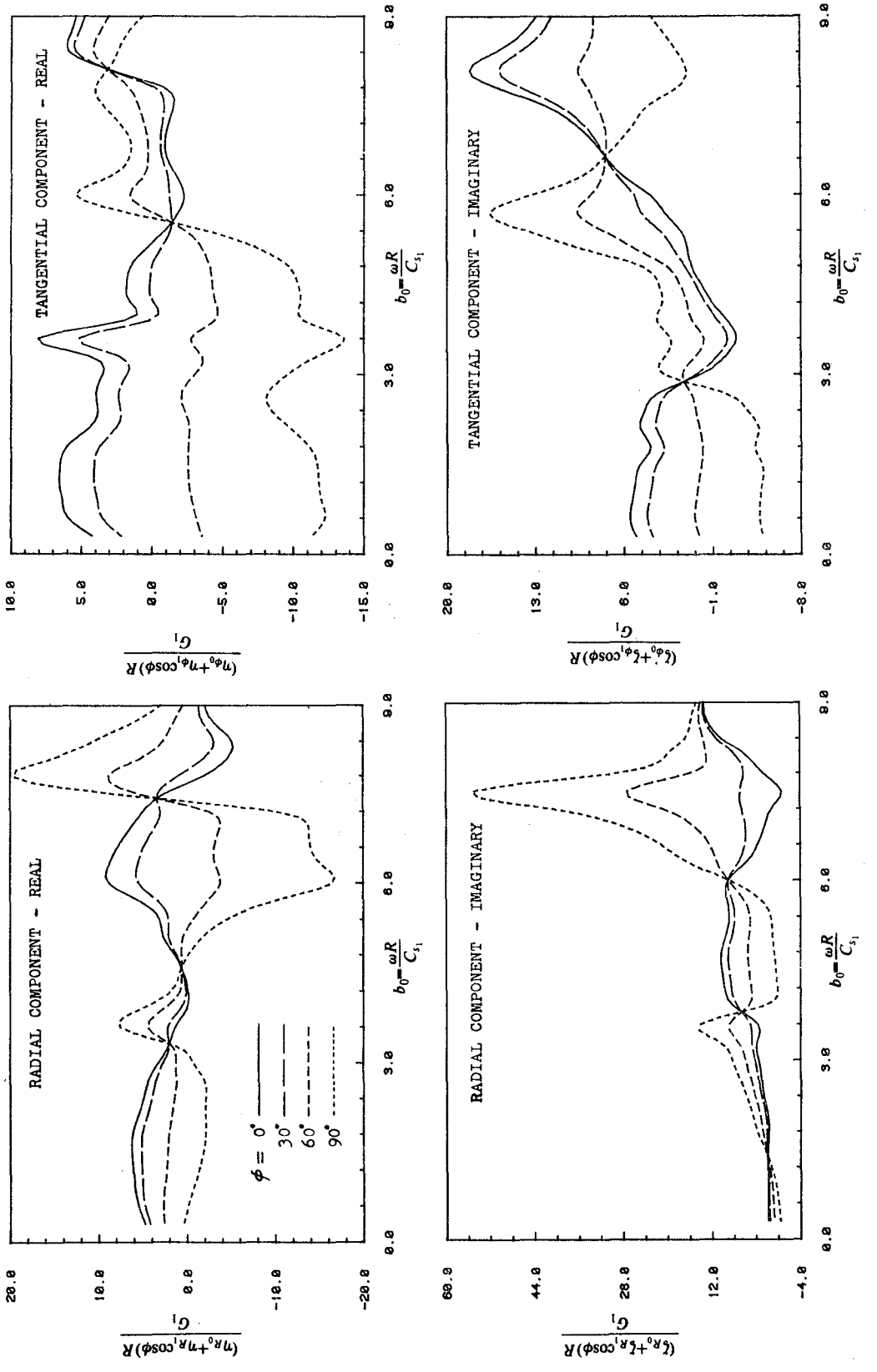

FIG. 3.10 FAR-FIELD IMPEDANCE FUNCTIONS AT DIFFERENT LOCATIONS
($C_{s_2}^2/C_{s_1}^2 = 10.0$, $\nu_1 = \nu_2 = 1/3$, $\xi_1 = \xi_2 = 0.02$, H/R = 4/3)

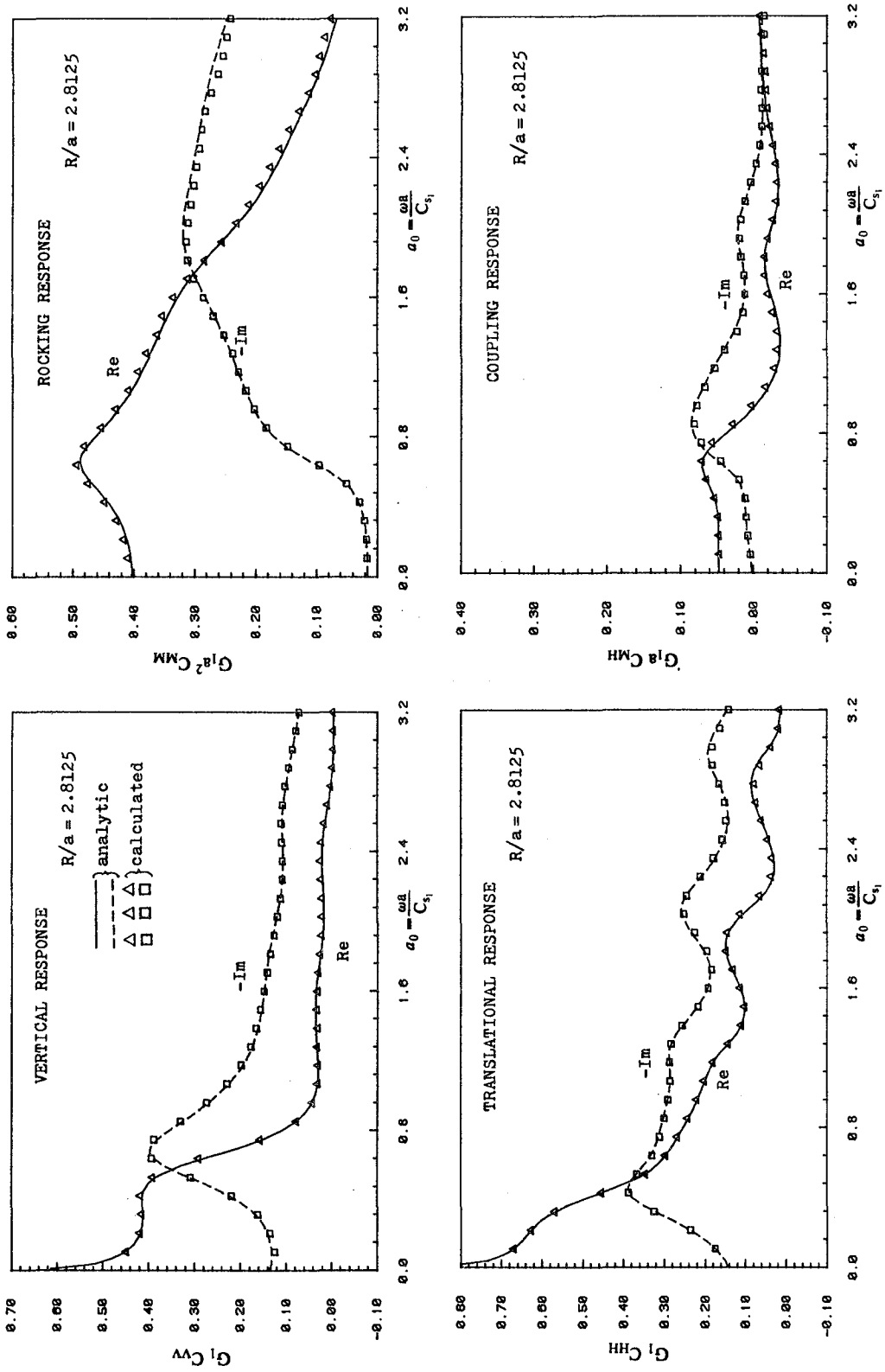

FIG. 3.11 COMPARISON OF STRIP COMPLIANCES USING IDENTIFIED IMPEDANCE FUNCTIONS ($C_{s_2}^2/C_{s_1}^2 = 3.0$, $\xi_1 = \xi_2 = 0.02$, $\nu_1 = \nu_2 = 1/3$, H/R =4/3)

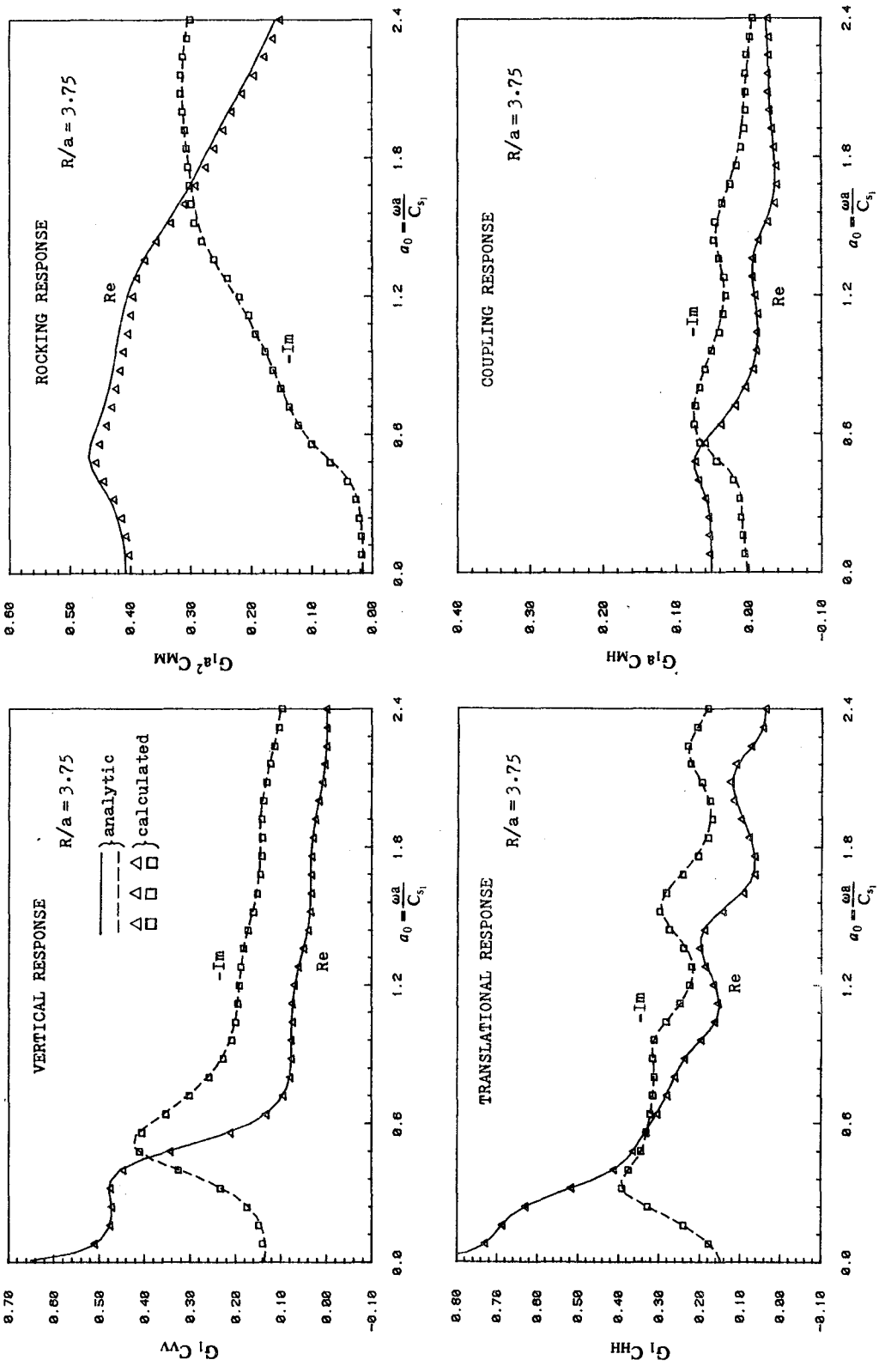

FIG. 3.12 COMPARISON OF STRIP COMPLIANCES USING IDENTIFIED IMPEDANCE FUNCTIONS ($C_{s_2}^2/C_{s_1}^2 = 3.0$, $\xi_1 = \xi_2 = 0.02$, $\nu_1 = \nu_2 = 1/3$, H/R = 4/3)

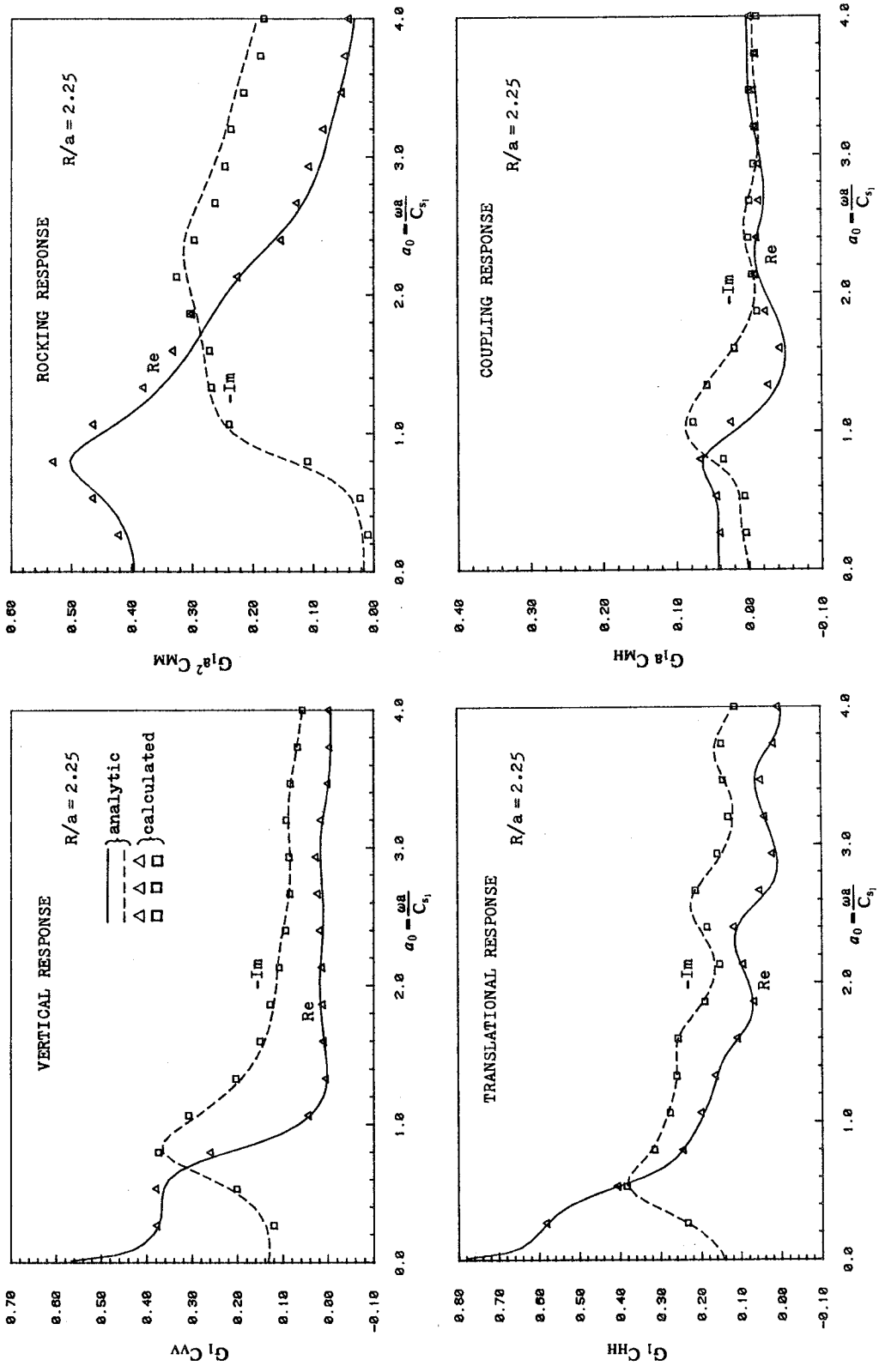

FIG. 3.13 COMPARISON OF STRIP COMPLIANCES USING IDENTIFIED IMPEDANCE FUNCTIONS ($C_{s_2}^2/C_{s_1}^2 = 3.0$, $\xi_1 = \xi_2 = 0.02$, $\nu_1 = \nu_2 = 1/3$, H/R = 4/3)

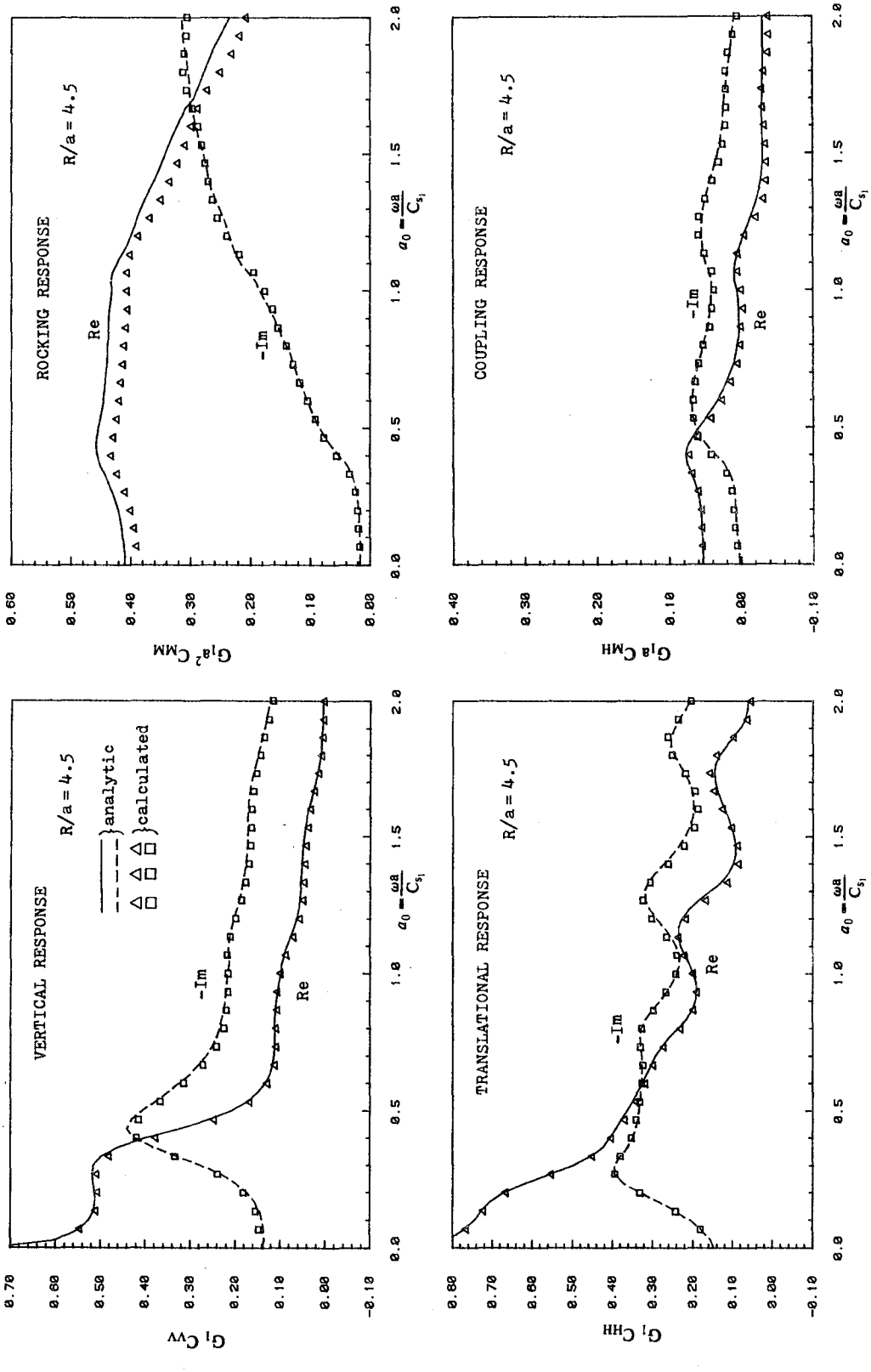

FIG. 3.14 COMPARISON OF STRIP COMPLIANCES USING IDENTIFIED IMPEDANCE FUNCTIONS ($C_{s_2}^2/C_{s_1}^2 = 3.0$, $\xi_1 = \xi_2 = 0.02$, $\nu_1 = \nu_2 = 1/3$, H/R = 4/3)

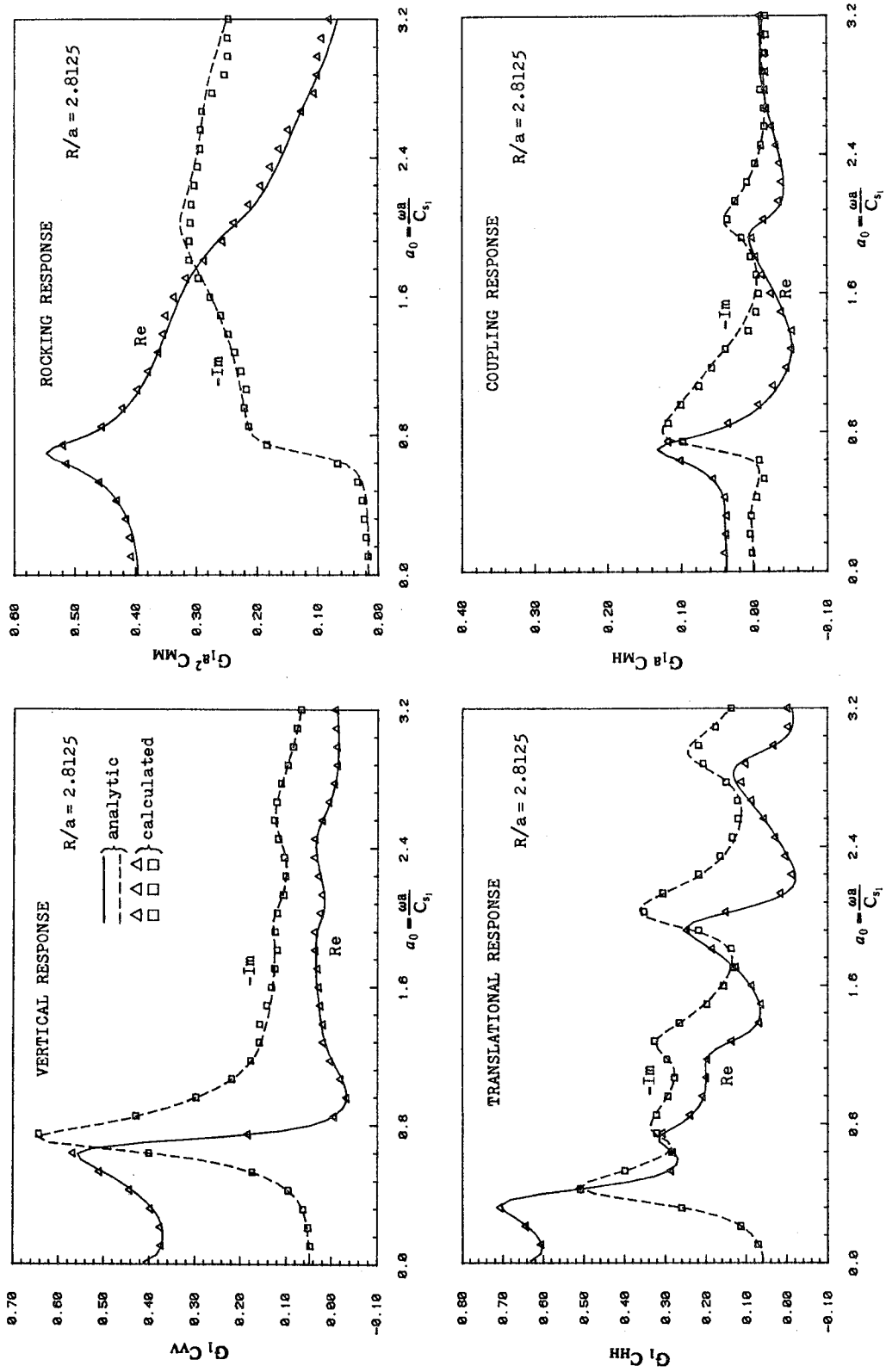

FIG. 3.15 COMPARISON OF STRIP COMPLIANCES USING IDENTIFIED IMPEDANCE FUNCTIONS ($C_{s_2}^2/C_{s_1}^2 = 10.0$, $\xi_1 = \xi_2 = 0.02$, $\nu_1 = \nu_2 = 1/3$, H/R =4/3)

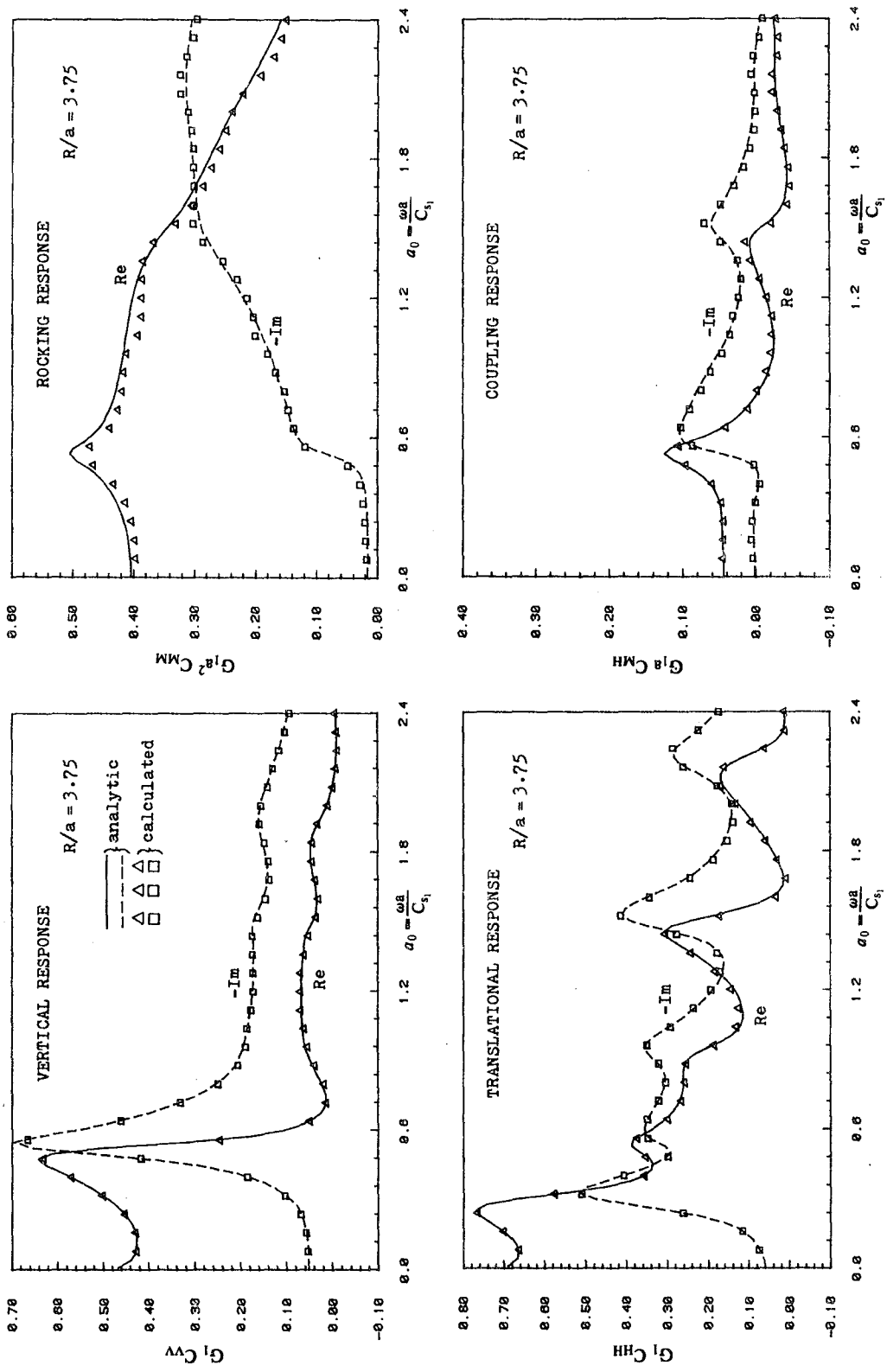

FIG. 3.16 COMPARISON OF STRIP COMPLIANCES USING IDENTIFIED IMPEDANCE FUNCTIONS ($C_{s_2}^2/C_{s_1}^2 = 10.0$, $\xi_1 = \xi_2 = 0.02$, $\nu_1 = \nu_2 = 1/3$, H/R =4/3)

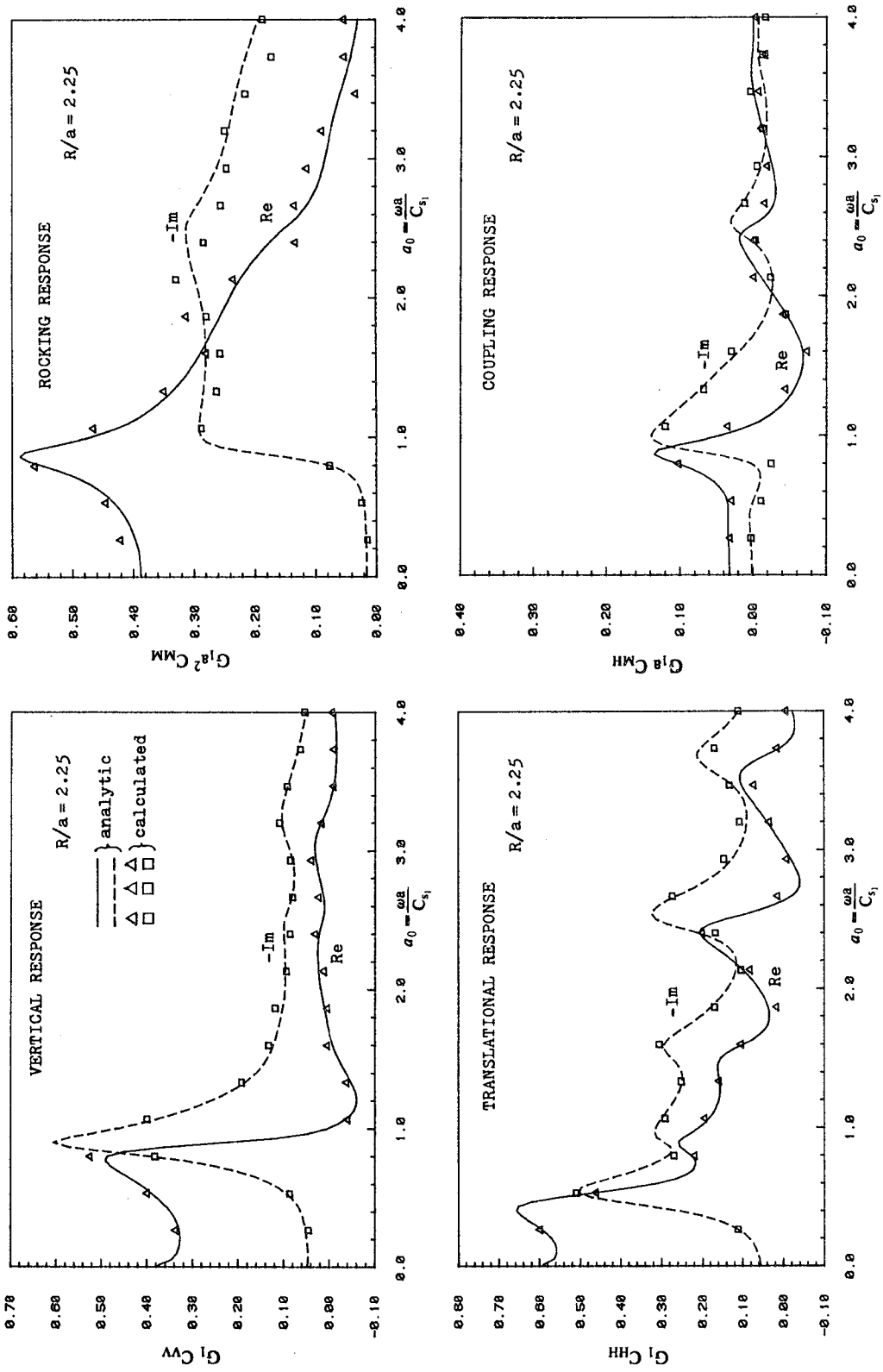

FIG. 3.17 COMPARISON OF STRIP COMPLIANCES USING IDENTIFIED IMPEDANCE FUNCTIONS ($C_{s_2}^2/C_{s_1}^2 = 10.0$, $\xi_1 = \xi_2 = 0.02$, $\nu_1 = \nu_2 = 1/3$, H/R = 4/3)

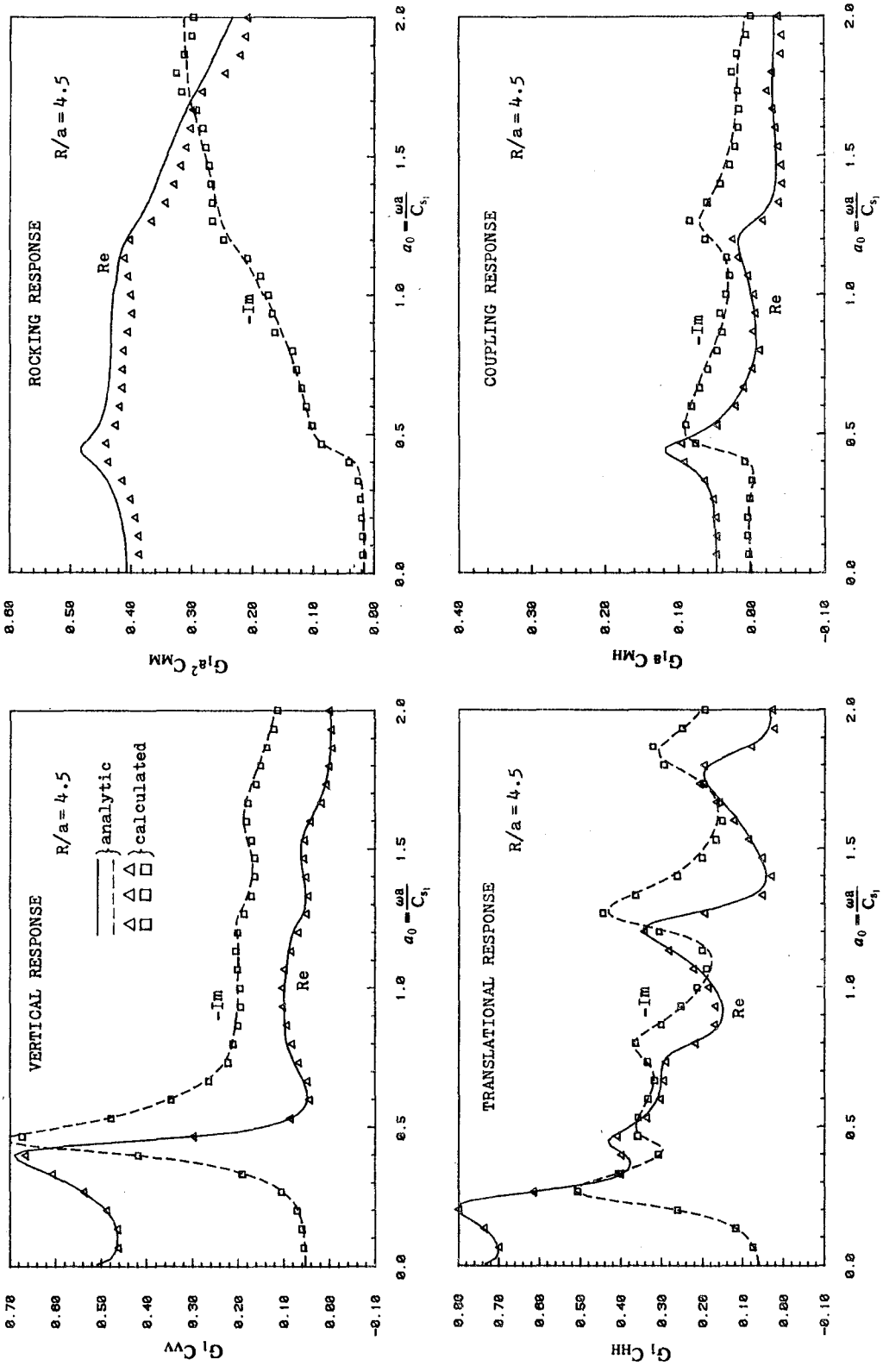

FIG. 3.18 COMPARISON OF STRIP COMPLIANCES USING IDENTIFIED IMPEDANCE FUNCTIONS ($C_{s_2}^2/C_{s_1}^2 = 10.0$, $\xi_1 = \xi_2 = 0.02$, $\nu_1 = \nu_2 = 1/3$, H/R = 4/3)

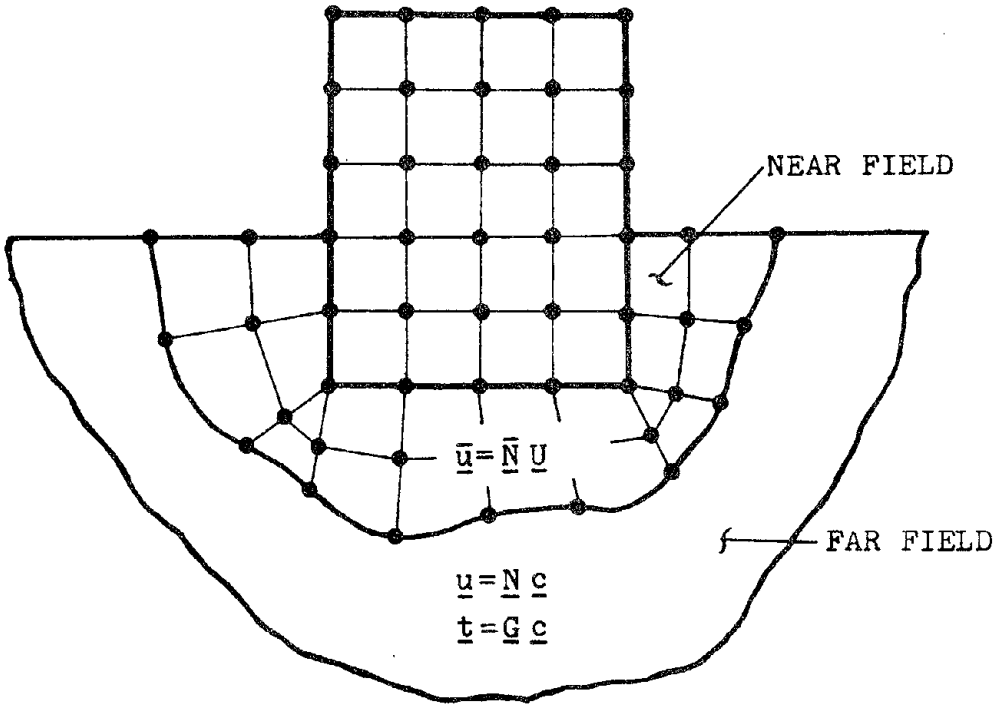

FIG. 4.1 HYBRID MODELLING USING BOUNDARY SOLUTION METHOD

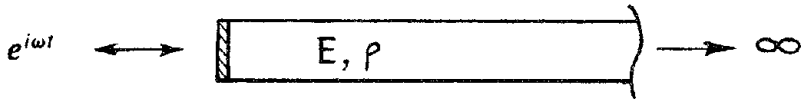

(a) HOMOGENEOUS BAR

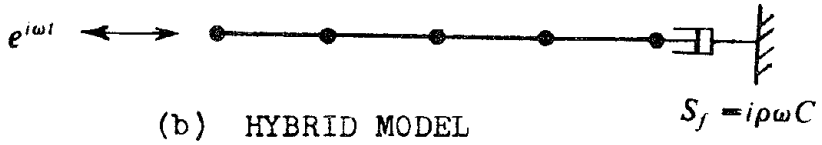

(b) HYBRID MODEL

FIG. 4.2 HARMONIC LOADING ON SEMI-INFINITE BAR

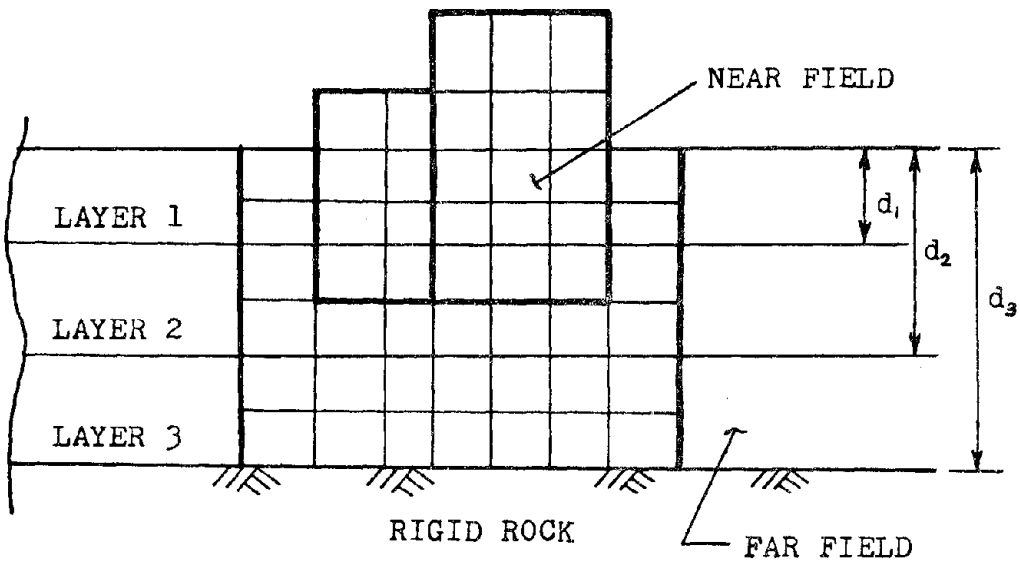

FIG. 4.3 HYBRID MODELLING OF LAYERED SOIL SYSTEM

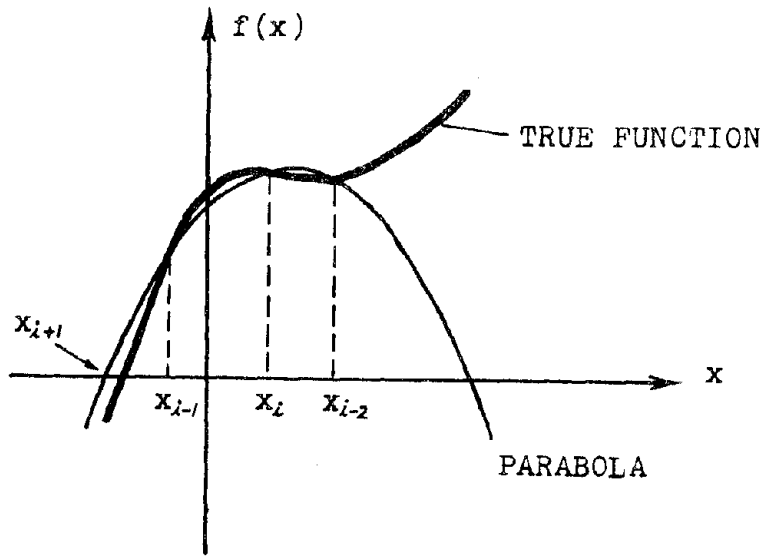

FIG. 4.4 ROOT-FINDING USING MULLER'S METHOD

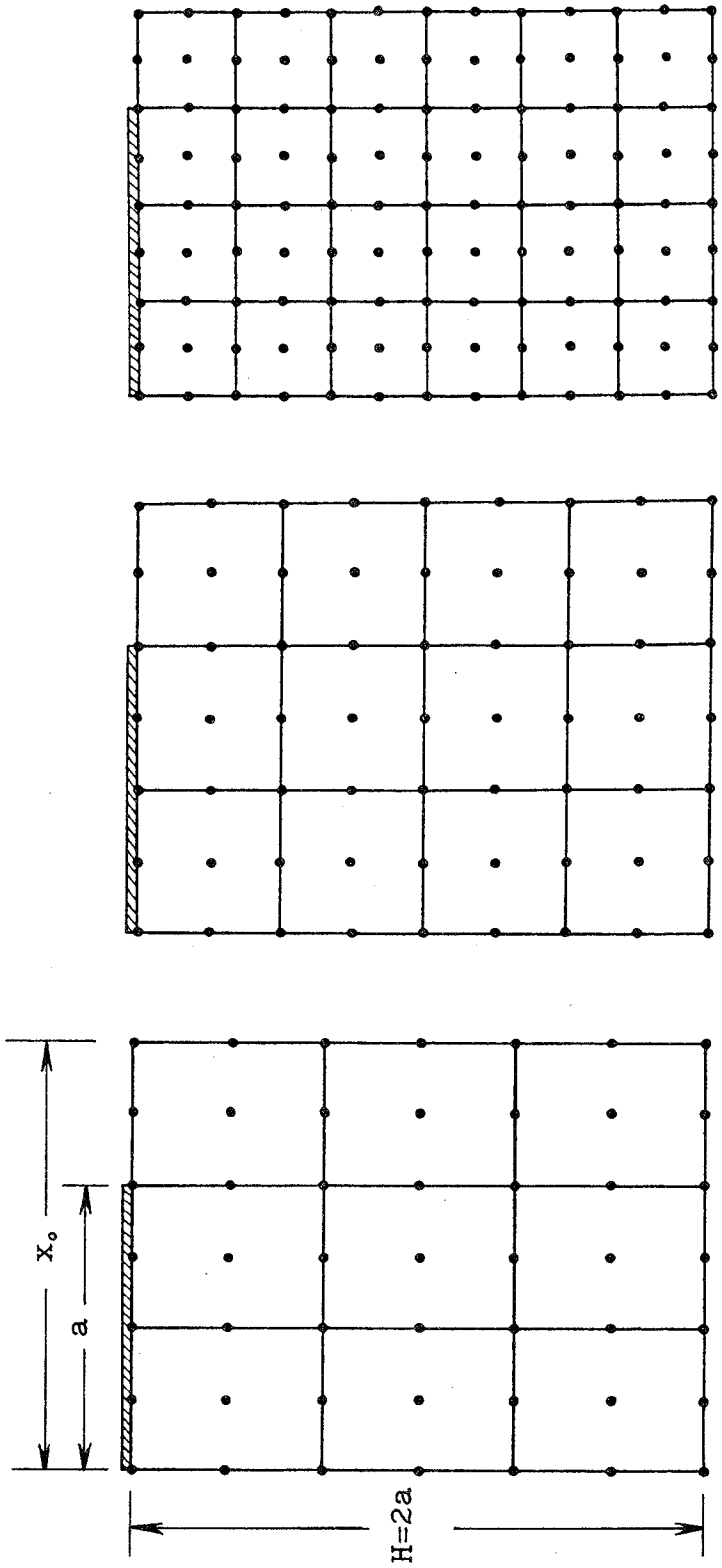

FIG. 4.5 NEAR-FIELD FINITE ELEMENT MODELS FOR INFINITELY LONG RIGID STRIP

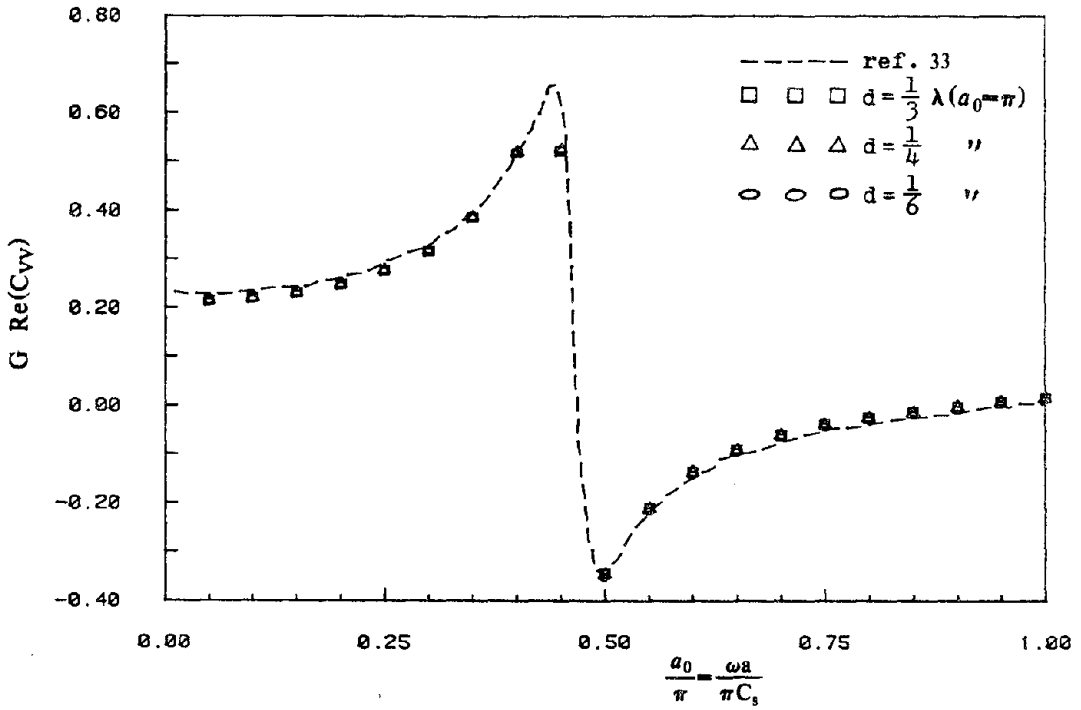

(a) REAL PART

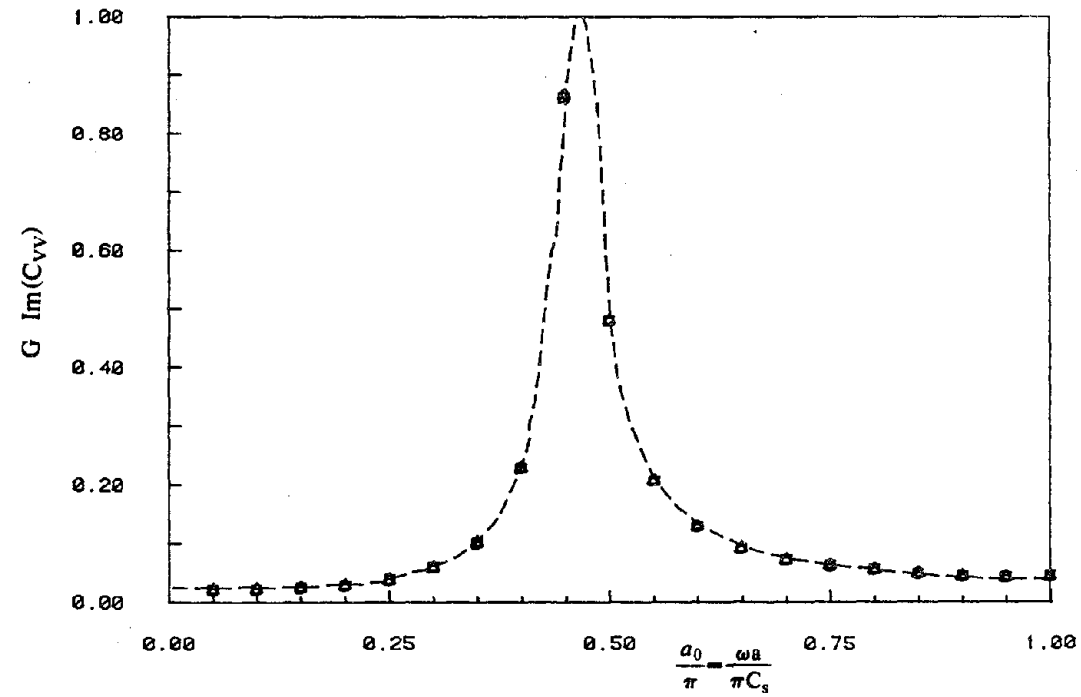

(b) IMAGINARY PART

FIG. 4.6 VERTICAL COMPLIANCE OF RIGID STRIP USING BOUNDARY SOLUTION METHOD (ν =0.3, ξ =0.05, H/a =2.0)

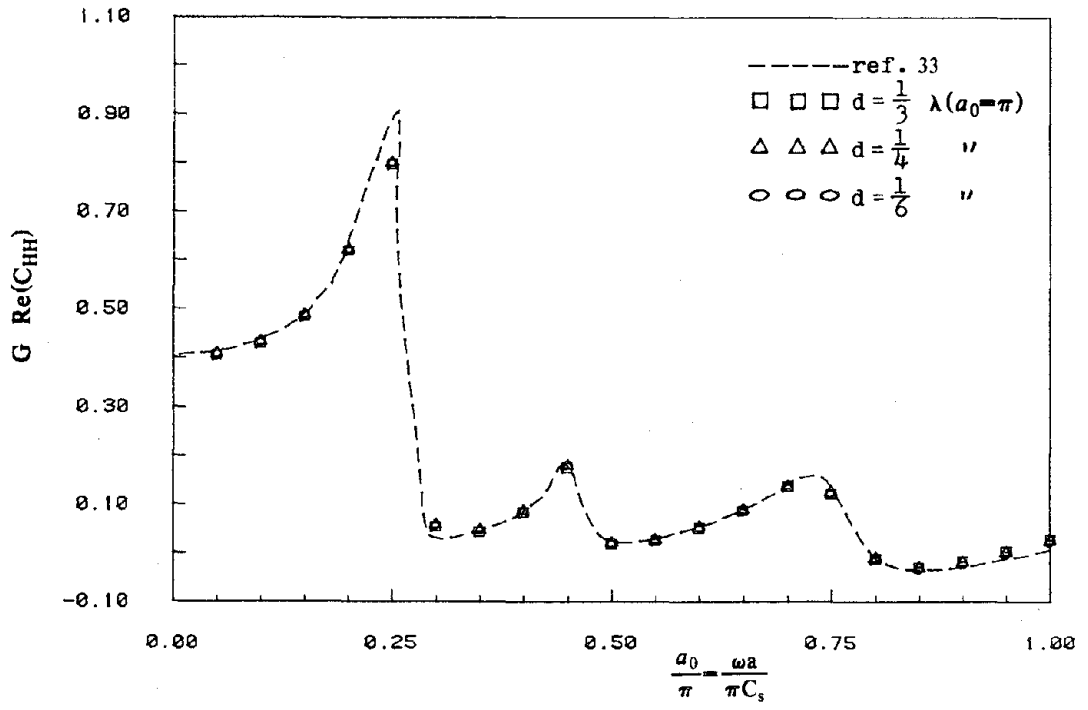

(a) REAL PART

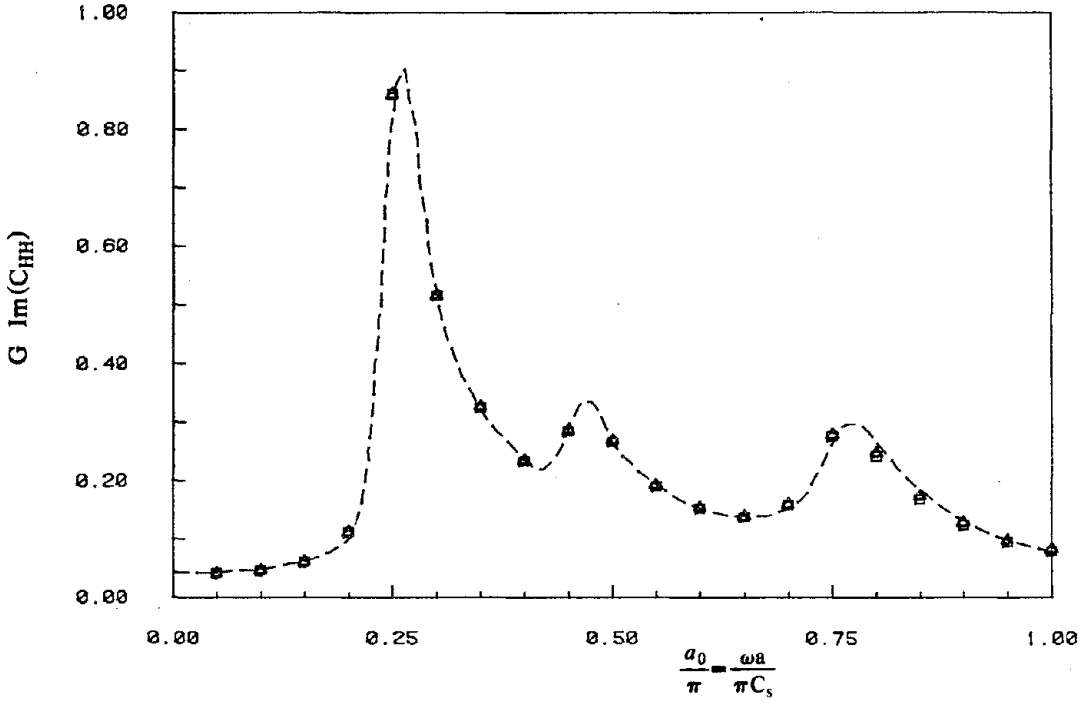

(b) IMAGINARY PART

FIG. 4.7 TRANSLATIONAL COMPLIANCE OF RIGID STRIP USING BOUNDARY SOLUTION METHOD (ν =0.3, ξ =0.05, H/a =2.0)

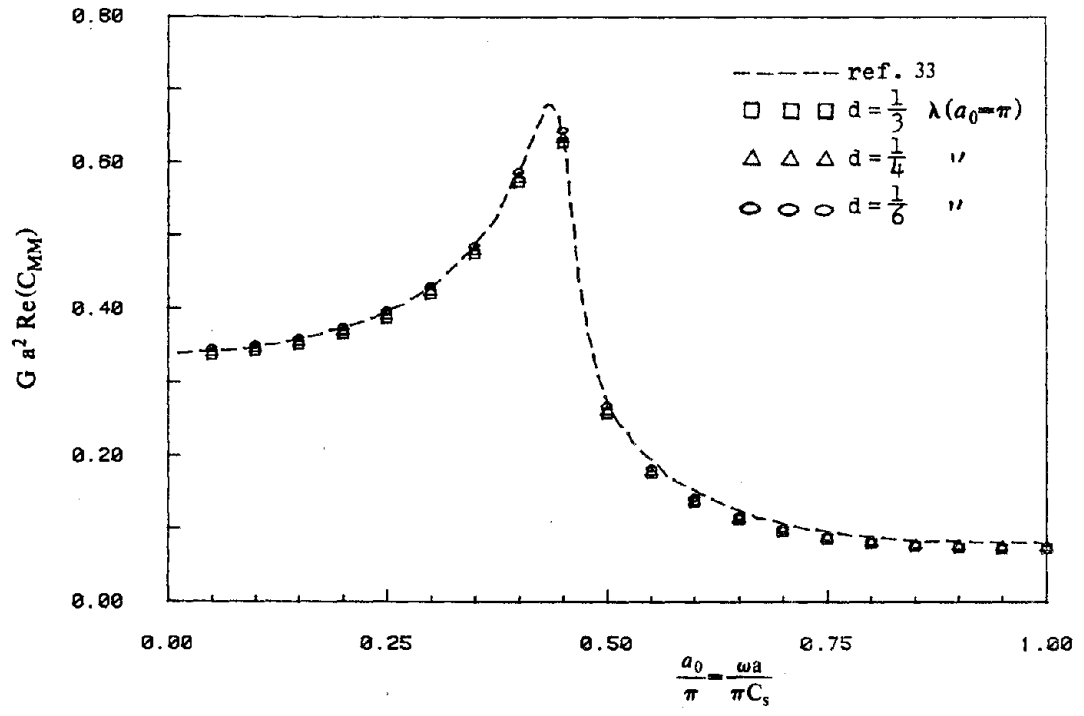

(a) REAL PART

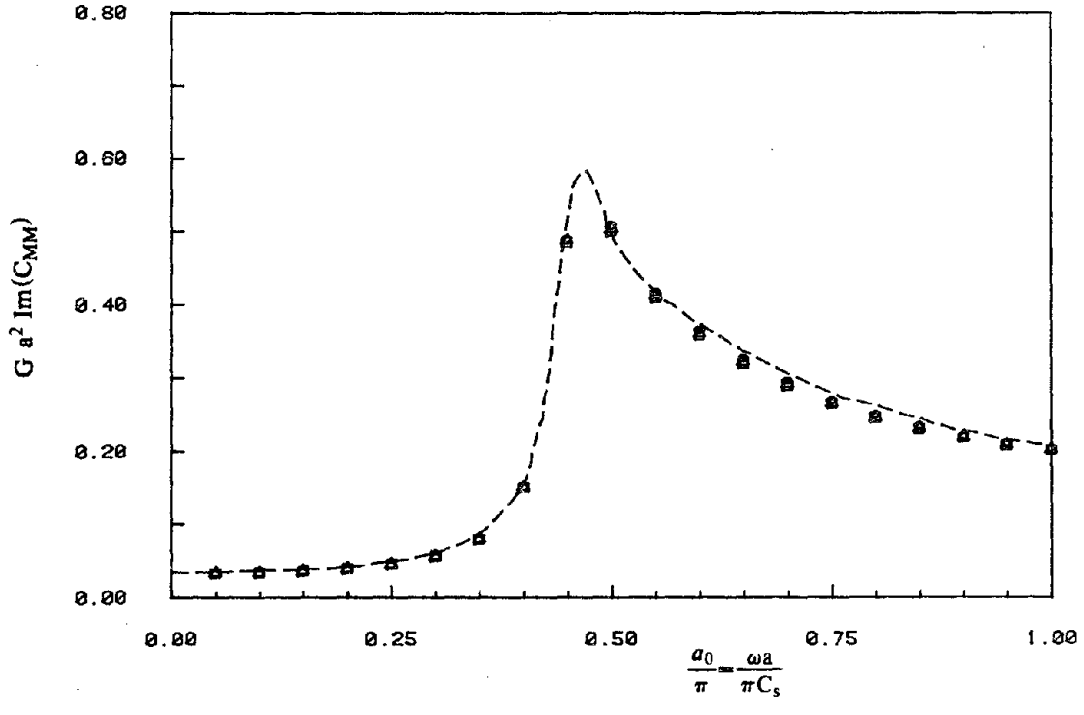

(b) IMAGINARY PART

FIG. 4.8 ROCKING COMPLIANCE OF RIGID STRIP USING BOUNDARY SOLUTION METHOD (ν =0.3, ξ =0.05, H/a =2.0)

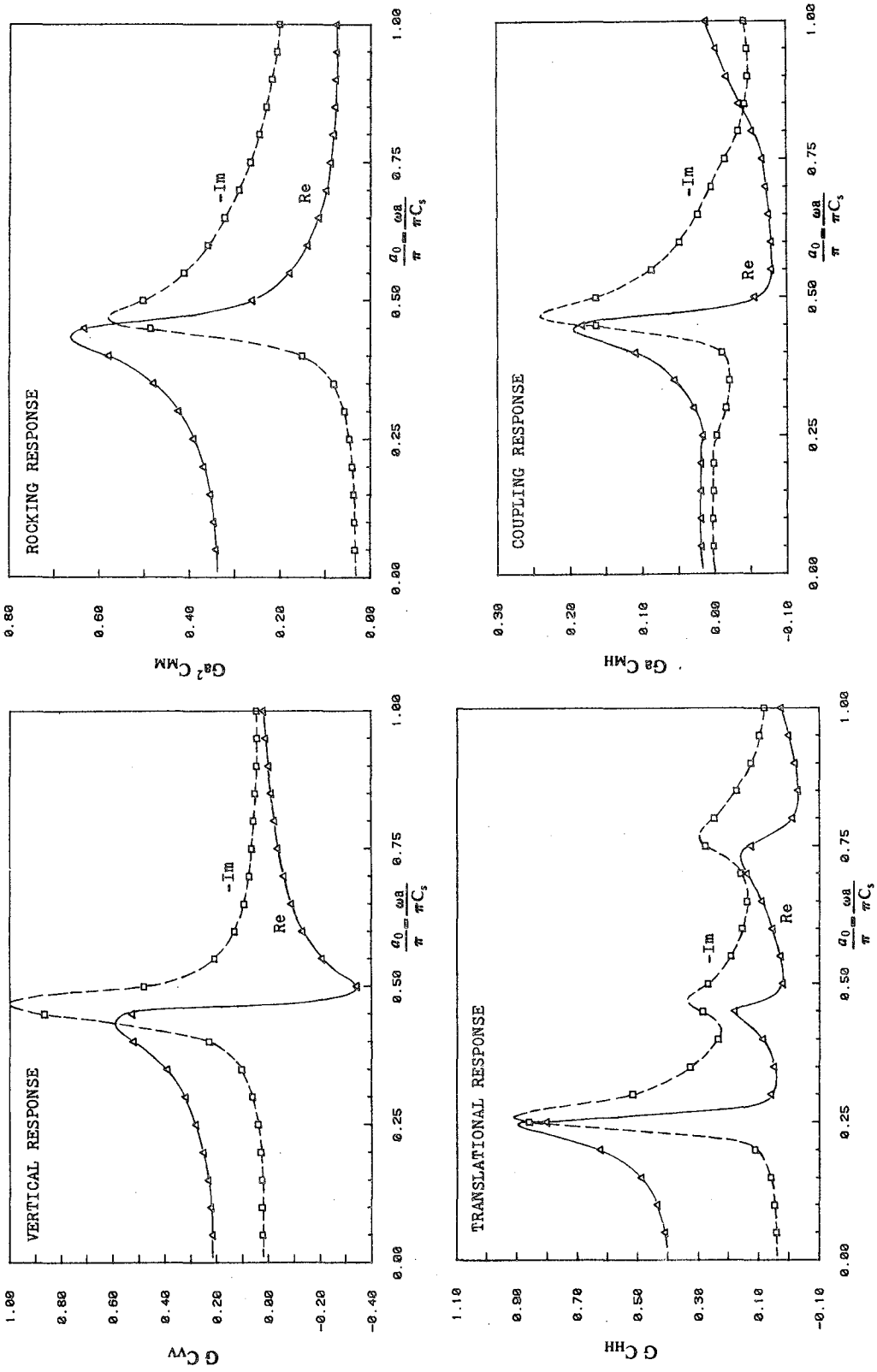

FIG. 4.9 STRIP COMPLIANCES FOR DIFFERENT NUMBERS OF INTEGRATION POINTS ($\nu = 0.3$, $\xi = 0.05$, $H/a = 2.0$)

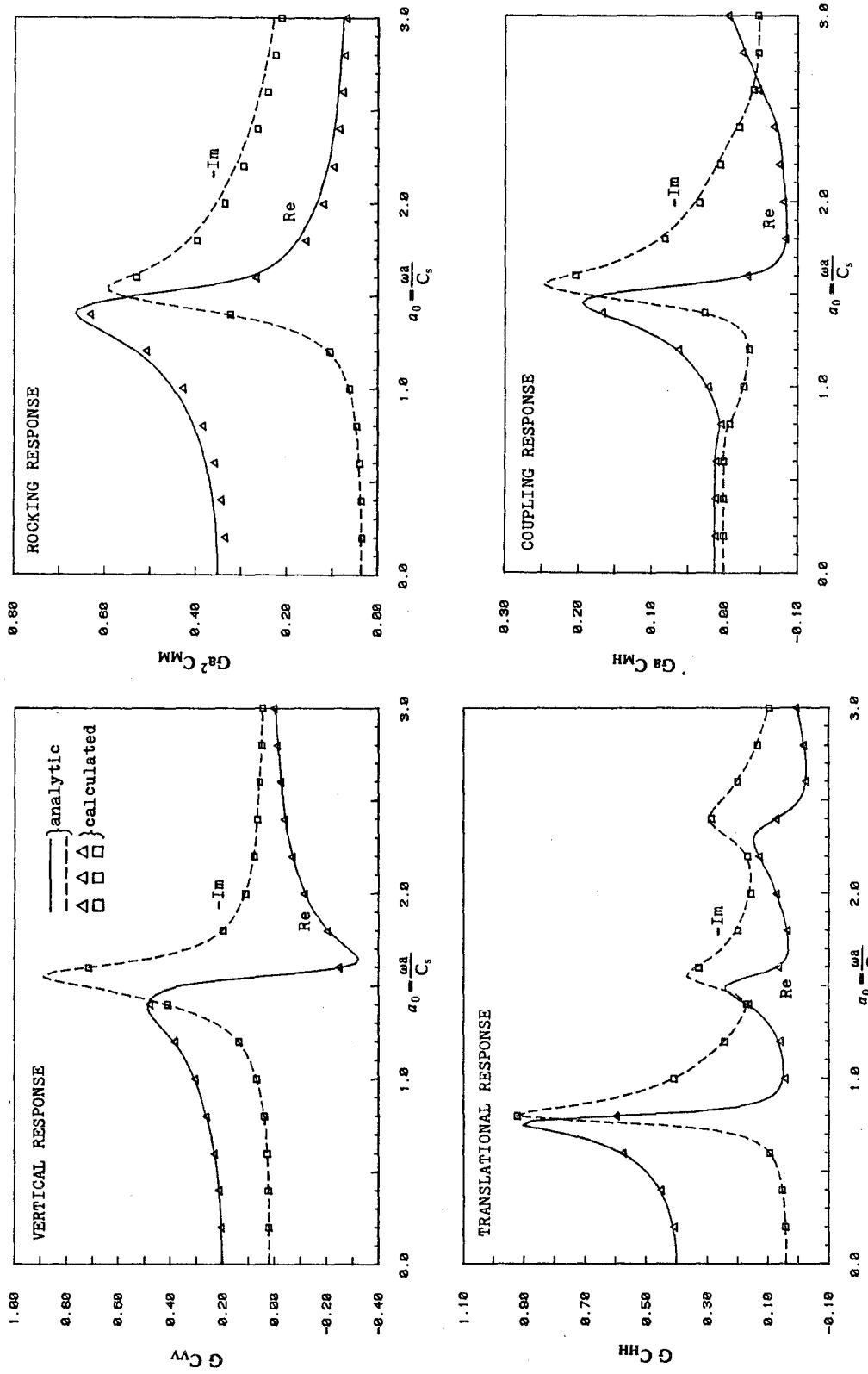

FIG. 4.10 COMPARISON OF STRIP COMPLIANCES USING BOUNDARY SOLUTION METHOD ($\nu = 1/3$, $\xi = 0.05$, H/a = 2.0)

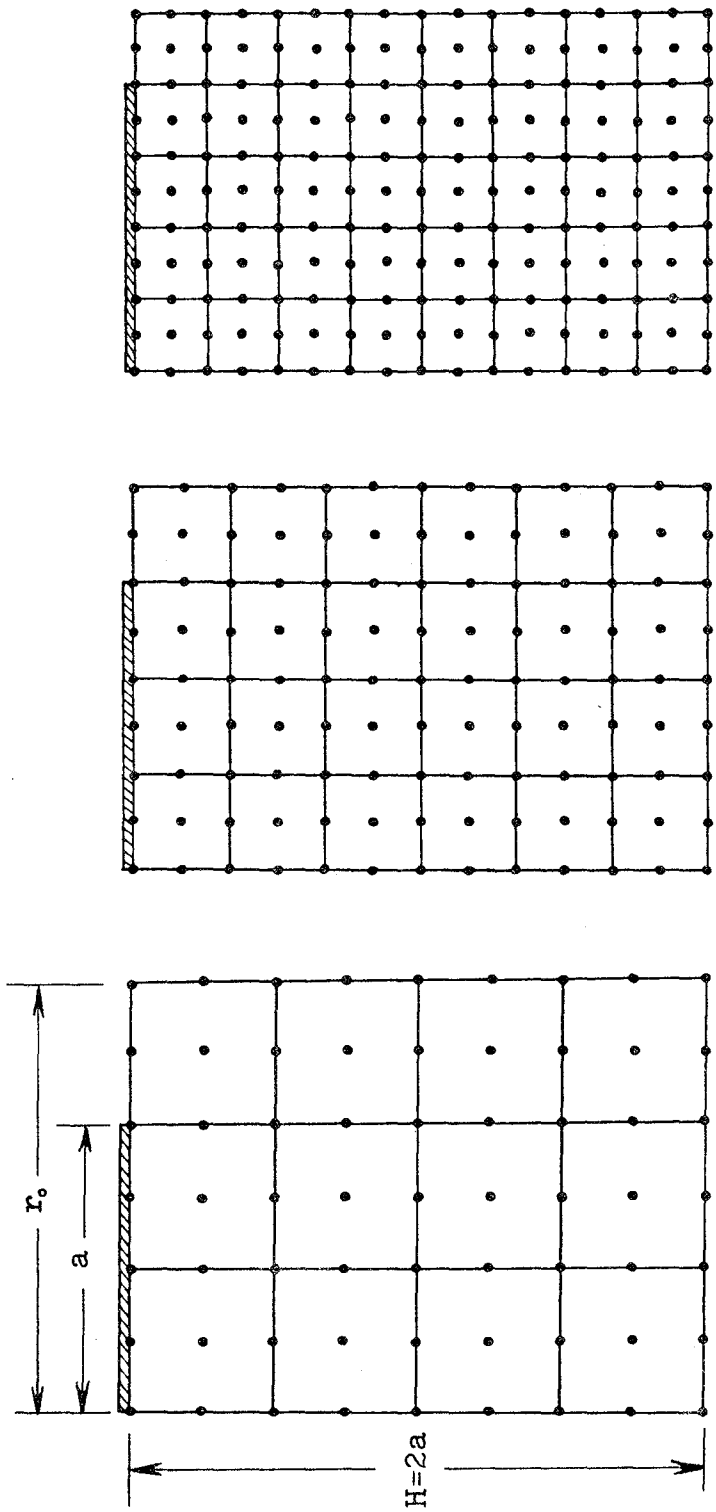

(a) COARSE MESH $d=\frac{1}{2}\lambda(a_0=2\pi)$

(b) MEDIUM MESH $d=\frac{1}{3}\lambda(a_0=2\pi)$

(c) FINE MESH $d=\frac{1}{4}\lambda(a_0=2\pi)$

FIG. 4.11 NEAR-FIELD FINITE ELEMENT MODELS FOR RIGID CIRCULAR DISK

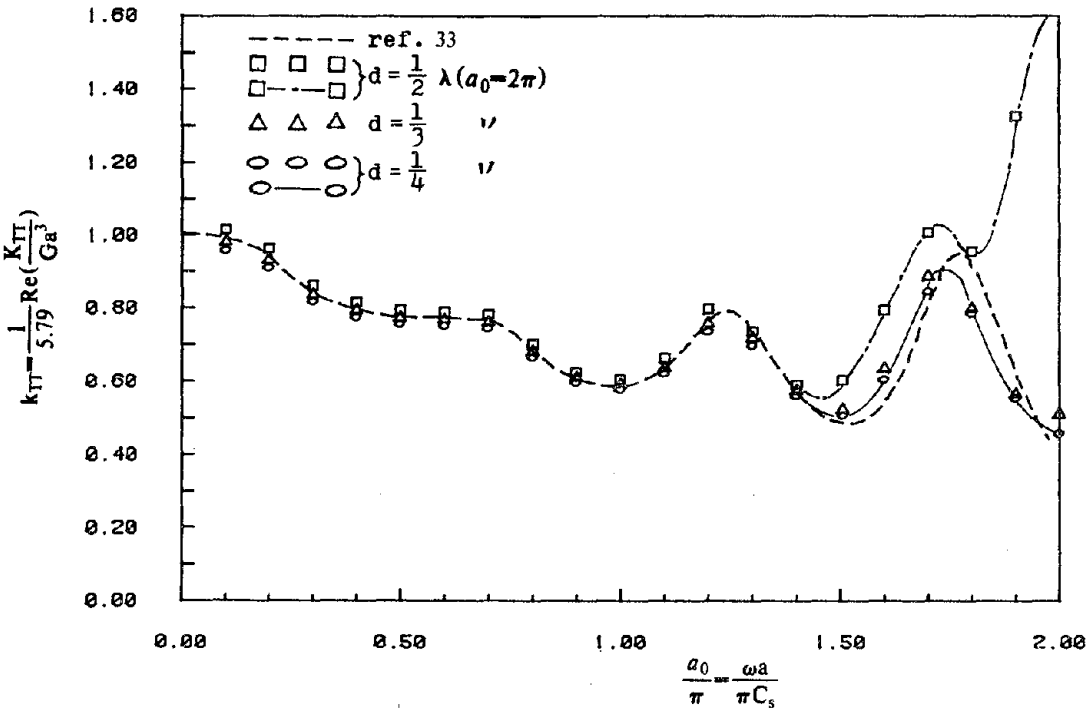

(a) STIFFNESS COEFFICIENT

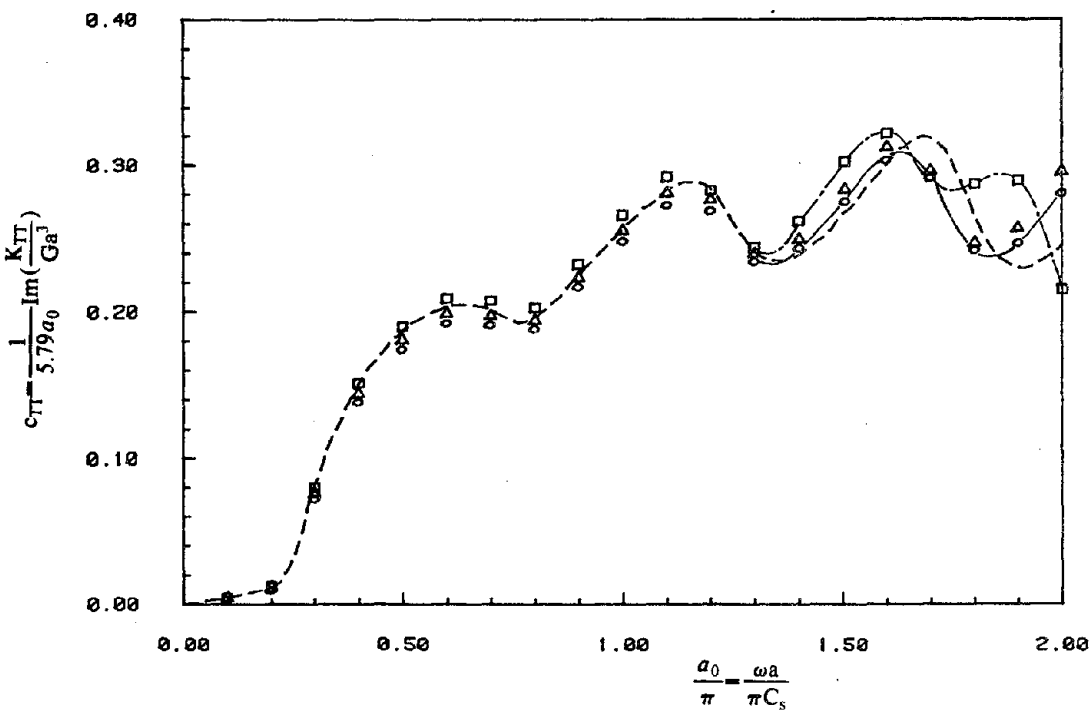

(b) DAMPING COEFFICIENT

FIG. 4.12 TORSIONAL IMPEDANCE OF CIRCULAR DISK USING BOUNDARY SOLUTION METHOD (ν =1/3, ξ =0.05, H/a =2.0)

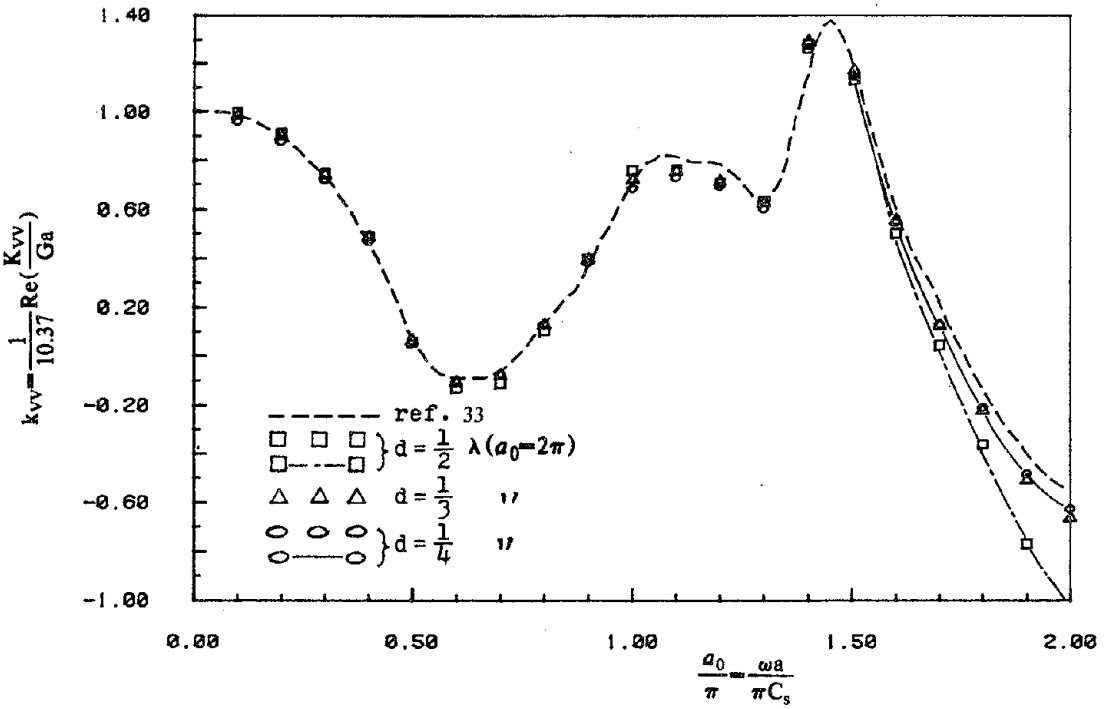

(a) STIFFNESS COEFFICIENT

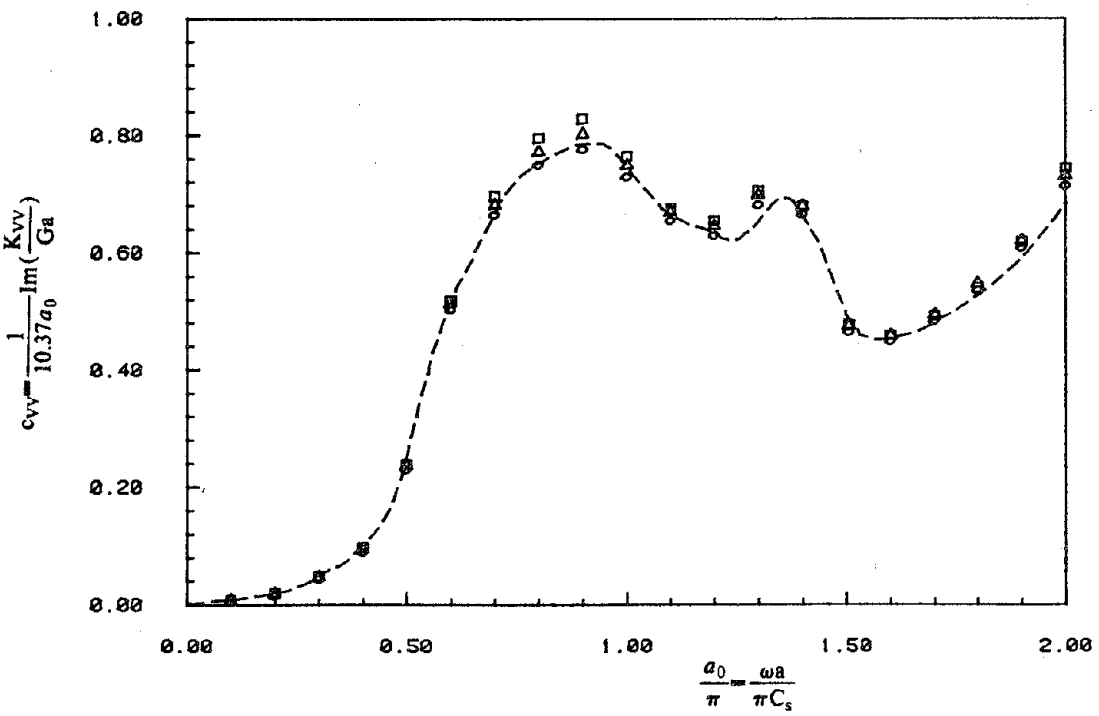

(b) DAMPING COEFFICIENT

FIG. 4.13 VERTICAL IMPEDANCE OF CIRCULAR DISK USING BOUNDARY SOLUTION METHOD (ν =1/3, ξ =0.05, H/a =2.0)

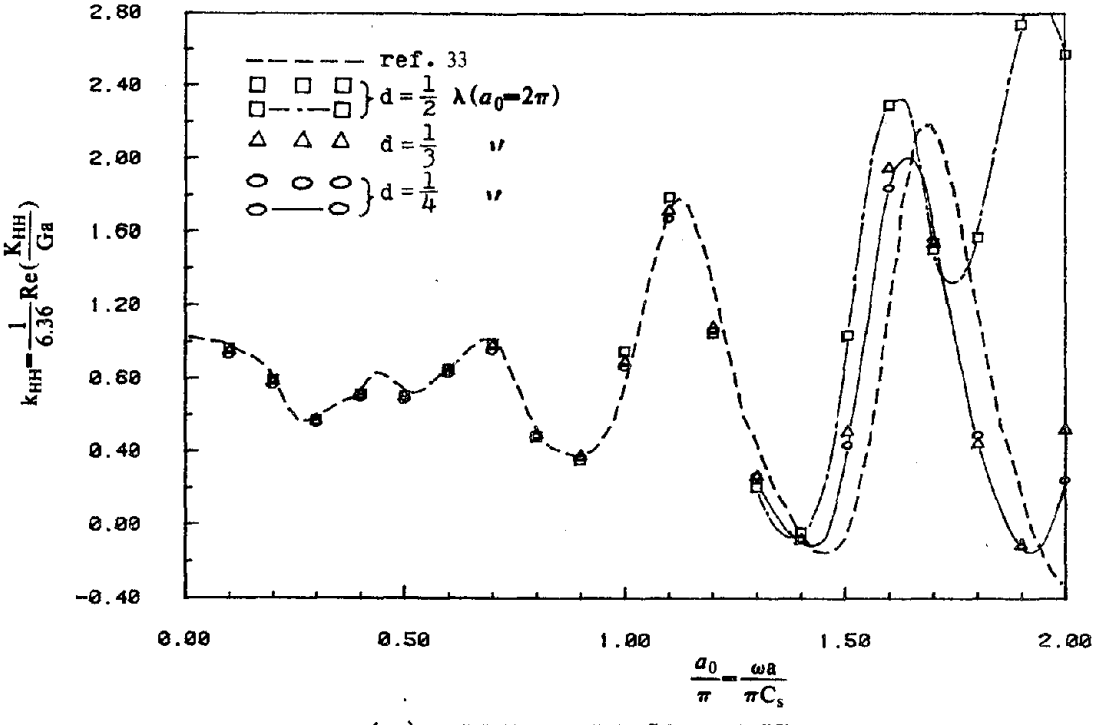

(a) STIFFNESS COEFFICIENT

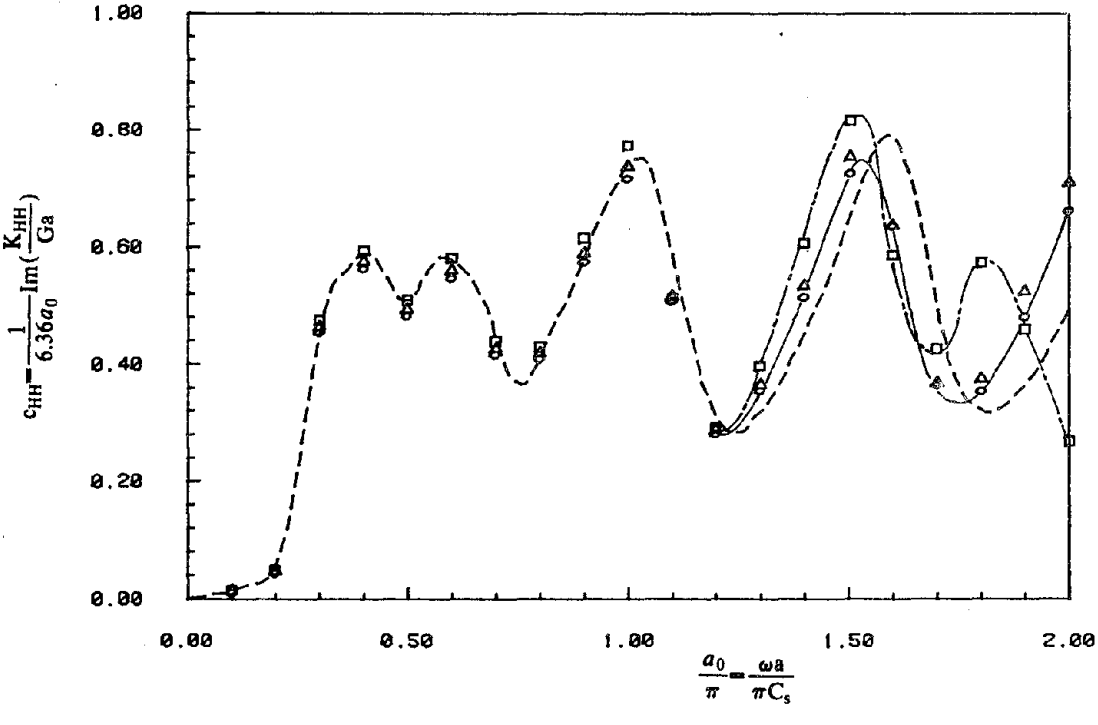

(b) DAMPING COEFFICIENT

FIG. 4.14 TRANSLATIONAL IMPEDANCE OF CIRCULAR DISK USING BOUNDARY SOLUTION METHOD (ν =1/3, ξ =0.05, H/a =2.0)

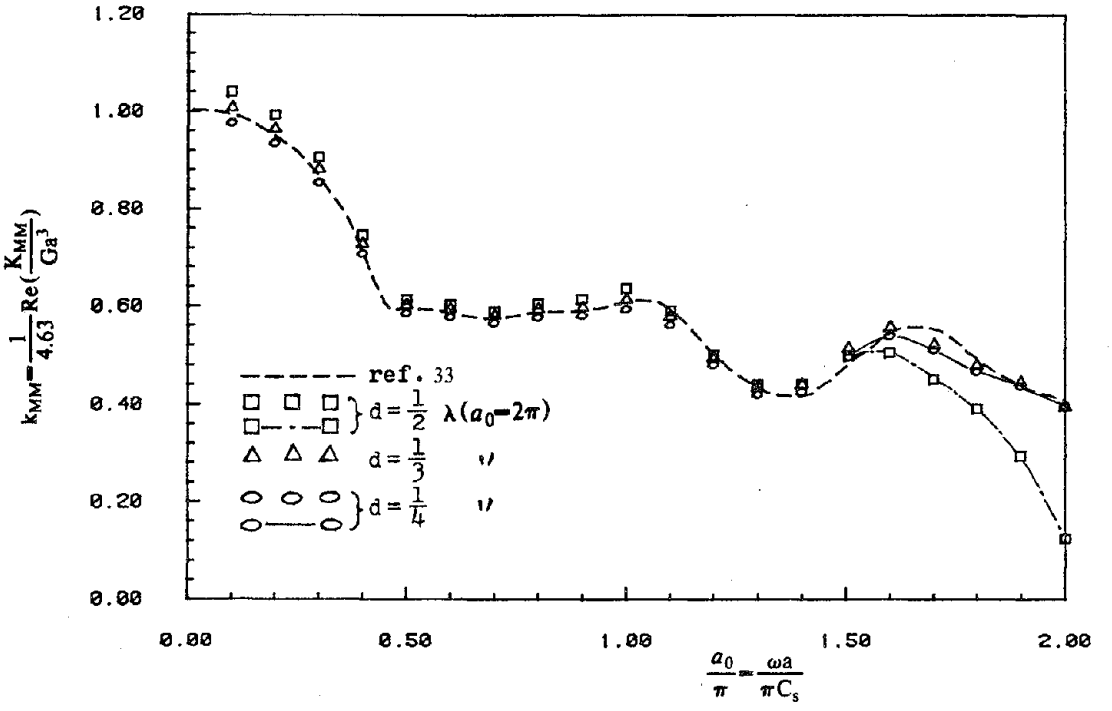

(a) STIFFNESS COEFFICIENT

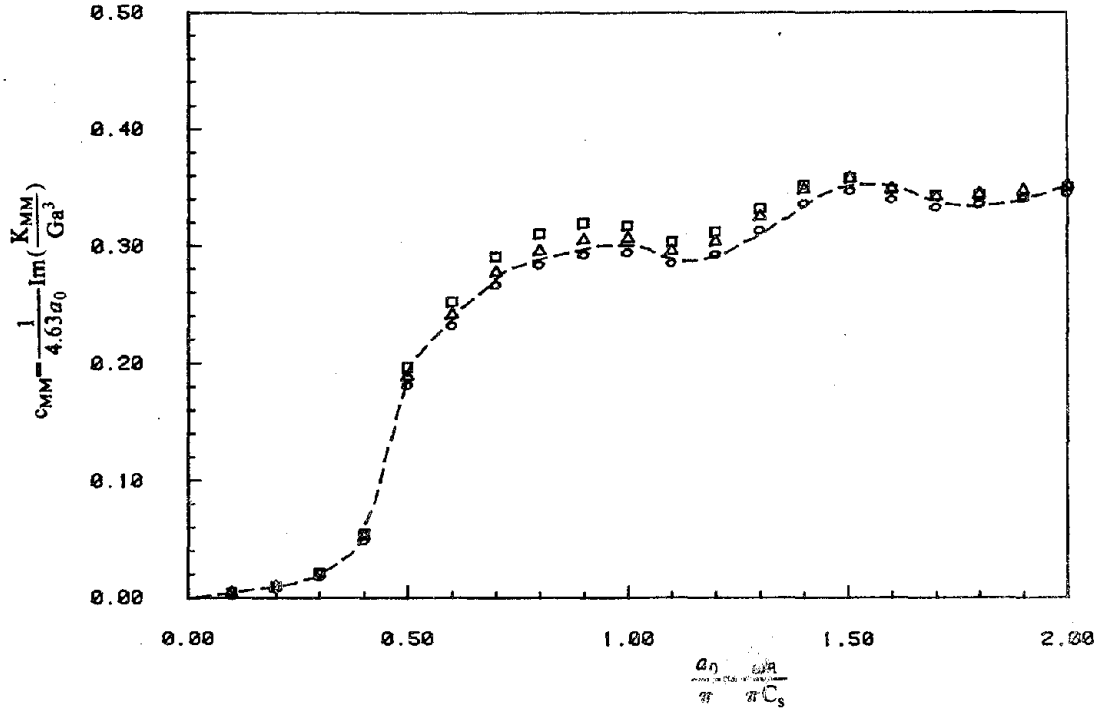

(b) DAMPING COEFFICIENT

FIG. 4.15 ROCKING IMPEDANCE OF CIRCULAR DISK USING BOUNDARY SOLUTION METHOD (ν =1/3, ξ =0.05, H/a =2.0)

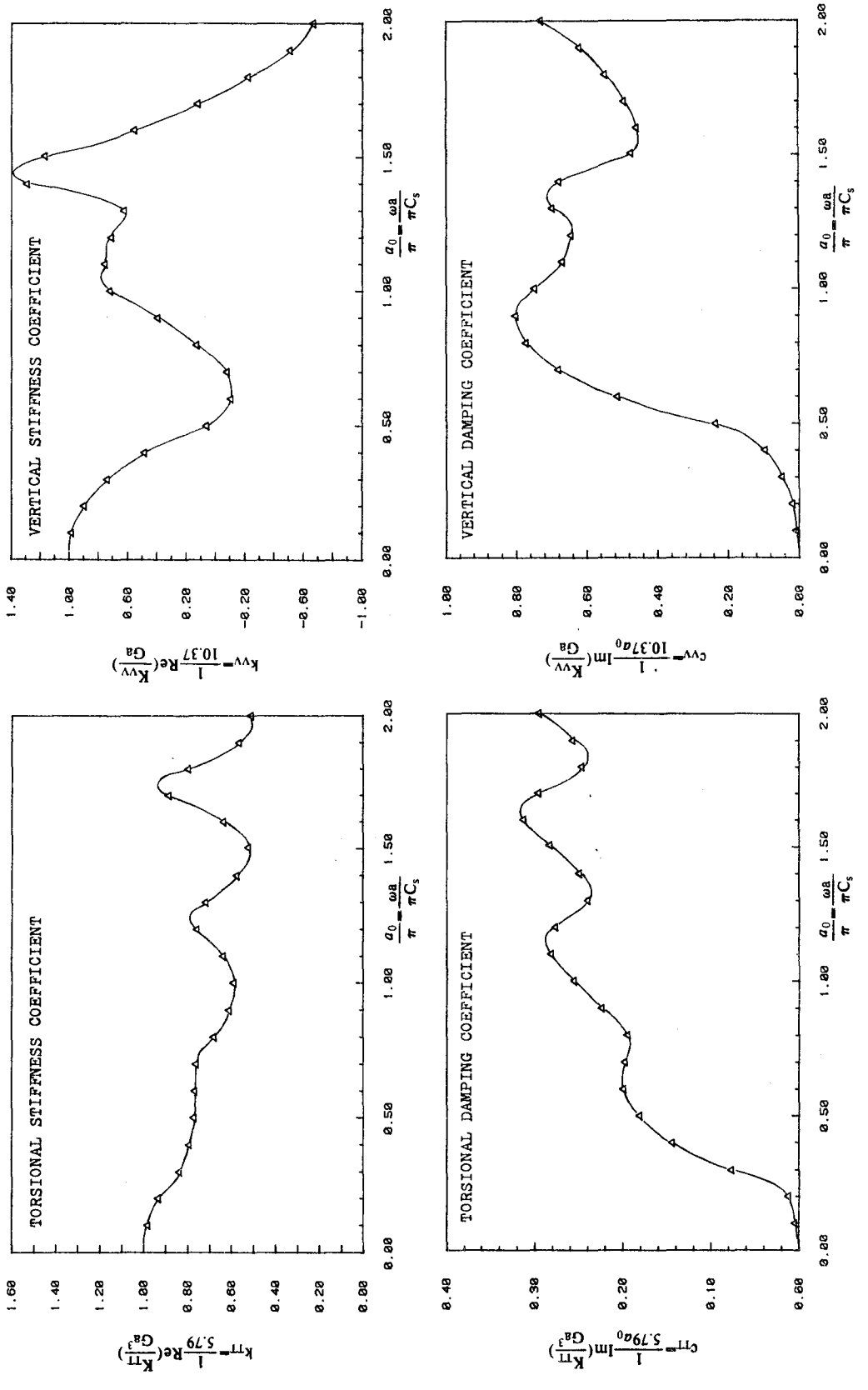

FIG. 4.16 TORSIONAL AND VERTICAL IMPEDANCES OF CIRCULAR DISK FOR DIFFERENT NUMBERS OF INTEGRATION POINTS (ν =1/3, ξ =0.05, H/a =2.0)

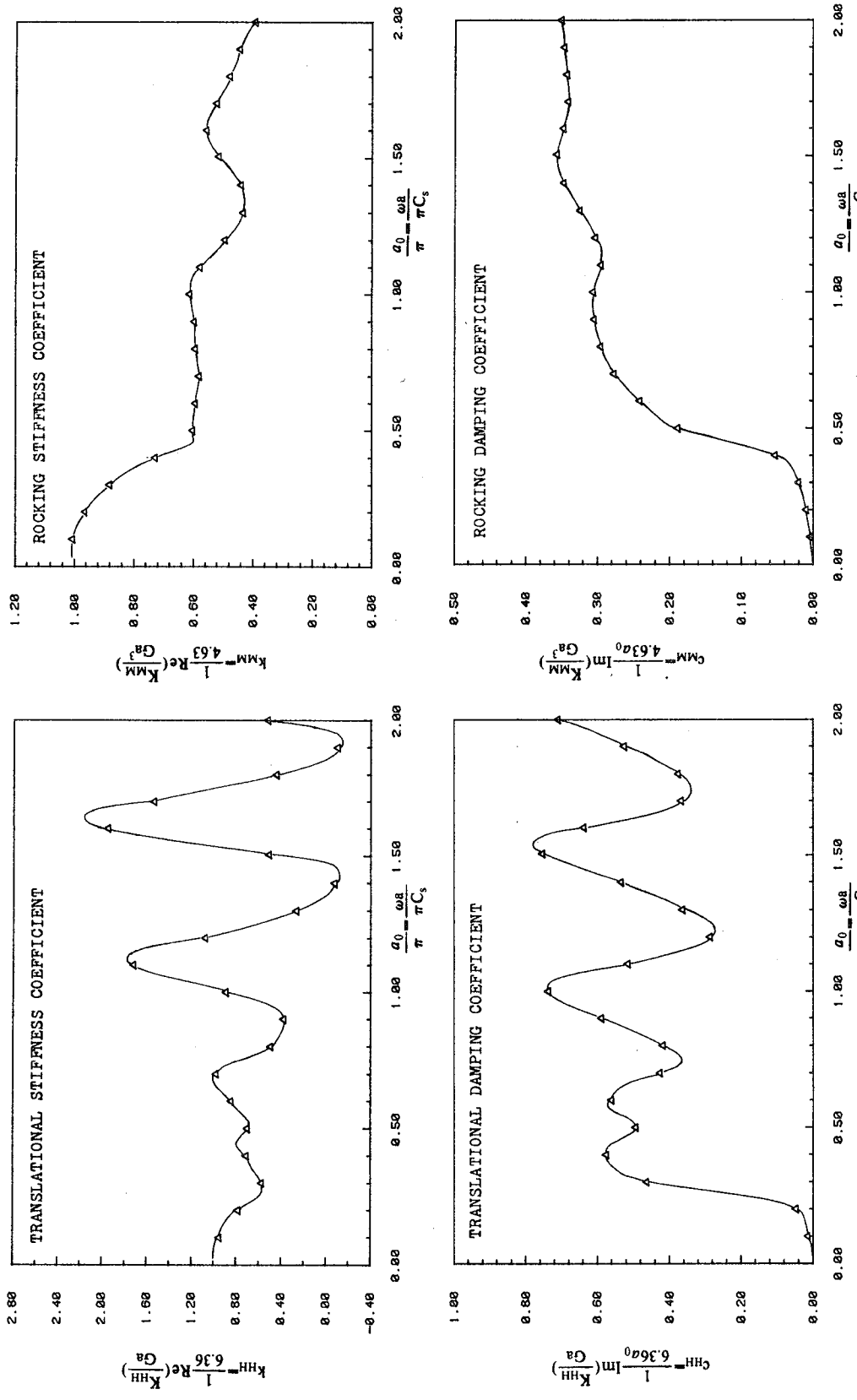

FIG. 4.17 TRANSLATIONAL AND ROCKING IMPEDANCES OF CIRCULAR DISK FOR DIFFERENT NUMBERS OF INTEGRATION POINTS (ν =1/3, ξ =0.05, H/a =2.0)

EARTHQUAKE ENGINEERING RESEARCH CENTER REPORTS

NOTE: Numbers in parentheses are Accession Numbers assigned by the National Technical Information Service; these are followed by a price code. Copies of the reports may be ordered from the National Technical Information Service, 5285 Port Royal Road, Springfield, Virginia, 22161. Accession Numbers should be quoted on orders for reports (PB --- ---) and remittance must accompany each order. Reports without this information were not available at time of printing. The complete list of EERC reports (from EERC 67-1) is available upon request from the Earthquake Engineering Research Center, University of California, Berkeley, 47th Street and Hoffman Boulevard, Richmond, California 94804.

UCB/EERC-77/01 "PLUSH - A Computer Program for Probabilistic Finite Element Analysis of Seismic Soil-Structure Interaction," by M.P. Romo Organista, J. Lysmer and H.B. Seed - 1977 (PB81 177 651)A05

UCB/EERC-77/02 "Soil-Structure Interaction Effects at the Humboldt Bay Power Plant in the Ferndale Earthquake of June 7, 1975," by J.E. Valera, H.B. Seed, C.F. Tsai and J. Lysmer - 1977 (PB 265 795)A04

UCB/EERC-77/03 "Influence of Sample Disturbance on Sand Response to Cyclic Loading," by K. Mori, H.B. Seed and C.K. Chan - 1977 (PB 267 352)A04

UCB/EERC-77/04 "Seismological Studies of Strong Motion Records," by J. Shoja-Taheri - 1977 (PB 269 655)A10

UCB/EERC-77/05 Unassigned

UCB/EERC-77/06 "Developing Methodologies for Evaluating the Earthquake Safety of Existing Buildings," by No. 1 - B. Bresler; No. 2 - B. Bresler, T. Okada and D. Zisling; No. 3 - T. Okada and B. Bresler; No. 4 - V.V. Bertero and B. Bresler - 1977 (PB 267 354)A08

UCB/EERC-77/07 "A Literature Survey - Transverse Strength of Masonry Walls," by Y. Omote, R.L. Mayes, S.W. Chen and R.W. Clough - 1977 (PB 277 933)A07

UCB/EERC-77/08 "DRAIN-TABS: A Computer Program for Inelastic Earthquake Response of Three Dimensional Buildings," by R. Guendelman-Israel and G.H. Powell - 1977 (PB 270 693)A07

UCB/EERC-77/09 "SUBWALL: A Special Purpose Finite Element Computer Program for Practical Elastic Analysis and Design of Structural Walls with Substructure Option," by D.Q. Le, H. Peterson and E.P. Popov - 1977 (PB 270 567)A05

UCB/EERC-77/10 "Experimental Evaluation of Seismic Design Methods for Broad Cylindrical Tanks," by D.P. Clough (PB 272 280)A13

UCB/EERC-77/11 "Earthquake Engineering Research at Berkeley - 1976," - 1977 (PB 273 507)A09

UCB/EERC-77/12 "Automated Design of Earthquake Resistant Multistory Steel Building Frames," by N.D. Walker, Jr. - 1977 (PB 276 526)A09

UCB/EERC-77/13 "Concrete Confined by Rectangular Hoops Subjected to Axial Loads," by J. Vallenas, V.V. Bertero and E.P. Popov - 1977 (PB 275 165)A06

UCB/EERC-77/14 "Seismic Strain Induced in the Ground During Earthquakes," by Y. Sugimura - 1977 (PB 284 201)A04

UCB/EERC-77/15 Unassigned

UCB/EERC-77/16 "Computer Aided Optimum Design of Ductile Reinforced Concrete Moment Resisting Frames," by S.W. Zagajeski and V.V. Bertero - 1977 (PB 280 137)A07

UCB/EERC-77/17 "Earthquake Simulation Testing of a Stepping Frame with Energy-Absorbing Devices," by J.M. Kelly and D.F. Tsztoo - 1977 (PB 273 506)A04

UCB/EERC-77/18 "Inelastic Behavior of Eccentrically Braced Steel Frames under Cyclic Loadings," by C.W. Roeder and E.P. Popov - 1977 (PB 275 526)A15

UCB/EERC-77/19 "A Simplified Procedure for Estimating Earthquake-Induced Deformations in Dams and Embankments," by F.I. Makdisi and H.B. Seed - 1977 (PB 276 820)A04

UCB/EERC-77/20 "The Performance of Earth Dams during Earthquakes," by H.B. Seed, F.I. Makdisi and P. de Alba - 1977 (PB 276 821)A04

UCB/EERC-77/21 "Dynamic Plastic Analysis Using Stress Resultant Finite Element Formulation," by P. Lukkunapvasit and J.M. Kelly - 1977 (PB 275 453)A04

UCB/EERC-77/22 "Preliminary Experimental Study of Seismic Uplift of a Steel Frame," by R.W. Clough and A.A. Huckelbridge 1977 (PB 278 769)A08

UCB/EERC-77/23 "Earthquake Simulator Tests of a Nine-Story Steel Frame with Columns Allowed to Uplift," by A.A. Huckelbridge - 1977 (PB 277 944)A09

UCB/EERC-77/24 "Nonlinear Soil-Structure Interaction of Skew Highway Bridges," by M.-C. Chen and J. Penzien - 1977 (PB 276 176)A07

UCB/EERC-77/25 "Seismic Analysis of an Offshore Structure Supported on Pile Foundations," by D.D.-N. Liou and J. Penzien 1977 (PB 283 180)A06

UCB/EERC-77/26 "Dynamic Stiffness Matrices for Homogeneous Viscoelastic Half-Planes," by G. Dasgupta and A.K. Chopra - 1977 (PB 279 654)A06

UCB/EERC-77/27 "A Practical Soft Story Earthquake Isolation System," by J.M. Kelly, J.M. Eidinger and C.J. Derham - 1977 (PB 276 814)A07

UCB/EERC-77/28 "Seismic Safety of Existing Buildings and Incentives for Hazard Mitigation in San Francisco: An Exploratory Study," by A.J. Meltsner - 1977 (PB 281 970)A05

UCB/EERC-77/29 "Dynamic Analysis of Electrohydraulic Shaking Tables," by D. Rea, S. Abedi-Hayati and Y. Takahashi 1977 (PB 282 569)A04

UCB/EERC-77/30 "An Approach for Improving Seismic - Resistant Behavior of Reinforced Concrete Interior Joints," by B. Galunic, V.V. Bertero and E.P. Popov - 1977 (PB 290 870)A06

UCB/EERC-78/01 "The Development of Energy-Absorbing Devices for Aseismic Base Isolation Systems," by J.M. Kelly and D.F. Tsztoo - 1978 (PB 284 978)A04

UCB/EERC-78/02 "Effect of Tensile Prestrain on the Cyclic Response of Structural Steel Connections, by J.G. Bouwkamp and A. Mukhopadhyay - 1978

UCB/EERC-78/03 "Experimental Results of an Earthquake Isolation System using Natural Rubber Bearings," by J.M. Eidinger and J.M. Kelly - 1978 (PB 281 686)A04

UCB/EERC-78/04 "Seismic Behavior of Tall Liquid Storage Tanks," by A. Niwa - 1978 (PB 284 017)A14

UCB/EERC-78/05 "Hysteretic Behavior of Reinforced Concrete Columns Subjected to High Axial and Cyclic Shear Forces," by S.W. Zagajeski, V.V. Bertero and J.G. Bouwkamp - 1978 (PB 283 858)A13

UCB/EERC-78/06 "Three Dimensional Inelastic Frame Elements for the ANSR-I Program," by A. Riahi, D.G. Row and G.H. Powell - 1978 (PB 295 755)A04

UCB/EERC-78/07 "Studies of Structural Response to Earthquake Ground Motion," by O.A. Lopez and A.K. Chopra - 1978 (PB 282 790)A05

UCB/EERC-78/08 "A Laboratory Study of the Fluid-Structure Interaction of Submerged Tanks and Caissons in Earthquakes," by R.C. Byrd - 1978 (PB 284 957)A08

UCB/EERC-78/09 Unassigned

UCB/EERC-78/10 "Seismic Performance of Nonstructural and Secondary Structural Elements," by I. Sakamoto - 1978 (PB81 154 593)A05

UCB/EERC-78/11 "Mathematical Modelling of Hysteresis Loops for Reinforced Concrete Columns," by S. Nakata, T. Sproul and J. Penzien - 1978 (PB 298 274)A05

UCB/EERC-78/12 "Damageability in Existing Buildings," by T. Blejwas and B. Bresler - 1978 (PB 80 166 978)A05

UCB/EERC-78/13 "Dynamic Behavior of a Pedestal Base Multistory Building," by R.M. Stephen, E.L. Wilson, J.G. Bouwkamp and M. Button - 1978 (PB 286 650)A08

UCB/EERC-78/14 "Seismic Response of Bridges - Case Studies," by R.A. Imbsen, V. Nutt and J. Penzien - 1978 (PB 286 503)A10

UCB/EERC-78/15 "A Substructure Technique for Nonlinear Static and Dynamic Analysis," by D.G. Row and G.H. Powell - 1978 (PB 288 077)A10

UCB/EERC-78/16 "Seismic Risk Studies for San Francisco and for the Greater San Francisco Bay Area," by C.S. Oliveira - 1978 (PB 81 120 115)A07

UCB/EERC-78/17 "Strength of Timber Roof Connections Subjected to Cyclic Loads," by P. Gülkan, R.L. Mayes and R.W. Clough - 1978 (HUD-000 1491)A07

UCB/EERC-78/18 "Response of K-Braced Steel Frame Models to Lateral Loads," by J.G. Bouwkamp, R.M. Stephen and E.P. Popov - 1978

UCB/EERC-78/19 "Rational Design Methods for Light Equipment in Structures Subjected to Ground Motion," by J.L. Sackman and J.M. Kelly - 1978 (PB 292 357)A04

UCB/EERC-78/20 "Testing of a Wind Restraint for Aseismic Base Isolation," by J.M. Kelly and D.E. Chitty - 1978 (PB 292 833)A03

UCB/EERC-78/21 "APOLLO - A Computer Program for the Analysis of Pore Pressure Generation and Dissipation in Horizontal Sand Layers During Cyclic or Earthquake Loading," by P.P. Martin and H.B. Seed - 1978 (PB 292 835)A04

UCB/EERC-78/22 "Optimal Design of an Earthquake Isolation System," by M.A. Bhatti, K.S. Pister and E. Polak - 1978 (PB 294 735)A06

UCB/EERC-78/23 "MASH - A Computer Program for the Non-Linear Analysis of Vertically Propagating Shear Waves in Horizontally Layered Deposits," by P.P. Martin and H.B. Seed - 1978 (PB 293 101)A05

UCB/EERC-78/24 "Investigation of the Elastic Characteristics of a Three Story Steel Frame Using System Identification," by I. Kaya and H.D. McNiven - 1978 (PB 296 225)A06

UCB/EERC-78/25 "Investigation of the Nonlinear Characteristics of a Three-Story Steel Frame Using System Identification," by I. Kaya and H.D. McNiven - 1978 (PB 301 363)A05

UCB/EERC-78/26 "Studies of Strong Ground Motion in Taiwan," by Y.M. Hsiung, B.A. Bolt and J. Penzien - 1978 (PB 298 436)A06

UCB/EERC-78/27 "Cyclic Loading Tests of Masonry Single Piers: Volume 1 - Height to Width Ratio of 2," by P.A. Hidalgo, R.L. Mayes, H.D. McNiven and R.W. Clough - 1978 (PB 296 211)A07

UCB/EERC-78/28 "Cyclic Loading Tests of Masonry Single Piers: Volume 2 - Height to Width Ratio of 1," by S.-W.J. Chen, P.A. Hidalgo, R.L. Mayes, R.W. Clough and H.D. McNiven - 1978 (PB 296 212)A09

UCB/EERC-78/29 "Analytical Procedures in Soil Dynamics," by J. Lysmer - 1978 (PB 298 445)A06

UCB/EERC-79/01 "Hysteretic Behavior of Lightweight Reinforced Concrete Beam-Column Subassemblages," by B. Forzani, E.P. Popov and V.V. Bertero - April 1979(PB 298 267)A06

UCB/EERC-79/02 "The Development of a Mathematical Model to Predict the Flexural Response of Reinforced Concrete Beams to Cyclic Loads, Using System Identification," by J. Stanton & H. McNiven - Jan. 1979(PB 295 875)A10

UCB/EERC-79/03 "Linear and Nonlinear Earthquake Response of Simple Torsionally Coupled Systems," by C.L. Kan and A.K. Chopra - Feb. 1979(PB 298 262)A06

UCB/EERC-79/04 "A Mathematical Model of Masonry for Predicting its Linear Seismic Response Characteristics," by Y. Mengi and H.D. McNiven - Feb. 1979(PB 298 266)A06

UCB/EERC-79/05 "Mechanical Behavior of Lightweight Concrete Confined by Different Types of Lateral Reinforcement," by M.A. Manrique, V.V. Bertero and E.P. Popov - May 1979(PB 301 114)A06

UCB/EERC-79/06 "Static Tilt Tests of a Tall Cylindrical Liquid Storage Tank," by R.W. Clough and A. Niwa - Feb. 1979 (PB 301 167)A06

UCB/EERC-79/07 "The Design of Steel Energy Absorbing Restrainers and Their Incorporation into Nuclear Power Plants for Enhanced Safety: Volume 1 - Summary Report," by P.N. Spencer, V.F. Zackay, and E.R. Parker - Feb. 1979(UCB/EERC-79/07)A09

UCB/EERC-79/08 "The Design of Steel Energy Absorbing Restrainers and Their Incorporation into Nuclear Power Plants for Enhanced Safety: Volume 2 - The Development of Analyses for Reactor System Piping,""Simple Systems" by M.C. Lee, J. Penzien, A.K. Chopra and K, Suzuki "Complex Systems" by G.H. Powell, E.L. Wilson, R.W. Clough and D.G. Row - Feb. 1979(UCB/EERC-79/08)A10

UCB/EERC-79/09 "The Design of Steel Energy Absorbing Restrainers and Their Incorporation into Nuclear Power Plants for Enhanced Safety: Volume 3 - Evaluation of Commercial Steels," by W.S. Owen, R.M.N. Pelloux, R.O. Ritchie, M. Faral, T. Ohhashi, J. Toplosky, S.J. Hartman, V.F. Zackay and E.R. Parker - Feb. 1979(UCB/EERC-79/09)A04

UCB/EERC-79/10 "The Design of Steel Energy Absorbing Restrainers and Their Incorporation into Nuclear Power Plants for Enhanced Safety: Volume 4 - A Review of Energy-Absorbing Devices," by J.M. Kelly and M.S. Skinner - Feb. 1979(UCB/EERC-79/10)A04

UCB/EERC-79/11 "Conservatism In Summation Rules for Closely Spaced Modes," by J.M. Kelly and J.L. Sackman - May 1979(PB 301 328)A03

UCB/EERC-79/12 "Cyclic Loading Tests of Masonry Single Piers; Volume 3 - Height to Width Ratio of 0.5," by P.A. Hidalgo, R.L. Mayes, H.D. McNiven and R.W. Clough - May 1979(PB 301 321)A08

UCB/EERC-79/13 "Cyclic Behavior of Dense Course-Grained Materials in Relation to the Seismic Stability of Dams," by N.G. Banerjee, H.B. Seed and C.K. Chan - June 1979(PB 301 373)A13

UCB/EERC-79/14 "Seismic Behavior of Reinforced Concrete Interior Beam-Column Subassemblages," by S. Viwathanatepa, E.P. Popov and V.V. Bertero - June 1979(PB 301 326)A10

UCB/EERC-79/15 "Optimal Design of Localized Nonlinear Systems with Dual Performance Criteria Under Earthquake Excitations," by M.A. Bhatti - July 1979(PB 80 167 109)A06

UCB/EERC-79/16 "OPTDYN - A General Purpose Optimization Program for Problems with or without Dynamic Constraints," by M.A. Bhatti, E. Polak and K.S. Pister - July 1979(PB 80 167 091)A05

UCB/EERC-79/17 "ANSR-II, Analysis of Nonlinear Structural Response, Users Manual," by D.P. Mondkar and G.H. Powell July 1979(PB 80 113 301)A05

UCB/EERC-79/18 "Soil Structure Interaction in Different Seismic Environments," A. Gomez-Masso, J. Lysmer, J.-C. Chen and H.B. Seed - August 1979(PB 80 101 520)A04

UCB/EERC-79/19 "ARMA Models for Earthquake Ground Motions," by M.K. Chang, J.W. Kwiatkowski, R.F. Nau, R.M. Oliver and K.S. Pister - July 1979(PB 301 166)A05

UCB/EERC-79/20 "Hysteretic Behavior of Reinforced Concrete Structural Walls," by J.M. Vallenas, V.V. Bertero and E.P. Popov - August 1979(PB 80 165 905)A12

UCB/EERC-79/21 "Studies on High-Frequency Vibrations of Buildings - 1: The Column Effect," by J. Lubliner - August 1979 (PB 80 158 553)A03

UCB/EERC-79/22 "Effects of Generalized Loadings on Bond Reinforcing Bars Embedded in Confined Concrete Blocks," by S. Viwathanatepa, E.P. Popov and V.V. Bertero - August 1979(PB 81 124 018)A14

UCB/EERC-79/23 "Shaking Table Study of Single-Story Masonry Houses, Volume 1: Test Structures 1 and 2," by P. Gülkan, R.L. Mayes and R.W. Clough - Sept. 1979 (HUD-000 1763)A12

UCB/EERC-79/24 "Shaking Table Study of Single-Story Masonry Houses, Volume 2: Test Structures 3 and 4," by P. Gülkan, R.L. Mayes and R.W. Clough - Sept. 1979 (HUD-000 1836)A12

UCB/EERC-79/25 "Shaking Table Study of Single-Story Masonry Houses, Volume 3: Summary, Conclusions and Recommendations," by R.W. Clough, R.L. Mayes and P. Gülkan - Sept. 1979 (HUD-000 1837)A06

UCB/EERC-79/26 "Recommendations for a U.S.-Japan Cooperative Research Program Utilizing Large-Scale Testing Facilities," by U.S.-Japan Planning Group - Sept. 1979(PB 301 407)A06

UCB/EERC-79/27 "Earthquake-Induced Liquefaction Near Lake Amatitlan, Guatemala," by H.B. Seed, I. Arango, C.K. Chan, A. Gomez-Masso and R. Grant de Ascoli - Sept. 1979(NUREG-CR1341)A03

UCB/EERC-79/28 "Infill Panels: Their Influence on Seismic Response of Buildings," by J.W. Axley and V.V. Bertero Sept. 1979(PB 80 163 371)A10

UCB/EERC-79/29 "3D Truss Bar Element (Type 1) for the ANSR-II Program," by D.P. Mondkar and G.H. Powell - Nov. 1979 (PB 80 169 709)A02

UCB/EERC-79/30 "2D Beam-Column Element (Type 5 - Parallel Element Theory) for the ANSR-II Program," by D.G. Row, G.H. Powell and D.P. Mondkar - Dec. 1979(PB 80 167 224)A03

UCB/EERC-79/31 "3D Beam-Column Element (Type 2 - Parallel Element Theory) for the ANSR-II Program," by A. Riahi, G.H. Powell and D.P. Mondkar - Dec. 1979(PB 80 167 216)A03

UCB/EERC-79/32 "On Response of Structures to Stationary Excitation," by A. Der Kiureghian - Dec. 1979(PB 80166 929)A03

UCB/EERC-79/33 "Undisturbed Sampling and Cyclic Load Testing of Sands," by S. Singh, H.B. Seed and C.K. Chan Dec. 1979(ADA 087 298)A07

UCB/EERC-79/34 "Interaction Effects of Simultaneous Torsional and Compressional Cyclic Loading of Sand," by P.M. Griffin and W.N. Houston - Dec. 1979(ADA 092 352)A15

UCB/EERC-80/01 "Earthquake Response of Concrete Gravity Dams Including Hydrodynamic and Foundation Interaction Effects," by A.K. Chopra, P. Chakrabarti and S. Gupta - Jan. 1980(AD-A087297)A10

UCB/EERC-80/02 "Rocking Response of Rigid Blocks to Earthquakes," by C.S. Yim, A.K. Chopra and J. Penzien - Jan. 1980 (PB80 166 002)A04

UCB/EERC-80/03 "Optimum Inelastic Design of Seismic-Resistant Reinforced Concrete Frame Structures," by S.W. Zagajeski and V.V. Bertero - Jan. 1980(PB80 164 635)A06

UCB/EERC-80/04 "Effects of Amount and Arrangement of Wall-Panel Reinforcement on Hysteretic Behavior of Reinforced Concrete Walls," by R. Iliya and V.V. Bertero - Feb. 1980(PB81 122 525)A09

UCB/EERC-80/05 "Shaking Table Research on Concrete Dam Models," by A. Niwa and R.W. Clough - Sept. 1980(PB81 122 368)A06

UCB/EERC-80/06 "The Design of Steel Energy-Absorbing Restrainers and their Incorporation into Nuclear Power Plants for Enhanced Safety (Vol 1A): Piping with Energy Absorbing Restrainers: Parameter Study on Small Systems," by G.H. Powell, C. Oughourlian and J. Simons - June 1980

UCB/EERC-80/07 "Inelastic Torsional Response of Structures Subjected to Earthquake Ground Motions," by Y. Yamazaki April 1980(PB81 122 327)A08

UCB/EERC-80/08 "Study of X-Braced Steel Frame Structures Under Earthquake Simulation," by Y. Ghanaat - April 1980 (PB81 122 335)A11

UCB/EERC-80/09 "Hybrid Modelling of Soil-Structure Interaction," by S. Gupta, T.W. Lin, J. Penzien and C.S. Yeh May 1980(PB81 122 319)A07

UCB/EERC-80/10 "General Applicability of a Nonlinear Model of a One Story Steel Frame," by B.I. Sveinsson and H.D. McNiven - May 1980(PB81 124 877)A06

UCB/EERC-80/11 "A Green-Function Method for Wave Interaction with a Submerged Body," by W. Kioka - April 1980 (PB81 122 269)A07

UCB/EERC-80/12 "Hydrodynamic Pressure and Added Mass for Axisymmetric Bodies," by F. Nilrat - May 1980(PB81 122 343)A08

UCB/EERC-80/13 "Treatment of Non-Linear Drag Forces Acting on Offshore Platforms," by B.V. Dao and J. Penzien May 1980(PB81 153 413)A07

UCB/EERC-80/14 "2D Plane/Axisymmetric Solid Element (Type 3 - Elastic or Elastic-Perfectly Plastic) for the ANSR-II Program," by D.P. Mondkar and G.H. Powell - July 1980(PB81 122 350)A03

UCB/EERC-80/15 "A Response Spectrum Method for Random Vibrations," by A. Der Kiureghian - June 1980(PB81 122 301)A03

UCB/EERC-80/16 "Cyclic Inelastic Buckling of Tubular Steel Braces," by V.A. Zayas, E.P. Popov and S.A. Mahin June 1980(PB81 124 885)A10

UCB/EERC-80/17 "Dynamic Response of Simple Arch Dams Including Hydrodynamic Interaction," by C.S. Porter and A.K. Chopra - July 1980(PB81 124 000)A13

UCB/EERC-80/18 "Experimental Testing of a Friction Damped Aseismic Base Isolation System with Fail-Safe Characteristics," by J.M. Kelly, K.E. Beucke and M.S. Skinner - July 1980(PB81 148 595)A04

UCB/EERC-80/19 "The Design of Steel Energy-Absorbing Restrainers and their Incorporation into Nuclear Power Plants for Enhanced Safety (Vol 1B): Stochastic Seismic Analyses of Nuclear Power Plant Structures and Piping Systems Subjected to Multiple Support Excitations," by M.C. Lee and J. Penzien - June 1980

UCB/EERC-80/20 "The Design of Steel Energy-Absorbing Restrainers and their Incorporation into Nuclear Power Plants for Enhanced Safety (Vol 1C): Numerical Method for Dynamic Substructure Analysis," by J.M. Dickens and E.L. Wilson - June 1980

UCB/EERC-80/21 "The Design of Steel Energy-Absorbing Restrainers and their Incorporation into Nuclear Power Plants for Enhanced Safety (Vol 2): Development and Testing of Restraints for Nuclear Piping Systems," by J.M. Kelly and M.S. Skinner - June 1980

UCB/EERC-80/22 "3D Solid Element (Type 4-Elastic or Elastic-Perfectly-Plastic) for the ANSR-II Program," by D.P. Mondkar and G.H. Powell - July 1980(PB81 123 242)A03

UCB/EERC-80/23 "Gap-Friction Element (Type 5) for the ANSR-II Program," by D.P. Mondkar and G.H. Powell - July 1980 (PB81 122 285)A03

UCB/EERC-80/24 "U-Bar Restraint Element (Type 11) for the ANSR-II Program," by C. Oughourlian and G.H. Powell July 1980(PB81 122 293)A03

UCB/EERC-80/25 "Testing of a Natural Rubber Base Isolation System by an Explosively Simulated Earthquake," by J.M. Kelly - August 1980(PB81 201 360)A04

UCB/EERC-80/26 "Input Identification from Structural Vibrational Response," by Y. Hu - August 1980(PB81 152 308)A05

UCB/EERC-80/27 "Cyclic Inelastic Behavior of Steel Offshore Structures," by V.A. Zayas, S.A. Mahin and E.P. Popov August 1980(PB81 196 180)A15

UCB/EERC-80/28 "Shaking Table Testing of a Reinforced Concrete Frame with Biaxial Response," by M.G. Oliva October 1980(PB81 154 304)A10

UCB/EERC-80/29 "Dynamic Properties of a Twelve-Story Prefabricated Panel Building," by J.G. Bouwkamp, J.P. Kollegger and R.M. Stephen - October 1980(PB82 117 128)A06

UCB/EERC-80/30 "Dynamic Properties of an Eight-Story Prefabricated Panel Building," by J.G. Bouwkamp, J.P. Kollegger and R.M. Stephen - October 1980(PB81 200 313)A05

UCB/EERC-80/31 "Predictive Dynamic Response of Panel Type Structures Under Earthquakes," by J.P. Kollegger and J.G. Bouwkamp - October 1980(PB81 152 316)A04

UCB/EERC-80/32 "The Design of Steel Energy-Absorbing Restrainers and their Incorporation into Nuclear Power Plants for Enhanced Safety (Vol 3): Testing of Commercial Steels in Low-Cycle Torsional Fatigue," by P. Spencer, E.R. Parker, E. Jongewaard and M. Drory

UCB/EERC-80/33 "The Design of Steel Energy-Absorbing Restrainers and their Incorporation into Nuclear Power Plants for Enhanced Safety (Vol 4): Shaking Table Tests of Piping Systems with Energy-Absorbing Restrainers," by S.F. Stiemer and W.G. Godden - Sept. 1980

UCB/EERC-80/34 "The Design of Steel Energy-Absorbing Restrainers and their Incorporation into Nuclear Power Plants for Enhanced Safety (Vol 5): Summary Report," by P. Spencer

UCB/EERC-80/35 "Experimental Testing of an Energy-Absorbing Base Isolation System," by J.M. Kelly, M.S. Skinner and K.E. Beucke - October 1980(PB81 154 072)A04

UCB/EERC-80/36 "Simulating and Analyzing Artificial Non-Stationary Earthquake Ground Motions," by R.F. Nau, R.M. Oliver and K.S. Pister - October 1980(PB81 153 397)A04

UCB/EERC-80/37 "Earthquake Engineering at Berkeley - 1980," - Sept. 1980(PB81 205 874)A09

UCB/EERC-80/38 "Inelastic Seismic Analysis of Large Panel Buildings," by V. Schricker and G.H. Powell - Sept. 1980 (PB81 154 338)A13

UCB/EERC-80/39 "Dynamic Response of Embankment, Concrete-Gravity and Arch Dams Including Hydrodynamic Interaction," by J.F. Hall and A.K. Chopra - October 1980(PB81 152 324)A11

UCB/EERC-80/40 "Inelastic Buckling of Steel Struts Under Cyclic Load Reversal," by R.G. Black, W.A. Wenger and E.P. Popov - October 1980(PB81 154 312)A08

UCB/EERC-80/41 "Influence of Site Characteristics on Building Damage During the October 3, 1974 Lima Earthquake," by P. Repetto, I. Arango and H.B. Seed - Sept. 1980(PB81 161 739)A05

UCB/EERC-80/42 "Evaluation of a Shaking Table Test Program on Response Behavior of a Two Story Reinforced Concrete Frame," by J.M. Blondet, R.W. Clough and S.A. Mahin

UCB/EERC-80/43 "Modelling of Soil-Structure Interaction by Finite and Infinite Elements," by F. Medina - December 1980(PB81 229 270)A04

UCB/EERC-81/01 "Control of Seismic Response of Piping Systems and Other Structures by Base Isolation," edited by J.M. Kelly - January 1981 (PB81 200 735)A05

UCB/EERC-81/02 "OPTNSR - An Interactive Software System for Optimal Design of Statically and Dynamically Loaded Structures with Nonlinear Response," by M.A. Bhatti, V. Ciampi and K.S. Pister - January 1981 (PB81 218 851)A09

UCB/EERC-81/03 "Analysis of Local Variations in Free Field Seismic Ground Motions," by J.-C. Chen, J. Lysmer and H.B. Seed - January 1981 (AD-A099508)A13

UCB/EERC-81/04 "Inelastic Structural Modeling of Braced Offshore Platforms for Seismic Loading," by V.A. Zayas, P.-S.B. Shing, S.A. Mahin and E.P. Popov - January 1981(PB82 138 777)A07

UCB/EERC-81/05 "Dynamic Response of Light Equipment in Structures," by A. Der Kiureghian, J.L. Sackman and B. Nour-Omid - April 1981 (PB81 218 497)A04

UCB/EERC-81/06 "Preliminary Experimental Investigation of a Broad Base Liquid Storage Tank," by J.G. Bouwkamp, J.P. Kollegger and R.M. Stephen - May 1981(PB82 140 385)A03

UCB/EERC-81/07 "The Seismic Resistant Design of Reinforced Concrete Coupled Structural Walls," by A.E. Aktan and V.V. Bertero - June 1981(PB82 113 358)A11

UCB/EERC-81/08 "The Undrained Shearing Resistance of Cohesive Soils at Large Deformations," by M.R. Pyles and H.B. Seed - August 1981

UCB/EERC-81/09 "Experimental Behavior of a Spatial Piping System with Steel Energy Absorbers Subjected to a Simulated Differential Seismic Input," by S.F. Stiemer, W.G. Godden and J.M. Kelly - July 1981

UCB/EERC-81/10 "Evaluation of Seismic Design Provisions for Masonry in the United States," by B.I. Sveinsson, R.L. Mayes and H.D. McNiven - August 1981 (PB82 166 075)A08

UCB/EERC-81/11 "Two-Dimensional Hybrid Modelling of Soil-Structure Interaction," by T.-J. Tzong, S. Gupta and J. Penzien - August 1981(PB82 142 118)A04

UCB/EERC-81/12 "Studies on Effects of Infills in Seismic Resistant R/C Construction," by S. Brokken and V.V. Bertero - September 1981 (PB82 166 190)A09

UCB/EERC-81/13 "Linear Models to Predict the Nonlinear Seismic Behavior of a One-Story Steel Frame," by H. Valdimarsson, A.H. Shah and H.D. McNiven - September 1981(PB82 138 793)A07

UCB/EERC-81/14 "TLUSH: A Computer Program for the Three-Dimensional Dynamic Analysis of Earth Dams," by T. Kagawa, L.H. Mejia, H.B. Seed and J. Lysmer - September 1981(PB82 139 940)A06

UCB/EERC-81/15 "Three Dimensional Dynamic Response Analysis of Earth Dams," by L.H. Mejia and H.B. Seed - September 1981 (PB82 137 274)A12

UCB/EERC-81/16 "Experimental Study of Lead and Elastomeric Dampers for Base Isolation Systems," by J.M. Kelly and S.B. Hodder - October 1981 (PB82 166 182)A05

UCB/EERC-81/17 "The Influence of Base Isolation on the Seismic Response of Light Secondary Equipment," by J.M. Kelly - April 1981 (PB82 255 266)A04

UCB/EERC-81/18 "Studies on Evaluation of Shaking Table Response Analysis Procedures," by J. Marcial Blondet - November 1981 (PB82 197 278)A10

UCB/EERC-81/19 "DELIGHT.STRUCT: A Computer-Aided Design Environment for Structural Engineering," by R.J. Balling, K.S. Pister and E. Polak - December 1981 (PB82 218 496)A07

UCB/EERC-81/20 "Optimal Design of Seismic-Resistant Planar Steel Frames," by R.J. Balling, V. Ciampi, K.S. Pister and E. Polak - December 1981 (PB82 220 179)A07

UCB/EERC-82/01 "Dynamic Behavior of Ground for Seismic Analysis of Lifeline Systems," by T. Sato and A. Der Kiureghian - January 1982 (PB82 218 926)A05

UCB/EERC-82/02 "Shaking Table Tests of a Tubular Steel Frame Model," by Y. Ghanaat and R. W. Clough - January 1982 (PB82 220 161)A07

UCB/EERC-82/03 "Behavior of a Piping System under Seismic Excitation: Experimental Investigations of a Spatial Piping System supported by Mechanical Shock Arrestors and Steel Energy Absorbing Devices under Seismic Excitation," by S. Schneider, H.-M. Lee and W. G. Godden - May 1982 (PB83 172 544)A09

UCB/EERC-82/04 "New Approaches for the Dynamic Analysis of Large Structural Systems," by E. L. Wilson - June 1982 (PB83 148 080)A05

UCB/EERC-82/05 "Model Study of Effects of Damage on the Vibration Properties of Steel Offshore Platforms," by F. Shahrivar and J. G. Bouwkamp - June 1982 (PB83 148 742)A10

UCB/EERC-82/06 "States of the Art and Practice in the Optimum Seismic Design and Analytical Response Prediction of R/C Frame-Wall Structures," by A. E. Aktan and V. V. Bertero - July 1982 (PB83 147 736)A05

UCB/EERC-82/07 "Further Study of the Earthquake Response of a Broad Cylindrical Liquid-Storage Tank Model," by G. C. Manos and R. W. Clough - July 1982 (PB83 147 744)A11

UCB/EERC-82/08 "An Evaluation of the Design and Analytical Seismic Response of a Seven Story Reinforced Concrete Frame - Wall Structure," by F. A. Charney and V. V. Bertero - July 1982(PB83 157 628)A09

UCB/EERC-82/09 "Fluid-Structure Interactions: Added Mass Computations for Incompressible Fluid," by J. S.-H. Kuo - August 1982 (PB83 156 281)A07

UCB/EERC-82/10 "Joint-Opening Nonlinear Mechanism: Interface Smeared Crack Model," by J. S.-H. Kuo - August 1982 (PB83 149 195)A05

UCB/EERC-82/11 "Dynamic Response Analysis of Techi Dam," by R. W. Clough, R. M. Stephen and J. S.-H. Kuo - August 1982 (PB83 147 496)A06

UCB/EERC-82/12 "Prediction of the Seismic Responses of R/C Frame-Coupled Wall Structures," by A. E. Aktan, V. V. Bertero and M. Piazza - August 1982 (PB83 149 203)A09

UCB/EERC-82/13 "Preliminary Report on the SMART 1 Strong Motion Array in Taiwan," by B. A. Bolt, C. H. Loh, J. Penzien, Y. B. Tsai and Y. T. Yeh - August 1982 (PB83 159 400)A10

UCB/EERC-82/14 "Shaking-Table Studies of an Eccentrically X-Braced Steel Structure," by M. S. Yang - September 1982

UCB/EERC-82/15 "The Performance of Stairways in Earthquakes," by C. Roha, J. W. Axley and V. V. Bertero - September 1982 (PB83 157 693)A07

UCB/EERC-82/16 "The Behavior of Submerged Multiple Bodies in Earthquakes," by W.-G. Liao - Sept. 1982 (PB83 158 709)A07

UCB/EERC-82/17 "Effects of Concrete Types and Loading Conditions on Local Bond-Slip Relationships," by A. D. Cowell, E. P. Popov and V. V. Bertero - September 1982 (PB83 153 577)A04

UCB/EERC-82/18 "Mechanical Behavior of Shear Wall Vertical Boundary Members: An Experimental Investigation," by M. T. Wagner and V. V. Bertero - October 1982 (PB83 159 764)A05

UCB/EERC-82/19 "Experimental Studies of Multi-support Seismic Loading on Piping Systems," by J. M. Kelly and A. D. Cowell - November 1982

UCB/EERC-82/20 "Generalized Plastic Hinge Concepts for 3D Beam-Column Elements," by P. F.-S. Chen and G. H. Powell - November 1982

UCB/EERC-82/21 "ANSR-III: General Purpose Computer Program for Nonlinear Structural Analysis," by C. V. Oughourlian and G. H. Powell - November 1982

UCB/EERC-82/22 "Solution Strategies for Statically Loaded Nonlinear Structures," by J. W. Simons and G. H. Powell - November 1982

UCB/EERC-82/23 "Analytical Model of Deformed Bar Anchorages under Generalized Excitations," by V. Ciampi, R. Eligehausen, V. V. Bertero and E. P. Popov - November 1982 (PB83 169 532)A06

UCB/EERC-82/24 "A Mathematical Model for the Response of Masonry Walls to Dynamic Excitations," by H. Sucuoğlu, Y. Mengi and H. D. McNiven - November 1982 (PB83 169 011)A07

UCB/EERC-82/25 "Earthquake Response Considerations of Broad Liquid Storage Tanks," by F. J. Cambra - November 1982

UCB/EERC-82/26 "Computational Models for Cyclic Plasticity, Rate Dependence and Creep," by B. Mosaddad and G. H. Powell - November 1982

UCB/EERC-82/27 "Inelastic Analysis of Piping and Tubular Structures," by M. Mahasuverachai and G. H. Powell - November 1982

UCB/EERC-83/01 "The Economic Feasibility of Seismic Rehabilitation of Buildings by Base Isolation," by J. M. Kelly - January 1983

UCB/EERC-83/02 "Seismic Moment Connections for Moment-Resisting Steel Frames," by E. P. Popov - January 1983

UCB/EERC-83/03 "Design of Links and Beam-to-Column Connections for Eccentrically Braced Steel Frames," by E. P. Popov and J. O. Malley - January 1983

UCB/EERC-83/04 "Numerical Techniques for the Evaluation of Soil-Structure Interaction Effects in the Time Domain," by E. Bayo and E. L. Wilson - February 1983

UCB/EERC-83/05 "A Transducer for Measuring the Internal Forces in the Columns of a Frame-Wall Reinforced Concrete Structure," by R. Sause and V. V. Bertero - May 1983

UCB/EERC-83/06 "Dynamic Interactions between Floating Ice and Offshore Structures," by P. Croteau - May 1983

UCB/EERC-83/07 "Dynamic Analysis of Multiply Tuned and Arbitrarily Supported Secondary Systems," by T. Igusa and A. Der Kiureghian - June 1983

UCB/EERC-83/08 "A Laboratory Study of Submerged Multi-body Systems in Earthquakes," by G. R. Ansari - June 1983

UCB/EERC-83/09 "Effects of Transient Foundation Uplift on Earthquake Response of Structures," by C.-S. Yim and A. K. Chopra - June 1983

UCB/EERC-83/10 "Optimal Design of Friction-Braced Frames under Seismic Loading," by M. A. Austin and K. S. Pister - June 1983

UCB/EERC-83/11 "Shaking Table Study of Single-Story Masonry Houses: Dynamic Performance under Three Component Seismic Input and Recommendations," by G. C. Manos, R. W. Clough and R. L. Mayes - June 1983

UCB/EERC-83/12 "Experimental Error Propagation in Pseudodynamic Testing," by P. B. Shing and S. A. Mahin - June 1983

UCB/EERC-83/13 "Experimental and Analytical Predictions of the Mechanical Characteristics of a 1/5-scale Model of a 7-story R/C Frame-Wall Building Structure," by A. E. Aktan, V. V. Bertero, A. A. Chowdhury and T. Nagashima - August 1983

UCB/EERC-83/14 "Shaking Table Tests of Large-Panel Precast Concrete Building System Assemblages," by M. G. Oliva and R. W. Clough - August 1983

UCB/EERC-83/15 "Seismic Behavior of Active Beam Links in Eccentrically Braced Frames," by K. D. Hjelmstad and E. P. Popov - July 1983

UCB/EERC-83/16 "System Identification of Structures with Joint Rotation," by J. S. Dimsdale and H. D. McNiven - July 1983

UCB/EERC-83/17 "Construction of Inelastic Response Spectra for Single-Degree-of-Freedom Systems," by S. Mahin and J. Lin - July 1983

UCB/EERC-83/18 "Interactive Computer Analysis Methods for Predicting the Inelastic Cyclic Behavior of Sections," by S. Kaba and S. Mahin - July 1983

UCB/EERC-83/19 "Effects of Bond Deterioration on Hysteretic Behavior of Reinforced Concrete Joints," by F. C. Filippou, E. P. Popov and V. V. Bertero - August 1983

UCB/EERC-83/20 "Analytical and Experimental Correlation of Large-Panel Precast Building System Performance," by M. G. Oliva, R. W. Clough, M. Velkov, P. Gavrilovic and J. Petrovski - November 1983

UCB/EERC-83/21 "Mechanical Characteristics of the Materials Used in the 1/5 Scale and Full Scale Models of the 7-Story Reinforced Concrete Test Structure," by V. V. Bertero, A. E. Aktan and A. A. Chowdhury - September 1983

UCB/EERC-83/22 "Hybrid Modelling of Soil-Structure Interaction in Layered Media," by T.-J. Tzong and J. Penzien - October 1983